Design and application of small circular RNAs with antisense function

Kumulative Inauguraldissertation

vorgelegt von

Christina Pfafenrot

(M. Sc. Biologie)

zur Erlangung des akademischen Grades

doctor rerum naturalium

(Dr. rer. nat.)

Eingereicht am Fachbereich 08 - Biologie und Chemie

der Justus-Liebig-Universität Gießen

Gießen, Februar 2022

„Was wir wissen, ist ein Tropfen; was wir nicht wissen, ein Ozean.“
— Isaac Newton

...Für meine Eltern.

Die vorliegende Arbeit wurde am Institut für Biochemie des Fachbereiches 08 der Justus-Liebig-Universität Gießen in der Zeit von Oktober 2016 bis Februar 2022 unter der Leitung von Prof. Dr. Albrecht Bindereif angefertigt.

Dekan	**Prof. Dr. Thomas Wilke** Institut für Tierökologie und Spezielle Zoologie, FB08 Justus-Liebig-Universität Gießen
1. Gutachter	**Prof. Dr. Albrecht Bindereif** Institut für Biochemie, FB08 Justus-Liebig-Universität Gießen
2. Gutachter	**Prof. Dr. John Ziebuhr** Institut für Medizinische Virologie, FB11 Justus-Liebig-Universität Gießen

Eidesstattliche Erklärung

Ich habe die vorgelegte Dissertation selbständig und ohne unerlaubte fremde Hilfe und nur mit den Hilfen angefertigt, die ich in der Dissertation angegeben habe. Alle Textstellen, die wörtlich oder sinngemäß aus veröffentlichten Schriften entnommen sind, und alle Angaben, die auf mündlichen Auskünften beruhen, sind als solche kenntlich gemacht. Bei den von mir durchgeführten und in der Dissertation erwähnten Untersuchungen habe ich die Grundsätze guter wissenschaftlicher Praxis, wie sie in der „Satzung der Justus-Liebig-Universität Gießen zur Sicherung guter wissenschaftlicher Praxis“ niedergelegt sind, eingehalten.

Gießen, 17.02.2022

Christina Pfafenrot

Index

Zusammenfassung

Zirkuläre RNAs (circRNAs) gehören zu einer Klasse von nichtkodierenden RNAs (ncRNAs) und zeichnen sich durch ihre kovalent geschlossene, zirkuläre Struktur aus. Die Biogenese beruht dabei auf einer Art von alternativem Spleißmechanismus, der auch als *Backsplicing* bezeichnet wird. Funktionell gesehen sind circRNAs jedoch bis heute weitgehend unerforscht, mit Ausnahme einer microRNA-Schwammfunktion, die nur in wenigen Fällen experimentell bestätigt werden konnte.

Auf Grundlage von Hochdurchsatz-Sequenzierungsverfahren wächst die Zahl der in der Literatur beschriebenen circRNAs stetig, welche sich unter anderem als neuartige und attraktive Biomarker herauskristallisieren. Da jedoch endogene, *trans*-gespleißte, Transkripte zur falsch-positiven Detektion von circRNA-*Junction*-Sequenzen führen können, ist es essentiell, dass für die Validierung nicht ausschließlich bioinformatische Auswertungen verwendet werden. Im Rahmen dieser Arbeit wurde daher auf die essentielle Notwendigkeit von Qualitätskriterien für die Validierung und Charakterisierung von zirkulären RNAs hingewiesen. Neben der bioinformatischen Analyse sind klassische biochemische Methoden für die Charakterisierung von circRNAs und die überzeugende Bestätigung ihrer Zirkularität unerlässlich **(Pfafenrot und Preußer 2019, siehe Abschnitt I)**.

Unter Einbezug dieser Validierungskriterien wurden in diesem Kontext diverse biochemische Methoden zusammengefasst, die sich besonders dafür eignen, circRNA-Protein-Komplexe (circRNPs) zu untersuchen. Hierfür wurden zwei Kategorien von Methoden vorgestellt, die sich entweder gezielt auf eine bestimmte RNA oder ein bestimmtes Protein konzentrierten, und sowohl Gen-spezifisch als auch auf globaler Ebene angewendet werden können. Darauf aufbauend wurden die Vorteile und Herausforderungen der verfügbaren Ansätze diskutiert (**Ulshöfer *et al.* 2021, siehe Abschnitt J)**.

Neben anderen RNAs wurden auch zirkuläre RNAs bereits als ein Bestandteil von aus Thrombozyten hervorgehenden extrazellulären Vesikeln (EVs) beschrieben, jedoch ist der zugrundeliegende selektive Sortierungsmechanismus bisher unbekannt. In diesem Kontext wurde die Sequenzabhängigkeit, Größenverteilung, sowie der Einfluss des Biogenese- und Prozessierungsmechanismus von verschiedenen linearen Reporter- und endogenen RNAs auf deren Sekretion in EVs untersucht. Mittels dieser Analysen konnte gezeigt werden, dass kurze RNAs effizienter sekretiert werden als lange und dass Pol III-Transkripte im Vergleich zu Pol II-Transkripten ebenfalls effizienter in EVs verpackt werden. Eine generelle Anreicherung der untersuchten RNAs in EVs im Vergleich zum zellulären Level konnte dabei jedoch nicht bestätigt werden **(Mosbach *et al.* 2021, siehe Abschnitt K)**.

Da circRNAs keine freien 5‘- bzw. 3‘-Enden enthalten, weisen sie im Vergleich zu ihren linearen Gegenstücken eine sehr hohe intrazelluläre Stabilität auf. Somit stellen circRNAs eine attraktive Grundlage für die Entwicklung von RNA-basierten Therapeutika im Bereich der molekularen Medizin dar. Um dieses Potential ausschöpfen zu können, wurde des Weiteren der Fokus auf die Etablierung von kleinen *antisense*-circRNAs (AS-circRNAs) gelegt, welche als molekulare Werkzeuge verwendet werden sollen, um gezielt die Translationsinitiation in Eukaryonten zu regulieren.

In einer *Proof-of-principle* Studie konnte anhand eines Luziferase-Konstrukts, das die β-Globin (*HBB*, Hämoglobin-Untereinheit beta-Gen) 5'-UTR enthielt, sowie einer Reihe von synthetischen AS-circRNAs, eine dosisabhängige Abnahme der Translationsaktivität demonstriert werden. In diesem Zusammenhang wurde die Cap- sowie die Startkodon-proximale Region als effektivste Zielregion identifiziert.

Basierend auf diesen Erkenntnissen, wurde nachfolgend zur Überprüfung dieses Ansatzes eine endogene mRNA (*MDM2*; mouse double minute 2 homolog) für weitere Untersuchungen als Ziel herangezogen. Hierbei konnte sowohl auf Ebene des Proteinlevels eine Reduktion der Translationsaktivität mittels Western blot, wie auch auf Ebene des mRNA-Levels eine Reduktion der mRNA Stabilität mittels RT-qPCR, belegt werden **(siehe Abschnitt M)**.

Im Kontext der aktuellen COVID-19 Pandemie mit ihren weltweiten Auswirkungen auf die menschliche Gesundheit sowie die Wirtschaft, wurde die etablierte AS-circRNA Technologie aus den vorangegangenen Studien auch auf SARS-CoV-2 angewendet. Auf der Grundlage einer Reihe von AS-circRNAs, die auf spezifische 5′-UTR-Regionen des SARS-CoV-2-Genoms und der subgenomischen RNAs abzielen, wurde die Cap-proximale Region (einschließlich eines Teils der 5′-Leader-Sequenz) als effektivste Zielregion identifiziert. Hierbei konnte eine Reduktion der viralen Translation von bis zu 90% erreicht werden. Basierend auf Luziferase- und Infektions-Assays konnte des Weiteren gezeigt werden, dass die inhibitorische Aktivität von zirkulären RNAs durchweg effektiver ist als die von linearen RNAs und dass der antivirale Effekt der AS-circRNAs um bis zu 48 h länger andauert. Ein Vergleich gegenüber modifizierten *antisense*-Oligonukleotiden, die nach dem neuesten Stand der Technik hergestellt wurden, verdeutlichte außerdem den stärkeren Effekt der AS-circRNAs.

Dieser Ansatz zur Untersuchung der Wirksamkeit von AS-circRNA gegen SARS-CoV-2 basiert auf einer circRNA-Transfektion mit anschließender Virusinfektion, was wiederum einer prophylaktischen Behandlung entspricht. In diesem Zusammenhang konnte jedoch ebenfalls bestätigt werden, dass mit einer umgekehrten Reihenfolge, sprich Virusinfektion gefolgt von circRNA-Transfektion, die Effizienz und die Dauerhaftigkeit der antiviralen Wirkung bestehen bleibt. Dies legt nahe, dass der AS-circRNA-Ansatz nicht nur für prophylaktische Strategien, sondern auch für den Schutz vor viralen Infektionen und für die antivirale Therapie nützlich ist (**Pfafenrot *et al.* 2021, siehe Abschnitt L)**.

Zusammenfassend weisen die Ergebnisse darauf hin, dass die in dieser Arbeit etablierten Designer-AS-circRNAs eine neue Generation vielseitiger und anpassungsfähiger RNA-Therapeutika mit großem Potenzial darstellen.

Abstract

Circular RNAs (circRNAs) belong to a class of noncoding RNAs (ncRNAs) and are particularly characterized by their covalently closed ring structure. The biogenesis of circRNAs is based on a kind of alternative splicing mechanism, also known as *backsplicing*. Functionally, however, the vast majority of circRNAs are still largely uncharacterized, with the exception of a microRNA sponge function, which could only be experimentally confirmed in a few cases.

Based on high-throughput sequencing technologies, the number of circRNAs described in the literature is steadily growing, emerging as novel and attractive biomarkers. However, since endogenous *trans*-spliced transcripts can lead to false-positive detection of circRNA-junction sequences, it is crucial that not only bioinformatic analyses alone are used for validation. In the context of this work, the important need for quality criteria for the validation and characterization of circular RNAs was therefore pointed out. In addition to bioinformatic analysis, classical biochemical methods are essential for the characterization of circRNAs and the convincing confirmation of their circularity (**Pfafenrot and Preußer 2019**, **see section I).**

Considering these validation criteria, various biochemical methods were summarized that are particularly suitable for investigating circRNA-protein complexes (circRNPs). Two categories of methods were presented, focusing on either a specific RNA or a specific protein, which can be applied on a gene-specific as well as on a global level. Based on this, the advantages and challenges of the available approaches have been discussed (**Ulshöfer *et al.* 2021, see section J)**.

Among other RNAs, circular RNAs have been described as a component of platelet-derived extracellular vesicles (EVs), but the underlying selective sorting mechanism is currently unknown. In this context, the sequence dependence, size distribution, and the influence of the biogenesis and processing pathways of different linear reporter and endogenous RNAs on their secretion into EVs were investigated. This analysis revealed that short RNAs are secreted more efficiently than longer ones, and that Pol III transcripts are also packaged more efficiently into EVs compared to Pol II transcripts. However, a general enrichment of the investigated RNAs in EVs compared to the corresponding cellular levels could not be confirmed **(Mosbach *et al.* 2021, see section K)**.

Since circRNAs do not contain free 5' and 3' ends, they have a very high intracellular stability compared to their linear counterparts. Thus, circRNAs represent an attractive basis for the development of RNA-based therapeutics in the field of molecular medicine. In order to exploit this potential, the focus was placed on the establishment of small antisense circRNAs (AS-circRNAs), which could be used as molecular tools to specifically regulate translation initiation in eukaryotes.

In a proof-of-principle study, a luciferase construct containing the β-globin (*HBB*, hemoglobin subunit beta gene) 5'-UTR and a series of synthetic AS-circRNAs demonstrated a dose-dependent decrease in translational activity. In this context, the cap- as well as the start codon-proximal regions were identified as the most effective target regions.

Based on these findings, an endogenous mRNA (*MDM2*; mouse double minute 2 homologue) was subsequently used as a target for further investigations to verify this approach. A reduction of the translational

activity at the protein level by Western blot as well as a reduction of the mRNA stability at the mRNA level by RT-qPCR could be demonstrated **(see section M)**.

In the context of the current COVID-19 pandemic with its global impact on human health and the economy, the established AS-circRNA technology from the previous studies was also applied to SARS-CoV-2. Based on a series of AS-circRNAs targeting specific 5′-UTR regions of the SARS-CoV-2 genome and subgenomic RNAs, the cap-proximal region (including part of the 5′-leader sequence) was identified as the most effective target region. Here, a reduction of viral translation of up to 90% could be achieved. Based on luciferase and infection assays, it was further shown that the inhibitory activity of circular RNAs is consistently more effective than that of linear RNAs and that the antiviral effect of AS-circRNAs persists for up to 48 h longer. A comparison with modified antisense oligonucleotides produced according to the state-of-the-art also confirmed the significantly stronger effect of AS-circRNAs.

This approach to investigate the efficacy of AS-circRNA against SARS-CoV-2 is based on circRNA transfection followed by viral infection, which in turn corresponds to prophylactic treatment. In this context, however, it could also be confirmed that in the reverse order, i.e. viral infection followed by circRNA transfection, the efficiency and durability of the antiviral effect remains. This suggests that the AS-circRNA approach is useful not only for prophylactic strategies, but also for protection against viral infections and for antiviral therapy (**Pfafenrot *et al.* 2021, see section L)**.

In summary, the results indicate that the designer AS-circRNAs established in this work represent a new generation of versatile and adaptable RNA therapeutics with great potential.

Introduction

Therapeutic antisense strategies for regulation of gene expression

Interest in antisense technology started to grow already more than 40 years ago, opening up possibilities to manipulate gene expression and study gene functions, as well as the development of powerful therapeutic tools to treat various diseases. Especially the work of **Zamecnik and Stephenson** in 1978 showed for the first time that DNA antisense oligonucleotides can bind complementary to the Rous Sarcoma Virus RNA by hybridization, subsequently leading to suppressed replication by blocking viral translation **(Zamecnik and Stephenson 1978, Stephenson and Zamecnik 1978)**. Furthermore, catalytically active RNAs, so-called ribozymes, which were described only a few years later **(Cech *et al.* 1981, Kruger *et al.* 1982, Guerrier-Takada *et al.* 1983)**, also raised interest in using them for therapeutic purposes. With the discovery of the natural mechanism of RNA interference (RNAi), the field received a new impetus. In this context, it was first reported in 1998 that double-stranded RNA molecules could be used in *Caenorhabditis elegans* to silence the expression of a gene in a sequence-specific manner **(Fire *et al.* 1998)**. Initially, this method could only be used in lower eukaryotes, as long double-stranded RNA molecules triggered the interferon response in mammalian cells. However, Tuschl and his colleagues were able to specifically inhibit the expression of target genes without eliciting an immune response. This was achieved using so-called small interfering RNAs (siRNAs), which are only 21 nts long **(Elbashir *et al.* 2001)**. Nowadays the RNAi technique has become a standard method in molecular biology, as it allows the investigation of gene function, for genome-wide identification of new targets, and validation of potential targets for new drugs. To this day, there are over 100 registered clinical trials, of which 10 oligonucleotide drugs have received approval from the FDA/EMA (reviewed by **Kilanowska and Studzinska 2020**).

Molecular mechanisms

Antisense oligonucleotides (ASOs) are defined as short, chemically synthesized, and single-stranded DNA or RNA oligomers approximately 12-30 nts in length, that bind a complementary target RNA through Watson-Crick base pairing **(De Mesmaeker *et al.* 1995)**. ASOs have been known for decades, and from the beginning, it was said that they 'promise to open up a new era of drug research with the possibility of rational drug design based on the nucleotide sequences of the genes causing the disease' **(Uhlmann and Peyman 1990)**. In principle, the mechanisms can be classified into two mechanistic categories, either RNA cleavage and degradation or occupancy (also known as steric blocking) (reviewed by **Bennett 2019**) **(Figure 1).**

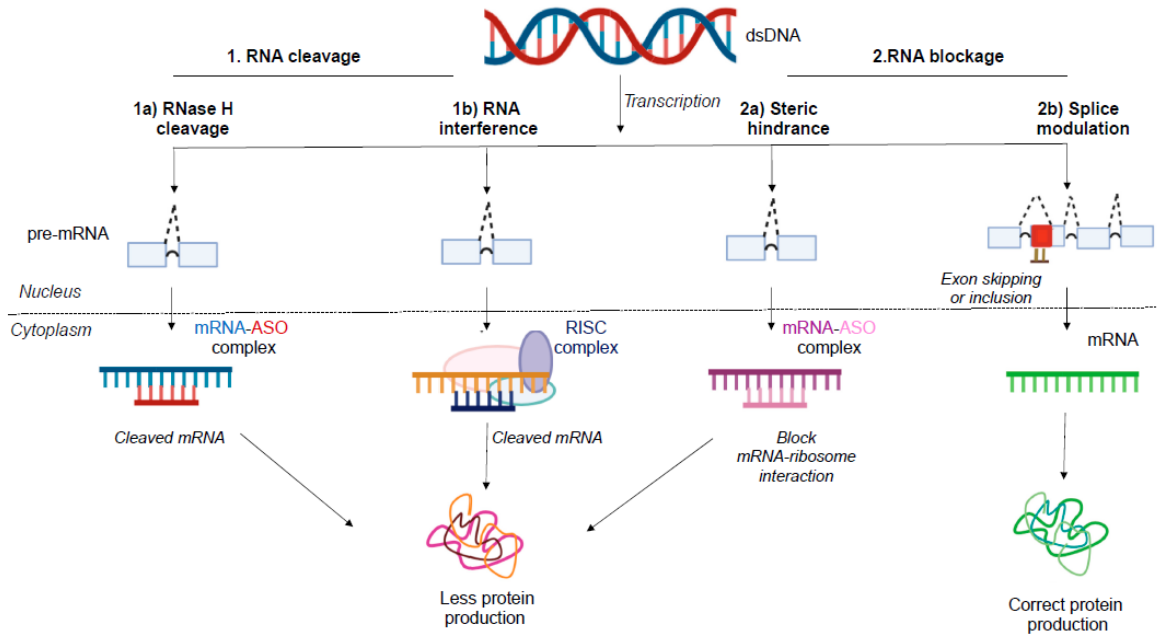

Figure 1: Functional mechanisms of ASOs.
The mechanisms can be classified into two categories (1) RNA cleavage and (2) RNA blocking.
[1a] RNA cleavage is induced by hybridization of DNA or Gapmer ASOs, and RNase H-dependent recognition of the DNA-RNA heteroduplexes in the cytoplasm. If cleavage occurs, translation is prevented and less target protein is formed.
[1b] RNA cleavage is promoted by synthetic and fully complementary siRNAs through AGO2 and the RNA interference (RNAi) pathway. In this process, the siRNA associates with the AGO2 and forms the RNA-induced silencing complex (RISC). Thereby, the passenger strand is degraded and the remaining guide strand directs the RISC to the complementary mRNA region. This causes mRNA to be cleaved by AGO2.
[2a] Steric hindrance can occur by using ASOs that bind the target RNA sequence in the cytoplasm and lead to translational arrest by inhibiting the interaction of the target mRNA with the 40S ribosomal subunit or preventing its assembly at the 40S or 60S subunit.
[2b] Splicing modulation can be achieved by blocking splice sites or splice enhancer/silencer elements. Generally, there are two ASO strategies to interfere with the splicing process: First, exon skipping can be induced by binding of an ASO to the pre-mRNA, thereby leading to splicing of a shortened mRNA, or, secondly, ASOs can promote the inclusion of exons in the final mRNA, resulting in a longer transcript isoform. Modified after **Dhuri *et al*. 2020.**

RNA cleavage and degradation

The majority of ASOs that have been developed fall into the first category and promote RNA cleavage either by RNase H, or Argonaute 2 (AGO2) **(Crooke *et al.* 2018)**. RNase H is an endogenous nuclease, which is found mostly in the nucleus, but also mitochondria and the cytoplasm. This enzyme recognizes RNA-DNA heteroduplexes and catalyzes the degradation of the RNA strand in this duplex **(Wu *et al*. 1999, Cerritelli and Crouch 2009)**. This enzymatic property is utilized in antisense technology, where hybridization and cleavage lead to a reduction of the target mRNA and its corresponding protein expression **(Figure 1 part 1a)**. An advantage of this method is that the ASO can be used substochiometrically, as it is released after cleavage, allowing it to bind an mRNA target once again. However, it should be noted that a target RNA may have strong secondary structures as well as binding sites for many RNA binding proteins (RBPs), which explains why not all ASOs can display their inhibitory effect. To overcome this problem, bioinformatic analysis and ASO screening are often required to identify suitable binding

sites **(Sohail and Southern 2000)**. To date, 4 ASOs received marketing authorization: Fomivirsen, Mipomersen, Inotersen as well as Volanesorsen.

Fomivirsen, commercially named Vitraven, was the first ASO-based drug developed and used intravitreally for the treatment of retinitis caused by opportunistic cytomegalovirus (CMV) infection in immunocompromised AIDS patients in 1998 **(Vitravene Study Group 2002)**. It is a antisense phosphorothioate oligonucleotide (PS)-based 21-mer that targets the viral mRNA encoding the immediate early-2 (IE-2) protein, required for viral replication, through the RNase H-mediated mRNA degradation mechanism **(Mulamba *et al.* 1998**, **Anderson *et al.* 1996)**. Due to reduced market demand, Fomiversen was voluntarily withdrawn from the market by its manufacturers.

In 2019, another RNase H-mediated antisense drug Volanesorsen (commercially called Waylivra) **(Rocha *et al.* 2017)** was released for the treatment of familial chylomicronaemia syndrome (FSC). This disease is a genetic disorder, leading to high concentrations of triglycerides in the blood, related to overexpression of apolipoprotein (Apo) C-III **(Digenio *et al.* 2016, Graham *et al.* 2013)**. This drug is a second-generation 20-mer ASO, based on a phosphorothioate backbone and 2'O-methoxyethylated RNA bases (reviewed by **Kilanowska and Studzinska 2020**).

Naturally occurring ribozymes and artificial DNA enzymes **(Breaker and Joyce 1994)** provide an alternative strategy to RNase H recruitment. Ribozymes are RNA molecules that occur naturally in many organisms and exhibit enzymatic activity. Naturally occurring ribozymes catalyze the hydrolysis or transesterification of phosphodiester bonds between nucleotides. The main difference to RNase H-dependent ASOs is that they do not rely on cellular enzymes. In addition, unlike ASOs, they can also be expressed *in vivo* in cells.

Ribozymes can be divided into two groups depending on their size. Large ribozymes, comprising several hundred nucleotides, include RNA self-splicing introns (group I and II) and RNase P, which processes the 5'-end of tRNA precursors. The splicing activity of group I introns has been used to replace mutated segments of ß-globin mRNA with the γ-globin 3' exon in cells from patients with sickle cell disease to prevent pathological hemoglobin aggregation **(Lan *et al.* 1998)**. Different variants of RNase P were used to inhibit the proliferation of various viruses in cell culture **(Kilani *et al.* 2000)**.

In contrast, small ribozymes are only 30 to 150 nts long and play a major role in clinical applications. These include, for example, hammerhead and hairpin ribozymes. Here, cleavage by these ribozymes occurs via a nucleophilic attack of the 2'-OH group on the cleavage site of its neighboring phosphorus atom, requiring only metal ions and producing cleavage products with 2'-3'-cyclophosphate and 5'-OH ends. The RNA is then released and degraded by cellular enzymes.

Although ribozymes can be directed against any target RNA, proper cleavage site selection has to be considered. For example, hammerhead ribozymes preferentially cleave downstream of the sequence NUH (N = any nucleotide, U = uridine, H = any nucleotide except G), and hairpin ribozymes cleave downstream of the sequence NGUC. Since many studies have shown that small ribozymes can be successfully used in animal models of cardiovascular disease, cancer, viral infections, and arthritis **(Wright and Kearney 2001, Peracchi 2004, Schubert and Kurreck 2004)**, many have also entered clinical trials **(Sullenger and Gilboa 2002)**.

Among others, approaches against HIV-1 were pursued **(Michienzi *et al*. 2003)**.

Chemically stabilized ribozymes, such as ANGIOZYME directed against the receptor tyrosine kinase VEGF-R1, which plays an important role in angiogenesis and cancer therapy, HEPTAZYME directed against Hepatitis C Virus **(Peracchi 2004)**, or HERZYME directed against epidermal growth factor receptor 2 (HER-2) were also evaluated in clinical trials. Although all these studies were promising, they failed to show convincing efficacy in all clinical phases, and to date, no ribozyme-based drug has been approved. With the discovery of RNAi, interest in ribozymes eventually waned.

RNA interference (RNAi) is a cellular process in which the degradation of an mRNA is induced by small interfering RNA (siRNA). The basic structure of such a siRNA is based on a 19+2-mer. This means that in a duplex consisting of two 21 nts long RNA molecules (guide and sense strand), 19 nts are complementary to each other and 2 nts are overhanging at the 3'-end **(Elbashir *et al*. 2001)**. The guide or antisense strand is designed to be complementary to the target RNA. In the cytoplasm, the duplex binds to the AGO2 protein, which is part of the RNA-induced silencing complex (RISC) and releases the passenger strand, which is subsequently degraded. Through the guide strand, the RISC complex is guided to its complementary RNA target **(Figure 1 part 1b)**.

In cases where the siRNA is fully complementary to the target RNA, binding leads to cleavage of the target RNA via slicer activity catalyzed by AGO2 **(Matranga *et al*. 2005, Rand *et al*. 2005)**. As of May 2020, two siRNAs have been approved by the FDA. These include Patisiran and Givosiran.

Patisiran (commercially called Onpattro) is the first RNAi-based drug, which was approved in August 2018 **(Rüger *et al*. 2020, Kristen *et al*. 2019, Zhang *et al*. 2019, Hoy 2018)**. It was developed to treat polyneuropathy in patients with hereditary transthyretin amyloidosis (hATTR). This siRNA, consisting of two complementary 21-mer strands encapsulated in lipid nanoparticles, which also protects against nucleases, is delivered to hepatocytes **(Zhang *et al*. 2019)**.

Another RNAi-based drug is Givosiran, which was approved in November 2019 by the FDA and in March 2020 by the EMA. It is used to treat acute hepatic porphyria (AHP) **(Scott 2020)**. In contrast to Patisiran, stability against nucleases results in this case from modifications using terminal phosphorothioate backbone linkages and the introduction of 2'-O-fluorine and 2'O-methyl groups on the ribose **(Scott 2020)**. Similar to RNase H, AGO2 also has limiting possibilities for modification as it involves specific structural requirements for the oligonucleotide.

Occupancy mechanisms (steric blocking)

An alternative to target RNA degradation is steric blocking, or occupancy of regulatory RNA elements, to manipulate gene expression. For example, this includes the modulation of splicing **(Figure 1 part 2b)**, inhibition or increasing translation, and RNA processing (e.g. viral replication). Specifically, for splicing modulation, it is essential that no degradation of the target RNA is induced. Since many diseases are associated with mutations that result in incorrect splicing of RNA, such splice-modulating ASOs can be used to correct aberrant splicing by promoting either exclusion or inclusion of an exon of interest.

The first proof-of-principle in 1993 by **Dominski and Kole** demonstrated that ASOs are able to restore splicing defects in patients with β-thalassemia. These results opened up new therapeutic perspectives, which has become interesting in several diseases like Duchenne muscular dystrophy (DMD) **(Cohn and Campbell 2000)**, spinal muscular atrophy (SMA) **(Porensky and Burghes 2013)**, familial hypercholesterolemia (FH) **(Khoo and Krainer 2009)**, and X-linked agammaglobulinemia (XLA) **(Bestas *et al.* 2014 and 2015)**.

Especially in the context of splicing, positioning of the ASO is very important, and their design has to ensure that the target sequences are located in, or in close proximity to the exon of interest. The binding position is important, because it affects the recruitment and binding of splicing factors, or occupies splice sites **(Havens and Hastings 2016)**. However, this also means that the search for a suitable splice-modulating ASO is limited (compared to RNase H ASOs), while it should also be noted that these ASOs are only active in the nucleus. Chemical modifications can ensure that RNase H recruitment is circumvented so that the ASOs do not inadvertently cause a target knockdown. In the context of splicing modulation, three drugs are currently on the market: Eteplirsen is used to induce exon skipping of exon 51 in the dystrophin mRNA **(Kinali *et al.* 2009)**. On the other hand, Nusinersen (commercially called Spinraza), promotes the inclusion of exon 7 in the survival motor neuron (*SMN2)* gene, and is used for the treatment of spinal muscular atrophy. Recently in December 2019, a third drug called Golodirsen was approved by the FDA. This ASO induces exon skipping of exon 53 in the dystrophin gene, leading to an increased amount of dystrophin protein available to muscle fibers **(Passini *et al.* 2011)**.

Although blocking protein translation appears to be quite feasible, it is rarely used as a therapeutic strategy and to date, no drug based on this mechanism of action has been approved yet. In this approach, the inhibition of translation relies on steric blocking of ribosomes and its screening process **(Bennett *et al.* 2017) (Figure 1 part 2a)**. This leads to a reduction in the protein level, but not on the overall RNA abundance. In this context, 5'-untranslated regions (5'-UTR) are often chosen as binding sites, so that initiation of translation can be diminished. This mechanism is very commonly used in zebrafish as a research tool for performing gene knockdowns **(Nasevicius and Ekker 2000, Bill *et al.* 2009)**. Most steric-blocking ASOs target either a sequence in the 5'-UTR directly upstream of the start codon **(Faria *et al.* 2001)** or spanning the start codon **(Gambacorti-Passerini *et al.* 1996)** as well as within ~25 bases downstream of the start codon **(Summerton 1999)**. Studies on viruses such as HIV and vesicular stomatitis virus have shown that this mechanism of action is able to inhibit their replication **(Agrawal et *al.* 1988, Lemaitre *et al.* 1987)**. Related to this, we could very recently demonstrate that targeting of the 5´-UTR sequence of SARS-CoV-2 by small antisense circular RNAs interferes with viral RNA replication and processing **(Pfafenrot *et al.* 2021, section L)**.

For many diseases, the therapeutic goal is to increase protein abundance. Several approaches have been shown to positively influence translation. The translation rate of certain human genes can be regulated by upstream open reading frames (uORFs) located upstream of the canonical start codon. An example of this is ATF4 **(Harding *et al.* 2000, Vattem and Wek 2004)**. Here, it was observed that translation from the canonical AUG increased due to reduced initiation at an associated uORF. Moreover, recent studies

indicate that uORFs that affect translation efficiency are not unusual and approximately half of all human genes have them **(Calvo *et al.* 2009, Barbosa *et al.* 2013)**.

Liang and colleagues (2016) designed ASOs against uORFs of four different genes and were able to increase protein abundance by 30-150%. Since microRNAs (miRNA; short RNAs of approximately 21 to 23 nucleotides) are involved in the control of gene networks while repressing the translation of multiple mRNA targets, it is also possible to design ASOs against them to increase translation. Regarding this, the binding of ASOs would block the ability of miRNAs to bind their target RNAs **(Krützfeldt *et al*. 2005, Esau *et al*. 2004)**.

Chemical modifications

Many chemical modifications have been established over time, that improved ASOs in various aspects, such as efficacy, increased enzymatic stability, reduced immune response and toxicity. To date, intensive work is ongoing to develop new chemical modifications as well as vehicles to improve delivery efficiency and target specificity **(Juliano 2016, Bennett 2019)**. This is of importance because unmodified ASOs have the disadvantage of being susceptible to nuclease degradation **(Bennett *et al*. 2017)**. The modification of oligonucleotides is possible for both, DNA as well as RNA nucleotides, and can be introduced either at the base, the phosphate backbone, or at the 2'-position of the sugar which mainly protects against nucleases while maintaining the desired properties of the antisense interaction **(Kurreck 2003) (Figure 2)**. Furthermore, ligands such as N-acetylgalactosamine (GalNAc) can also be included to improve tissue targeting and cellular uptake **(Bennett 2019)**. Chemically modified ASOs can be classified into three categories.

First-generation ASOs have modified phosphodiester linkages. Here, the non-bridging oxygen atoms are replaced by another atom or a chemical group like methyl. This group includes the most commonly investigated modifications, which are phosphorothioate oligonucleotides (PS), with a sulfur atom instead of an oxygen atom **(Studzińska *et al*. 2017, Lobue *et al*. 2019, Fountain *et al*. 2003, Zhang *et al*. 2005)**. These oligonucleotides have the advantage of retaining the ability to recruit RNase H after binding to the complementary RNA. However, they show a lower affinity for the target RNA compared to unmodified ASOs. Because of their higher stability, an improvement in pharmacokinetic properties can be reached due to their ability to remain longer in the bloodstream. However, undesirable side effects are also frequently observed for these ASOs **(Levin 1999)**, including toxic effects in the central nervous system. Based on these problems, ASOs of the second generation were designed.

The second generation includes modifications within sugar moieties, where the hydroxyl group at the 2'-position of the ribose is replaced by a fluorine atom, a methyl or a methoxyethyl group (ME and MOE). The advantage is a significantly reduced polarity **(Kaczmarkiewicz *et al*. 2019, Deleavey and Damha 2012, Urban and Noe 2003, Zimmermann *et al*. 2014)**. Compared to the first generation, the main improvement is that these ASOs are less toxic and have a high affinity for the target RNA. However, with these modifications they have lost the ability to recruit RNase H, meaning that degradation of the target RNA can no longer be initiated.

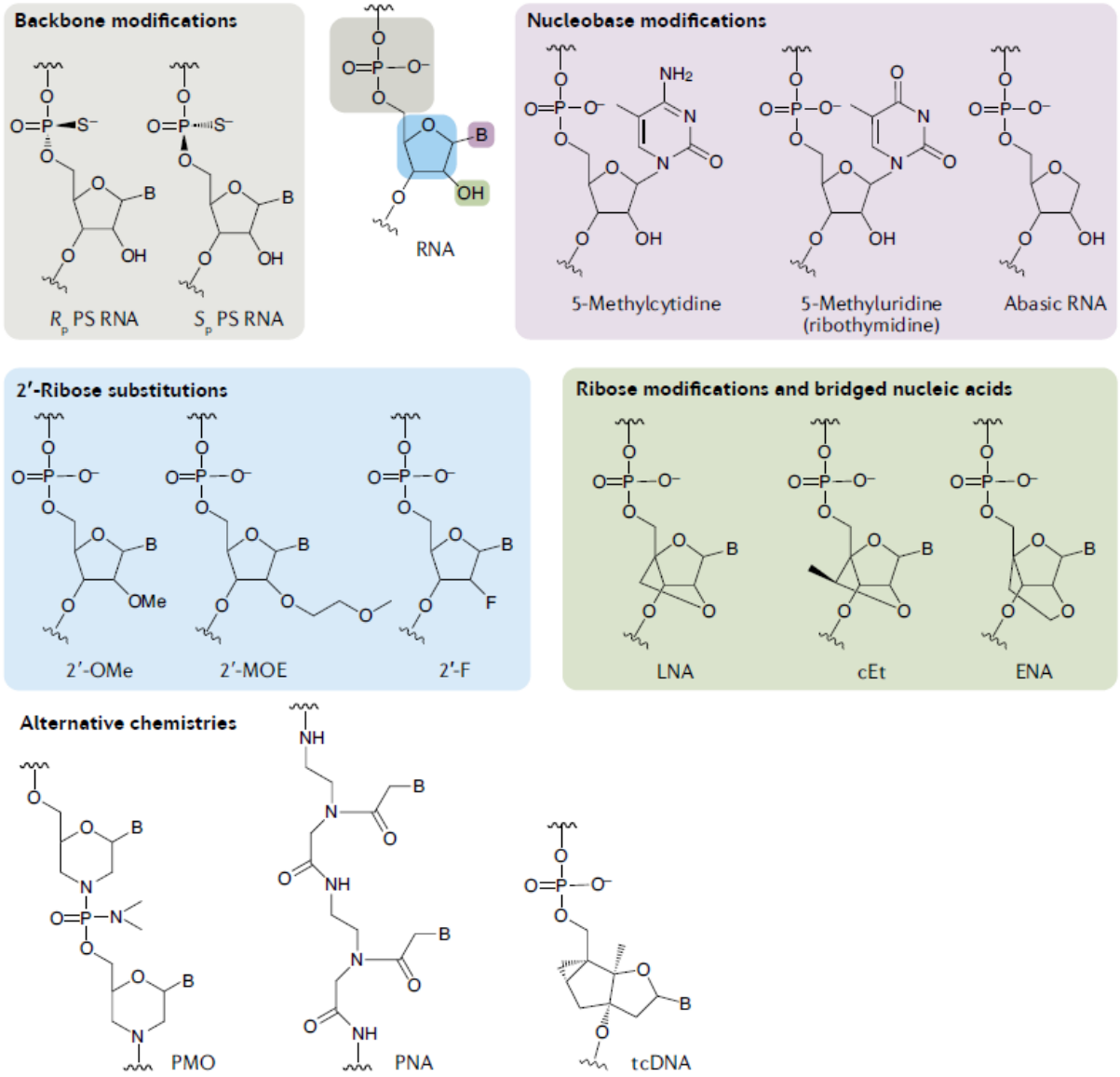

Figure 2: Common chemical modifications of antisense oligonucleotides to improve their properties. Representation of possible sites for chemical modification. ASOs can be modified at their backbone, nucleobase, ribose sugar and 2′-ribose substitutions. B, nucleobase; cEt, constrained ethyl bridged nucleic acid; ENA, ethylene-bridged nucleic acid; 2′-F, 2′-fluoro; LNA, locked nucleic acid; 2′-MOE, 2′-O-methoxyethyl; 2′-OMe, 2′-O-methyl; PMO, phosphorodiamidate morpholino oligonucleotide; PNA, peptide nucleic acid; PS, phosphorothioate; tcDNA, tricyclo DNA. Modified after **Roberts et al. 2020.**

However, RNase H recruitment can be ensured by the use of gapmers. These usually carry DNA or PS components at the center with at least 5 nts, and modified nucleotides at their ends with 7-10 nts, protecting from exonucleases.

The third generation can contain different modifications, either in phosphate groups, sugar moieties, or nucleobases. Modifications such as peptide nucleic acids (PNA), morpholino phosphoroamidates (PMOs), as well as locked nucleic acids (LNA) belong to this group **(Urban and Noe 2003)**. Almost all

of these modifications exhibit good binding properties and are also resistant to nucleases. However, these ASOs are also no longer able to induce RNase H-mediated cleavage. On the other hand, this makes them well-suited for steric blocking of translation and processing e.g. splicing. LNA and PMOs are also being tested in clinical trials. In LNAs, the 2'-oxygen atom is linked to the 4'-carbon of ribose by a methylene bridge.

This gives them a very high affinity and high protection against nucleases. Also, no toxic side effects have been observed, e.g. in the brain, as was the case with the first generation.

PMOs consist of an uncharged backbone **(Heasman 2002, Amantana and Iversen 2005)**, providing the advantage that non-specific interactions with cellular components are reduced, and undesirable side effects are omitted.

CircRNAs

Discovery of circRNAs

During the last four decades, circular RNAs (circRNAs) with covalently joined 5' and 3' ends emerged as a new class of mostly noncoding RNAs and have been found in all eukaryotes investigated so far, from protozoa, yeast to human (reviewed by **Lasda and Parker 2014, Chen and Yang 2015, Wilusz 2018, Kristensen *et al*. 2019, Chen 2020**). The first circRNA was discovered by **Sänger *et al*. (1976)** as a plant pathogen, a so-called viroid. Because of unsuccessful enzymatic labeling at their 5' and 3' ends, as well as resistance to degradation, only electron microscopy and additional sequencing of the viroid nucleotide sequence, demonstrated that viroids are indeed single-stranded circular RNAs **(Gross *et al*. 1978)**.

Some years later, again based on electron microscopy, the Hepatitis Delta (δ)-Virus (HDV) was the first animal virus shown to have a covalently closed and single-stranded RNA genome **(Kos *et al*. 1986)**. Furthermore, and in contrast to plant viroids, the circular molecule has also been shown to encode a single open reading frame for the Hepatitis Delta Antigen (HDAg), expanding knowledge about circRNA functions **(Sureau and Negro 2016, Weiner *et al*. 1988)**.

Moreover, circRNAs have also been described to arise from self-splicing introns in unicellular eukaryotes **(Grabowski *et al*. 1981)** as well as from ribosomal RNA introns in archaea **(Kjems and Garrett 1988)**. However, the first 'exonic circRNA' discoveries followed only from the 1990s onwards, with examples like *DCC*, *ETS-1*, *SRY*, *cytochrome P450 2C24* and *ANRIL* **(Nigro *et al.* 1991, Cocquerelle *et al.* 1992, Capel *et al.* 1993, Zaphiropoulos 1996, Burd *et al.* 2010)**.

Nigro *et al.* (1991) described the formation of circRNAs in their study as 'a creation of unexpected RNA products' for a tumor suppressor gene *DCC* (deleted in colorectal cancer/ netrin 1 receptor). In this case, they were able to identify four abnormally spliced transcripts with shuffled exons, which however were accurately joined by their canonical splice sites. More precisely, they could observe, that a 5'-splice site was joined to an upstream instead of a downstream 3'-splice site. Nowadays, this process is referred to as *backsplicing*. Furthermore, they also observed that these transcripts were expressed at very low levels compared to the normally spliced transcript, that they were not polyadenylated, and that they were enriched in the cytoplasm. One year later, these observations were confirmed in investigations on the *ETS-1* gene, which additionally revealed that the produced circRNAs were highly stable with a half-life over 48 h **(Cocquerelle *et al*. 1992)**.

Because of their low expression levels, only little importance was attributed to circRNAs up to this point. They were mainly assumed to be by-products generated by aberrant splicing events. Furthermore, it was also thought that they could be a possible intron-lariat intermediate of the mRNA splicing pathway. On the other hand, a circRNA derived from the *SRY* (sex-determining region of Y) gene was discovered in adult mouse testis with high expression levels and therefore thought to have a possible function **(Capel *et al.* 1993)**. Only with the help of high-throughput sequencing, a large number of circRNAs could be identified in

2012/13 based on boinformatic analyses **(Salzman *et al.* 2012 and 2013)**. The reason why circRNAs had remained undiscovered for such a long time is largely due to their special characteristics. Many RNA enrichment methods focused on the purification of 3´-polyadenylated RNA. Owing to the lack of 5' or 3' ends, and therefore also 3'-polyadenylated tails, most circRNAs could not be enriched, which in turn serves as an explanation for why they were overlooked by classical RNA sequencing approaches (reviewed by **Jeck and Sharpless 2014**).

In the meantime, many novel methods for the detection of circRNAs had been developed. Due to the overall low expression levels of most circRNAs, a greater sequencing depth is required in RNA-seq experiments. To achieve deep sequencing and to ensure transcriptome-wide annotation of all circular RNAs, a combination of different approaches should be used. For this, methods such as RNase R treatment or depletion of the poly(A) fraction for circRNA enrichment **(Salzman *et al.* 2012 and 2013, Zhang *et al.* 2014)** have become a part of the current standard. Furthermore, it should also be noted that reliable prediction and detection of circRNAs is not a trivial task. For example, the choice of library preparation itself, and especially reverse transcription, one of the first fundamental steps during RNA-Seq library preparations, can have a major impact on the results. In this context, it is well established that most of the reverse transcriptases used are error-prone and can cause mutations in their products **(Sebastián-Martín *et al.* 2018)**. Generation of aberrant *trans*-splicing products occurs mainly due to the template-switching activity of some enzymes **(Cocquet *et al.* 2006, Houseley and Tollervey 2010)**, and thus can easily lead to misinterpretation of the derived sequencing data. Furthermore, endogenously *trans*-spliced transcripts can lead to false-positive events. In particular, duplicated exon sequences within an mRNA (intragenic *trans*-splicing) or transcripts originating from different genes on different chromosomes (intergenic *trans*-splicing) can be detected and lead to false-positive events **(Preußer and Bindereif 2013)**. In addition, the library preparation from circRNAs either requires initial fragmentation to generate accessible 5′ and 3′ ends or relies on random hexamer priming, which may result in inefficiency and/or biased representation in RNA-Seq **(Hansen *et al.* 2016)**.

After sequencing, a large number of available circRNA prediction tools can be used. Some of them require an established annotation and some knowledge of existing exon-intron structures (e.g. CIRI), while others rely on *de novo* assembly and are thus able to identify novel backsplice junctions. These different options of evaluation tools can lead to dramatic differences between the results, depending on the algorithms used **(Hansen *et al.* 2016)**. A recent study compared 11 different circRNA detection tools on simulated and real datasets and was able to show that CIRI, CIRCexplorer, and KNIFE achieve a better balance between their precision and sensitivity compared to other methods **(Zeng *et al.* 2017)**. Nevertheless, many of these algorithms exhibit highly divergent results and a high level of false-positive results. These studies demonstrate that circRNA detection tools should be used with caution and that a combination of more than one method for bioinformatic analysis is needed to make reliable predictions as well as to minimize the number of false positives **(Hansen *et al.* 2016)**.

Another important point, which is often neglected, but should always follow after bioinformatic evaluation, is the stringent biochemical validation of circRNAs. To this

end, Northern blot analysis represents the gold standard for the detection of circular RNA (for details, see **Schneider *et al.* 2018**). In this method, suitable gel electrophoresis systems (agarose and/or polyacrylamide) allow the distinction between the possible configurations (linear or circular), while a combination with RNase R or RNase H ribonuclease digestion unequivocally proves circularity **(Starke *et al.* 2015, Jeck and Sharpless 2014, Preußer *et al.* 2018, Pfafenrot *et al.* 2021)**.

Beyond the fact that circRNAs have been detected in many different organs, tissues, and cell types **(Memczak *et al.* 2013)**, a significant enrichment in neuronal tissues has been observed for most organisms **(Rybak-Wolf *et al.* 2015)**, as well as in body fluids such as human blood **(Memczak *et al.* 2015)**. In particular, the platelet fraction shows a high accumulation of circRNAs, which is attributed to the general degradation of linear RNAs during the lifetime of platelets **(Alhasan *et al.* 2016)**.

Furthermore, different studies could prove that 'exonic circRNAs' are processed from pre-mRNA by a spliceosome-mediated mechanism **(Starke *et al.* 2015)**. Moreover, there is increasing evidence for the regulatory role of several RNA-binding proteins **(Conn *et al.* 2015, Kramer *et al.* 2015, Ivanov *et al.* 2015)**. Also interesting is the discovery that some circRNAs may have protein-coding potential and might be actively translated by ribosomes, indicating that not all circRNAs can be described as noncoding **(Legnini *et al.* 2017, Pamudurti *et al.* 2017, Yang *et al.* 2017)**. Nevertheless, there are still many open questions, which will be answered in the future. For example, it is still not known in detail how circRNAs are exported from the nucleus to the cytoplasm, although a study by **Huang *et al.* (2018)** assumes a length-dependent mechanism. Also, still unclear is a common degradation pathway of circRNAs. Interestingly, **Preußer *et al.* (2018)** observed a selective release of circRNAs into extracellular vesicles, which might suggest a specific sorting mechanism.

circRNA classes

Until now, circRNAs can be divided into five subclasses, depending on their origin and processing mechanism. These classes are summarized in the following table **(see Table 1**) by **Lasda and Parker** in 2014. Circular single-stranded RNA genomes such as from viroids (250-400 nts in length), and the human-pathogen Hepatitis Delta Virus (HDV, 1.7 kb) belong to the first subclass **(Sänger *et al.* 1976, Kos *et al.* 1986)**. Despite differences, however, they share a common feature such as the recruitment of a host DNA-dependent RNA polymerase to initiate rolling circle replication of the RNA genome (**Lasda and Parker 2014)**.

The second class includes intronic sequences, which are excised from precursors as circular molecules, and are referred to as circular RNA introns. For example, this class includes introns from tRNA, group I and II self-splicing introns, as well as 3'-processed lariat circles, which are formed from eukaryotic pre-mRNAs during canonical splicing **(Nielsen *et al.* 2003, Molina-Sanchéz *et al.* 2006, Zhang *et al.* 2013)**. The latter example includes a subclass called circular intronic RNAs (ciRNA), in which the characteristic 2'-5' lariat-bond is resistant to debranching due to specific sequence elements near the 5'-splice site. The functions of ciRNAs are not yet fully understood, but it has been reported that they associate with RNA polymerase II and thereby regulate the expression of their own gene **(Zhang *et al.* 2013)**.

The third class comprises processing intermediates, which occur for example

during tRNA or rRNA maturation, and are mainly found in archaea **(Kjems and Garrett 1988, Soma *et al.* 2007, Danan *et al.* 2012)**.

Functional noncoding RNAs in some archaeal species, such as some snoRNAs or RNase P RNA can be formed from excised and circularized tRNA introns and belong to the fourth class **(Lasda and Parker 2014)**.

The last and largest group comprises exonic circRNAs in eukaryotes that are derived from spliceosome-mediated pre-mRNA splicing. In this process, a downstream 5′-splice site (splice donor) is joined to an upstream 3′-splice site (splice acceptor), resulting in a circular product, consisting of a single or several adjacent exons **(Salzman *et al.* 2012 and 2013, Jeck *et al.* 2013, Memczak *et al.* 2013)**. These circRNAs are processed from 20% of all protein-coding genes **(Holdt *et al.* 2018)**. On average, they consist of one to five exons of their precursor transcript, with an enrichment for the second exon and depletion for the first and last exon. The size of the spliced circular molecule can range from less than 100 nts to more than 4 kb. Furthermore, it is also known that a gene can code for one or more circular isoforms. The abundance of the circRNA compared to the linear isoform can differ strongly due to cell type specific expression **(Jeck *et al.* 2013)**. Only a few studies describe an exclusively circular form, these include *CDR1as* and the platelet-specific *Plt-circR4* (platelet-specific circRNA expressed from chromosome 4, **Memczak *et al.* 2013, Hansen *et al.* 2013, Preußer *et al.* 2018**).

Table 1: Types and characteristics of circRNAs (Lasda and Parker 2014).
Overview of various features of the individual circRNA classes. The following points are discussed: RNA circle type, organism, biogenesis, function as well as the size of the circular molecules.

	RNA circle	Type	Organism	Formed by	Possible function (of the circular molecule)	Size
I. Circular RNA genome	Viroids	Genomic and antigenomic	Pathogen of plants	3′–5′ end ligation	Transcription of multimeric copies, stability	~250–400 nt
	Hepatitis delta virus (HDV)	Genomic and antigenomic	Pathogen of humans	3′–5′ end ligation	Transcription of multimeric copies, stability	1.7 kb
II. Circular RNA intron	Excised group I introns	RNA processing byproduct and end product (5′ truncated introns, introns with additional residue at site of circularization, and full-length introns)	Some eukaryotes, some bacteria, some viruses	Ribozyme	Genetic element mobility (?)	250–500 nt
	Group II intron circles and intron lariats	mRNA processing byproduct and end product	Bacteria, some archaea, and some eukaryotic organelles	Ribozyme, 2′–5′ bulged A attack	Genetic element mobility (?)	Up to 3 kb
	Circular intronic RNAs (ciRNAs)	mRNA processing byproduct and end product	Eukaryotes	2′–5′ branchpoint attack (spliceosome mediated) and subsequent degradation of downstream intron sequence	May regulate transcription	<200 nt to >3 kb
	Excised tRNA introns	tRNA processing byproduct and end product	Some archaea	3′–5′ end ligation	Can contain snoRNAs	
III. Circular RNA processing intermediate	rRNA precursors	Intermediate in rRNA processing reaction	Some archaea	3′–5′ end ligation		
	Permuted tRNAs	Intermediate in tRNA processing reaction	Some algae and archaea	3′–5′ end ligation	Rearrange genomic order of sequence	
IV. Circular noncoding RNA	Some snoRNAs		Some archaea	3′–5′ end ligation	Stability	
	RNase P		Some archaea	3′–5′ end ligation	Stability	
V. Circular RNA spliced exons	Exonic circular RNAs (circRNAs)	mRNA processing byproduct and end product	Eukaryotes	Backsplicing (spliceosome mediated)	ceRNAs (sponges), regulators of mRNA levels or translation, other	<100 nt to >4 kb

Biogenesis of exonic circRNAs

The biogenesis of circRNAs through *backsplicing* differs from the canonical splicing process of linear RNA, which are both catalyzed by a large ribonucleoprotein complex called the spliceosome. After recognition of conserved splicing signals, including 5´- and 3´-splice sites (5´-ss, 3´-ss) important to define exon-intron boundaries, as well as a branch point essential for the first catalytic step, the process results in the removal of introns and the precise joining of exons by a two-step mechanism.

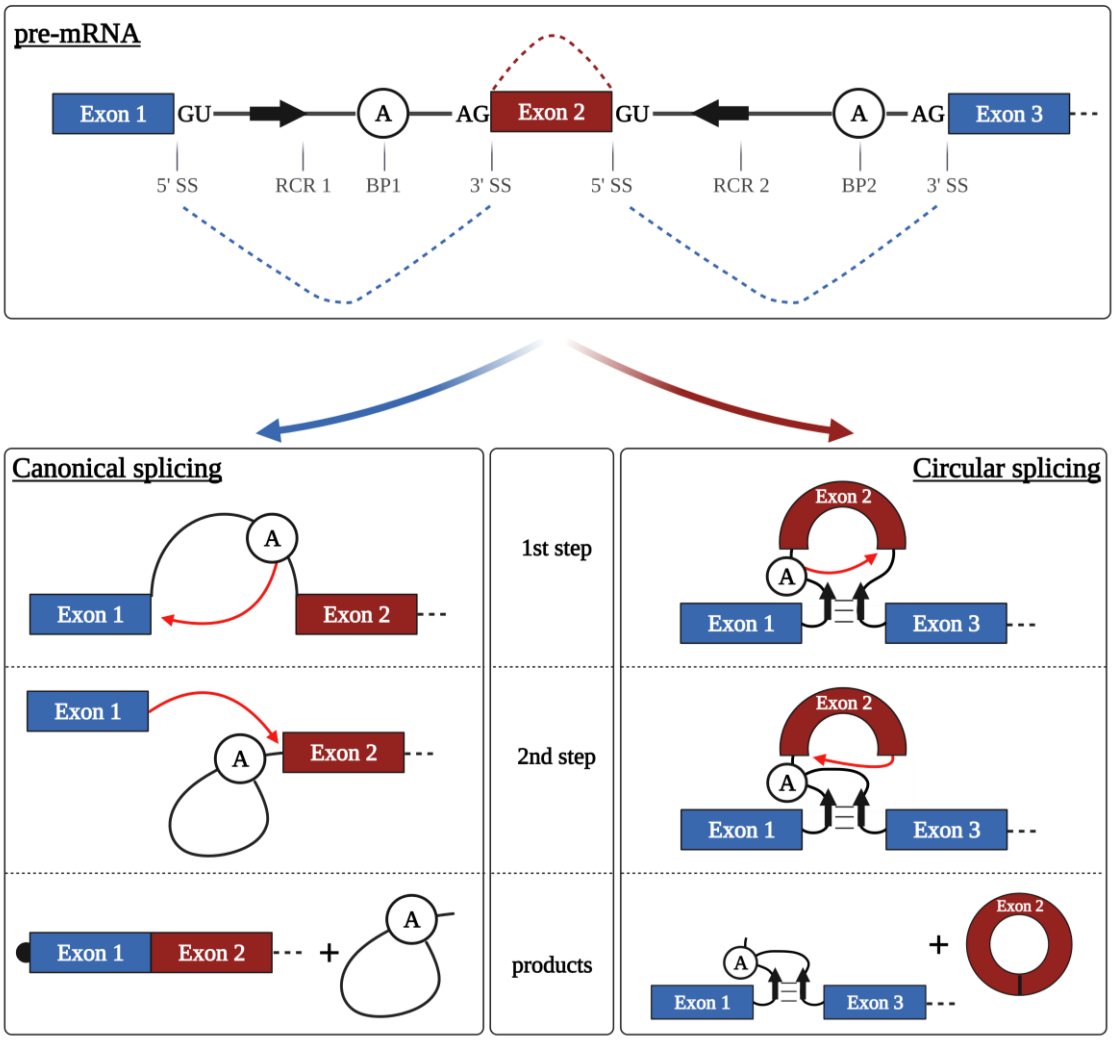

Figure 3: Comparison of canonical and non-canonical splicing.
Canonical (linear) pre-mRNA splicing **(left)** leads to one stable linear mRNA product as well as one 2´-5´ linked intron lariat. In the first transesterification step, the branch point (BP1) 2´-OH of adenosine (A) attacks the upstream 5´-SS, leading to the formation of an intron lariat (2´-5´ linkage). During the second transesterification step, the 3´-SS is attacked by the free 3´-OH of the 5´-SS. This leads to ligation of the two exons (3´-5´ linkage). In the case of circular splicing **(right)** the branch point attacks the downstream 5´-ss, followed by two transesterification steps. The products of this pathway are a circularized exon 2 (3´-5´ linkage) and a linear pre-mRNA intermediate (2´-5´ linkage). This intermediate still includes the intron sequence and can be further processed to a linear mRNA. Created with **BioRender.com**.

Although the spliceosome is formed by a stepwise and dynamic assembly of five small nuclear RNAs (snRNAs) and more than 100 proteins, the basic mechanism consists of two transesterification reactions **(Wahl *et al.* 2009, Shi 2017)**.

The first step of splicing is initiated by a nucleophilic attack on the phosphate of the guanine nucleotide at the 5′-splice site by the 2´-hydroxyl group of the branch point adenosine. This results in cleavage of the 3′-5′-phosphodiester bond at the 5′-splice site and the formation of a 2‘-5′ phosphodiester bond between the first nucleotide of the intron and the branch site adenosine. This reaction produces two splicing intermediates, the 5′ exon, and a lariat, containing the intron and the 3′ exon. In the second step, the 3´-hydroxyl group of the 5′ exon, which is released by the first transesterification reaction, performs a nucleophilic attack on the phosphate at the 3′-splice site. This results in excision and degradation of the intron lariat, and a linear mRNA, in which the donor splice site of an upstream exon is precisely linked to the acceptor splice site of the downstream exon. In contrast, *backsplicing* involves the reverse ligation of a downstream donor splice site with an upstream acceptor splice site **(Chen and Yang 2015) (Figure 3)**. The resulting circular RNA is characterized by a covalently closed circular structure, and it was shown that both canonical splicing signals and the splicing machinery are involved in circularization. This was in detail validated by mutational analysis of splicing signals in the context of circRNA-producing minigenes as well as by splicing inhibitors, like isoginkgetin **(Ashwal-Fluss *et al.* 2014, Starke *et al.* 2015).**

Furthermore, several *cis*-elements and *trans*-factors have been identified that promote circularization by bringing the donor and acceptor splice sites into close proximity **(Figure 4)**. Such *cis*-elements include inversely oriented repeat sequences in flanking introns, like *Alu* repeats, which are specific to primates **(Jeck *et al.* 2013)**. Such sequences were already identified in early studies on the *SRY* circRNA, showing that 400 nts of inverted repeats flanking the exon to be circularized are sufficient for circularization of ectopically expressed *SRY* circRNA **(Dubin *et al.* 1995)**. Moreover, recent studies have shown that the deletion of reverse-complementary repeats by using CRISPR/Cas9 technology can prevent circularization. However, bioinformatic analyses revealed that not every circRNA to be circularized is always flanked by complementary repeats **(Zhang *et al.* 2016 a, Zhang *et al.* 2016 b)**. Nowadays, it is assumed that most *backsplicing* events do not require special sequence motifs (beyond the splice sites and branch point), but are instead promoted by base-pairing interactions between flanking intronic elements (reviewed by **Wilusz 2018**). In the case of *trans*-acting factors, RNA-binding proteins (RBPs) bind to recognition motifs in the flanking introns and thereby bring the splice sites into close proximity to each other. Several proteins have already been linked to circularization. On the one hand, there are proteins, which promote circRNA biogenesis like NF90/NF110 **(Li *et al.* 2017)**, as well as the alternative splicing factor Quaking (QKI), and the *Drosophila* Muscleblind (Mbl) protein. QKI for example is involved in the production of circRNAs during human epithelial-mesenchymal transition (EMT) because it binds to flanking introns and forms dimers, thereby bringing the splice sites into close proximity **(Conn *et al.* 2015)**. The Mbl protein promotes the production of circular RNAs, due to binding to intronic elements of its own pre-mRNA, thereby auto-regulating *Mbl* gene expression and Mbl protein levels **(Ashwal-Fluss *et al.***

2014). On the other hand, there are also proteins, which have suppressive effects on circRNA biogenesis like RNA helicase DHX9 (DExH-Box Helicase 9) that binds to double-stranded RNAs **(Aktas *et al.* 2017)**. In this particular case, unwinding of the double-stranded intronic regions and recruiting of ADAR (adenosine deaminase acting on RNA) enzymes that convert adenosines to inosines, lead to decreased circularization **(Aktas *et al.* 2017, Ivanov *et al.* 2015, Rybak-Wolf *et al.* 2015)**. However, circRNA production is also controlled by other proteins such as FUS **(Errichelli *et al.* 2017)** and several hnRNP (heterogeneous nuclear ribonucleoprotein) and SR (serine-arginine) proteins **(Fei *et al.* 2017, Kramer *et al.* 2015, Liang *et al.* 2017)**.

In sum, this suggests a combinatorial regulation of circRNA production, whereby intronic repeats provide the opportunity for *backsplicing* to occur, and in contrast, a variety of transacting factors act to fine-tune the efficiency.

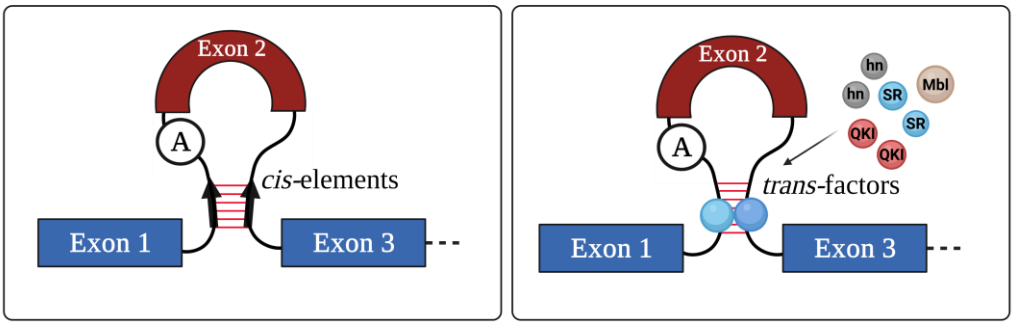

Figure 4: *Cis*-elements and *trans*-factors contribute to *backsplicing*.
Schematic representation of reverse complementary repeats, which are known to enhance circularization via base-pairing **(left)**. *Trans*-factors like hnRNPs, SR, QKI, Mbl proteins can bind intronic sequences, leading to looping that favors circularization **(right)**. Created with **BioRender.com**

Potential functions and applications of circRNAs

Although thousands of circRNAs have been identified, a general function is still under debate. This can be partially explained by low copy numbers of many circRNAs in cells and accompanied experimental difficulties. Only two studies convincingly revealed a microRNA sponge function **(Figure 5A)** of naturally occurring circRNAs like *CDR1as* (a circular isoform of human antisense to cerebellar degeneration-related protein 1 RNA) and *SRY* **(Hansen *et al.* 2013, Memczak *et al.* 2013)**. *CDR1as* (also known as *ciRS-7*), is one of the best characterized naturally occurring circRNAs, derived from an antisense transcript from the *CDR1* locus, and shown to sequester microRNA-7. This circRNA is mainly expressed in brain and contains over 70 conserved miR-7 seed sequences **(Hansen *et al.* 2013, Memczak *et al.* 2013)**. Besides the miR-7 binding sites, there is also one almost perfectly complementary binding site for miR-671. This site can be cleaved by the RNA-induced silencing complex (RISC) **(Hansen *et al.***

2011). A study by **Piwecka *et al.* (2017)** demonstrated specific and opposite deregulation of miR-7 (downregulation) and miR-671 (upregulation) upon loss of *CDR1as* in a knockout mouse model generated by *CRISPR/Cas9*. First, these data suggest a stabilizing effect of miR-7 during interaction with *CDR1as*. And second, they could also show, that a loss of *CDR1as* causes increased synaptic vesicle release and neurophysiological changes that are correlated with various neuropsychiatric disorders. A second study by **Kleaveland *et al.* (2018)** revealed that *CDR1as* is embedded in a regulatory RNA network, consisting of the circRNA itself, miR-7, and the *Cyrano* long noncoding RNA. Thus, this indicates that *CDR1as* has an important role in brain activity.

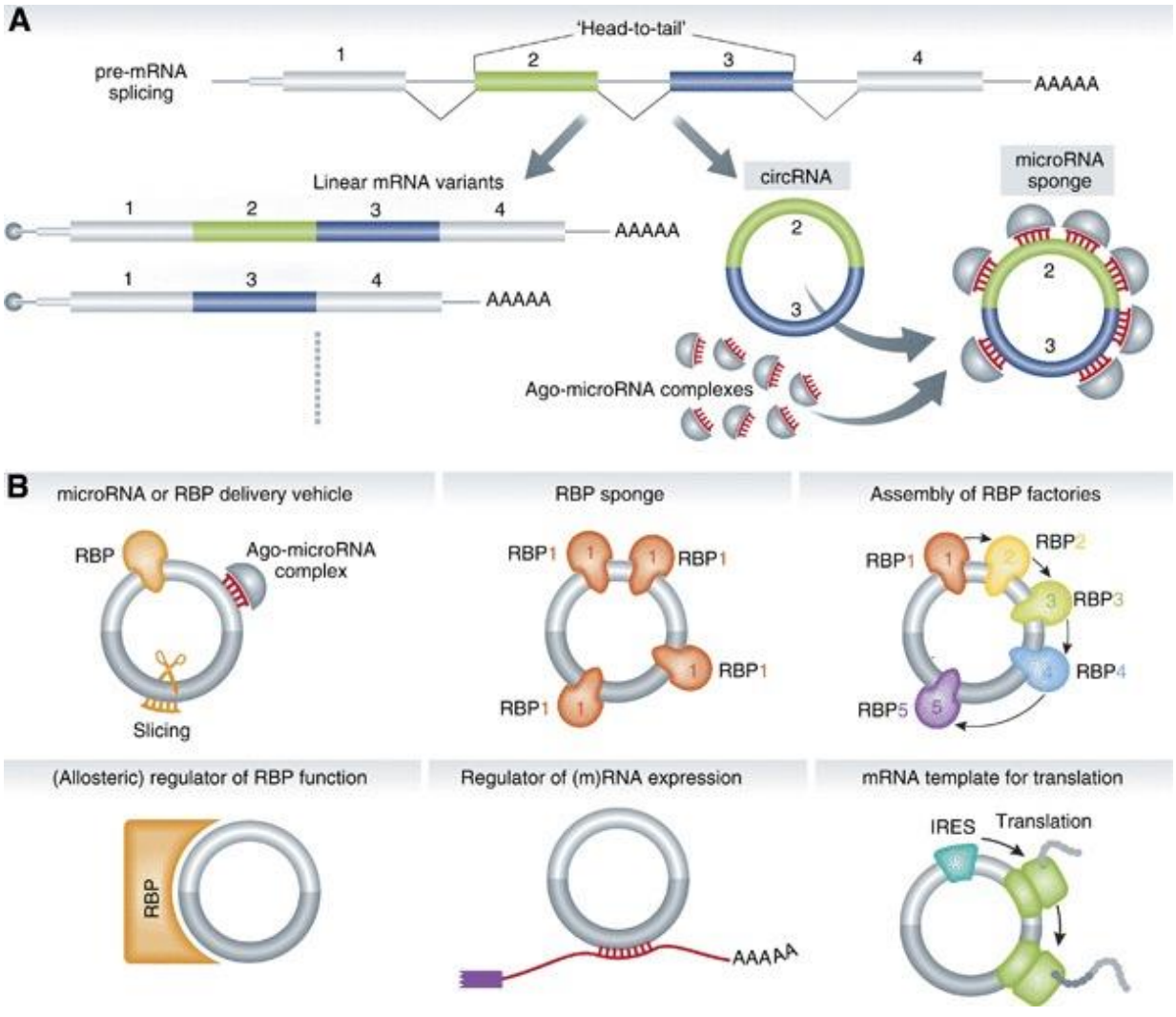

Figure 5: Functions of circular RNAs.
[A] CircRNA generation by alternative splicing: standard linear (left) versus circular splicing (right). Note that in the circular RNA the two splice sites of the exons (green/blue) are joined (5'/3'-ss circ-junction). So far, the best characterized function of circRNAs is sponging of microRNAs.
[B] Examples of other hypothetical functions of circular RNAs**.** Modified after **Hentze and Preiss 2013**.

Another circRNA that also acts as a molecular sponge is the testis-specific *SRY* (sex-determining region Y) circRNA. This 1.2 kb single-exon circRNA contains up to 16 binding sites for miR-138 in mice (the human homologue has only one binding site) **(Andreeva *et al.* 2015)**. However, until now no developmental phenotype could be identified **(Hansen *et al.* 2013)**. This type of function was also predicted for other circRNAs, like human circHIPK3, circZNF91, and circHECTD1, as well as a subset of circular RNAs in *Drosophila* **(Kristensen *et al.* 2018, Wang *et al.* 2016, Westholm *et al.* 2014, Zheng *et al.* 2016)**. CircHIPK3 (homeodomain interacting protein kinase 3) for example, has 18 potential seed sequences for 9 different miRNAs. In this context, it was also shown that circHIPK3 is associated with a growth-promoting function **(Zheng *et al*. 2016)**. However, since a sponge function could only be demonstrated for a few cases, the question remains whether these are rare cases or a general function of circRNAs. In addition to the sponge function, other functions have been identified. For example, **Burd *et al*. (2010)** discovered the circular isoform of ANRIL with its atheroprotective role. In addition, the study by **Holdt *et al*. (2016)** was able to show that this circRNA also appears to be involved in the maturation of rRNA.

Meanwhile, many studies have been published reporting that circRNAs are involved in different biological processes like regulation of transcription **(Zhang *et al.* 2013)**, neuronal development **(You *et al.* 2015)**, cell cycle control **(Du *et al.* 2016)** as well as tumorigenesis and chemoresistance **(Guarnerio *et al.* 2016, Yang *et al.* 2017)**. Although many of these functions are the result of circRNA-RBP interactions, no endogenous protein sponge function has yet been demonstrated. Another possibility that is still highly debated, is the potential protein-coding function of circRNAs. Already in 1995, **Chen and Sarnow** were able to demonstrate cap-independent translation *in vitro* by using constructs that contained an IRES element (internal ribosome entry site). Further studies could also demonstrate *in vivo* expression of a circularization-dependent split-GFP construct in *E. coli* **(Perriman and Ares 1998)** as well as in eukaryotic cells **(Wang and Wang 2015)**. In 2017, three groups have provided complementary sets of data that argue for active translation of a few endogenous circRNAs and highlight important advances **(Yang *et al.* 2017, Legnini *et al.* 2017, Pamudurti *et al.* 2017, summarized by Tatomer and Wilusz 2017, and Schneider and Bindereif 2017)**.

Using circRNA-expressing minigene reporters in conjunction with mutation and knockdown analyses, **Yang *et al*. (2017)** were able to show that m^6A modifications influence the translation of circular RNA templates. The initiation mechanism here is based on a known m^6A recognition factor, YTHDF3, and, similar to cap-independent mRNA translation, on an IRES-specialized translation initiation factor, eIF4G2. Furthermore, it was also shown that m^6A-dependent translation efficiency can be modulated by the m^6A methyltransferase METTL3/14 and the demethylase FTO.

In parallel, **Legnini *et al*. (2017)** identified cap-independent translation of a ZNF609 pre-mRNA-derived circRNA expressed in murine and human myoblasts. In addition, they were also able to link the expression of the ZNF609 circRNA to the modulation of myoblast proliferation**.**

Pamudurti *et al*. (2017) examined *Drosophila* heads to analyze ribosome footprinting data, as circRNAs are highly expressed in the brain. This analysis resulted in a subset of 122 circRNAs possibly

associated with actively translating ribosomes.

However, many questions remain unanswered, since the last two studies lacked evidence on protein functionality. In this context, a study by **Ho-Xuan *et al.* (2020)** very clearly shows the problem of such circRNA overexpression constructs used and how important it is to critically and accurately evaluate them. Here, a comprehensive mutational analysis revealed that deletion constructs that were deficient in circZNF609 production were still able to generate the observed protein products. This suggests that the apparent circZNF609 translation results from *trans*-splicing by-products of the overexpression plasmids. Another issue is also that in most studies, an association of circRNA with actively translating ribosomes is usually the only evidence of the circRNA-derived protein isoform. In order to prove the existence of the circRNA-derived protein isoform, this step is not sufficient; further lines of evidence are required, such as antibody-based detection of a circRNA-specific protein isoform via Western blot, preferably in combination with circRNA-specific siRNA knockdown, as well as mass spectrometry. Although circRNAs have so far generally been considered noncoding, these studies show that they can indeed serve as templates for protein translation. However, this issue is still very controversially discussed in the circRNA field (reviewed by **Schneider and Bindereif 2017, Stagsted *et al.* 2019, Ho-Xuan *et al.* 2020, Hansen 2021**).

Due to their circular configuration as well as the correlation with various human diseases, including cardiovascular diseases **(Holdt *et al.* 2016 and 2018)**, disorders of the nervous system **(Piwecka *et al.* 2017, Errichelli *et al.* 2017)**, diabetic retinopathy **(Liu *et al.* 2017)** and cancer **(Qu *et al.* 2018)**, it becomes clear that circRNAs may be used as specific biomarkers.

Since circRNAs are also found in extracellular vesicles circulating in various body fluids such as blood and saliva, this should greatly extend the potential of circRNAs as prognostic and diagnostic biomarkers, especially for liquid biopsies **(Memczak *et al.* 2015, Preußer *et al.* 2018)**.

Since the majority of circRNAs do not have a common or general function, many hypotheses and speculations have been made about their possible roles within cells. Additional considerations regarding function, which have not yet been experimentally proven, relate to the involvement of circRNAs as platforms for RBPs (RNA-binding proteins) interactions in so-called ‘RBP factories’, in the allosteric regulation of RBP functions, as well as in the regulation of (m)RNA expression **(Hentze and Preiss 2013) (Figure 5B)**. These hypotheses, as well as the unusually high stability of circRNAs in comparison to their linear counterparts, are also the basis for potential future applications. For example, in a proof-of-principle study, **Jost *et al.* (2018)** showed that artificial circRNAs can be successfully produced to act as miRNA sponges. In this context, functional sequestration of a host-specific factor, which is microRNA-122, could be obtained. This microRNA is the most abundant in the adult liver **(Bandiera *et al.* 2015)** and also has binding sites within the 5'-UTR of the HCV genome **(Conrad *et al.* 2013)**. Despite a high mutation rate of the virus, these binding sites are conserved in all HCV genotypes and thus also indicate an important functional significance of this sequence **(Jopling 2012)**.

Here, microRNA-122 exerts a positive effect on the life cycle of the virus through its binding within the 5'-UTR of the HCV genome by promoting viral translation as well as stabilizing the 5'-end **(Conrad *et al.* 2013)**.

Sequestration of miRNA-122 is a potentially promising therapeutic approach against HCV.

In another recently published study, short circRNAs designed to act as protein sponges, and carrying high-affinity binding sites for hnRNP L, were generated by enzymatic *in vitro* circularization, and subsequently transfected for modulating hnRNP L-dependent alternative splicing **(Schreiner *et al.* 2020)**.

In a further study, which is also discussed in more detail in this dissertation, we combined for the first time the classical antisense (AS) RNA approach with synthetic short circRNAs by integrating antisense sequences into a circRNA backbone. Thereby, we were able to show that the expression of the SARS-CoV-2 genome and viral replication can be successfully inhibited by targeting the structurally conserved 5'-UTR of SARS-CoV-2 **(Pfafenrot *et al.* 2021, section L)**.

In vivo circRNA expression systems

The majority of circRNAs are lowly abundant in cells and therefore difficult to study. To circumvent this problem, easily manipulable overexpression vectors are often used that enable the study of functions and biogenesis of circRNAs in detail. In this context, knowledge of circRNA biogenesis gained over the last few years was used to design vectors that allow ectopic expression of endogenous and artificial circular RNAs in eukaryotic cells.

These vectors contain the sequence to be circularized, which in turn is flanked by the necessary splicing signals, as well as complementary intron sequences with inverted repeats to facilitate circularization (reviewed by **Barrett and Salzman 2016**). These constructs can be transfected making use of the cell's splicing machinery to produce the desired circRNA. Well-known examples of circRNA expression vectors are based on *ciRS-7* **(Hansen *et al.* 2013)** as well as the *ZKSCAN1* gene **(Liang and Wilusz 2014)**.

In addition, there are also some spliceosome-independent strategies available, e.g. based on the tRNA-based splicing mechanism. In archaea and eukaryotes, pre-tRNAs are spliced enzymatically, in a two-step reaction. First, the intron is excised by a splicing endonuclease (SEN) and in the second step, the resulting tRNA exon halves are ligated by the RtcB tRNA ligase to form a fully mature functional tRNA **(Greer *et al.* 1983, Peebles *et al.* 1983)**. With this knowledge, **Lu *et al.* (2015)** and **Noto *et al.* (2017)** designed a vector, which is based on the intron from the *Drosophila tRNA:TyrGUA* gene. In contrast to the exonic circRNA vector-based expression systems, which are typically driven by an RNA Pol II promoter, transcription in the tRNA-splicing-based vectors relies on RNA polymerase III, like in the case of the U6 promoter **(Schmidt *et al.* 2016)**. Additionally, this promoter includes the first 27 nts of U6 snRNA, which is required for γ-monomethyl phosphate 5′-capping **(Good *et al.* 1997)**, and enhances the stability of the expressed RNA.

Since aptamer sequences can be incorporated in circRNA-overexpression constructs, direct visualization of the expressed circRNA in living cells or a total RNA sample on a gel is also possible. Aptamers used in this approach are often obtained by an *in vitro* selection and amplification technique, also known as SELEX (Systematic Evolution of Ligands by Exponential Enrichment), and are selected based on their ability to bind fluorophores and activate fluorescence. Broccoli is such an aptamer, which is a 49-nt long RNA and can be used in mammalian or bacterial live-cell imaging for direct localization of RNA

molecules, by staining with Broccoli-binding fluorophore DFHBI **(Filonov *et al.* 2014)**.

Despite all this, the described methods for overexpression also have disadvantages. These include, for example, low expression efficiency, the time required to produce the constructs, and inaccurate splicing, often resulting in multiple products **(Hansen *et al.* 2013, Du *et al.* 2016, Schmidt *et al.* 2016, Ho-Xuan *et al.* 2020, Hansen 2021)**.

A recently published study by **Litke and Jaffrey (2019)** proposed a solution to this via the insertion of ribozymes. These introduced ribozymes belong to the naturally occurring class of twister ribozymes that were discovered through bioinformatic predictions and represent one of the most efficient ribozyme classes **(Roth *et al.* 2014)**. Mechanistically, these ribozymes undergo spontaneous self-cleavage, producing 5′-hydroxyl and 2′,3′-cyclic phosphate ends, identical to TSEN-driven pre-tRNA intron excision during tRNA splicing, and have been implemented in the so-called Tornado (Twister-optimized RNA for durable overexpression) expression system. Here, the circularized region (Broccoli aptamer or sequence of interest) is flanked by 5′- and 3′-stem-forming tRNA intron sequences, each of which is flanked by a 5′- (P3 Twister U2A) and 3′ (P1 Twister) -self-cleaving ribozyme. Once transcribed, this RNA will be autocatalytically cleaved by the ribozyme, generating a linear RNA with 2′,3′-cyclic phosphate and 5′-OH ends. The stem-forming sequences hybridize and become circularized by the endogenous tRNA ligase (RtcB). Impressively, the Tornado expression system can lead to very high levels of RNA expression, corresponding to the levels of highly expressed endogenous RNAs, e.g. tRNAs and snRNAs. These advantages combined in the described approach already have been used to achieve high-level expression of artificial designer circRNAs, like protein sponges and antisense circRNAs **(Schreiner *et al.* 2020, Pfafenrot *et al.* 2021)**.

In vitro circRNA synthesis strategies

In addition to plasmid-based overexpression in mammalian cells, circRNAs can also be produced *in vitro*. In principle, there are three general strategies for RNA circularization in a cell-free system. These include chemical (e.g. cyanogen bromide), enzymatic (e.g. RNA or DNA ligases), and ribozymatic (e.g. self-splicing introns) methods (**Beaudry and Perreault 1995**, **Petkovic and Müller 2015**, **Wesselhoeft *et al.* 2018)**. The first step in producing the desired circRNA *in vitro* is to create a DNA template for *in vitro* transcription. For this purpose, a T7 promoter sequence is usually included upstream in order to perform the reaction with the highly efficient T7 polymerase. It is important to note that both chemical, as well as enzymatic end joining, usually require a 5'-monophosphate for circularization. Therefore, the 5'-terminal triphosphate must be removed before ligation. To obtain 5′-monophosphorylated linear RNA substrates, there are several possibilities. For example, an RNA 5'-pyrophosphohydrolase (RppH) can be used after transcription, or an excess of guanosine 5′-monophosphate (GMP) during transcription (**Müller and Appel 2017, Breuer and Rossbach 2020)**. Different sequences can vary in their circularization efficiency. To enhance the circularization efficiency, several strategies are available, such as the application of DNA oligonucleotides (splint oligonucleotides) or the insertion of secondary structure elements (e.g. terminal stem) in the construct itself. However, it should be noted, that more than one product can be generated during the

circularization reaction. For example, intermolecular ligation may result in linear dimers and oligomers, while only intramolecular ligation leads to the desired circularized products **(Petkovic and Müller 2015)**. Circular integrity of the circRNAs can be confirmed by their characteristic aberrant running behavior in polyacrylamide gels as well as their resistance to RNase R, an exoribonuclease able to digest linear, but not circular RNA. After purification of the circRNA products, transfection in mammalian cell culture can be performed, comparable with the described vector-based strategy (see chapter **'*in vivo* circRNA expression systems'**).

Selection of a circularization method should be chosen depending on the circRNA sequence size. In general, *in vitro* circRNA production is more suitable for shorter (up to several hundred nucleotides) RNAs, while ribozymatic methods are more suitable for the circularization of long RNA (up to several kilobases). This reaction only requires the addition of GTP and Mg^{2+} as cofactors **(Petkovic and Müller, 2015)**.

Wesselhoeft *et al.* (2018) described an *in vitro* vector-based system using group I self-splicing introns [permuted intron-exon (PIE)] from *Anabaena* pre-tRNA for *in vitro* circRNA synthesis. After performing run-off transcription from PIE vector constructs, circRNA formation is achieved by an autocatalytic reaction. Because different products are also formed here, purification is subsequently carried out using RNase R and HPLC.

MDM2

The mouse double minute 2 gene (*MDM2*, also termed *HDM2* in humans) encodes a cellular phosphoprotein **(Momand *et al.* 1992)** that plays a key role in a variety of fundamental cellular processes **(Marine and Lozano 2010)**. However, it is mostly known as the master regulator of the tumor suppressor protein p53, because it negatively modulates its activity as well as stability via ubiquitylation and proteasomal-dependent degradation **(Klein and Vassilev 2004)**. Since MDM2 is overexpressed in several human tumors like human breast **(McCann *et al.* 1995)**, prostate **(Osman *et al.* 1999)**, pancreas **(Müller-Höcker *et al.* 2001)**, and glioma cancer **(Ehrmann *et al.* 1997)**, it is a valuable molecular target for cancer therapy.

MDM2 gene and protein structure

The MDM2 gene belongs to a large family of RING finger-containing proteins and is located on chromosome 12q13-14 **(Nag *et al.* 2014)**, encoding a protein with multiple domains (in human, its gel-electrophoretic mobility is at ~ 90 kDa, due to post-transcriptional modifications) **(Hou *et al.* 2019).** The N-terminal domain harbors binding sites for p53, p73, and E2F, the acidic domain on the other hand is necessary for the interaction with the tumor suppressor $p14^{ARF}$ protein, and a putative Zn-finger binding site interacts with the retinoblastoma protein Rb. On the C-terminal end, it contains a RING-finger as well as the E3 ligase domain, responsible for the ubiquitylation of p53. Furthermore, MDM2 also contains nuclear localization (NLS), nucleolar localization (NoLS), and nuclear export signals (NES) **(Momand *et al.* 2000)**.

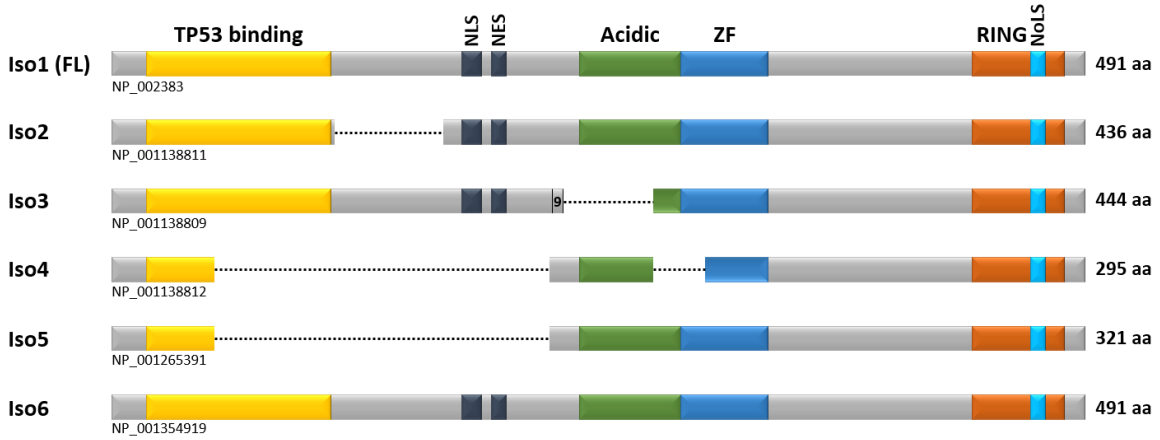

Figure 6: Schematic representation of the functional domains of human MDM2 proteins derived from different isoforms.
The respective functional domains are indicated. Yellow: p53 binding site. Grey, NLS: Nuclear Localization Signal, NES: Nuclear Export Signal, and NoLS: Nucleolar Localization Signal. Green: Acidic region. Blue, ZF: Zing finger domain.

Interestingly, two of the MDM2 transcripts (isoform 1 and 2) contain two upstream open reading frames (uORFs), which cooperate to decrease the translational output of MDM2 **(Figure 7)**. In general, uORFs represent important mediators of transcript-specific translational control, and in this context, it is known that a class of tumors derives from cells expressing transcript versions of MDM2 that do not harbor the uORFs (alternative first exon and short 5´-UTR). The strong effects of these uORFs on translation could be confirmed by studies through mutational analysis, leading to a 10-fold increase in the translation efficiency **(Jin *et al.* 2003)**.

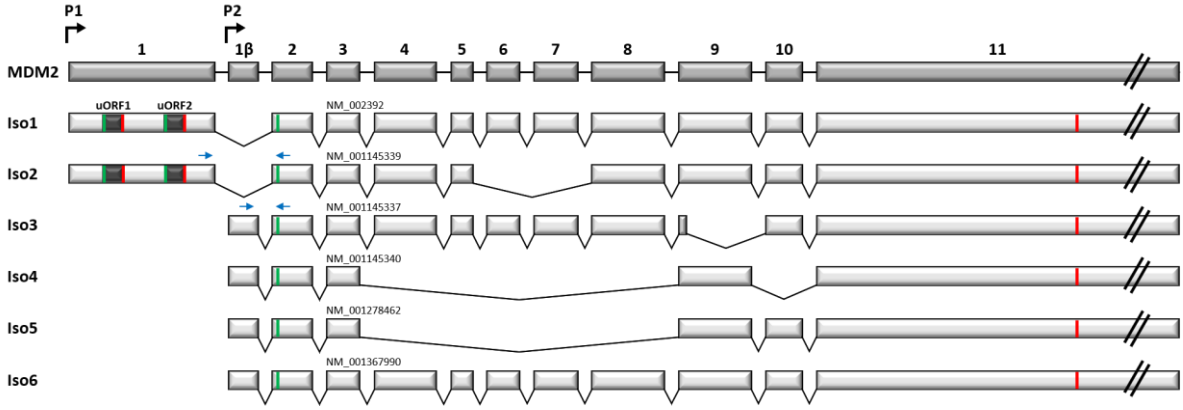

Figure 7: Schematic structure of MDM2 mRNAs.
The genomic structure is represented on top (not to scale), including two alternative promoters (P1 and 2), as well as the alternative first exon 1β. On the bottom section the different mRNA isoforms are depicted. Isoforms 1 and 2 have a longer 5'-UTR (exon 1) than isoforms 3-6 (alternative exon 1β). The longer 5'-UTR also harbors two additional upstream UTRs (uORF 1 and 2). The start and stop codons are shown in green and red respectively. The arrows represent the primers that can be used to detect and distinguish between the respective isoforms.

The biological functions of MDM2

Functionally, MDM2 and p53 act in an auto-regulatory feedback loop **(Figure 8)**. Thereby, p53 induces the transcription of MDM2, leading to higher levels of expressed proteins that can in turn bind p53 with high affinity **(Nag *et al.* 2014)**, resulting in inhibited p53 activity through several mechanisms. For example, after binding of MDM2 to p53, it induces the nuclear export of p53 **(Kubbutat *et al.* 1997)** and inhibits its ability to act as a transcription factor **(Oliner *et al.* 1993)**. Furthermore, MDM2 is also able to induce the degradation of p53 by the proteasome, through its ubiquitin ligase activity **(Kubbutat *et al.* 1997)**. Under normal conditions, p53 is thus only present at low levels **(Chène 2003)**. In the case of cellular stress, MDM2-mediated ubiquitination of p53 is abolished. As a consequence, p53 can activate the transcription of, for example, apoptotic genes **(Wade *et al.* 2013)**.

Nevertheless, it was shown that MDM2 also exerts multiple p53-independent functions. For example, it is involved in various biological processes such as cell proliferation, cell fate determination, and DNA repair.

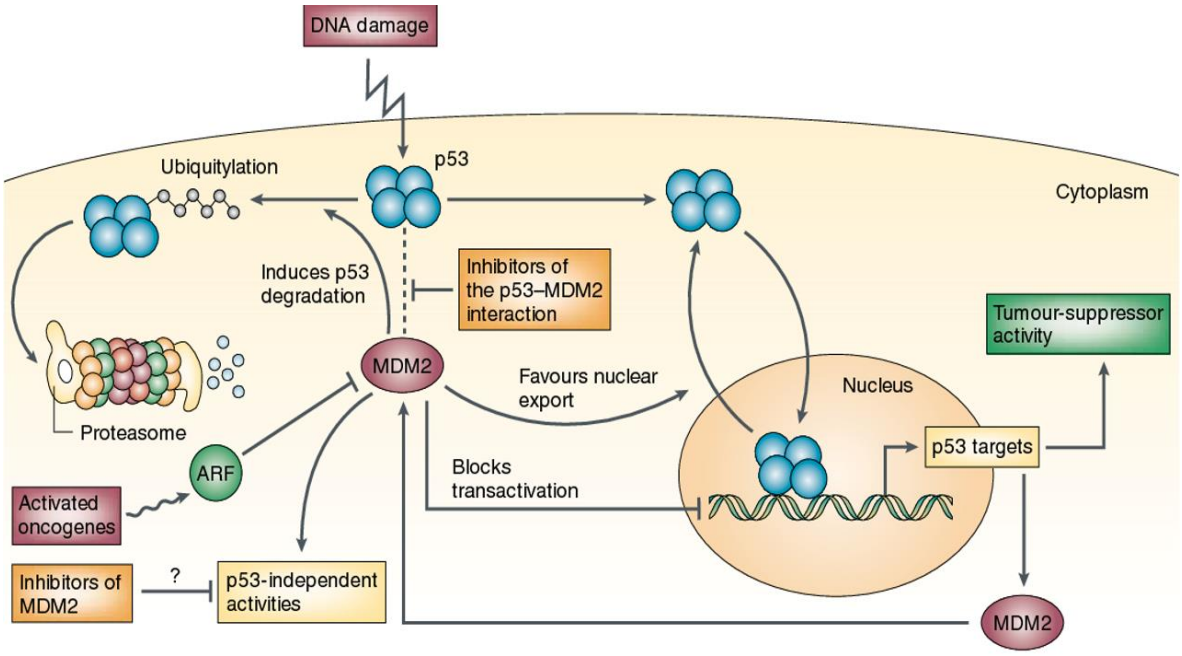

Figure 8: Feedback loop of p53 and MDM2.
MDM2 expression is stimulated by p53. MDM2 subsequently inhibits the activity of p53 by blocking its transcriptional activity. In addition, it promotes nuclear export of p53 and stimulates its subsequent degradation in the cytoplasm. If cellular signals occur, such as DNA damage or the activation of oncogenes, p53 is activated. With this activation, MDM2 can no longer be bound. Furthermore, activated oncogenes can activate ARF proteins, which in turn prevent MDM2-mediated degradation of p53. This MDM2-p53 feedback loop offers a good target in cancer therapy. Modified after **Chène (2003)**.

MDM2 as target for cancer therapy

In many cancers, the MDM2-p53 feedback loop is dysregulated, making it important in therapeutic strategies. Furthermore, the overexpression of MDM2 can promote the formation, progression and drug resistance of malignant tumors **(Hou *et al.* 2019)**. Inhibition of MDM2 and thereby restored p53 functionality with subsequent p53 cell cycle arrest and apoptosis induction represents a particularly attractive approach to new targeted therapies. In this context, two different approaches have been described and pursued so far **(Chène 2003)**.

The first approach includes studies, in which MDM2 antisense-oligodeoxy-nucleotides have been used. For example, the studies by **Chen *et al.* (1998 and 1999)** show that 20-mer antisense oligonucleotides directed against the MDM2 coding sequence can be successfully used alone or in combination with other therapeutics to inhibit MDM2 expression. Comparing the current state of research, there are hardly any studies or clinical trials on this approach.

The focus has shifted to the second approach, in which several small-molecule compounds are used to inhibit the interaction between p53 and MDM2. These inhibitors are *cis*-imidazolines (Nutlins), described first by **Vassilev (2004)**. This group of inhibitors (Nutlin-1, Nutlin-2, Nutlin-3) prevents the interaction between MDM2 and p53 and restores p53 functionality by binding MDM2 at the p53 binding site via three amino acid residues.

SARS-CoV-2

Late in 2019, there was an outbreak of a pandemic of acute respiratory illness referred to as Coronavirus Disease 2019 (COVID-19). The trigger for this was a new, highly transmissible, and pathogenic coronavirus, designated severe acute respiratory syndrome coronavirus type 2 (SARS-CoV-2) **(Hu *et al*. 2021)**. Coronaviruses represent a diverse group of viruses that can infect both animals and humans due to their ability to undergo homologous recombination **(Graham and Baric 2010)** and cause mild to severe respiratory infections in the latter. Outbreaks caused by two coronaviruses of zoonotic origin occurred as early as 2002 and 2012. These were severe acute respiratory syndrome coronavirus (SARS-CoV) and Middle East coronavirus (MERS-CoV). However, the SARS-CoV-2 pandemic has been much worse compared to the SARS-CoV and MERS-CoV outbreaks in terms of the number of people infected, as well as the spatial extent of the epidemic areas. Coronaviruses are classified in the family *Coronaviridae* (suborder: *Cornidovirineae*, order: *Nidovirales*, realm: *Riboviria*), in which the large subfamily *Orthocoronavirinae* can be divided into four genera: *Alphacoronavirus*, *Betacoronavirus*, *Gammacoronavirus*, and *Deltacoronavirus* **(coronaviridae study group of the international committee on taxonomy of viruses 2020)**. To date, seven human pathogenic coronavirus (HCoV) species are known, classified as *Alphacoronaviruses* (HCoV-229E, HCoV-NL63) and *Betacoronaviruses* (HCoV-HKU1, HCoV-OC43, SARS-CoV, MERS-CoV, SARS-CoV-2).

Virion structure of SARS-CoV-2

SARS-CoV-2 is a membrane-enveloped RNA virus that forms virions with a diameter of approximately 80-140 nm (**Laue *et al*. 2021**). There are three structural proteins, spike (S), envelope (E), and membrane (M) proteins, embedded in the membrane. Inside the virion is the nucleocapsid, which is composed of the single-stranded RNA genome of positive polarity and the fourth structural protein, nucleocapsid (N) (**Fehr and Perlman 2015**). The approximately 30 kilobases long polycistronic RNA genome encodes both nonstructural proteins that play a major role in replication, and the four structural proteins (S, E, M, and N) **(Figure 9)**. The spike protein is responsible for entry into the host cell and consists of two subunits (S1 and S2). The first subunit contains a receptor-binding domain (RBD) that can bind to the host receptor, which is the transmembrane enzyme ACE-2 (angiotensin-converting enzyme 2). The second subunit subsequently initiates the fusion of the viral membrane envelope with the host cell membrane. Entry into the host cell is additionally supported by a cell-surface serine protease TMPRSS2 (**Hoffmann *et al*. 2020**).

Replication and transcription of SARS-CoV-2

Following receptor-mediated entry of coronavirus into host cells, the two large open reading frames (ORFs) 1a and 1b, located in the 5'-terminal two-thirds of the capped and polyadenylated coronavirus genome, are translated.

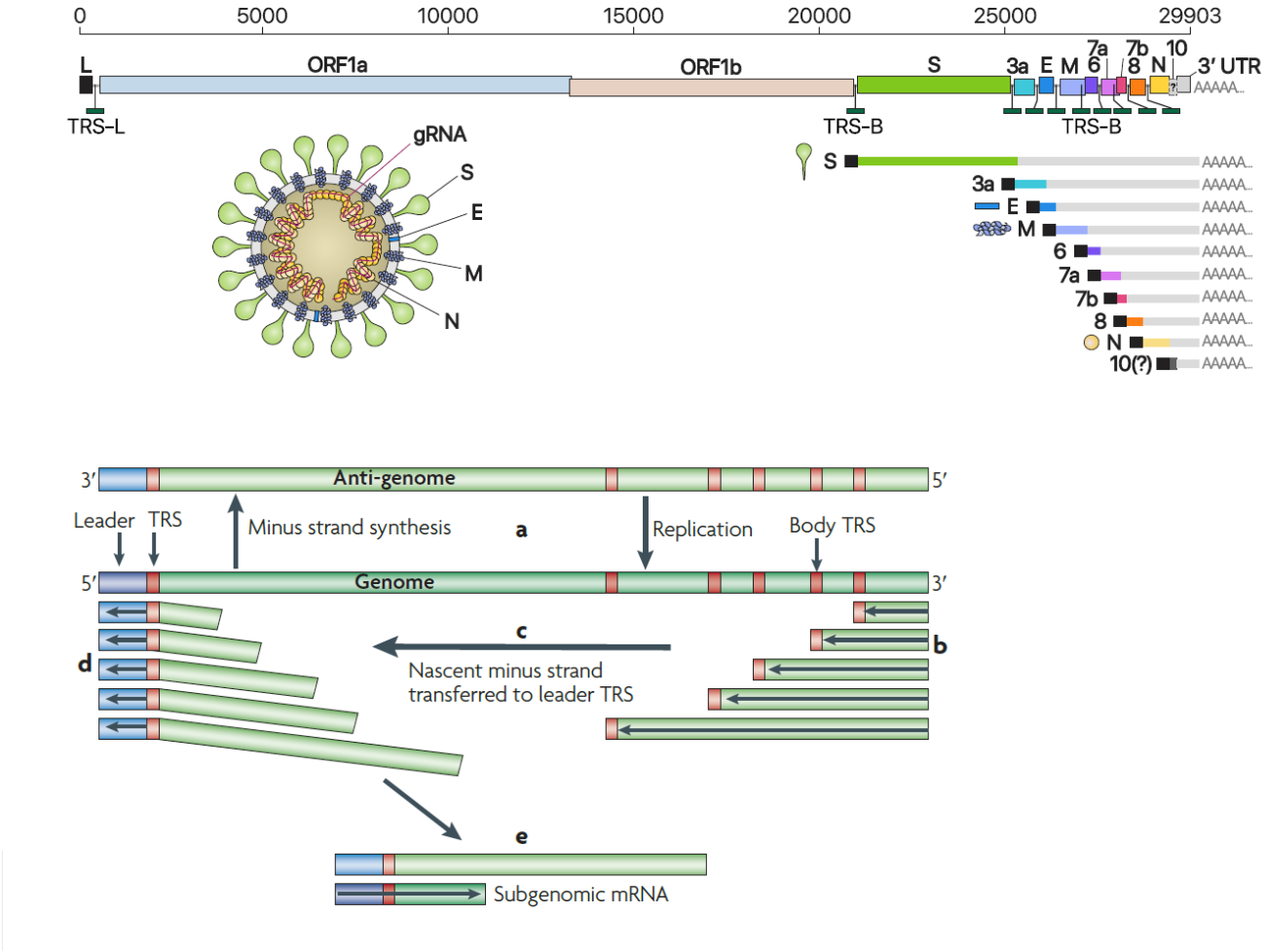

Figure 9: SARS-CoV-2 genome organization, virion structure, and discontinuous synthesis of sgRNAs.
[top] SARS-CoV-2 is an enveloped virus with a positive-sense, single-stranded RNA genome of 29,903 nts. The first two thirds of the genome harbor ORF1a and ORF1b, which encode non-structural proteins (nsp). The remaining one-third of the genome at the 3'-end encodes four structural proteins, spike (S), envelope (E), membrane (M) and nucleocapsid (N) proteins. S, M and E are embedded in the membrane, while N is inside the virion together with the RNA (building the nucleocapsid). Modified after **Kim *et al.* 2020**.
[bottom] (a) The full-length genome is used as a template to generate negative-sense RNA, which then serves as a template for the synthesis of additional copies of the full-length genomic RNA (gRNA), and the subgenomic RNAs (sgRNAs).
(b) All coronavirus sgRNAs have a 5'-leader sequence in common, which is added by discontinuous transcription of minus-sense subgenomic RNAs. Synthesis of sgRNAs is initiated at the 3'-end of the genome and proceeds until it reaches one of the transcriptional regulatory sequences (TRS, red).
(c) Nascent transcripts are transferred to the complementary leader TRS through base-pairing interactions.
(d) This transfer is followed by transcription through the 5'-end of the genome, thereby including the 5'-leader sequence.
(e) These transcribed subgenomic mRNAs serve as templates for viral mRNA production.
Modified after **Perlman and Netland 2009**.

Specifically, translation from ORF1b occurs through a -1 ribosomal frameshift at the short overlap of ORF1a and ORF1b. This results in two polyproteins that are processed by viral proteases to produce 15-16 nonstructural proteins (NSPs) that form the viral replication and transcription complex **(Perlman and Masters 2021)**.

Negative strand RNA is produced from the genome, subsequently serving as a template for synthesis of positive-sense genomic (gRNA) and subgenomic RNAs (sgRNAs). The latter represents a series of 5'-coterminal subgenomic (sg) minus-strand RNAs of varying lengths produced from the 3'-end of the genome by a process referred to as 'discontinuous transcription' of minus strands **(Figure 9)**. In this case, RNA synthesis proceeds until one of the transcriptional regulatory sequences (TRS) is reached. Through base-pairing interactions, the nascent transcript is then transferred to the complementary leader TRS, and the leader sequence is added. These produced minus strands serve as a template for the production of a nested set of sg mRNAs that share a common 5'-leader sequence. The produced viral RNA copies and viral proteins are then taken up into the endoplasmic reticulum (ER) of the host cell and assembled into new viruses. Subsequently, the assembled viral particles are released through the ER and Golgi and transported out of the host cell by exocytosis, where they are present as virions and can infect new host cells.

Potential therapeutic approaches

Since the outbreak of SARS-CoV-2, there are intense worldwide efforts to develop and apply new therapeutic strategies to fight this life-threatening disease. Most of these approaches focus on, first, small-molecule drugs targeting viral enzymes (nucleoside analogs, protease inhibitors, and others), and second, on antibodies interfering with virus entry, in particular virus-receptor interactions. In addition, immunomodulatory agents are being used and a large number of SARS-CoV-2 vaccines (including virus vector- and mRNA-based vaccines) are being developed and tested, many of which provide promising new approaches to prevent or treat COVID-19 more effectively **(Polack *et al.* 2020)**. However, alternative novel strategies should also be considered and pursued. Antisense approaches represent such a classical line of sequence-based interference. Regarding antiviral strategies, earlier studies had evaluated HIV-Tat peptide-coupled morpholino ASO against SARS-CoV and the related mouse hepatitis virus (MHV) **(Neuman *et al.* 2005, Burrer *et al.* 2007)**.

Specific aims of this work

Translation of proteins is a tightly regulated cellular process. However, in many diseases dysregulated protein expression patterns are observed and the translation machinery can be hijacked e.g. during viral infections. In this context, many strategies have been developed to interfere with these mechanisms. In this thesis we focused on the potential of designer circRNAs as molecular tools to regulate translational output of mRNAs due to their superior intracellular stability compared to linear RNAs. For this purpose, we utilized small *in vitro* produced, or intracellularly overexpressed circular RNAs as a backbone for the presentation of antisense sequence that are targeted to the 5´-UTRs of cellular and viral mRNAs. In summary, the approach proofed as an efficient and elegant way to interfere with translation of endogenous, mRNAs and the propagation of SARS-CoV-2 infections in cell culture, opening up new potential and possibilities for the utilization of circular RNAs in molecular medicine.

References

Agrawal, S., Goodchild, J., Civeira, M. P., Thornton, A. H., Sarin, P. S., & Zamecnik, P. C. (1988). Oligodeoxynucleoside phosphoramidates and phosphorothioates as inhibitors of human immunodeficiency virus. *Proceedings of the National Academy of Sciences of the United States of America*, *85*(19), 7079–7083. https://doi.org/10.1073/pnas.85.19.7079

Aktaş, T., Avşar Ilık, İ., Maticzka, D., Bhardwaj, V., Pessoa Rodrigues, C., Mittler, G., Manke, T., Backofen, R., & Akhtar, A. (2017). DHX9 suppresses RNA processing defects originating from the Alu invasion of the human genome. *Nature*, *544*(7648), 115–119. https://doi.org/10.1038/nature21715

Alhasan, A. A., Izuogu, O. G., Al-Balool, H. H., Steyn, J. S., Evans, A., Colzani, M., Ghevaert, C., Mountford, J. C., Marenah, L., Elliott, D. J., Santibanez-Koref, M., & Jackson, M. S. (2016). Circular RNA enrichment in platelets is a signature of transcriptome degradation. *Blood*, *127*(9), e1–e11. https://doi.org/10.1182/blood-2015-06-649434

Amantana, A., & Iversen, P. L. (2005). Pharmacokinetics and biodistribution of phosphorodiamidate morpholino antisense oligomers. *Current opinion in pharmacology*, *5*(5), 550–555. https://doi.org/10.1016/j.coph.2005.07.001

Anderson, K. P., Fox, M. C., Brown-Driver, V., Martin, M. J., & Azad, R. F. (1996). Inhibition of human cytomegalovirus immediate-early gene expression by an antisense oligonucleotide complementary to immediate-early RNA. *Antimicrobial agents and chemotherapy*, *40*(9), 2004–2011. https://doi.org/10.1128/AAC.40.9.2004

Andreeva, K., Soliman, M. M., & Cooper, N. G. (2015). Regulatory networks in retinal ischemia-reperfusion injury. *BMC genetics*, *16*, 43. https://doi.org/10.1186/s12863-015-0201-4

Ashwal-Fluss, R., Meyer, M., Pamudurti, N. R., Ivanov, A., Bartok, O., Hanan, M., Evantal, N., Memczak, S., Rajewsky, N., & Kadener, S. (2014). circRNA biogenesis competes with pre-mRNA splicing. *Molecular cell*, *56*(1), 55–66. https://doi.org/10.1016/j.molcel.2014.08.019

Bandiera, S., Pfeffer, S., Baumert, T. F., & Zeisel, M. B. (2015). miR-122--a key factor and therapeutic target in liver disease. *Journal of hepatology*, *62*(2), 448–457. https://doi.org/10.1016/j.jhep.2014.10.004

Barbosa, C., Peixeiro, I., & Romão, L. (2013). Gene expression regulation by upstream open reading frames and human disease. *PLoS genetics*, *9*(8), e1003529. https://doi.org/10.1371/journal.pgen.1003529

Barrett, S. P., & Salzman, J. (2016). Circular RNAs: analysis, expression and potential functions. *Development (Cambridge, England)*, *143*(11), 1838–1847. https://doi.org/10.1242/dev.128074

Beaudry, D., & Perreault, J. P. (1995). An efficient strategy for the synthesis of circular RNA molecules. *Nucleic acids research*, *23*(15), 3064–3066. https://doi.org/10.1093/nar/23.15.3064

Bennett C. F. (2019). Therapeutic Antisense Oligonucleotides Are Coming of Age. *Annual review of medicine*, *70*, 307–321. https://doi.org/10.1146/annurev-med-041217-010829

Bennett, C. F., Baker, B. F., Pham, N., Swayze, E., & Geary, R. S. (2017). Pharmacology of Antisense Drugs. *Annual review of pharmacology and toxicology*, *57*, 81–105. https://doi.org/10.1146/annurev-pharmtox-010716-104846

Bestas, B., Moreno, P. M., Blomberg, K. E., Mohammad, D. K., Saleh, A. F., Sutlu, T., Nordin, J. Z., Guterstam, P., Gustafsson, M. O., Kharazi, S., Piątosa, B., Roberts, T. C., Behlke, M. A., Wood, M. J., Gait, M. J., Lundin, K. E., El Andaloussi, S., Månsson, R., Berglöf, A., Wengel, J., … Smith, C. I. (2014). Splice-correcting oligonucleotides restore BTK function in X-linked agammaglobulinemia model. *The Journal of clinical investigation*, *124*(9), 4067–4081. https://doi.org/10.1172/JCI76175

Bestas, B., Turunen, J. J., Blomberg, K. E., Wang, Q., Månsson, R., El Andaloussi, S., Berglöf, A., & Smith, C. I. (2015). Splice-correction strategies for treatment of X-linked agammaglobulinemia. *Current allergy and asthma reports*, *15*(3), 510. https://doi.org/10.1007/s11882-014-0510-0

Bill, B. R., Petzold, A. M., Clark, K. J., Schimmenti, L. A., & Ekker, S. C. (2009). A primer for morpholino use in zebrafish. *Zebrafish*, *6*(1), 69–77. https://doi.org/10.1089/zeb.2008.0555

Breaker, R. R., & Joyce, G. F. (1994). A DNA enzyme that cleaves RNA. *Chemistry & biology*, *1*(4), 223–229. https://doi.org/10.1016/1074-5521(94)90014-0

Breuer, J., & Rossbach, O. (2020). Production and Purification of Artificial Circular RNA Sponges for Application in Molecular Biology and Medicine. *Methods and protocols*, *3*(2), 42. https://doi.org/10.3390/mps3020042

Burd, C. E., Jeck, W. R., Liu, Y., Sanoff, H. K., Wang, Z., & Sharpless, N. E. (2010). Expression of linear and novel circular forms of an INK4/ARF-associated non-coding RNA correlates with atherosclerosis risk. *PLoS genetics*, *6*(12), e1001233. https://doi.org/10.1371/journal.pgen.1001233

Burrer, R., Neuman, B. W., Ting, J. P., Stein, D. A., Moulton, H. M., Iversen, P. L., Kuhn, P., & Buchmeier, M. J. (2007). Antiviral effects of antisense morpholino oligomers in murine coronavirus infection models. *Journal of virology*, *81*(11), 5637–5648. https://doi.org/10.1128/JVI.02360-06

Calvo, S. E., Pagliarini, D. J., & Mootha, V. K. (2009). Upstream open reading frames cause widespread reduction of protein expression and are polymorphic among humans. *Proceedings of the National Academy of Sciences of the United States of America*, *106*(18), 7507–7512. https://doi.org/10.1073/pnas.0810916106

Capel, B., Swain, A., Nicolis, S., Hacker, A., Walter, M., Koopman, P., Goodfellow, P., & Lovell-Badge, R. (1993). Circular transcripts of the testis-determining gene Sry in adult mouse testis. *Cell*, *73*(5), 1019–1030. https://doi.org/10.1016/0092-8674(93)90279-y

Cech, T. R., Zaug, A. J., & Grabowski, P. J. (1981). In vitro splicing of the ribosomal RNA precursor of Tetrahymena: involvement of a guanosine nucleotide in the excision of the intervening sequence. *Cell*, *27*(3 Pt 2), 487–496. https://doi.org/10.1016/0092-8674(81)90390-1

Cerritelli, S. M., & Crouch, R. J. (2009). Ribonuclease H: the enzymes in eukaryotes. *The FEBS journal*, *276*(6), 1494–1505. https://doi.org/10.1111/j.1742-4658.2009.06908.x

Chen, C. Y., & Sarnow, P. (1995). Initiation of protein synthesis by the eukaryotic translational apparatus on circular RNAs. *Science (New York, N.Y.)*, *268*(5209), 415–417. https://doi.org/10.1126/science.7536344

Chen L. L. (2020). The expanding regulatory mechanisms and cellular functions of circular RNAs. *Nature reviews. Molecular cell biology*, *21*(8), 475–490. https://doi.org/10.1038/s41580-020-0243-y

Chen, L. L., & Yang, L. (2015). Regulation of circRNA biogenesis. *RNA biology*, *12*(4), 381–388. https://doi.org/10.1080/15476286.2015.1020271

Chen, L., Agrawal, S., Zhou, W., Zhang, R., & Chen, J. (1998). Synergistic activation of p53 by inhibition of MDM2 expression and DNA damage. *Proceedings of the National Academy of Sciences of the United States of America*, *95*(1), 195–200. https://doi.org/10.1073/pnas.95.1.195

Chen, L., Lu, W., Agrawal, S., Zhou, W., Zhang, R., & Chen, J. (1999). Ubiquitous induction of p53 in tumor cells by antisense inhibition of MDM2 expression. *Molecular medicine (Cambridge, Mass.)*, *5*(1), 21–34.

Chène P. (2003). Inhibiting the p53-MDM2 interaction: an important target for cancer therapy. *Nature reviews. Cancer*, *3*(2), 102–109. https://doi.org/10.1038/nrc991

Cocquerelle, C., Daubersies, P., Majérus, M. A., Kerckaert, J. P., & Bailleul, B. (1992). Splicing with inverted order of exons occurs proximal to large introns. *The EMBO journal*, *11*(3), 1095–1098.

Cocquet, J., Chong, A., Zhang, G., & Veitia, R. A. (2006). Reverse transcriptase template switching and false alternative transcripts. *Genomics*, *88*(1), 127–131. https://doi.org/10.1016/j.ygeno.2005.12.013

Cohn, R. D., & Campbell, K. P. (2000). Molecular basis of muscular dystrophies. *Muscle & nerve*, *23*(10), 1456–1471. https://doi.org/10.1002/1097-4598(200010)23:10<1456::aid-mus2>3.0.co;2-t

Conn, S. J., Pillman, K. A., Toubia, J., Conn, V. M., Salmanidis, M., Phillips, C. A., Roslan, S., Schreiber, A. W., Gregory, P. A., & Goodall, G. J. (2015). The RNA binding protein quaking regulates formation of circRNAs. *Cell*, *160*(6), 1125–1134. https://doi.org/10.1016/j.cell.2015.02.014

Conrad, K. D., Giering, F., Erfurth, C., Neumann, A., Fehr, C., Meister, G., & Niepmann, M. (2013). MicroRNA-122 dependent binding of Ago2 protein to hepatitis C virus RNA is associated with enhanced RNA stability and translation stimulation. *PloS one*, *8*(2), e56272. https://doi.org/10.1371/journal.pone.0056272

Coronaviridae Study Group of the International Committee on Taxonomy of Viruses (2020). The species Severe acute respiratory syndrome-related coronavirus: classifying 2019-nCoV and naming it SARS-CoV-2. *Nature microbiology*, *5*(4), 536–544. https://doi.org/10.1038/s41564-020-0695-z

Crooke, S. T., Witztum, J. L., Bennett, C. F., & Baker, B. F. (2018). RNA-Targeted Therapeutics. *Cell metabolism*, *27*(4), 714–739. https://doi.org/10.1016/j.cmet.2018.03.004

Danan, M., Schwartz, S., Edelheit, S., & Sorek, R. (2012). Transcriptome-wide discovery of circular RNAs in Archaea. *Nucleic acids research*, *40*(7), 3131–3142. https://doi.org/10.1093/nar/gkr1009

De Mesmaeker A., Haener R., Martin P., & Moser HE. (1995). Antisense Oligonucleotides. *Accounts of Chemical Research.*, 28, 9, 366–374 https://doi.org/10.1021/ar00057a002

Deleavey, G. F., & Damha, M. J. (2012). Designing chemically modified oligonucleotides for targeted gene silencing. *Chemistry & biology*, *19*(8), 937–954. https://doi.org/10.1016/j.chembiol.2012.07.011

Dhuri, K., Bechtold, C., Quijano, E., Pham, H., Gupta, A., Vikram, A., & Bahal, R. (2020). Antisense Oligonucleotides: An Emerging Area in Drug Discovery and Development. *Journal of clinical medicine*, *9*(6), 2004. https://doi.org/10.3390/jcm9062004

Digenio, A., Dunbar, R. L., Alexander, V. J., Hompesch, M., Morrow, L., Lee, R. G., Graham, M. J., Hughes, S. G., Yu, R., Singleton, W., Baker, B. F., Bhanot, S., & Crooke, R. M. (2016). Antisense-Mediated Lowering of Plasma Apolipoprotein C-III by Volanesorsen Improves Dyslipidemia and Insulin Sensitivity in Type 2 Diabetes. *Diabetes care*, *39*(8), 1408–1415. https://doi.org/10.2337/dc16-0126

Dominski, Z., & Kole, R. (1993). Restoration of correct splicing in thalassemic pre-mRNA by antisense oligonucleotides. *Proceedings of the National Academy of Sciences of the United States of America*, *90*(18), 8673–8677. https://doi.org/10.1073/pnas.90.18.8673

Du, W. W., Yang, W., Liu, E., Yang, Z., Dhaliwal, P., & Yang, B. B. (2016). Foxo3 circular RNA retards cell cycle progression via forming ternary complexes with p21 and CDK2. *Nucleic acids research*, *44*(6), 2846–2858. https://doi.org/10.1093/nar/gkw027

Dubin, R. A., Kazmi, M. A., & Ostrer, H. (1995). Inverted repeats are necessary for circularization of the mouse testis Sry transcript. *Gene*, *167*(1-2), 245–248. https://doi.org/10.1016/0378-1119(95)00639-7

Ehrmann, J., Jr, Kolár, Z., Vojtěsek, B., Kala, M., Komenda, S., & Oulton, A. (1997). Prognostic factors in astrocytomas: relationship of p53, MDM-2, BCL-2 and PCNA immunohistochemical expression to tumor grade and overall patient survival. *Neoplasma*, *44*(5), 299–304.

Elbashir, S. M., Harborth, J., Lendeckel, W., Yalcin, A., Weber, K., & Tuschl, T. (2001). Duplexes of 21-nucleotide RNAs mediate RNA interference in cultured mammalian cells. *Nature*, *411*(6836), 494–498. https://doi.org/10.1038/35078107

Errichelli, L., Dini Modigliani, S., Laneve, P., Colantoni, A., Legnini, I., Capauto, D., Rosa, A., De Santis, R., Scarfò, R., Peruzzi, G., Lu, L., Caffarelli, E., Shneider, N. A., Morlando, M., & Bozzoni, I. (2017). FUS affects circular RNA expression in murine embryonic stem cell-derived motor neurons. *Nature communications*, *8*, 14741. https://doi.org/10.1038/ncomms14741

Esau, C., Kang, X., Peralta, E., Hanson, E., Marcusson, E. G., Ravichandran, L. V., Sun, Y., Koo, S., Perera, R. J., Jain, R., Dean, N. M., Freier, S. M., Bennett, C. F., Lollo, B., & Griffey, R. (2004). MicroRNA-143 regulates adipocyte differentiation. *The Journal of biological chemistry*, *279*(50), 52361–52365. https://doi.org/10.1074/jbc.C400438200

Faria, M., Spiller, D. G., Dubertret, C., Nelson, J. S., White, M. R., Scherman, D., Hélène, C., & Giovannangeli, C. (2001). Phosphoramidate oligonucleotides as potent antisense molecules in cells and in vivo. *Nature biotechnology*, *19*(1), 40–44. https://doi.org/10.1038/83489

Fehr, A. R., & Perlman, S. (2015). Coronaviruses: an overview of their replication and pathogenesis. *Methods in molecular biology (Clifton, N.J.)*, *1282*, 1–23. https://doi.org/10.1007/978-1-4939-2438-7_1

Fei, T., Chen, Y., Xiao, T., Li, W., Cato, L., Zhang, P., Cotter, M. B., Bowden, M., Lis, R. T., Zhao, S. G., Wu, Q., Feng, F. Y., Loda, M., He, H. H., Liu, X. S., & Brown, M. (2017). Genome-wide CRISPR screen identifies HNRNPL as a prostate cancer dependency regulating RNA splicing. *Proceedings of the National Academy of Sciences of the United States of America*, *114*(26), E5207–E5215. https://doi.org/10.1073/pnas.1617467114

Filonov, G. S., Moon, J. D., Svensen, N., & Jaffrey, S. R. (2014). Broccoli: rapid selection of an RNA mimic of green fluorescent protein by fluorescence-based selection and directed evolution. *Journal of the American Chemical Society*, *136*(46), 16299–16308. https://doi.org/10.1021/ja508478x

Fire, A., Xu, S., Montgomery, M. K., Kostas, S. A., Driver, S. E., & Mello, C. C. (1998). Potent and specific genetic interference by double-stranded RNA in Caenorhabditis elegans. *Nature*, *391*(6669), 806–811. https://doi.org/10.1038/35888

Fountain, K. J., Gilar, M., & Gebler, J. C. (2003). Analysis of native and chemically modified oligonucleotides by tandem ion-pair reversed-phase high-performance liquid chromatography/electrospray ionization mass spectrometry. *Rapid communications in mass spectrometry: RCM*, *17*(7), 646–653. https://doi.org/10.1002/rcm.959

Gambacorti-Passerini, C., Mologni, L., Bertazzoli, C., le Coutre, P., Marchesi, E., Grignani, F., & Nielsen, P. E. (1996). In vitro transcription and translation inhibition by anti-promyelocytic leukemia (PML)/retinoic acid receptor alpha and anti-PML peptide nucleic acid. *Blood*, *88*(4), 1411–1417.

Good, P. D., Krikos, A. J., Li, S. X., Bertrand, E., Lee, N. S., Giver, L., Ellington, A., Zaia, J. A., Rossi, J. J., & Engelke, D. R. (1997). Expression of small, therapeutic RNAs in human cell nuclei. *Gene therapy*, *4*(1), 45–54. https://doi.org/10.1038/sj.gt.3300354

Grabowski, P. J., Zaug, A. J., & Cech, T. R. (1981). The intervening sequence of the ribosomal RNA precursor is converted to a circular RNA in isolated nuclei of Tetrahymena. *Cell*, *23*(2), 467–476. https://doi.org/10.1016/0092-8674(81)90142-2

Graham, M. J., Lee, R. G., Bell, T. A., 3rd, Fu, W., Mullick, A. E., Alexander, V. J., Singleton, W., Viney, N., Geary, R., Su, J., Baker, B. F., Burkey, J., Crooke, S. T., & Crooke, R. M. (2013). Antisense oligonucleotide inhibition of apolipoprotein C-III reduces plasma triglycerides in rodents, nonhuman primates, and humans. *Circulation research*, *112*(11), 1479–1490. https://doi.org/10.1161/CIRCRESAHA.111.300367

Graham, R. L., & Baric, R. S. (2010). Recombination, reservoirs, and the modular spike: mechanisms of coronavirus cross-species transmission. *Journal of virology*, *84*(7), 3134–3146. https://doi.org/10.1128/JVI.01394-09

Greer, C. L., Peebles, C. L., Gegenheimer, P., & Abelson, J. (1983). Mechanism of action of a yeast RNA ligase in tRNA splicing. *Cell*, *32*(2), 537–546. https://doi.org/10.1016/0092-8674(83)90473-7

Gross, H. J., Domdey, H., Lossow, C., Jank, P., Raba, M., Alberty, H., & Sänger, H. L. (1978). Nucleotide sequence and secondary structure of potato spindle tuber viroid. *Nature*, *273*(5659), 203–208. https://doi.org/10.1038/273203a0

Guarnerio, J., Bezzi, M., Jeong, J. C., Paffenholz, S. V., Berry, K., Naldini, M. M., Lo-Coco, F., Tay, Y., Beck, A. H., & Pandolfi, P. P. (2016). Oncogenic Role of Fusion-circRNAs Derived from Cancer-Associated Chromosomal Translocations. *Cell*, *165*(2), 289–302. https://doi.org/10.1016/j.cell.2016.03.020

Guerrier-Takada, C., Gardiner, K., Marsh, T., Pace, N., & Altman, S. (1983). The RNA moiety of ribonuclease P is the catalytic subunit of the enzyme. *Cell*, *35*(3 Pt 2), 849–857. https://doi.org/10.1016/0092-8674(83)90117-4

Hansen T. B. (2021). Signal and noise in circRNA translation. *Methods (San Diego, Calif.)*, *196*, 68–73. https://doi.org/10.1016/j.ymeth.2021.02.007

Hansen, T. B., Jensen, T. I., Clausen, B. H., Bramsen, J. B., Finsen, B., Damgaard, C. K., & Kjems, J. (2013). Natural RNA circles function as efficient microRNA sponges. *Nature*, *495*(7441), 384–388. https://doi.org/10.1038/nature11993

Hansen, T. B., Venø, M. T., Damgaard, C. K., & Kjems, J. (2016). Comparison of circular RNA prediction tools. *Nucleic acids research*, *44*(6), e58. https://doi.org/10.1093/nar/gkv1458

Hansen, T. B., Wiklund, E. D., Bramsen, J. B., Villadsen, S. B., Statham, A. L., Clark, S. J., & Kjems, J. (2011). miRNA-dependent gene silencing involving Ago2-mediated cleavage of a circular antisense RNA. *The EMBO journal*, *30*(21), 4414–4422. https://doi.org/10.1038/emboj.2011.359

Harding, H. P., Novoa, I., Zhang, Y., Zeng, H., Wek, R., Schapira, M., & Ron, D. (2000). Regulated translation initiation controls stress-induced gene expression in mammalian cells. *Molecular cell*, *6*(5), 1099–1108. https://doi.org/10.1016/s1097-2765(00)00108-8

Havens, M. A., & Hastings, M. L. (2016). Splice-switching antisense oligonucleotides as therapeutic drugs. *Nucleic acids research*, *44*(14), 6549–6563. https://doi.org/10.1093/nar/gkw533

Heasman J. (2002). Morpholino oligos: making sense of antisense? *Developmental biology*, *243*(2), 209–214. https://doi.org/10.1006/dbio.2001.0565

Hentze, M. W., & Preiss, T. (2013). Circular RNAs: splicing's enigma variations. *The EMBO journal*, *32*(7), 923–925. https://doi.org/10.1038/emboj.2013.53

Hoffmann, M., Kleine-Weber, H., Schroeder, S., Krüger, N., Herrler, T., Erichsen, S., Schiergens, T. S., Herrler, G., Wu, N. H., Nitsche, A., Müller, M. A., Drosten, C., & Pöhlmann, S. (2020). SARS-CoV-2 Cell Entry Depends on ACE2 and TMPRSS2 and Is Blocked by a Clinically Proven Protease Inhibitor. *Cell*, *181*(2), 271–280.e8. https://doi.org/10.1016/j.cell.2020.02.052

Holdt, L. M., Kohlmaier, A., & Teupser, D. (2018). Molecular roles and function of circular RNAs in eukaryotic cells. *Cellular and molecular life sciences: CMLS*, *75*(6), 1071–1098. https://doi.org/10.1007/s00018-017-2688-5

Holdt, L. M., Stahringer, A., Sass, K., Pichler, G., Kulak, N. A., Wilfert, W., Kohlmaier, A., Herbst, A., Northoff, B. H., Nicolaou, A., Gäbel, G., Beutner, F., Scholz, M., Thiery, J., Musunuru, K., Krohn, K., Mann, M., & Teupser, D. (2016). Circular non-coding RNA ANRIL modulates ribosomal RNA maturation and atherosclerosis in humans. *Nature communications*, *7*, 12429. https://doi.org/10.1038/ncomms12429

Hou, H., Sun, D., & Zhang, X. (2019). The role of *MDM2* amplification and overexpression in therapeutic resistance of malignant tumors. *Cancer cell international*, *19*, 216. https://doi.org/10.1186/s12935-019-0937-4

Houseley, J., & Tollervey, D. (2010). Apparent non-canonical trans-splicing is generated by reverse transcriptase in vitro. *PloS one*, *5*(8), e12271. https://doi.org/10.1371/journal.pone.0012271

Ho-Xuan, H., Glažar, P., Latini, C., Heizler, K., Haase, J., Hett, R., Anders, M., Weichmann, F., Bruckmann, A., Van den Berg, D., Hüttelmaier, S., Rajewsky, N., Hackl, C., & Meister, G. (2020). Comprehensive analysis of translation from overexpressed circular RNAs reveals pervasive translation from linear transcripts. *Nucleic acids research*, *48*(18), 10368–10382. https://doi.org/10.1093/nar/gkaa704

Hoy S. M. (2018). Patisiran: First Global Approval. *Drugs*, *78*(15), 1625–1631. https://doi.org/10.1007/s40265-018-0983-6

Hu, B., Guo, H., Zhou, P., & Shi, Z. L. (2021). Characteristics of SARS-CoV-2 and COVID-19. *Nature reviews. Microbiology*, *19*(3), 141–154. https://doi.org/10.1038/s41579-020-00459-7

Huang, C., Liang, D., Tatomer, D. C., & Wilusz, J. E. (2018). A length-dependent evolutionarily conserved pathway controls nuclear export of circular RNAs. *Genes & development*, *32*(9-10), 639–644. https://doi.org/10.1101/gad.314856.118

Ivanov, A., Memczak, S., Wyler, E., Torti, F., Porath, H. T., Orejuela, M. R., Piechotta, M., Levanon, E. Y., Landthaler, M., Dieterich, C., & Rajewsky, N. (2015). Analysis of intron sequences reveals hallmarks of circular RNA biogenesis in animals. *Cell reports*, *10*(2), 170–177. https://doi.org/10.1016/j.celrep.2014.12.019

Jeck, W. R., & Sharpless, N. E. (2014). Detecting and characterizing circular RNAs. *Nature biotechnology*, *32*(5), 453–461. https://doi.org/10.1038/nbt.2890

Jeck, W. R., Sorrentino, J. A., Wang, K., Slevin, M. K., Burd, C. E., Liu, J., Marzluff, W. F., & Sharpless, N. E. (2013). Circular RNAs are abundant, conserved, and associated with ALU repeats. *RNA (New York, N.Y.)*, *19*(2), 141–157. https://doi.org/10.1261/rna.035667.112

Jin, X., Turcott, E., Englehardt, S., Mize, G. J., & Morris, D. R. (2003). The two upstream open reading frames of oncogene mdm2 have different translational regulatory properties. *The Journal of biological chemistry*, *278*(28), 25716–25721. https://doi.org/10.1074/jbc.M300316200

Jopling C. (2012). Liver-specific microRNA-122: Biogenesis and function. *RNA biology*, *9*(2), 137–142. https://doi.org/10.4161/rna.18827

Jost, I., Shalamova, L. A., Gerresheim, G. K., Niepmann, M., Bindereif, A., & Rossbach, O. (2018). Functional sequestration of microRNA-122 from Hepatitis C Virus by circular RNA sponges. *RNA biology*, *15*(8), 1032–1039. https://doi.org/10.1080/15476286.2018.1435248

Juliano R. L. (2016). The delivery of therapeutic oligonucleotides. *Nucleic acids research*, *44*(14), 6518–6548. https://doi.org/10.1093/nar/gkw236

Kaczmarkiewicz, A., Nuckowski, Ł., Studzińska, S., & Buszewski, B. (2019). Analysis of Antisense Oligonucleotides and Their Metabolites with the Use of Ion Pair Reversed-Phase Liquid Chromatography Coupled with Mass Spectrometry. *Critical reviews in analytical chemistry*, *49*(3), 256–270. https://doi.org/10.1080/10408347.2018.1517034

Khoo, B., & Krainer, A. R. (2009). Splicing therapeutics in SMN2 and APOB. *Current opinion in molecular therapeutics*, *11*(2), 108–115.

Kilani, A. F., Trang, P., Jo, S., Hsu, A., Kim, J., Nepomuceno, E., Liou, K., & Liu, F. (2000). RNase P ribozymes selected in vitro to cleave a viral mRNA effectively inhibit its expression in cell culture. *The Journal of biological chemistry*, *275*(14), 10611–10622. https://doi.org/10.1074/jbc.275.14.10611

Kilanowska, A., & Studzińska, S. (2020). *In vivo* and *in vitro* studies of antisense oligonucleotides – a review. *RSC Advances.* 10, 34501. https://doi.org/10.1039/D0RA04978F

Kim, D., Lee, J. Y., Yang, J. S., Kim, J. W., Kim, V. N., & Chang, H. (2020). The Architecture of SARS-CoV-2 Transcriptome. *Cell*, *181*(4), 914–921.e10. https://doi.org/10.1016/j.cell.2020.04.011

Kinali, M., Arechavala-Gomeza, V., Feng, L., Cirak, S., Hunt, D., Adkin, C., Guglieri, M., Ashton, E., Abbs, S., Nihoyannopoulos, P., Garralda, M. E., Rutherford, M., McCulley, C., Popplewell, L., Graham, I. R., Dickson, G., Wood, M. J., Wells, D. J., Wilton, S. D., Kole, R., … Muntoni, F. (2009). Local restoration of dystrophin expression with the morpholino oligomer AVI-4658 in Duchenne muscular dystrophy: a single-blind, placebo-controlled, dose-escalation, proof-of-concept study. *The Lancet. Neurology*, *8*(10), 918–928. https://doi.org/10.1016/S1474-4422(09)70211-X

Kjems, J., & Garrett, R. A. (1988). Novel splicing mechanism for the ribosomal RNA intron in the archaebacterium Desulfurococcus mobilis. *Cell*, *54*(5), 693–703. https://doi.org/10.1016/s0092-8674(88)80014-x

Kleaveland, B., Shi, C. Y., Stefano, J., & Bartel, D. P. (2018). A Network of Noncoding Regulatory RNAs Acts in the Mammalian Brain. *Cell*, *174*(2), 350–362.e17. https://doi.org/10.1016/j.cell.2018.05.022

Klein, C., & Vassilev, L. T. (2004). Targeting the p53-MDM2 interaction to treat cancer. *British journal of cancer*, *91*(8), 1415–1419. https://doi.org/10.1038/sj.bjc.6602164

Kos, A., Dijkema, R., Arnberg, A. C., van der Meide, P. H., & Schellekens, H. (1986). The hepatitis delta (delta) virus possesses a circular RNA. *Nature*, *323*(6088), 558–560. https://doi.org/10.1038/323558a0

Kramer, M. C., Liang, D., Tatomer, D. C., Gold, B., March, Z. M., Cherry, S., & Wilusz, J. E. (2015). Combinatorial control of Drosophila circular RNA expression by intronic repeats, hnRNPs, and SR proteins. *Genes & development*, *29*(20), 2168–2182. https://doi.org/10.1101/gad.270421.115

Kristen, A. V., Ajroud-Driss, S., Conceição, I., Gorevic, P., Kyriakides, T., & Obici, L. (2019). Patisiran, an RNAi therapeutic for the treatment of hereditary transthyretin-mediated amyloidosis. *Neurodegenerative disease management*, *9*(1), 5–23. https://doi.org/10.2217/nmt-2018-0033

Kristensen, L. S., Andersen, M. S., Stagsted, L., Ebbesen, K. K., Hansen, T. B., & Kjems, J. (2019). The biogenesis, biology and characterization of circular RNAs. *Nature reviews. Genetics*, *20*(11), 675–691. https://doi.org/10.1038/s41576-019-0158-7

Kristensen, L. S., Okholm, T., Venø, M. T., & Kjems, J. (2018). Circular RNAs are abundantly expressed and upregulated during human epidermal stem cell differentiation. *RNA biology*, *15*(2), 280–291. https://doi.org/10.1080/15476286.2017.1409931

Kruger, K., Grabowski, P. J., Zaug, A. J., Sands, J., Gottschling, D. E., & Cech, T. R. (1982). Self-splicing RNA: autoexcision and autocyclization of the ribosomal RNA intervening sequence of Tetrahymena. *Cell*, *31*(1), 147–157. https://doi.org/10.1016/0092-8674(82)90414-7

Krützfeldt, J., Rajewsky, N., Braich, R., Rajeev, K. G., Tuschl, T., Manoharan, M., & Stoffel, M. (2005). Silencing of microRNAs in vivo with 'antagomirs'. *Nature*, *438*(7068), 685–689. https://doi.org/10.1038/nature04303

Kubbutat, M. H., Jones, S. N., & Vousden, K. H. (1997). Regulation of p53 stability by Mdm2. *Nature*, *387*(6630), 299–303. https://doi.org/10.1038/387299a0

Kurreck J. (2003). Antisense technologies. Improvement through novel chemical modifications. *European journal of biochemistry*, *270*(8), 1628–1644. https://doi.org/10.1046/j.1432-1033.2003.03555.x

Lan, N., Howrey, R. P., Lee, S. W., Smith, C. A., & Sullenger, B. A. (1998). Ribozyme-mediated repair of sickle beta-globin mRNAs in erythrocyte precursors. *Science (New York, N.Y.)*, *280*(5369), 1593–1596. https://doi.org/10.1126/science.280.5369.1593

Lasda, E., & Parker, R. (2014). Circular RNAs: diversity of form and function. *RNA (New York, N.Y.)*, *20*(12), 1829–1842. https://doi.org/10.1261/rna.047126.114

Laue, M., Kauter, A., Hoffmann, T., Möller, L., Michel, J., & Nitsche, A. (2021). Morphometry of SARS-CoV and SARS-CoV-2 particles in ultrathin plastic sections of infected Vero cell cultures. *Scientific reports*, *11*(1), 3515. https://doi.org/10.1038/s41598-021-82852-7

Legnini, I., Di Timoteo, G., Rossi, F., Morlando, M., Briganti, F., Sthandier, O., Fatica, A., Santini, T., Andronache, A., Wade, M., Laneve, P., Rajewsky, N., & Bozzoni, I. (2017). Circ-ZNF609 Is a Circular RNA that Can Be Translated and Functions in Myogenesis. *Molecular cell*, *66*(1), 22–37.e9. https://doi.org/10.1016/j.molcel.2017.02.017

Lemaitre, M., Bayard, B., & Lebleu, B. (1987). Specific antiviral activity of a poly(L-lysine)-conjugated oligodeoxyribonucleotide sequence complementary to vesicular stomatitis virus N protein mRNA initiation site. *Proceedings of the National Academy of Sciences of the United States of America*, *84*(3), 648–652. https://doi.org/10.1073/pnas.84.3.648

Levin A. A. (1999). A review of the issues in the pharmacokinetics and toxicology of phosphorothioate antisense oligonucleotides. *Biochimica et biophysica acta*, *1489*(1), 69–84. https://doi.org/10.1016/s0167-4781(99)00140-2

Li, X., Liu, C. X., Xue, W., Zhang, Y., Jiang, S., Yin, Q. F., Wei, J., Yao, R. W., Yang, L., & Chen, L. L. (2017). Coordinated circRNA Biogenesis and Function with NF90/NF110 in Viral Infection. *Molecular cell*, *67*(2), 214–227.e7. https://doi.org/10.1016/j.molcel.2017.05.023

Liang, D., & Wilusz, J. E. (2014). Short intronic repeat sequences facilitate circular RNA production. *Genes & development*, *28*(20), 2233–2247. https://doi.org/10.1101/gad.251926.114

Liang, D., Tatomer, D. C., Luo, Z., Wu, H., Yang, L., Chen, L. L., Cherry, S., & Wilusz, J. E. (2017). The Output of Protein-Coding Genes Shifts to Circular RNAs When the Pre-mRNA Processing Machinery Is Limiting. *Molecular cell*, *68*(5), 940–954.e3. https://doi.org/10.1016/j.molcel.2017.10.034

Liang, X. H., Shen, W., Sun, H., Migawa, M. T., Vickers, T. A., & Crooke, S. T. (2016). Translation efficiency of mRNAs is increased by antisense oligonucleotides targeting upstream open reading frames. *Nature biotechnology*, *34*(8), 875–880. https://doi.org/10.1038/nbt.3589

Litke, J. L., & Jaffrey, S. R. (2019). Highly efficient expression of circular RNA aptamers in cells using autocatalytic transcripts. *Nature biotechnology*, *37*(6), 667–675. https://doi.org/10.1038/s41587-019-0090-6

Liu, C., Yao, M. D., Li, C. P., Shan, K., Yang, H., Wang, J. J., Liu, B., Li, X. M., Yao, J., Jiang, Q., & Yan, B. (2017). Silencing Of Circular RNA-ZNF609 Ameliorates Vascular Endothelial Dysfunction. *Theranostics*, *7*(11), 2863–2877. https://doi.org/10.7150/thno.19353

Lobue, P. A., Jora, M., Addepalli, B., & Limbach, P. A. (2019). Oligonucleotide analysis by hydrophilic interaction liquid chromatography-mass spectrometry in the absence of ion-pair reagents. *Journal of chromatography. A*, *1595*, 39–48. https://doi.org/10.1016/j.chroma.2019.02.016

Lu, Z., Filonov, G. S., Noto, J. J., Schmidt, C. A., Hatkevich, T. L., Wen, Y., Jaffrey, S. R., & Matera, A. G. (2015). Metazoan tRNA introns generate stable circular RNAs in vivo. *RNA (New York, N.Y.)*, *21*(9), 1554–1565. https://doi.org/10.1261/rna.052944.115

Marine, J. C., & Lozano, G. (2010). Mdm2-mediated ubiquitylation: p53 and beyond. *Cell death and differentiation*, *17*(1), 93–102. https://doi.org/10.1038/cdd.2009.68

Matranga, C., Tomari, Y., Shin, C., Bartel, D. P., & Zamore, P. D. (2005). Passenger-strand cleavage facilitates assembly of siRNA into Ago2-containing RNAi enzyme complexes. *Cell*, *123*(4), 607–620. https://doi.org/10.1016/j.cell.2005.08.044

McCann, A. H., Kirley, A., Carney, D. N., Corbally, N., Magee, H. M., Keating, G., & Dervan, P. A. (1995). Amplification of the MDM2 gene in human breast cancer and its association with MDM2 and p53 protein status. *British journal of cancer*, *71*(5), 981–985. https://doi.org/10.1038/bjc.1995.189

Memczak, S., Jens, M., Elefsinioti, A., Torti, F., Krueger, J., Rybak, A., Maier, L., Mackowiak, S. D., Gregersen, L. H., Munschauer, M., Loewer, A., Ziebold, U., Landthaler, M., Kocks, C., le Noble, F., & Rajewsky, N. (2013). Circular RNAs are a large class of animal RNAs with regulatory potency. *Nature*, *495*(7441), 333–338. https://doi.org/10.1038/nature11928

Memczak, S., Papavasileiou, P., Peters, O., & Rajewsky, N. (2015). Identification and Characterization of Circular RNAs As a New Class of Putative Biomarkers in Human Blood. *PloS one*, *10*(10), e0141214. https://doi.org/10.1371/journal.pone.0141214

Michienzi, A., Castanotto, D., Lee, N., Li, S., Zaia, J. A., & Rossi, J. J. (2003). RNA-mediated inhibition of HIV in a gene therapy setting. *Annals of the New York Academy of Sciences*, *1002*, 63–71. https://doi.org/10.1196/annals.1281.008

Molina-Sánchez, M. D., Martinez-Abarca, F., & Toro, N. (2006). Excision of the Sinorhizobium meliloti group II intron RmInt1 as circles in vivo. *The Journal of biological chemistry*, *281*(39), 28737–28744. https://doi.org/10.1074/jbc.M602695200

Momand, J., Wu, H. H., & Dasgupta, G. (2000). MDM2--master regulator of the p53 tumor suppressor protein. *Gene*, *242*(1-2), 15–29. https://doi.org/10.1016/s0378-1119(99)00487-4

Momand, J., Zambetti, G. P., Olson, D. C., George, D., & Levine, A. J. (1992). The mdm-2 oncogene product forms a complex with the p53 protein and inhibits p53-mediated transactivation. *Cell*, *69*(7), 1237–1245. https://doi.org/10.1016/0092-8674(92)90644-r

Mulamba, G. B., Hu, A., Azad, R. F., Anderson, K. P., & Coen, D. M. (1998). Human cytomegalovirus mutant with sequence-dependent resistance to the phosphorothioate oligonucleotide fomivirsen (ISIS 2922). *Antimicrobial agents and chemotherapy*, *42*(4), 971–973. https://doi.org/10.1128/AAC.42.4.971

Müller, S., & Appel, B. (2017). In vitro circularization of RNA. *RNA biology*, *14*(8), 1018–1027. https://doi.org/10.1080/15476286.2016.1239009

Müller-Höcker, J., Zietz, C. H., & Sendelhofert, A. (2001). Deregulated expression of cell cycle-associated proteins in solid pseudopapillary tumor of the pancreas. *Modern pathology : an official journal of the United States and Canadian Academy of Pathology, Inc*, *14*(2), 47–53. https://doi.org/10.1038/modpathol.3880255

Nag, S., Zhang, X., Srivenugopal, K. S., Wang, M. H., Wang, W., & Zhang, R. (2014). Targeting MDM2-p53 interaction for cancer therapy: are we there yet? *Current medicinal chemistry*, *21*(5), 553–574. https://doi.org/10.2174/09298673113206660325

Nasevicius, A., & Ekker, S. C. (2000). Effective targeted gene 'knockdown' in zebrafish. *Nature genetics*, *26*(2), 216–220. https://doi.org/10.1038/79951

Neuman, B. W., Stein, D. A., Kroeker, A. D., Churchill, M. J., Kim, A. M., Kuhn, P., Dawson, P., Moulton, H. M., Bestwick, R. K., Iversen, P. L., & Buchmeier, M. J. (2005). Inhibition, escape, and attenuated growth of severe acute respiratory syndrome coronavirus treated with antisense morpholino oligomers. *Journal of virology*, *79*(15), 9665–9676. https://doi.org/10.1128/JVI.79.15.9665-9676.2005

Nielsen, H., Fiskaa, T., Birgisdottir, A. B., Haugen, P., Einvik, C., & Johansen, S. (2003). The ability to form full-length intron RNA circles is a general property of nuclear group I introns. *RNA (New York, N.Y.)*, *9*(12), 1464–1475. https://doi.org/10.1261/rna.5290903

Nigro, J. M., Cho, K. R., Fearon, E. R., Kern, S. E., Ruppert, J. M., Oliner, J. D., Kinzler, K. W., & Vogelstein, B. (1991). Scrambled exons. *Cell*, *64*(3), 607–613. https://doi.org/10.1016/0092-8674(91)90244-s

Noto, J. J., Schmidt, C. A., & Matera, A. G. (2017). Engineering and expressing circular RNAs via tRNA splicing. *RNA biology*, *14*(8), 978–984. https://doi.org/10.1080/15476286.2017.1317911

Oliner, J. D., Pietenpol, J. A., Thiagalingam, S., Gyuris, J., Kinzler, K. W., & Vogelstein, B. (1993). Oncoprotein MDM2 conceals the activation domain of tumour suppressor p53. *Nature*, *362*(6423), 857–860. https://doi.org/10.1038/362857a0

Osman, I., Drobnjak, M., Fazzari, M., Ferrara, J., Scher, H. I., & Cordon-Cardo, C. (1999). Inactivation of the p53 pathway in prostate cancer: impact on tumor progression. *Clinical cancer research : an official journal of the American Association for Cancer Research*, *5*(8), 2082–2088.

Pamudurti, N. R., Bartok, O., Jens, M., Ashwal-Fluss, R., Stottmeister, C., Ruhe, L., Hanan, M., Wyler, E., Perez-Hernandez, D., Ramberger, E., Shenzis, S., Samson, M., Dittmar, G., Landthaler, M., Chekulaeva, M., Rajewsky, N., & Kadener, S. (2017). Translation of CircRNAs. *Molecular cell*, *66*(1), 9–21.e7. https://doi.org/10.1016/j.molcel.2017.02.021

Passini, M. A., Bu, J., Richards, A. M., Kinnecom, C., Sardi, S. P., Stanek, L. M., Hua, Y., Rigo, F., Matson, J., Hung, G., Kaye, E. M., Shihabuddin, L. S., Krainer, A. R., Bennett, C. F., & Cheng, S. H. (2011). Antisense oligonucleotides delivered to the mouse CNS ameliorate symptoms of severe spinal muscular atrophy. *Science translational medicine*, *3*(72), 72ra18. https://doi.org/10.1126/scitranslmed.3001777

Peebles, C. L., Gegenheimer, P., & Abelson, J. (1983). Precise excision of intervening sequences from precursor tRNAs by a membrane-associated yeast endonuclease. *Cell*, *32*(2), 525–536. https://doi.org/10.1016/0092-8674(83)90472-5

Peracchi A. (2004). Prospects for antiviral ribozymes and deoxyribozymes. *Reviews in medical virology*, *14*(1), 47–64. https://doi.org/10.1002/rmv.415

Perlman, S., & Masters, PS. (2021). Coronaviridae: The viruses and their replication, p 410-448. In Howley PM, Knipe DM, Whelan S (ed), Fields Virology, 7th ed, vol 1. Wolters Kluwer, Philadelphia, PA.

Perlman, S., & Netland, J. (2009). Coronaviruses post-SARS: update on replication and pathogenesis. *Nature reviews. Microbiology*, *7*(6), 439–450. https://doi.org/10.1038/nrmicro2147

Perriman, R., & Ares, M., Jr (1998). Circular mRNA can direct translation of extremely long repeating-sequence proteins in vivo. *RNA (New York, N.Y.)*, *4*(9), 1047–1054. https://doi.org/10.1017/s135583829898061x

Petkovic, S., & Müller, S. (2015). RNA circularization strategies in vivo and in vitro. *Nucleic acids research*, *43*(4), 2454–2465. https://doi.org/10.1093/nar/gkv045

Pfafenrot, C., Schneider, T., Müller, C., Hung, L. H., Schreiner, S., Ziebuhr, J., & Bindereif, A. (2021). Inhibition of SARS-CoV-2 coronavirus proliferation by designer antisense-circRNAs. *Nucleic acids research*, *49*(21), 12502–12516. https://doi.org/10.1093/nar/gkab1096

Piwecka, M., Glažar, P., Hernandez-Miranda, L. R., Memczak, S., Wolf, S. A., Rybak-Wolf, A., Filipchyk, A., Klironomos, F., Cerda Jara, C. A., Fenske, P., Trimbuch, T., Zywitza, V., Plass, M., Schreyer, L., Ayoub, S., Kocks, C., Kühn, R., Rosenmund, C., Birchmeier, C., & Rajewsky, N. (2017). Loss of a mammalian circular RNA locus causes miRNA deregulation and affects brain function. *Science (New York, N.Y.)*, *357*(6357), eaam8526. https://doi.org/10.1126/science.aam8526

Polack, F. P., Thomas, S. J., Kitchin, N., Absalon, J., Gurtman, A., Lockhart, S., Perez, J. L., Pérez Marc, G., Moreira, E. D., Zerbini, C., Bailey, R., Swanson, K. A., Roychoudhury, S., Koury, K., Li, P., Kalina, W. V., Cooper, D., Frenck, R. W., Jr, Hammitt, L. L., Türeci, Ö., … C4591001 Clinical Trial Group (2020). Safety and Efficacy of the BNT162b2 mRNA Covid-19 Vaccine. *The New England journal of medicine*, *383*(27), 2603–2615. https://doi.org/10.1056/NEJMoa2034577

Porensky, P. N., & Burghes, A. H. (2013). Antisense oligonucleotides for the treatment of spinal muscular atrophy. *Human gene therapy*, *24*(5), 489–498. https://doi.org/10.1089/hum.2012.225

Preußer, C., & Bindereif, A. (2013). Exo-endo trans splicing: a new way to link. *Cell research*, *23*(9), 1071–1072. https://doi.org/10.1038/cr.2013.105

Preußer, C., Hung, L. H., Schneider, T., Schreiner, S., Hardt, M., Moebus, A., Santoso, S., & Bindereif, A. (2018). Selective release of circRNAs in platelet-derived extracellular vesicles. *Journal of extracellular vesicles*, *7*(1), 1424473. https://doi.org/10.1080/20013078.2018.1424473

Qu, S., Liu, Z., Yang, X., Zhou, J., Yu, H., Zhang, R., & Li, H. (2018). The emerging functions and roles of circular RNAs in cancer. *Cancer letters*, *414*, 301–309. https://doi.org/10.1016/j.canlet.2017.11.022

Rand, T. A., Petersen, S., Du, F., & Wang, X. (2005). Argonaute2 cleaves the anti-guide strand of siRNA during RISC activation. *Cell*, *123*(4), 621–629. https://doi.org/10.1016/j.cell.2005.10.020

Roberts, T. C., Langer, R., & Wood, M. (2020). Advances in oligonucleotide drug delivery. *Nature reviews. Drug discovery*, *19*(10), 673–694. https://doi.org/10.1038/s41573-020-0075-7

Rocha, N. A., East, C., Zhang, J., & McCullough, P. A. (2017). ApoCIII as a Cardiovascular Risk Factor and Modulation by the Novel Lipid-Lowering Agent Volanesorsen. *Current atherosclerosis reports*, *19*(12), 62. https://doi.org/10.1007/s11883-017-0697-3

Roth, A., Weinberg, Z., Chen, A. G., Kim, P. B., Ames, T. D., & Breaker, R. R. (2014). A widespread self-cleaving ribozyme class is revealed by bioinformatics. *Nature chemical biology*, *10*(1), 56–60. https://doi.org/10.1038/nchembio.1386

Rüger, J., Ioannou, S., Castanotto, D., & Stein, C. A. (2020). Oligonucleotides to the (Gene) Rescue: FDA Approvals 2017-2019. *Trends in pharmacological sciences*, *41*(1), 27–41. https://doi.org/10.1016/j.tips.2019.10.009

Rybak-Wolf, A., Stottmeister, C., Glažar, P., Jens, M., Pino, N., Giusti, S., Hanan, M., Behm, M., Bartok, O., Ashwal-Fluss, R., Herzog, M., Schreyer, L., Papavasileiou, P., Ivanov, A., Öhman, M., Refojo, D., Kadener, S., & Rajewsky, N. (2015). Circular RNAs in the Mammalian Brain Are Highly Abundant, Conserved, and Dynamically Expressed. *Molecular cell*, *58*(5), 870–885. https://doi.org/10.1016/j.molcel.2015.03.027

Salzman, J., Chen, R. E., Olsen, M. N., Wang, P. L., & Brown, P. O. (2013). Cell-type specific features of circular RNA expression. *PLoS genetics*, *9*(9), e1003777. https://doi.org/10.1371/journal.pgen.1003777

Salzman, J., Gawad, C., Wang, P. L., Lacayo, N., & Brown, P. O. (2012). Circular RNAs are the predominant transcript isoform from hundreds of human genes in diverse cell types. *PloS one*, *7*(2), e30733. https://doi.org/10.1371/journal.pone.0030733

Sanger, H. L., Klotz, G., Riesner, D., Gross, H. J., & Kleinschmidt, A. K. (1976). Viroids are single-stranded covalently closed circular RNA molecules existing as highly base-paired rod-like structures. *Proceedings of the National Academy of Sciences of the United States of America*, *73*(11), 3852–3856. https://doi.org/10.1073/pnas.73.11.3852

Schmidt, C. A., Noto, J. J., Filonov, G. S., & Matera, A. G. (2016). A Method for Expressing and Imaging Abundant, Stable, Circular RNAs In Vivo Using tRNA Splicing. *Methods in enzymology*, *572*, 215–236. https://doi.org/10.1016/bs.mie.2016.02.018

Schneider, T., & Bindereif, A. (2017). Circular RNAs: Coding or noncoding? *Cell research*, *27*(6), 724–725. https://doi.org/10.1038/cr.2017.70

Schneider, T., Schreiner, S., Preußer, C., Bindereif, A., & Rossbach, O. (2018). Northern Blot Analysis of Circular RNAs. *Methods in molecular biology (Clifton, N.J.)*, *1724*, 119–133. https://doi.org/10.1007/978-1-4939-7562-4_10

Schreiner, S., Didio, A., Hung, L. H., & Bindereif, A. (2020). Design and application of circular RNAs with protein-sponge function. *Nucleic acids research*, *48*(21), 12326–12335. https://doi.org/10.1093/nar/gkaa1085

Schubert, S., & Kurreck, J. (2004). Ribozyme- and deoxyribozyme-strategies for medical applications. *Current drug targets*, *5*(8), 667–681. https://doi.org/10.2174/1389450043345092

Scott L. J. (2020). Givosiran: First Approval. *Drugs*, *80*(3), 335–339. https://doi.org/10.1007/s40265-020-01269-0

Sebastián-Martín, A., Barrioluengo, V., & Menéndez-Arias, L. (2018). Transcriptional inaccuracy threshold attenuates differences in RNA-dependent DNA synthesis fidelity between retroviral reverse transcriptases. *Scientific reports*, *8*(1), 627. https://doi.org/10.1038/s41598-017-18974-8

Shi Y. (2017). Mechanistic insights into precursor messenger RNA splicing by the spliceosome. *Nature reviews. Molecular cell biology*, *18*(11), 655–670. https://doi.org/10.1038/nrm.2017.86

Sohail, M., & Southern, E. M. (2000). Selecting optimal antisense reagents. *Advanced drug delivery reviews*, *44*(1), 23–34. https://doi.org/10.1016/s0169-409x(00)00081-8

Soma, A., Onodera, A., Sugahara, J., Kanai, A., Yachie, N., Tomita, M., Kawamura, F., & Sekine, Y. (2007). Permuted tRNA genes expressed via a circular RNA intermediate in Cyanidioschyzon merolae. *Science (New York, N.Y.)*, *318*(5849), 450–453. https://doi.org/10.1126/science.1145718

Stagsted, L. V., Nielsen, K. M., Daugaard, I., & Hansen, T. B. (2019). Noncoding AUG circRNAs constitute an abundant and conserved subclass of circles. *Life science alliance*, *2*(3), e201900398. https://doi.org/10.26508/lsa.201900398

Starke, S., Jost, I., Rossbach, O., Schneider, T., Schreiner, S., Hung, L. H., & Bindereif, A. (2015). Exon circularization requires canonical splice signals. *Cell reports*, *10*(1), 103–111. https://doi.org/10.1016/j.celrep.2014.12.002

Stephenson, M. L., & Zamecnik, P. C. (1978). Inhibition of Rous sarcoma viral RNA translation by a specific oligodeoxyribonucleotide. *Proceedings of the National Academy of Sciences of the United States of America*, *75*(1), 285–288. https://doi.org/10.1073/pnas.75.1.285

Studzińska, S., Rola, R., & Buszewski, B. (2017). The impact of ion-pairing reagents on the selectivity and sensitivity in the analysis of modified oligonucleotides in serum samples by liquid chromatography coupled with tandem mass spectrometry. *Journal of pharmaceutical and biomedical analysis*, *138*, 146–152. https://doi.org/10.1016/j.jpba.2017.02.014

Sullenger, B. A., & Gilboa, E. (2002). Emerging clinical applications of RNA. *Nature*, *418*(6894), 252–258. https://doi.org/10.1038/418252a

Summerton J. (1999). Morpholino antisense oligomers: the case for an RNase H-independent structural type. *Biochimica et biophysica acta*, *1489*(1), 141–158. https://doi.org/10.1016/s0167-4781(99)00150-5

Sureau, C., & Negro, F. (2016). The hepatitis delta virus: Replication and pathogenesis. *Journal of hepatology*, *64*(1 Suppl), S102–S116. https://doi.org/10.1016/j.jhep.2016.02.013

Tatomer, D. C., & Wilusz, J. E. (2017). An Unchartered Journey for Ribosomes: Circumnavigating Circular RNAs to Produce Proteins. *Molecular cell*, *66*(1), 1–2. https://doi.org/10.1016/j.molcel.2017.03.011

Uhlmann E., & Peyman A. (1990). Antisense oligonucleotides: a new therapeutic principle. *Chemical Reviews*, 90, 4, 543–584 https://doi.org/10.1021/cr00102a001

Ulshöfer, C. J., Pfafenrot, C., Bindereif, A., & Schneider, T. (2021). Methods to study circRNA-protein interactions. *Methods (San Diego, Calif.)*, *196*, 36–46. https://doi.org/10.1016/j.ymeth.2021.04.014

Urban, E., & Noe, C. R. (2003). Structural modifications of antisense oligonucleotides. *Farmaco (Societa chimica italiana : 1989)*, *58*(3), 243–258. https://doi.org/10.1016/S0014-827X(03)00022-3

Vassilev L. T. (2004). Small-molecule antagonists of p53-MDM2 binding: research tools and potential therapeutics. *Cell cycle (Georgetown, Tex.)*, *3*(4), 419–421.

Vattem, K. M., & Wek, R. C. (2004). Reinitiation involving upstream ORFs regulates ATF4 mRNA translation in mammalian cells. *Proceedings of the National Academy of Sciences of the United States of America*, *101*(31), 11269–11274. https://doi.org/10.1073/pnas.0400541101

Vitravene Study Group (2002). A randomized controlled clinical trial of intravitreous fomivirsen for treatment of newly diagnosed peripheral cytomegalovirus retinitis in patients with AIDS. *American journal of ophthalmology*, *133*(4), 467–474. https://doi.org/10.1016/s0002-9394(02)01327-2

Wade, M., Li, Y. C., & Wahl, G. M. (2013). MDM2, MDMX and p53 in oncogenesis and cancer therapy. *Nature reviews. Cancer*, *13*(2), 83–96. https://doi.org/10.1038/nrc3430

Wahl, M. C., Will, C. L., & Lührmann, R. (2009). The spliceosome: design principles of a dynamic RNP machine. *Cell*, *136*(4), 701–718. https://doi.org/10.1016/j.cell.2009.02.009

Wang, K., Long, B., Liu, F., Wang, J. X., Liu, C. Y., Zhao, B., Zhou, L. Y., Sun, T., Wang, M., Yu, T., Gong, Y., Liu, J., Dong, Y. H., Li, N., & Li, P. F. (2016). A circular RNA protects the heart from pathological hypertrophy and heart failure by targeting miR-223. *European heart journal*, *37*(33), 2602–2611. https://doi.org/10.1093/eurheartj/ehv713

Wang, Y., & Wang, Z. (2015). Efficient backsplicing produces translatable circular mRNAs. *RNA (New York, N.Y.)*, *21*(2), 172–179. https://doi.org/10.1261/rna.048272.114

Weiner, A. J., Choo, Q. L., Wang, K. S., Govindarajan, S., Redeker, A. G., Gerin, J. L., & Houghton, M. (1988). A single antigenomic open reading frame of the hepatitis delta virus encodes the epitope(s) of both hepatitis delta antigen polypeptides p24 delta and p27 delta. *Journal of virology*, *62*(2), 594–599. https://doi.org/10.1128/JVI.62.2.594-599.1988

Wesselhoeft, R. A., Kowalski, P. S., & Anderson, D. G. (2018). Engineering circular RNA for potent and stable translation in eukaryotic cells. *Nature communications*, *9*(1), 2629. https://doi.org/10.1038/s41467-018-05096-6

Westholm, J. O., Miura, P., Olson, S., Shenker, S., Joseph, B., Sanfilippo, P., Celniker, S. E., Graveley, B. R., & Lai, E. C. (2014). Genome-wide analysis of drosophila circular RNAs reveals their structural and sequence properties and age-dependent neural accumulation. *Cell reports*, *9*(5), 1966–1980. https://doi.org/10.1016/j.celrep.2014.10.062

Wilusz J. E. (2018). A 360° view of circular RNAs: From biogenesis to functions. *Wiley interdisciplinary reviews. RNA*, *9*(4), e1478. https://doi.org/10.1002/wrna.1478

Wright, L., & Kearney, P. (2001). Current status of ribozymes as gene therapy agents for cancer. *Cancer investigation*, *19*(5), 495–509. https://doi.org/10.1081/cnv-100103848

Wu, H., Lima, W. F., & Crooke, S. T. (1999). Properties of cloned and expressed human RNase H1. *The Journal of biological chemistry*, *274*(40), 28270–28278. https://doi.org/10.1074/jbc.274.40.28270

Yang, Y., Fan, X., Mao, M., Song, X., Wu, P., Zhang, Y., Jin, Y., Yang, Y., Chen, L. L., Wang, Y., Wong, C. C., Xiao, X., & Wang, Z. (2017). Extensive translation of circular RNAs driven by N^6-methyladenosine. *Cell research*, *27*(5), 626–641. https://doi.org/10.1038/cr.2017.31

You, X., Vlatkovic, I., Babic, A., Will, T., Epstein, I., Tushev, G., Akbalik, G., Wang, M., Glock, C., Quedenau, C., Wang, X., Hou, J., Liu, H., Sun, W., Sambandan, S., Chen, T., Schuman, E. M., & Chen, W. (2015). Neural circular RNAs are derived from synaptic genes and regulated by development and plasticity. *Nature neuroscience*, *18*(4), 603–610. https://doi.org/10.1038/nn.3975

Zamecnik, P. C., & Stephenson, M. L. (1978). Inhibition of Rous sarcoma virus replication and cell transformation by a specific oligodeoxynucleotide. *Proceedings of the National Academy of Sciences of the United States of America*, *75*(1), 280–284. https://doi.org/10.1073/pnas.75.1.280

Zaphiropoulos P. G. (1996). Circular RNAs from transcripts of the rat cytochrome P450 2C24 gene: correlation with exon skipping. *Proceedings of the National Academy of Sciences of the United States of America*, *93*(13), 6536–6541. https://doi.org/10.1073/pnas.93.13.6536

Zeng, X., Lin, W., Guo, M., & Zou, Q. (2017). A comprehensive overview and evaluation of circular RNA detection tools. *PLoS computational biology*, *13*(6), e1005420. https://doi.org/10.1371/journal.pcbi.1005420

Zhang, W., Leighl, N., Zawisza, D., Moore, M. J., & Chen, E. X. (2005). Determination of GTI-2040, a novel antisense oligonucleotide, in human plasma by using HPLC combined with solid phase and liquid-liquid extractions. *Journal of chromatography. B, Analytical technologies in the biomedical and life sciences*, *829*(1-2), 45–49. https://doi.org/10.1016/j.jchromb.2005.09.036

Zhang, X. O., Dong, R., Zhang, Y., Zhang, J. L., Luo, Z., Zhang, J., Chen, L. L., & Yang, L. (2016 a). Diverse alternative back-splicing and alternative splicing landscape of circular RNAs. *Genome research*, *26*(9), 1277–1287. https://doi.org/10.1101/gr.202895.115

Zhang, X. O., Wang, H. B., Zhang, Y., Lu, X., Chen, L. L., & Yang, L. (2014). Complementary sequence-mediated exon circularization. *Cell*, *159*(1), 134–147. https://doi.org/10.1016/j.cell.2014.09.001

Zhang, X., Goel, V., & Robbie, G. J. (2019). Pharmacokinetics of Patisiran, the First Approved RNA Interference Therapy in Patients With Hereditary Transthyretin-Mediated Amyloidosis. *Journal of clinical pharmacology*, *60*(5), 573–585. Advance online publication. https://doi.org/10.1002/jcph.1553

Zhang, Y., Xue, W., Li, X., Zhang, J., Chen, S., Zhang, J. L., Yang, L., & Chen, L. L. (2016 b). The Biogenesis of Nascent Circular RNAs. *Cell reports*, *15*(3), 611–624. https://doi.org/10.1016/j.celrep.2016.03.058

Zhang, Y., Zhang, X. O., Chen, T., Xiang, J. F., Yin, Q. F., Xing, Y. H., Zhu, S., Yang, L., & Chen, L. L. (2013). Circular intronic long noncoding RNAs. *Molecular cell*, *51*(6), 792–806. https://doi.org/10.1016/j.molcel.2013.08.017

Zheng, Q., Bao, C., Guo, W., Li, S., Chen, J., Chen, B., Luo, Y., Lyu, D., Li, Y., Shi, G., Liang, L., Gu, J., He, X., & Huang, S. (2016). Circular RNA profiling reveals an abundant circHIPK3 that regulates cell growth by sponging multiple miRNAs. *Nature communications*, *7*, 11215. https://doi.org/10.1038/ncomms11215

Zimmermann, A., Greco, R., Walker, I., Horak, J., Cavazzini, A., & Lämmerhofer, M. (2014). Synthetic oligonucleotide separations by mixed-mode reversed-phase/weak anion-exchange liquid chromatography. *Journal of chromatography. A*, *1354*, 43–55. https://doi.org/10.1016/j.chroma.2014.05.048

Biomolecular Detection and Quantification 17 (2019) 100085

Contents lists available at ScienceDirect

Biomolecular Detection and Quantification

journal homepage: www.elsevier.com/locate/bdq

Short Communication

Establishing essential quality criteria for the validation of circular RNAs as biomarkers

Christina Pfafenrot, Christian Preußer*

Institute of Biochemistry, Justus Liebig University of Giessen, D-35392 Giessen, Germany

ARTICLE INFO

Handled by Guest Editor Chennai

Keywords:
Non-coding RNA
Circular RNA
Biomarker

ABSTRACT

Non-coding RNAs were established in the last decade as a new valuable biomarker class for human diseases. Specifically, circular RNAs (circRNAs) were only recently discovered as a new large group of non-coding RNAs that, due to their circular configuration, are metabolically more stable compared to their linear counterparts and therefore highly suitable for biomarker use. Based on high-throughput sequencing, the catalogs of endogenous circRNAs with disease relevance and correlation continue to grow steadily. As a consequence, circRNAs emerged as novel and attractive biomarkers, indicated by numerous recent publications. Here we would like to stress the need of essential quality criteria for validation and characterization of circular RNAs. In addition to high-throughput sequencing, classical biochemical methods are essential and should be applied for the characterization of this special class of RNAs, in particular to convincingly confirm their circularity.

The rapid evolution of next generation sequencing technologies resulted in the nearly exponential development of putative RNA biomarkers in recent years. In particular, different classes of non-coding RNAs (ncRNA) appear promising for a wide range of clinical applications. This is also reflected in the so-called “Non-coding RNA revolution” [1] and the current focus in non-coding RNA research on investigating the underlying global RNA networks within cells, tissues, or organisms. As a relatively new class of ncRNA biomarkers, circular RNAs (circRNAs) have come more into focus within the last decade (Fig. 1). Although single examples of these particular RNA species had been known for more than forty years [2], circRNAs were established as a large RNA class only a few years ago, based on high-throughput sequencing and bioinformatics [3]. CircRNAs derived from pre-mRNAs (in some cases also from pre-ncRNAs) are characterized by a covalently closed loop structure, which is generated by a special mode of alternative splicing of pre-mRNAs, also called “backsplicing”: A 5′ splice site is joined to an upstream instead of a downstream 3′ splice site (Fig. 2). Some studies also showed that constitutive splice signals as well as the canonical splicing machinery are involved in circularization [4,5]. The average size of a circRNAs can range from under 100 nts to over 4 kb in which the commonly observed circular RNAs consist of 2–3 exons with internal introns removed [6]. Furthermore, circRNA biogenesis can be promoted by *cis*-elements and *trans*-factors by bringing the corresponding splice sites in close proximity, resulting in circularization [7]. In addition to this major, exon-type circRNAs, there are also circular intronic RNAs (ciRNAs) and exon-intron circular RNAs (EIciRNAs) [6]. Although a defined function of circRNAs is still under debate, some studies revealed a microRNA sponge function of naturally occurring circRNAs like ciRS-7 and SRY [8,9]. In addition, several other, hypothetical roles have been discussed, such as templates for translation into peptides or proteins, protein sponging, allostery, scaffold functions in RNA-protein complex assembly, or antisense activity. CircRNAs are cell type-specifically expressed and, due to their structure, very stable compared to their linear counterparts [9]. Because of these biological properties and the correlation with various human diseases, including cardiovascular diseases [10,11], disorders of the nervous system [12,13], diabetic retinopathy [14] and cancer [15], it becomes clear that circRNAs may play an important role as specific biomarkers. Since circRNAs are also found in extracellular vesicles circulating in various body fluids such as blood and saliva this should greatly extend the potential of circRNAs as prognostic and diagnostic biomarkers, especially for liquid biopsies. Specifically, RNA-Seq reads spanning the backsplice junction allow the genome-wide bioinformatic identification of circRNAs. However, we observe a certain amount of different and facile approaches to unequivocally prove circularity of this important ncRNA class. This comprises all stages of circRNA identification, ranging from RNA-Seq approaches, bioinformatics, to biochemical validation. Here we would like to stress that stringent quality criteria have to be defined, which distinguish real circular configuration from possible artifacts.

* Corresponding author.
E-mail address: christian.preusser@chemie.bio.uni-giessen.de (C. Preußer).

https://doi.org/10.1016/j.bdq.2019.100085
Received 1 November 2018; Received in revised form 4 February 2019; Accepted 5 March 2019

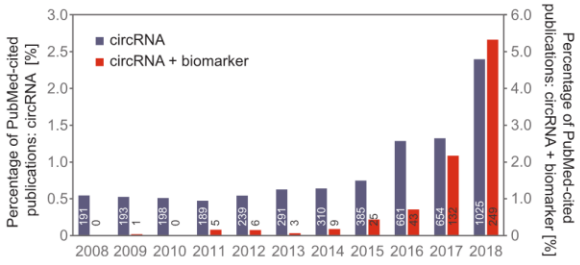

Fig. 1. Circular RNA as emerging novel biomarkers. The rapid development of circRNA research and circRNA in combination with biomarkers can be inferred from the percentage of PubMed-cited publications (https://www.ncbi.nlm.nih.gov/pubmed) using *circular RNA* (blue graphs) and *circular RNA + biomarker* (red graphs) as keywords in searches, of publications using the general terms *RNA* and *RNA + biomarker* as keywords, for publications between 2008 and 2018. The number inside the bars represents the absolute number of publications.

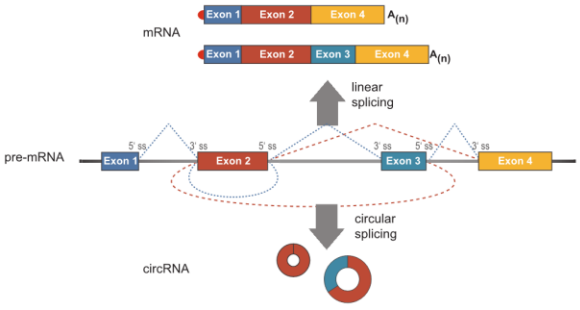

Fig. 2. Biogenesis of circular RNAs (circRNAs). Schematic representation of the biogenesis of linear mRNA and circular RNA. During canonical splicing, introns are removed and exons are joined with each other, generating either a single mRNA from the pre-mRNA (constitutive splicing) or several splice variants (alternative splicing). CircRNAs are generated by an alternative splicing mechanism, also referred to as backsplicing, in which a 5′ splice site (5′ ss) is joined to an upstream 3′ splice site (3′ ss) instead of a downstream 3′ ss. Different splice variants can be generated by alternative backsplicing resulting in single- or multi-exonic circular RNAs (circRNAs). Exons are depicted as colored boxes and introns as solid lines. The 5′ cap structure of mRNA is shown as red dots and the 3′ poly(A) tail as A(n). Constitutive (blue) and alternative splicing (red) is indicated by dashed lines.

Already the initial stage of identification of novel circRNAs requires the establishment and standardization of unbiased approaches. Several things have to be considered: The RNA integrity is critical, since neither RT-PCR might detect circRNAs molecules nor other methods such as Northern blotting, since the characteristic circular junction might get lost during partial degradation [16]. Even the choice of library preparation itself has a strong impact on the results. In particular, one of the first fundamental steps during RNA-Seq library preparation is crucial, namely the reverse transcription. Most of the reverse transcriptases used are known to be error prone and can frequently introduce mutations, which have been widely recognized [17]. As a result, aberrant *trans*-splicing products can be generated during reverse transcription, mainly based on a template-switching activity of some enzymes [18,19]. This phenomenon can also occur in the case of linear transcripts, but in particular for circRNAs can easily result in misinterpretations.

In addition, endogenous *trans*-spliced transcripts can lead to false positive events. In particular, duplicated exon sequences within one mRNA (intragenic *trans* splicing) or transcripts derived from different genes on different chromosomes (intergenic *trans* splicing) can be detected and result in false positive events [20]. Another critical step during library preparation is that most of the commercially available RNA-Seq library kits are designed to analyze either the RNA profile of long RNAs, such as mRNA and lncRNAs, or of small ncRNAs, for example miRNA. Again, this general limitation applies also to circRNAs. Furthermore, the library preparation from circRNAs either requires initial fragmentation to generate accessible 5′ and 3′ ends, or relies on random hexamer priming, which may result in inefficiency and/or biased representation in RNA-Seq [21]. This turns out to be especially challenging for the analysis of RNA profiles from extracellular vesicles, which primarily contain short RNAs less than 500 nts, however longer transcripts were reported as well [22,23].

After sequencing, the large number of available circRNA prediction tools can introduce additional variability. Some of them require an established annotation and some knowledge about existing exon-intron structures, while others, such as CIRI [24], rely on *de novo* assembly and thus are able to identify new backsplice junctions. These different options of evaluation tools can result in a dramatic differences between the outputs of algorithms used [21]. Referring thereto, a recent study compared 11 different circRNA detection tools on stimulated and on real datasets and could show that CIRI, CIRCexplorer and KNIFE achieved better balanced performance between their precision and sensitivity compared to other methods [25]. Nevertheless, many of these algorithms show strongly aberrant results and a high degree of false positive results, for example in relation to their resistance to RNase R treatment. These studies show that CircRNA detection tools should be treated with care, and that a combination of tools is required to make reliable predictions [21]. Therefore one should consider the combination of more than one method for the bioinformatic analysis to minimize the number of false positives.

However, from our point of view, most critical is the often neglected stringent biochemical validation of the circRNAs, which should follow the bioinformatic evaluation. Unfortunately, in many recent publications, including many on biomarker detection, this important and crucial issue is restricted to a minimum. As a method of choice, RNA-Seq and the bioinformatic analysis in combination with RT-(q)PCR approaches are employed as the only assays for validation. RT-qPCR approaches have the great advantage – in particular digital PCR- to check genome-wide data sets in a quantitative manner and represents the simplest and fastest method to detect the circularity of circRNAs. By designing divergent primer pairs relative to the circularizing exon/s, PCR products can be generated (usually 100–200 nts), which specifically include the characteristic circular splice site. Beyond the scope of this point of view, this method offers certain limitations, which are particularly relevant in the validation of circRNAs and are mainly based on the problems caused by the transcriptases as already mentioned above. One possibility to circumvent this problem is to combine the RT-PCR analysis with RNase R treatment. RNase R is a 3′ to 5′ exoribonuclease that degrades linear RNA, whereas most circRNAs are resistant due to their circular configuration. Unfortunately, relatively large circRNAs tend to be not absolutely RNase R resistant and in addition, complex secondary structures and chemical modifications in linear RNAs can influence the RNase R activity [16]. Moreover, variations in RNases R activities among different batches and manufacturers, experimental settings, as well as secondary RNA structure, might affect the efficiency of linear RNA removal as well.

To unequivocally demonstrate a circular configuration, Northern blot analysis, which is RNase R independent, should be defined as the gold standard and also as a method of choice (for details on the method, see [26]). Although this classic type of RNA analysis is often neglected because it is somewhat more time-consuming and requires some practical experience, Northern blotting is greatly versatile and thereby ideally suitable for circRNA characterization. For Northern blot detection, probes are designed that either span the backsplice junction or hybridize to the total transcript. By simply choosing a suitable gel-electrophoresis system (agarose and/or polyacrylamide), the two possible configurations (circular or linear) can be clearly distinguished

from each other.

Furthermore, Northern blotting can also be combined with RNase R or RNase H ribonuclease digestion. In particular, the RNase H cleavage assay has emerged as an elegant method for validation of circRNAs [4,27]. In brief, antisense oligonucleotides are designed directed against a specific circRNA. RNase H recognizes DNA-RNA hybrids and subsequent cuts the RNA within the duplex. The characteristic shift of mobility during denaturing polyacrylamide gel electrophoresis from an aberrantly slow migration of the circRNA to the expected linear behavior, as well as the cleavage patterns of RNase H digestion, can then be analyzed by Northern blotting. Furthermore, new approaches should be considered for a biochemical validation of the circular configuration. Here, among other things, probe-based systems (*in situ* hybridization) could play a crucial role. Moreover, current developments in next-generation sequencing such as the nanopore technology (Oxford Nanopore Technologies) should likely provide new options in the future. MinION's for example could provide emerging direct RNA sequencing capabilities.

In sum, all the problems mentioned here can only be circumvented by combining several biochemical validation methods and by maintaining stringent quality standards. Especially in the field of biomarker development, complete and convincing circRNA characterization should be a top priority. The commonly mentioned low reproducibility and the variable analytical standards are often an obstacle during the development of potential new biomarkers. CircRNAs highlighted here, indeed harbor great biomarker potential, but there is a strong need for standardization and for setting up minimal requirements for validating this class of ncRNA. How could this be achieved? The growing circRNA community should define what is essential to establish a new circRNA species as such. In recent years this has been successfully implemented for other issues, such as the MIQE (minimum information for publication of quantitative real-time PCR experiments) [28] and MISEV (minimal information for studies of EVs) [29], where the respective communities and their experts have provided recommendations on experimental methods and minimal information in reporting.

Acknowledgement

This work was funded by the LOEWE centre DRUID (Novel Drug Targets against Poverty-related and Neglected Tropical Infectious Diseases), Federal state of Hessen, Germany.

References

[1] T.R. Cech, J.A. Steitz, The noncoding RNA revolution-trashing old rules to forge new ones, Cell 157 (2014) 77–94, https://doi.org/10.1016/j.cell.2014.03.008.
[2] H.L. Sanger, G. Klotz, D. Riesner, H.J. Gross, A.K. Kleinschmidt, Viroids are single-stranded covalently closed circular RNA molecules existing as highly base-paired rod-like structures, Proc. Natl. Acad. Sci. U. S. A. 73 (1976) 3852–3856.
[3] L.L. Chen, The biogenesis and emerging roles of circular RNAs, Nat. Rev. Mol. Cell Biol. 17 (2016) 205–211, https://doi.org/10.1038/nrm.2015.32.
[4] S. Starke, I. Jost, O. Rossbach, T. Schneider, S. Schreiner, L.H. Hung, A. Bindereif, Exon circularization requires canonical splice signals, Cell Rep. 10 (2015) 103–111, https://doi.org/10.1016/j.celrep.2014.12.002.
[5] R. Ashwal-Fluss, M. Meyer, N.R. Pamudurti, A. Ivanov, O. Bartok, M. Hanan, N. Evantal, S. Memczak, N. Rajewsky, S. Kadener, circRNA biogenesis competes with pre-mRNA splicing, Mol. Cell 56 (2014) 55–66, https://doi.org/10.1016/j.molcel.2014.08.019.
[6] E. Lasda, R. Parker, Circular RNAs: diversity of form and function, RNA 20 (2014) 1829–1842, https://doi.org/10.1261/rna.047126.114.
[7] W.R. Jeck, J.A. Sorrentino, K. Wang, M.K. Slevin, C.E. Burd, J. Liu, W.F. Marzluff, N.E. Sharpless, Circular RNAs are abundant, conserved, and associated with ALU repeats, RNA 19 (2013) 141–157, https://doi.org/10.1261/rna.035667.112.
[8] T.B. Hansen, T.I. Jensen, B.H. Clausen, J.B. Bramsen, B. Finsen, C.K. Damgaard, J. Kjems, Natural RNA circles function as efficient microRNA sponges, Nature 495 (2013) 384–388 https://doi.org/10.1038/nature11993.
[9] S. Memczak, M. Jens, A. Elefsinioti, F. Torti, J. Krueger, A. Rybak, L. Maier, S.D. Mackowiak, L.H. Gregersen, M. Munschauer, A. Loewer, U. Ziebold, M. Landthaler, C. Kocks, F. le Noble, N. Rajewsky, Circular RNAs are a large class of animal RNAs with regulatory potency, Nature 495 (2013) 333–338, https://doi.org/10.1038/nature11928.
[10] L.M. Holdt, A. Stahringer, K. Sass, G. Pichler, N.A. Kulak, W. Wilfert, A. Kohlmaier, A. Herbst, B.H. Northoff, A. Nicolaou, G.F. Gäbel, F. Beutner, M. Scholz, J. Thiery, K. Musunuru, K. Krohn, M. Mann, D. Teupser, Circular non-coding RNA ANRIL modulates ribosomal RNA maturation and atherosclerosis in humans, Nat. Commun. 7 (2016) 12429, https://doi.org/10.1038/ncomms12429.
[11] L.M. Holdt, A. Kohlmaier, D. Teupser, Molecular roles and function of circular RNAs in eukaryotic cells, Cell. Mol. Life Sci. 75 (2018) 1071–1098, https://doi.org/10.1007/s00018-017-2688-5.
[12] M. Piwecka, P. Glažar, L.R. Hernandez-Miranda, S. Memczak, S.A. Wolf, A. Rybak-Wolf, A. Filipchyk, F. Klironomos, C.A. Cerda Jara, P. Fenske, T. Trimbuch, V. Zywitza, M. Plass, L. Schreyer, S. Ayoub, C. Kocks, R. Kühn, C. Rosenmund, C. Birchmeier, N. Rajewsky, Loss of a mammalian circular RNA locus causes miRNA deregulation and affects brain function, Science. 357 (2017), https://doi.org/10.1126/science.aam8526 pii: eaam8526.
[13] L. Errichelli, S. Dini Modigliani, P. Laneve, A. Colantoni, I. Legnini, D. Capauto, A. Rosa, R. De Santis, R. Scarfò, G. Peruzzi, L. Lu, E. Caffarelli, N.A. Shneider, M. Morlando, I. Bozzoni, FUS affects circular RNA expression in murine embryonic stem cell-derived motor neurons, Nat. Commun. 8 (2017) 14741, https://doi.org/10.1038/ncomms14741.
[14] C. Liu, M.D. Yao, C.P. Li, K. Shan, H. Yang, J.J. Wang, B. Liu, X.M. Li, J. Yao, Q. Jiang, B. Yan, Silencing of circular RNA-ZNF609 ameliorates vascular endothelial dysfunction, Theranostics. 7 (2017) 2863–2877, https://doi.org/10.7150/thno.19353.
[15] S. Qu, Z. Liu, X. Yang, J. Zhou, H. Yu, R. Zhang, H. Li, The emerging functions and roles of circular RNAs in cancer, Cancer Lett. 414 (2018) 301–309, https://doi.org/10.1016/j.canlet.2017.11.022.
[16] A.C. Panda, S. De, I. Grammatikakis, R. Munk, X. Yang, Y. Piao, D.B. Dudekula, K. Abdelmohsen, M. Gorospe, High-purity circular RNA isolation method (RPAD) reveals vast collection of intronic circRNAs, Nucleic Acids Res. 45 (2017) e116, https://doi.org/10.1093/nar/gkx297.
[17] A. Sebastián-Martín, V. Barriolluengo, L. Menéndez-Arias, Transcriptional inaccuracy threshold attenuates differences in RNA-dependent DNA synthesis fidelity between retroviral reverse transcriptases, Sci. Rep. 8 (2018) 627, https://doi.org/10.1038/s41598-017-18974-8.
[18] J. Cocquet, A. Chong, G. Zhang, R.A. Veitia, Reverse transcriptase template switching and false alternative transcripts, Genomics. 88 (2006) 127–131, https://doi.org/10.1016/j.ygeno.2005.12.013.
[19] J. Houseley, D. Tollervey, Apparent non-canonical trans-splicing is generated by reverse transcriptase in vitro, PLoS One 5 (2010) e12271, , https://doi.org/10.1371/journal.pone.0012271.
[20] C. Preußer, A. Bindereif, Exo-endo trans splicing: a new way to link, Cell Res. 23 (2013) 1071–1072, https://doi.org/10.1038/cr.2013.105.
[21] T.B. Hansen, M.T. Venø, C.K. Damgaard, J. Kjems, Comparison of circular RNA prediction tools, Nucleic Acids Res. 44 (2016) e58, https://doi.org/10.1093/nar/gkv1458.
[22] C. Preußer, L.H. Hung, T. Schneider, M. Hardt, A. Moebus, S. Santoso, A. Bindereif, Selective release of circRNAs in platelet-derived extracellular vesicles, J. Extracell. Vesicles 7 (2018) 1424473, , https://doi.org/10.1080/20013078.2018.1424473.
[23] R. Crescitelli, C. Lässer, T.G. Szabó, A. Kittel, M. Eldh, I. Dianzani, E.I. Buzás, J. Lötvall, Distinct RNA profiles in subpopulations of extracellular vesicles: apoptotic bodies, microvesicles and exosomes, J. Extracell. Vesicles 2 (2013), https://doi.org/10.3402/jev.v2i0.20677.
[24] Y. Gao, J. Wang, F. Zhao, CIRI: an efficient and unbiased algorithm for de novo circular RNA identification, Genome Biol. 16 (2015) 4, https://doi.org/10.1186/s13059-014-0571-3.
[25] X. Zeng, W. Lin, M. Guo, Q. Zou, A comprehensive overview and evaluation of circular RNA detection tools, PLoS Comput. Biol. 13 (2017) e1005420, , https://doi.org/10.1371/journal.pcbi.1005420.
[26] T. Schneider, S. Schreiner, C. Preußer, A. Bindereif, O. Rossbach, Northern blot analysis of circular RNAs, Methods Mol. Biol. 1724 (2018) 119–133, https://doi.org/10.1007/978-1-4939-7562-4_10.
[27] W.R. Jeck, N.E. Sharpless, Detecting and characterizing circular RNAs, Nat. Biotechnol. 32 (2014) 453–461, https://doi.org/10.1038/nbt.2890.
[28] S.A. Bustin, V. Benes, J.A. Garson, et al., The MIQE guidelines: minimum information for publication of quantitative real-time PCR experiments, Clin. Chem. 55 (2009) 611–622, https://doi.org/10.1373/clinchem.2008.112797.
[29] J. Lötvall, A.F. Hill, F. Hochberg, E.I. Buzás, D. Di Vizio, C. Gardiner, Y.S. Gho, I.V. Kurochkin, S. Mathivanan, P. Quesenberry, S. Sahoo, H. Tahara, M.H. Wauben, K.W. Witwer, C. Théry, Minimal experimental requirements for definition of extracellular vesicles and their functions: a position statement from the International Society for Extracellular Vesicles, J. Extracell. Vesicles 3 (2014) 26913, https://doi.org/10.3402/jev.v3.26913.

Methods 196 (2021) 36–46

Contents lists available at ScienceDirect

Methods

journal homepage: www.elsevier.com/locate/ymeth

Methods to study circRNA-protein interactions

Corinna J. Ulshöfer [1], Christina Pfafenrot [1], Albrecht Bindereif [*], Tim Schneider [*]

Institute of Biochemistry, Justus-Liebig-University of Giessen, 35392 Giessen, Germany

ARTICLE INFO

Keywords:
Circular RNAs (circRNAs)
RNA-binding proteins (RBPs)
Ribonucleoprotein complexes (RNPs)
RNA-protein interactions

ABSTRACT

Circular RNAs (circRNAs) have been studied extensively in the last few years, uncovering functional roles in a diverse range of cell types and organisms. As shown for a few cases, these functions may be mediated by *trans*-acting factors, in particular RNA-binding proteins (RBPs). However, the specific interaction partners for most circRNAs remain unknown. This is mainly due to technical difficulties in their identification and in differentiating between interactors of circRNAs and their linear counterparts. Here we review the currently used methodology to systematically study circRNA-protein complexes (circRNPs), focusing either on a specific RNA or protein, both on the gene-specific or global level, and discuss advantages and challenges of the available approaches.

1. Introduction

Circular RNAs (circRNAs) are classified as RNA molecules with covalently joined 5′ and 3′ ends, resulting in a closed, circular configuration. While their existence has been known for more than four decades [1], they were more recently re-discovered as a large class of noncoding RNAs, based on high-throughput sequencing and computational analyses, and identified in all eukaryotes investigated so far [2–7]. Several different subclasses of circRNAs have been described, varying in their origin and biogenesis, but most common is processing from pre-mRNAs through a type of alternative splicing, called back-splicing [8,9]. During this process, the 5′ and 3′ splice sites of a single, or several adjacent exons are joined to form a special splice junction, also referred to as backsplicing junction or circ-junction [10,11]. From a functional perspective, miRNA sponging by ciRS-7/CDR1as represents the by far best studied example [4,12] and was found to take part in a complex regulatory RNA network [13,14]. However, other hypothetical roles have been proposed for circRNAs, including scaffold functions in RNA-protein complex assembly, allostery, protein sponging, antisense activity, or acting as templates for protein synthesis [15]. Regarding circRNA biogenesis, extensive investigations revealed a wide range of regulatory *cis*-elements like *Alu* repeats [3,10,16,17] and RNA-binding proteins as *trans*-acting factors [18–26].

The understanding of RNA-protein interactions, in general, can provide many insights into biological processes and regulatory pathways [27]. These interactions are usually dynamic, for example during development or cell-cycle progression, or in response to external stimuli such as stress [28,29]. An array of methods to analyze protein-RNA interactions has been developed to address molecular structures of RNA-protein complexes and biological functions [30–32]. For circRNA-protein complexes, only a subset of these methods has been employed so far [33–37]. This is mostly due to the special challenges in circRNA research, i.e. their low endogenous abundance, difficulties to differentiate between circular and linear isoforms, and the use of overexpression techniques [35,38–40]. Since circRNAs carry the same sequence information as their linear counterparts except for the circ-junction, the latter represents the only criterion available for prediction of new circRNAs. This has two consequences: First, it emphasizes the importance of robust circRNA identification and essential quality criteria in the validation process [41–44]. Second, the missing full-length circRNA sequence makes functional circRNA studies difficult. A strategy for sequencing full-length circRNA-isoforms was recently published [45] and will hopefully contribute to understand the specific interplay between proteins and circRNAs, which is crucial to uncover circRNA functions and the underlying networks [46].

In this review, we summarize the currently used approaches to investigate the interaction of circRNAs and their protein partners. We have therefore organized the diverse methodology into two groups, protein- and circRNA-centric approaches, depending on from which component the analysis starts (see Fig. 1). Fig. 2 provides a detailed overview of the method workflows, and Table 1 further discusses advantages and challenges with respect to the unique characteristics of

* Corresponding author.
E-mail addresses: albrecht.bindereif@chemie.bio.uni-giessen.de (A. Bindereif), tim.schneider@chemie.bio.uni-giessen.de (T. Schneider).
[1] These authors contributed equally to this work.

https://doi.org/10.1016/j.ymeth.2021.04.014
Received 15 February 2021; Received in revised form 15 April 2021; Accepted 18 April 2021
Available online 22 April 2021

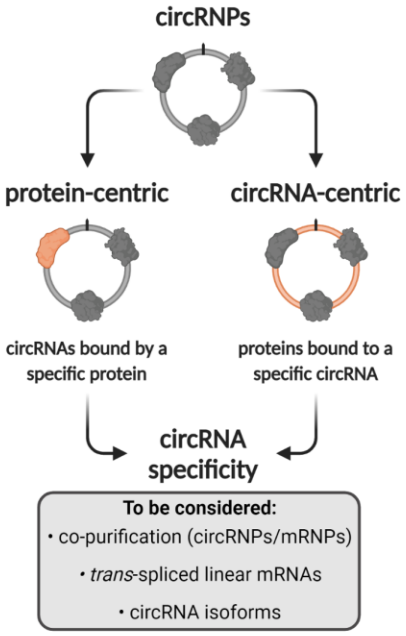

Fig. 1. *How to study circRNA-protein interactions*. CircRNPs can be studied using a variety of methods classified as protein- or circRNA-centric, depending on the component from which the analysis starts. As a crucial step in all protocols, circRNA specificity of the used method must be established in order to e.g. differentiate circRNAs from their linear mRNA counterparts, minimize detection of false-positive circ-junctions due to *trans*-spliced linear mRNAs, and taking into account that the same circ-junction can originate from different circRNA isoforms. Created with Biorender.com.

circular RNAs. Finally, we outline future perspectives for circRNP research.

2. Protein-centric methods to study circRNA-protein interactions

2.1. RNA immunoprecipitation (RIP)

RNA immunoprecipitation (RIP) has developed to one of the most common standard techniques for detecting and analyzing associations of an RNA-binding protein with its target RNAs, such as circRNAs. After antibody-mediated pulldown of the desired RBP from cell lysates, RBP-RNA complexes are washed so that unspecifically bound molecules are removed, but at the same time native complexes are preserved. Captured RNA is then purified, followed by RNA identification and analysis, for example, based on RT-qPCR or sequencing. Crosslinking of proteins to RNA prior to cell lysis is optional and mediated by formaldehyde or UV light to capture weak or transient interactions more efficiently [47].

Analysis of RIP experiments by RT-qPCR has been extensively applied in the circRNA field. For example, RNA polymerase II was shown to associate with ci-ankrd52 (circular intronic RNA) [48] or the pre-ribosomal assembly factor PES1 with circANRIL [49]. CircRNA-specific primers leading to PCR products spanning the circ-junction are used for this purpose. However, linear RNAs generated through *trans*-splicing, tandem DNA duplications, or during RT-PCR by template switching of the reverse transcriptase, can also be detected, resulting in false-positive events [35]. As a control, treatment of total RNA with the exoribonuclease RNase R prior to RT-PCR can be performed to digest linear RNAs. Although some circRNAs seem to be RNase R sensitive, whereas some linear RNAs have shown resistance towards RNase R [50], this digestion is widely used as a criterion for circularity. Recently, an improvement of this method has been published, in which RNase R digestion in Li^+-containing buffer combined with a preceding poly(A) tailing step achieved more complete degradation of linear RNA [51]. This extended RNase R protocol represents a useful tool for future circRNA research, also in the context of validating circRNA-protein interactions.

RIP-seq provides the advantage of transcriptome-wide detection of associated circRNAs. Deep sequencing is needed to gain reads spanning the circ-junction as most circRNAs are of low abundance. Several RIP-seq experiments revealed binding of specific proteins to circRNAs; for example, multiple circRNAs were shown to be associated with IMP3 in cancer cell lines [21], RIP of polysomes in RiboTag mouse hearts suggested a subset of circRNAs to be involved in translation regulation [52], and RIP-seq of fragile X mental retardation protein (FMRP) revealed competitive binding of circZKSCAN1 and a linear mRNA in hepatocellular carcinoma cells [53]. As for all RNA-seq experiments, biochemical validation should be performed. When new circRNAs are predicted, RNase R treatment of total RNA with subsequent RT-PCR analysis can be applied for screening a large number of circRNAs, or, alternatively and more stringently, Northern blotting (with probes spanning the circ-junction and the entire transcript, respectively) can be performed for smaller sets of circRNAs. Northern blotting in conjunction with RNase R or RNase H assays provides even more powerful and convincing tools for circRNA validation [35,54].

Independently of the RNA analysis method, RIP assays require a suitable antibody targeting the protein of interest, which can be the limiting factor. In addition, since the procedure is normally performed under native conditions, protein complexes are preserved, and thus also indirectly bound RNAs are detected. The latter aspect can be largely overcome by stringent washing, which is usually only possible for crosslinked RBP-RNA complexes, as e.g. in CLIP assays (see next section).

2.2. Crosslinking and immunoprecipitation (CLIP)

Crosslinking and immunoprecipitation (CLIP) is a widely used global method to detect *in vivo* protein-RNA interactions [55,56]. Different versions of this technique have been developed in recent years, such as iCLIP, HITS-CLIP, PAR-CLIP, eCLIP, etc. [57]. All these methods share a UV-crosslinking step in cells prior to cell lysis, which covalently tethers amino acid residues to RNA bases in close proximity. The protein of interest is then pulled down by a specific antibody, and non-crosslinked RNAs, as well as other proteins, are removed through stringent washing. In a multi-step procedure, crosslinked RNAs are fragmented, isolated, and reverse-transcribed to yield a library for sequencing. As a result, identification of the protein binding sites on the RNA can be identified at nucleotide-level, allowing predictions of binding motifs, which is a great advantage compared to RIP assays.

CLIP techniques have also been used to identify circRNA-protein interactions, but to a lesser extent than RIP experiments. The first CLIP applications in the circRNA field were AGO-CLIP experiments. Here, either available HITS-CLIP data were analyzed [12] or PAR-CLIP experiments performed [4] to identify the AGO proteins associated with ciRS-7/CDR1as, although this does not involve a direct protein-RNA contact, but instead a microRNA-mediated circRNA interaction of AGO. Direct protein-circRNA associations were revealed by an RNA polymerase II CLIP in HeLa cells [58]. Other studies used (available) CLIP data to confirm the interaction of a specific RBP with one or several circRNAs [21,59,60]. Recently, bioinformatic tools have been developed to predict circRNA-RBP interactions on a global level based on CLIP data [61–64]. Nevertheless, one should keep in mind that such results require further experimental validation.

Similarly to RIP experiments, a suitable antibody is essential for CLIP assays to pull down endogenous protein. The utilization of tagged protein might be a solution to approach this problem but suffers from other drawbacks, such as expression levels different from those of the

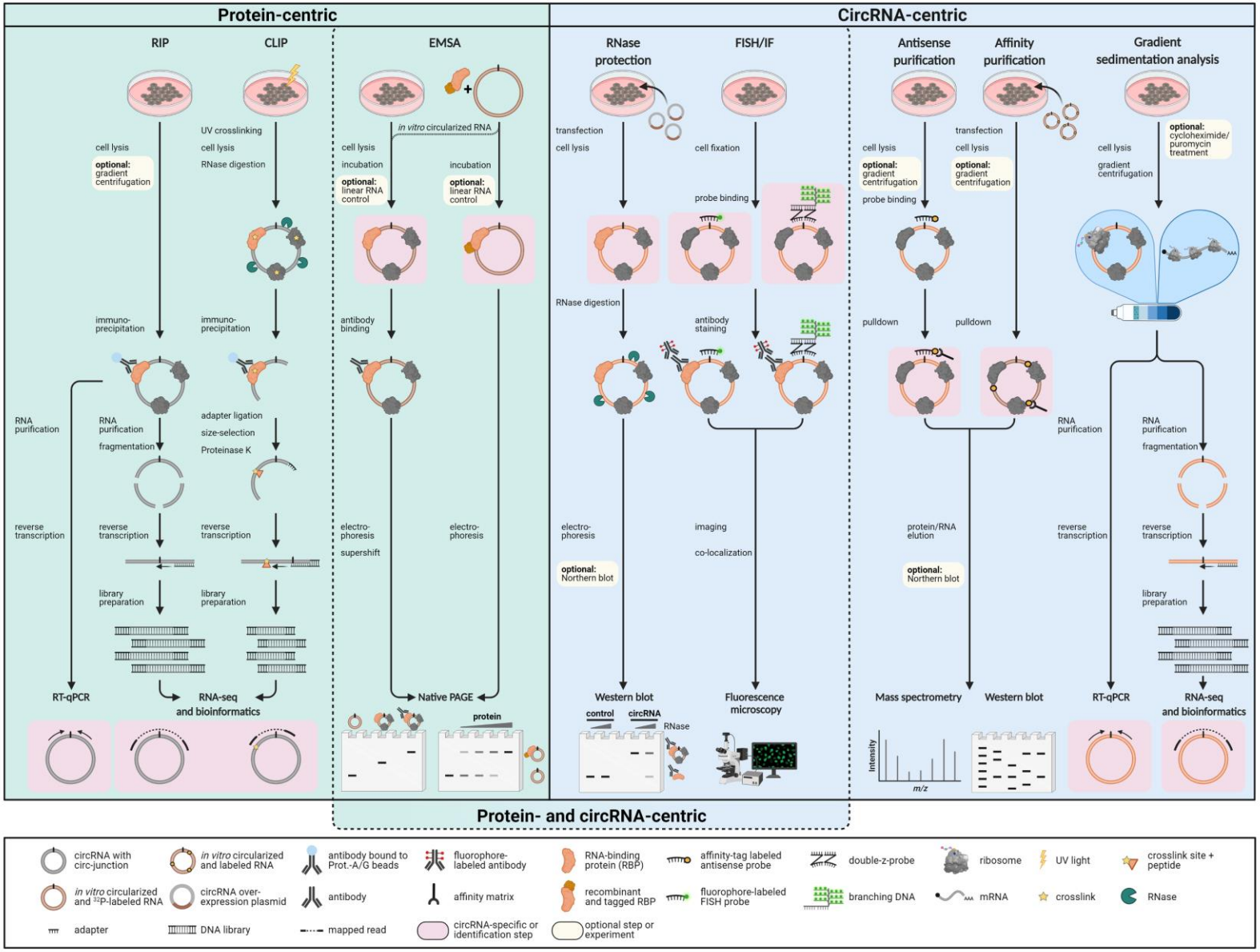
Protein-centric
CircRNA-centric
RIP
CLIP
EMSA
RNase protection
FISH/IF
Antisense purification
Affinity purification
Gradient sedimentation analysis
cell lysis
optional: gradient centrifugation
UV crosslinking
RNase digestion
in vitro circularized RNA
incubation
optional: linear RNA control
transfection
cell fixation
probe binding
optional: cyclohexamide/ puromycin treatment
gradient centrifugation
immuno-precipitation
antibody binding
RNase digestion
antibody staining
pulldown
RNA purification
fragmentation
adapter ligation
size-selection
Proteinase K
reverse transcription
library preparation
electro-phoresis
supershift
imaging
co-localization
protein/RNA elution
optional: Northern blot
RT-qPCR
RNA-seq and bioinformatics
Native PAGE
protein
Western blot
control
circRNA
RNase
Fluorescence microscopy
Mass spectrometry
intensity
m/z
Protein- and circRNA-centric
circRNA with circ-junction
in vitro circularized and labeled RNA
antibody bound to Prot.-A/G beads
fluorophore-labeled antibody
RNA-binding protein (RBP)
affinity-tag labeled antisense probe
double-z-probe
ribosome
UV light
crosslink site + peptide
in vitro circularized and 32P-labeled RNA
circRNA over-expression plasmid
antibody
affinity matrix
recombinant and tagged RBP
fluorophore-labeled FISH probe
branching DNA
mRNA
crosslink
RNase
adapter
DNA library
mapped read
circRNA-specific or identification step
optional step or experiment

Fig. 2. *How to study circRNA-protein interactions: workflow of methods presented. Protein-centric methods*: Both circRNA immunoprecipitation (RIP) as well as crosslinking and immunoprecipitation (CLIP) rely on the selection of associated circRNAs via antibody binding to the protein of interest. In RIP assays, immunoprecipitation (IP) is either followed by RT-qPCR using circ-junction detecting primers, or RNA-seq and bioinformatic filtering for circ-junction reads. In CLIP experiments, RNP complexes are first crosslinked by UV irradiation, treated with RNase to yield small RNA fragments protected by the bound protein, followed by IP, library preparation, and RNA-seq to identify circ-junction spanning CLIP tags. Electrophoretic mobility shift assays (EMSA) are based on differential running behavior of free or complexed circRNA in the presence of cell lysate or recombinant protein, allowing analysis of protein-binding characteristics, and comparing circRNAs with their linear counterparts in terms of affinity (K_d), specificity (e.g. binding motifs), RNA structure or complex assembly. *circRNA-centric methods*: RNase protection experiments are based on the local protection of a circRNA through bound proteins from RNase-mediated degradation, allowing analysis of complex formation, and mapping of protein binding sites (footprints). For this, circRNAs can be transiently overexpressed through plasmid-transfection, or directly by circRNA transfection. Fluorescence *in situ* hybridization (FISH) and immunofluorescence (IF) can be combined to detect circRNA-protein co-localization by fluorescence microscopy. The analyzed circRNA is detected by a single fluorophore-coupled, or a double-z-probe covering the circ-junction, while the protein of interest is immunostained with a labeled antibody (direct or sandwich method). Antisense purification of circRNPs relies on binding of a circ-junction-specific, and biotinylated probe, enabling pulldown with streptavidin-coated beads, followed by Western blot or mass spectrometry analysis. Affinity purification combines many possible strategies, ranging from internal RNA labeling by modified nucleotides to the addition of tag or aptamer sequences. The described example represents purification of circRNA-binding proteins based on *in vitro* circularized RNA containing biotinylated nucleotides, allowing pulldown with streptavidin-beads, followed by Western blot or mass spectrometry. Gradient sedimentation allows physical separation of RNA-protein complexes according to their size, shape, and corresponding density, by ultracentrifugation of cell extracts loaded on a gradient material (e.g. glycerol or sucrose). In the context of circRNAs, this can be used to analyze circRNP complex sizes and sedimentation profiles, as well as their potential association with ribosomes, but also as an enrichment step before proceeding with other methods. Methods that require knowledge about a specific circRNA and RNA-binding protein have been labeled as protein- and circRNA-centric methods (dashed box). Red boxes indicate steps within the experimental protocol that are either circRNA-specific or can be used to identify new circRNAs. Yellow boxes highlight optional steps or experiments in the method workflow. Created with Biorender.com.

endogenous protein. Crosslinking of the RBP-RNA complexes prior to immunoprecipitation has the advantage to allow stringent washing criteria but can introduce biases itself, e.g. preferred crosslinking to certain nucleotides and amino acids [56]. Concerning circRNAs, the limitation of the standard CLIP procedure is their reliable distinction from the corresponding linear counterparts, since reads spanning the circ-junction can only be obtained if the protein binds there directly or in immediate proximity, which rarely occurs. Furthermore, since CLIP methods tend to be biased to abundant RNAs, the detection of circRNAs, which are often only lowly expressed, requires deep sequencing of the samples. A possibility to address this issue might be a combination with newer techniques such as PTex (as discussed in the Conclusion, Section 4).

2.3. *In vitro assays to study circRNA-protein complexes*

Binding of proteins to nucleic acids, such as a specific circRNA, can be examined *in vitro* using electrophoretic mobility shift assays (EMSAs). This method relies on the principle that free nucleic acids migrate faster in a non-denaturing gel than protein-nucleic acid complexes. Conditions of complex formation and of the electrophoresis itself have to be adjusted so that distinct bands can be resolved [65,66]. Visualization is classically achieved through labeling of the nucleic acid, e.g. by ^{32}P or by fluorescence/chemiluminescence approaches, requiring only small amounts of material to start with. The protein is usually purified in recombinant form, but cell lysate can also be used. Depending on the goals of the experiment, EMSAs can be carried out qualitatively or quantitatively, the latter employing titration of the protein to obtain (non-equilibrium) dissociation constants.

EMSAs are also useful to analyze interactions between proteins in complex with circRNA in more detail. This has been done for circACC1, which plays a role in metabolic stress response and interacts with the heterotrimeric AMP-activated protein kinase (AMPK) complex [67]. Internally biotinylated circACC1 was generated by *in vitro* transcription and circularization, followed by the analysis of its association with the three FLAG-tagged subunits. Visualization was performed through horseradish peroxidase-mediated chemiluminescent reaction of the blotted EMSA-gel. The assay revealed binding of circACC1 only to the ß and γ subunit, but not to α, and complemented the available RNA pulldown and RIP data [67].

Other studies analyzed protein-circRNA interactions by using a linear RNA containing the circ-junction sequence in the EMSA experiment [68,69]. Results of these approaches should be interpreted with caution since the loss of the natural circRNA structure might influence binding. In addition, demonstrating that protein binding occurs at the circular junction requires further controls, e.g. RNAs of different lengths derived from variable distances to the circ-junction or mutant RNA sequences. This compromise might be an option especially to examine binding to larger, multi-exonic circRNAs, which are more difficult to synthesize and to separate on classical native polyacrylamide gels, although this is to some extent possible using e.g. composite or agarose gels and an appropriate circRNA production protocol (see references below).

Another approach besides EMSA assays to differentiate between protein-binding to the linear or circular form of an RNA has been developed by the Chen lab. Here, equal amounts of *in vitro* produced linear or circularized RNA were incubated with different His-tagged proteins and binding subsequently analyzed by anti-His antibody pulldown followed by RNA extraction and Northern blot [70]. Binding of both the linear and circular RNA was tested separately as well as simultaneously, i.e. in competition, and revealed preferences in the case of protein kinase R (PKR) for circular over linear RNA [70]. A similar version of this circular/linear RNA competition assay has been performed before with the immune factor NF90 (nuclear factor 90) [25]. Here, HeLa cells stably expressing Flag-NF90 were infected with vesicular stomatitis virus (VSV) to precipitate NF90 bound *VSV* mRNAs by native RIP. *In vitro* produced linear or circularized competitor RNA was then added to bound viral VSV mRNA and the dissociated amount quantified by RT-qPCR. Increasing amounts of added circular but not linear RNA led to stronger competition effects, supporting the evidence of RNA structural importance [25].

One critical aspect of all *in vitro* assays described in this article is the generation of pure circRNAs. While a detailed description of how they can be obtained is beyond the scope of this review, we would like to refer to several publications summarizing *in vitro* circRNA production methods [9,71–73]. Independently of the method chosen, the structure of *in vitro* produced circRNAs may differ from endogenous circRNAs. This in turn would influence binding to RBPs and biochemical parameters determined, such as binding constants. Nevertheless, *in vitro* assays represent useful tools to gain detailed insights into protein-circRNA interactions which are often not possible to gain *in vivo*. A combination with *in vivo* techniques such as RIP (see Section 2.1), antisense-based pulldown (see Section 3.1), or FISH/IF (see Section 3.5) will reinforce the findings and additionally give a broader picture of the observed interactions.

Table 1
Overview of benefits and drawbacks of circRNA-protein interaction methods.

Protein-centric		
Method	*Advantages*	*Disadvantages*
RIP (see Section 2.1)	- Fast, widely applied method - RBPs can be bound to long RNAs (good for detection of circ-junctions) - Purification of native complexes (no modifications needed)	- Suitable antibody required - Native conditions preserve protein complexes (also indirect binding of RNAs detected) - Deep sequencing needed to obtain circRNA reads
CLIP (see Section 2.2)	- Global identification of protein binding sites on RNA at single nucleotide resolution - Stringent washing conditions can be applied due to covalent crosslinking	- Suitable, high quality antibody required - UV-crosslinking can introduce biases - Number of sequencing reads containing circ-junctions are usually low
EMSA (see Section 2.3)	- Small amounts of material sufficient - Different RNA labeling techniques can be employed - Various methods available to determine biochemical parameters, e.g. dissociation constants or stoichiometry of complexes	- Complexes must be stable during gel run - Binding constants determined *in vitro* may differ from endogenous *in vivo* binding - Challenging for large circRNAs
CircRNA-centric		
Method	*Advantages*	*Disadvantages*
Antisense purification (see Section 3.1)	- Pulldown of native complexes and RBP identification via mass spectrometry - Can be combined with pre-purification/enrichment by gradient sedimentation	- Low pulldown efficiencies due to potential blocking of the circ-junction by RNA structure or bound RBPs - Potential off-target purification of linear mRNA counterparts
Affinity purification (see Section 3.2)	*In vitro* circularized RNA (internally labeled) - *In vitro* circularization assures circular configuration when transfected into cells, or exposed to cell extracts - Custom-made designer circRNAs can be used Overexpressed circRNA (aptamer-tagged) - Aptamer-specific pulldown of overexpressed circRNAs - Can be combined with pre-purification/enrichment by gradient sedimentation	*In vitro* circularized RNA (internally labeled) - Internal labeling can affect circularization efficiencies (transcription with modified nucleotides), and RNA structure Overexpressed circRNA (aptamer-tagged) - Co-expression of viral proteins necessary - circRNA overexpression might induce non-physiological RBP association - Potential off-target purification of linear mRNA counterparts or processing artifacts from overexpression constructs
RNase protection (see Section 3.3)	- Allows mapping of RBP binding sites *in vitro*	- Requires plasmid-based overexpression or *in vitro* circularized RNA - Requires knowledge of circRNA-interacting proteins
Gradient sedimentation (see Section 3.4)	- Allows estimation of circRNP complex sizes - Suitable for studying circRNA translation - Pre-purification/enrichment step before proceeding with other methods	- Laborious and time consuming - Does not yield circRNA-interacting protein candidates on its own
FISH/IF (see Section 3.5)	- Visualization of cellular localization and overall circRNP complex abundance - Single-molecule resolution (smFISH)	- Co-localization does not prove direct physical interaction - Potential off-target hybridization (to corresponding linear mRNAs) depending on the used method (FISH)

3. CircRNA-centric methods to study circRNA-protein interactions

3.1. Antisense-based pulldown purification of circRNPs

The principle of antisense pulldown is based on specific base-pairing of biotinylated antisense probes with its target RNA sequence, such as a circRNA, which has to be accessible within the RNP [74–76]. After cell lysis and probe hybridization, the target circRNA is captured via streptavidin-coupled beads. Through stringent washing steps, non-specific binders can be removed and the complex can be further analyzed, for example by Western blotting or by mass spectrometry, in order to identify associated proteins.

The first critical step when designing an antisense pulldown experiment is to select a region within the RNA of interest. Especially for circRNAs, it is necessary to choose antisense probes spanning the circ-junction to achieve circRNA specificity [60,77–79]. Applying this technique in combination with mass spectrometry, Li and colleagues could demonstrate that the EIciRNAs (exon–intron circRNA) circEIF3J, and circPAIP2 associate with RNA polymerase II, modulating expression of their parental genes [58]. Furthermore, the MALAT1-derived circular RNA circ2082 was identified to interact with DICER in the nucleus [80]. In another recent study, Zhao *et al.* performed pulldown assays from fibroblast lysates against the mitochondria-located circRNA SCAR, followed by mass spectrometry. In this example, binding of circSCAR to ATP5B (ATP synthase F1 subunit beta) resulted in shut down of the mitochondrial permeability transition pore [81].

Because in most cases the specific target sequence of a circRNA is restricted to its circ-junction, which may not be optimal for probe hybridization, or may be occupied by protein *in vivo*, low pulldown efficiencies represent a major drawback for antisense pulldown experiments. Therefore, multiple probes distributed over the circularized sequence have been used to increase pulldown efficiency, which then target both circular and linear isoforms, and which may reduce overall specificity [26]. However, there are special cases of circRNAs, for which there is practically no linear counterpart, such as ciRS-7 [4,12] or the platelet-specific Plt-circR4 RNA [82]. One option to minimize linear contamination is to introduce an initial purification step by density gradient centrifugation. In principle, this step allows the physical separation of circRNPs from mRNPs, although limited in resolution by the relative differences of corresponding RNA-protein complexes (see Section 3.4) [21].

3.2. CircRNP affinity purification by labeled circRNAs

An alternative to antisense-based purification of circRNPs is the use of internally labeled circRNAs. This can be subdivided into two general strategies:

3.2.1. Affinity purification with in vitro internally labeled circRNAs

This approach relies on the use of internally modified circRNAs that can be either transfected in cell culture (*in vivo*) or incubated with cell extract (*in vitro*), allowing the purification of circRNPs via an affinity matrix. Labeling of *in vitro* circularized RNAs is thereby achieved through the incorporation of modified, or modifiable nucleotides during transcription [83]. The most commonly used chemical moiety is biotin [67]. Because the addition of many biotin residues produces a relatively bulky molecule, this can severely reduce the efficiency of the subsequent circularization step. Although labeling efficiencies can be fine-tuned by altered ratios of labeled to unlabeled nucleotides during transcription, alternatively, modifiable nucleotides offer the advantage that they can be modified with biotin via click-chemistry [84], after the RNA is circularized. For example, in a recent study, short circRNAs designed to act as protein sponges and carrying high-affinity binding sites for hnRNP L were generated by enzymatic *in vitro* circularization, labeled with biotin via click-chemistry, and subsequently transfected for modulating hnRNP L-dependent alternative splicing [85]. Additionally, such *in vitro* modified, circularized, and transfected circRNAs can also be used to investigate protein binding *in vivo*. However, it should be noted that in both cases the observed binding does not entirely recreate a naturally occurring circRNP since the circRNA is not endogenously processed, and secondary structures might be perturbed due to modifications.

3.2.2. Affinity purification of aptamer-tagged and overexpressed circRNAs

A second approach is based on the endogenous overexpression of circular RNAs harboring an aptamer element. RNA aptamers are folded RNAs that specifically interact with their targets, such as small molecules, peptides, or proteins [86,87]. Until now, the application of MS2 and Box-b aptamer sequences has been described in the context of circRNAs. The MS2 stem-loop sequence is bound by the MS2 coat protein (MS2cp) derived from the MS2 bacteriophage [88], while the Box-b stem loop sequence is recognized by the λ bacteriophage N-protein [89–91]. Aptamer sequences can be incorporated in circRNA-overexpression constructs. Co-expression of the corresponding target molecule (MS2cp/λN) then allows pulldown through the use of a corresponding affinity matrix. Hollensen and colleagues generated cell lines stably overexpressing circZNF827 tagged with two MS2 hairpins, followed by anti-FLAG ChIP analysis [92]. As a result, they could observe that circZNF827 guides the hnRNP(K/L)-ZNF827-containing complex to chromatin. In another study, Holdt *et al.* generated cell lines stably overexpressing circANRIL, engineered to contain the Box-b RNA hairpin, allowing pulldown assays followed by mass spectrometry [49]. Taken together, pulldown of overexpressed circRNAs can give valuable insights into circRNA-protein interactions. However, one should be aware that circRNA overexpression may result in non-physiological RBP association and generation of linear RNA products [40].

3.3. RNase protection

The association of an RBP with RNA can locally protect the RNA from degradation by RNases, thereby defining the direct interaction site, also called protein footprint [93]. Mapping of RBP binding sites this way usually focuses on a specific, radioactively labeled RNA and incubation with recombinant protein or cellular extracts, but transcriptome-wide approaches are also available [94,95]. However, the basic principle of RNase protection was initially used for gene quantitation or transcription start site mapping, etc., through hybridization of an antisense probe and subsequent treatment with single-strand specific RNases [96,97]. While not directly linked to circRNP complexes, it is worth noting that RNase protection assays have been used to validate circ-junctions of *SMN*-derived circRNA isoforms [98]. In the context of circRNA-protein interactions, Du *et al.* validated complex formation of circFOXO3 with CDK2 (cyclin dependent kinase 2) and p21 (or CDKN1A, cyclin dependent kinase inhibitor 1A) in circFOXO3-overexpressing cells [73]. Although not very commonly used for the analysis of circRNPs until now, RNase protection experiments have good potential for *in vitro* assays in cases where protein interactors of a specific circRNA are identified, but the binding region remains unknown.

3.4. Gradient sedimentation analysis

A powerful general tool for the characterization of circRNA-protein interactions is the analysis of crude cell extracts by density gradient

ultracentrifugation [99,100]. Depending on the concentration range and gradient material used, resolution can be adjusted to study RNP complexes within a wide size range. In principle, two types of gradients can be differentiated: glycerol gradients (between 5% and 30%) for small- to medium-molecular-weight complexes (e.g. snRNPs, circRNPs), and sucrose gradients (between 5% and 50%) for analysis of high-molecular-weight complexes (e.g. mRNPs and polysomes).

3.4.1. Analysis of circRNA-protein complexes by glycerol gradient centrifugation

Since the majority of RNAs, including circRNAs, are associated with several different proteins, within the same or separate complexes, differential sedimentation profiles can be observed when comparing cell lysates and RNA prepared from the same lysate. The observed shift of specific RNAs within the gradient can yield an estimate of the total molecular weight of the bound protein components, as well as the overall complex size [21,82]. The sedimentation of a known circRNA is typically detected by RT-(q)PCR and circ-junction specific primers [101], but RNA-seq of individual fractions can give a global survey of all RNA-protein complexes [102]. Moreover, RNase treatment with subsequent mass spectrometry analysis reveals all RNA-binding proteins shifting in an RNA-dependent manner [103]. While sedimentation analysis alone does not allow identification of actual protein candidates bound directly to respective circRNAs, it can be a very useful first enrichment and purification step, separating circRNPs and mRNPs, before proceeding with immunoprecipitation strategies or antisense/affinity selection (see Fig. 2, and Sections 2.1, 3.1 and 3.2) [21].

3.4.2. Analysis of circRNA-ribosome association by sucrose gradient centrifugation

The discovery that exonic circRNAs comprise the largest class of circRNAs sparked the longstanding and still controversially discussed question of whether circRNAs can function as templates for translation into peptides or proteins [38–40,104,105]. Besides ribosome profiling [106–109], polysome gradient sedimentation analysis [110] has been proven to be particularly useful in determining whether a circular RNA is associated [111,112] with actively translating ribosomes, or not [3,21,107,113–115]. Because simple co-migration with monosome or polysome-containing fractions does not suffice as evidence for translation, treatments with e.g. cycloheximide (CHX) to stabilize, and puromycin to destabilize polysome complexes can be used as additional supportive criteria [21,111,112]. In the latter case, puromycin is incorporated into the nascent protein chain leading to premature termination [116], thereby inducing dissociation of actively translating ribosomes, which is subsequently visualized by a shift of the RNA within the gradient. As described in Section 3.4.1, the changes in sedimentation of known circRNAs can be assayed by PCR and circ-junction primers [21,111,112], while transcriptome-wide analysis by RNA-seq of selected gradient fractions [112,117], allows the discovery of new potential candidates. Based on the example of circZNF609, Legnini *et al.* identified cap-independent translation through polysome gradient analysis of CHX and puromycin treated cells, as well as mass spectrometry of the corresponding protein product after overexpression of a stably integrated and FLAG-tagged circZNF609 [111]. While the general expression of circZNF609 could be linked to modulation of myoblast proliferation, it remains unclear whether this is a function of the circRNA-derived protein or the circRNA itself [39]. It should be noted, that association with actively translating ribosomes is still just one first step towards validation of a truly translated circRNA, while additional lines of evidence are needed, for example, antibody-based detection of a circRNA-specific protein isoform via Western blot, best combined with circRNA-specific siRNA-knockdown, as well as mass spectrometry to unequivocally prove the existence of the circRNA-derived protein isoform. Finally, since all published evidence in favor of circRNA translation relies to some extent on mass spectrometry, detecting proteins at very low levels, the circRNA translation question remains controversial, and one has to seriously consider the signal-versus-noise issue [38,40].

3.5. Fluorescence in situ hybridization (FISH) and immunofluorescence (IF)

The expression status of many circRNAs can widely differ between cell types or tissues, with most circRNAs occurring at relatively low copy numbers per cell [11,79]; exceptions, and RNAs expressed in exclusively circular form, have been described [3,14]. The low abundance of circRNAs, as well as the need to distinguish them from their linear counterparts, makes the application of imaging methods like fluorescence *in situ* hybridization (FISH) particularly challenging. Therefore, most ISH protocols for circRNA detection rely on the hybridization of a single, labeled probe targeting the circ-junction [12,14,81,118]. However, recent advances in probe design and signal amplification enable single-molecule detection [119]. In principle, two types of single-molecule FISH (smFISH) can be differentiated that have been successfully used to detect circRNAs [37]:

1) CircRNA detection based on hybridization of a set of 3′-end fluorophore-labeled oligonucleotides (Stellaris) [4,120,121]. Because this set of probes can also detect the respective linear mRNA, this method is specifically suitable for circRNAs without abundant linear counterpart [4,12,82], or in combination with RNase R treatment.
2) Amplification-based visualization of circRNAs (ViewRNA, RNAscope, BaseScope) via double-z-probes across the circ-junction [13,79,107,122]. In this case, the hybridization of both probes of the double-z-pair leads to signal generation and amplification, thereby achieving circRNA specificity.

Because RNA FISH alone provides information on expression level and subcellular localization of circRNAs, only the simultaneous detection and co-localization of different molecules at once yields insights on potential interaction partners [123]. This was initially studied for CDR1as/ciRS-7 and its interaction with miR-7 [4,12], with an expanding list of other examples of circRNA-miRNA interactions [124–128]. In contrast to circRNA-miRNA co-localization, the study of circRNA-protein interactions requires the application of a specified ISH protocol, including immunostaining of the potentially circRNA-interacting RBP by IF. While broadly used for linear RNAs and their *trans*-acting factors, until now there is only a small set of publications with applications to circRNPs. CircERBB2 was found to be localized to nucleoli, associated with PA2G4 (proliferation-associated 2G4) [78]. CircHOT1 on the other hand co-localizes with TIP60 (or KAT5, lysine acetyltransferase 5) [69].

Even though co-localization represents only a weak argument for direct physical interaction of the analyzed protein with a circRNA, it can yield a detailed and valuable view of the overall cellular distribution of a circRNP. Therefore, smFISH techniques combined with immunofluorescence will likely contribute to future circRNP research.

4. Conclusion and future perspectives

CircRNAs were discovered as a separate large class of noncoding RNAs only in the last decade, and their functions are just beginning to be understood. This involves interactions with RNA-binding proteins as well as with other RNA classes, such as microRNAs [5,6,129]. The methods applied so far to discover circRNA-protein interactions significantly contribute to our understanding of circRNA function. Experimentally, most protein-centric methods require suitable, specific antibodies, whereas some circRNA-centric methods rely on the introduction of RNA modifications. The latter is especially challenging for

circRNAs, where the usual end-labeling techniques cannot be applied and modifications should not impede RNA circularization nor disturb RNA structure. Therefore, only few fluorescence-based approaches of the vast number of available techniques have been employed so far. For example, protein associations with linear RNAs can be measured by FRET-assays [28], but to our knowledge, this has not been applied for circRNAs. Furthermore, insights into the dynamics and localization of circRNA-protein complexes could be gained by live-cell imaging. Until now, fluorophore-binding aptamers were inserted into circRNAs for visualization, relying on tRNA-splicing related methods [73,130]; in principle, other circRNA tagging approaches could be used [37,91]. Application of visualizable circRNAs in CRISPR-Cas engineered cell lines, expressing fluorescently tagged proteins, has future potential for studying circRNA-protein interactions [37].

Currently, when studying protein binding by circRNAs, the focus lies on the recognition of the circRNA sequence but mostly does not take RNA structure into account. However, the majority of circRNAs are predicted to be highly structured [131]. Recently, two studies suggested that circRNA degradation by RNase L [70] or UPF1/G3BP1 (UPF1 RNA helicase and ATPase, Ras GTPase-activating protein-binding protein 1) [131] relies on its structure. Additionally, binding of PKR [70], as well as NF90 [25], to circRNAs depends on RNA structure rather than on sequence. Hence, systematic and global investigations of circRNA structure promise to enhance our understanding of the interaction with RBPs and should be addressed in future research.

Besides the investigation of specific circRNA-protein interactions, establishing and applying global "RNPome" techniques will certainly generate detailed insights into circRNA-protein networks. UV-crosslinking of RNPs prior to isolation stabilizes the complexes in currently used methods [132]. For example, the RICK (RNA interactome using click chemistry) technique uses the incorporation of the nucleoside analog 5-ethynyl-uridine into RNA prior to UV-crosslinking [133]. Crosslinked RNPs are then biotinylated via click chemistry, isolated by streptavidin affinity purification, and analyzed by mass spectrometry and RNA-seq. Backsplicing events were detected by this approach and shown to partially overlap with circBase-annotated datasets, but in-depth analysis of specific circRNAs was not performed [133]. Nevertheless, this shows that identification of circRNPs is possible and application of RICK, or the similar CARIC technique (click chemistry-assisted RNA interactome capture; [134]), are promising tools for global circRNP analysis. However, both methods are limited in their requirement for nucleoside analogs for RNA biotinylation and affinity purification. Three recently developed techniques (XRNAX: protein-crosslinked RNA extraction, [135]; OOPS: orthogonal organic phase separation, [136]; PTex: phenol toluol extraction, [137]) circumvent this drawback by isolating unlabeled RNPs on the basis of organic biphasic extractions. Although technically challenging, these methods can be combined with other techniques, e.g. PTex was used to replace a gel extraction step in PAR-CLIP and compared to classical PAR-CLIP procedures [134]. With the modified protocol, the authors obtained a larger fraction of longer reads [134]. Regarding circRNAs, this would be beneficial to also obtain more reads containing the circ-junction. In a future perspective, treatment with RNase R might also be included in the protocol to specifically enrich for circRNAs. Taken together, there are several promising techniques available, which should be developed further to be suitable for circRNA research, providing further insights in circRNA-protein networks.

Declaration of Competing Interest

The authors declare that they have no known competing financial interests or personal relationships that could have appeared to influence the work reported in this paper.

Acknowledgments

Funding is acknowledged from the Deutsche Forschungsgemeinschaft (RTG 2355; projects Bi 316/18-1 and 18-2 within SPP 1935; to A.B.), project Bi 316/20-1 within Research Unit FOR 5116 (to A.B.), and the Cardio-Pulmonary Institute (CPI) within the Excellence Strategy Program Exc 2026 (to T.S.); additional funding was from the State of Hessen, LOEWE Centre DRUID (project E2, to A.B.).

References

[1] H.L. Sanger, G. Klotz, D. Riesner, H.J. Gross, A.K. Kleinschmidt, Viroids are single stranded covalently closed circular RNA molecules existing as highly base paired rod like structures, Proc. Natl. Acad. Sci. U. S. A. 73 (1976) 3852–3856, https://doi.org/10.1073/pnas.73.11.3852.

[2] J. Salzman, C. Gawad, P.L. Wang, N. Lacayo, P.O. Brown, Circular RNAs are the predominant transcript isoform from hundreds of human genes in diverse cell types, PLoS ONE 7 (2012), https://doi.org/10.1371/journal.pone.0030733.

[3] W.R. Jeck, J.A. Sorrentino, K. Wang, M.K. Slevin, C.E. Burd, J. Liu, W.F. Marzluff, N.E. Sharpless, Circular RNAs are abundant, conserved, and associated with ALU repeats, RNA 19 (2013) 141–157, https://doi.org/10.1261/rna.035667.112.

[4] S. Memczak, M. Jens, A. Elefsinioti, F. Torti, J. Krueger, A. Rybak, L. Maier, S. D. Mackowiak, L.H. Gregersen, M. Munschauer, A. Loewer, U. Ziebold, M. Landthaler, C. Kocks, F. le Noble, N. Rajewsky, Circular RNAs are a large class of animal RNAs with regulatory potency, Nature 495 (2013) 333–338, https://doi.org/10.1038/nature11928.

[5] J.E. Wilusz, A 360° view of circular RNAs: From biogenesis to functions, Wiley Interdiscip. Rev. RNA. 9 (2018) 1–17, https://doi.org/10.1002/wrna.1478.

[6] L.S. Kristensen, M.S. Andersen, L.V.W. Stagsted, K.K. Ebbesen, T.B. Hansen, J. Kjems, The biogenesis, biology and characterization of circular RNAs, Nat. Rev. Genet. 20 (2019) 675–691, https://doi.org/10.1038/s41576-019-0158-7.

[7] L.L. Chen, The expanding regulatory mechanisms and cellular functions of circular RNAs, Nat. Rev. Mol. Cell Biol. 21 (2020) 475–490, https://doi.org/10.1038/s41580-020-0243-y.

[8] E. Lasda, R. Parker, Circular RNAs: diversity of form and function, RNA 20 (2014) 1829–1842, https://doi.org/10.1261/rna.047126.114.

[9] S. Petkovic, S. Müller, RNA circularization strategies in vivo and in vitro, Nucleic Acids Res. 43 (2015) 2454–2465, https://doi.org/10.1093/nar/gkv045.

[10] R. Ashwal-Fluss, M. Meyer, N. Pamudurti, A. Ivanov, O. Bartok, M. Hanan, N. Evantal, S. Memczak, N. Rajewsky, S. Kadener, CircRNA biogenesis competes with pre-mRNA splicing, Mol. Cell. 56 (2014) 55–66, https://doi.org/10.1016/j.molcel.2014.08.019.

[11] S. Starke, I. Jost, O. Rossbach, T. Schneider, S. Schreiner, L.-H. Hung, A. Bindereif, Exon circularization requires canonical splice signals, Cell Rep. 10 (2015) 103–111, https://doi.org/10.1016/j.celrep.2014.12.002.

[12] T.B. Hansen, T.I. Jensen, B.H. Clausen, J.B. Bramsen, B. Finsen, C.K. Damgaard, J. Kjems, Natural RNA circles function as efficient microRNA sponges, Nature 495 (2013) 384–388, https://doi.org/10.1038/nature11993.

[13] M. Piwecka, P. Glažar, L.R. Hernandez-Miranda, S. Memczak, S.A. Wolf, A. Rybak-Wolf, A. Filipchyk, F. Klironomos, C.A.C. Jara, P. Fenske, T. Trimbuch, V. Zywitza, M. Plass, L. Schreyer, S. Ayoub, C. Kocks, R. Kühn, C. Rosenmund, C. Birchmeier, N. Rajewsky, Loss of a mammalian circular RNA locus causes miRNA deregulation and affects brain function, Science 357 (2017) 1–14, https://doi.org/10.1126/science.aam8526.

[14] B. Kleaveland, C.Y. Shi, J. Stefano, D.P. Bartel, A network of noncoding regulatory RNAs acts in the mammalian brain, Cell 174 (2018) 350–362.e17, https://doi.org/10.1016/j.cell.2018.05.022.

[15] M.W. Hentze, T. Preiss, Circular RNAs: splicing's enigma variations, EMBO J. 32 (2013) 923–925, https://doi.org/10.1038/emboj.2013.53.

[16] X.-O. Zhang, H.-B. Wang, Y. Zhang, X. Lu, L.-L. Chen, L.i. Yang, Complementary sequence-mediated exon circularization, Cell 159 (2014) 134–147, https://doi.org/10.1016/j.cell.2014.09.001.

[17] D. Liang, J.E. Wilusz, Short intronic repeat sequences facilitate circular RNA production, Genes Dev. 28 (2014) 2233–2247, https://doi.org/10.1101/gad.251926.114.

[18] S. Conn, K. Pillman, J. Toubia, V. Conn, M. Salmanidis, C. Phillips, S. Roslan, A. Schreiber, P. Gregory, G. Goodall, The RNA binding protein quaking regulates formation of circRNAs, Cell 160 (2015) 1125–1134, https://doi.org/10.1016/j.cell.2015.02.014.

[19] M.C. Kramer, D. Liang, D.C. Tatomer, B. Gold, Z.M. March, S. Cherry, J.E. Wilusz, Combinatorial control of Drosophila circular RNA expression by intronic repeats, hnRNPs, and SR proteins, Genes Dev. 29 (2015) 2168–2182, https://doi.org/10.1101/gad.270421.115.

[20] A. Ivanov, S. Memczak, E. Wyler, F. Torti, H. Porath, M. Orejuela, M. Piechotta, E. Levanon, M. Landthaler, C. Dieterich, N. Rajewsky, Analysis of intron sequences reveals hallmarks of circular RNA biogenesis in animals, Cell Rep. 10 (2015) 170–177, https://doi.org/10.1016/j.celrep.2014.12.019.

[21] T. Schneider, L.H. Hung, S. Schreiner, S. Starke, H. Eckhof, O. Rossbach, S. Reich, J. Medenbach, A. Bindereif, CircRNA-protein complexes: IMP3 protein component defines subfamily of circRNPs, Sci. Rep. 6 (2016) 1–11, https://doi.org/10.1038/srep31313.

[22] M.A.F. Khan, Y.J. Reckman, S. Aufiero, M.M.G. van den Hoogenhof, I. van der Made, A. Beqqali, D.R. Koolbergen, T.B. Rasmussen, J. van der Velden, E. E. Creemers, Y.M. Pinto, RBM20 regulates circular RNA production from the titin gene, Circ. Res. 119 (2016) 996–1003, https://doi.org/10.1161/CIRCRESAHA.116.309568.

[23] T. Aktaş, İ. Avşar Ilık, D. Maticzka, V. Bhardwaj, C. Pessoa Rodrigues, G. Mittler, T. Manke, R. Backofen, A. Akhtar, DHX9 suppresses RNA processing defects originating from the Alu invasion of the human genome, Nature 544 (2017) 115–119, https://doi.org/10.1038/nature21715.

[24] L. Errichelli, S. Dini Modigliani, P. Laneve, A. Colantoni, I. Legnini, D. Capauto, A. Rosa, R. De Santis, R. Scarfò, G. Peruzzi, L. Lu, E. Caffarelli, N.A. Shneider, M. Morlando, I. Bozzoni, FUS affects circular RNA expression in murine embryonic stem cell-derived motor neurons, Nat. Commun. 8 (2017) 14741, https://doi.org/10.1038/ncomms14741.

[25] X. Li, C.-X. Liu, W. Xue, Y. Zhang, S. Jiang, Q.-F. Yin, J. Wei, R.-W. Yao, L.i. Yang, L.-L. Chen, Coordinated circRNA biogenesis and function with NF90/NF110 in viral infection, Mol. Cell. 67 (2017) 214–227.e7, https://doi.org/10.1016/j.molcel.2017.05.023.

[26] Y.G. Chen, M.V. Kim, X. Chen, P.J. Batista, S. Aoyama, J.E. Wilusz, A. Iwasaki, H. Y. Chang, Sensing self and foreign circular RNAs by intron identity, Mol. Cell. 67 (2017) 228–238.e5, https://doi.org/10.1016/j.molcel.2017.05.022.

[27] S. Liu, B. Li, Q. Liang, A. Liu, L. Qu, J. Yang, Classification and function of RNA–protein interactions, Wiley Interdiscip. Rev. RNA. 11 (2020) 1–27, https://doi.org/10.1002/wrna.1601.

[28] D.D. Licatalosi, X. Ye, E. Jankowsky, Approaches for measuring the dynamics of RNA–protein interactions, Wiley Interdiscip. Rev. RNA. 11 (2020) 1–23, https://doi.org/10.1002/wrna.1565.

[29] K. Zarnack, S. Balasubramanian, M.P. Gantier, V. Kunetsky, M. Kracht, M. L. Schmitz, K. Sträßer, Dynamic mRNP remodeling in response to internal and external stimuli, Biomolecules. 10 (2020) 1–32, https://doi.org/10.3390/biom10091310.

[30] J.K. Flores, S.F. Ataide, Structural changes of RNA in complex with proteins in the SRP, Front. Mol. Biosci. 5 (2018) 1–8, https://doi.org/10.3389/fmolb.2018.00007.

[31] M. Ramanathan, D.F. Porter, P.A. Khavari, Methods to study RNA–protein interactions, Nat. Methods. 16 (2019) 225–234, https://doi.org/10.1038/s41592-019-0330-1.

[32] L. Dimitrova-Paternoga, P.K.A. Jagtap, P.-C. Chen, J. Hennig, Integrative structural biology of protein-RNA complexes, Structure. 28 (2020) 6–28, https://doi.org/10.1016/j.str.2019.11.017.

[33] A. Huang, H. Zheng, Z. Wu, M. Chen, Y. Huang, Circular RNA-protein interactions: functions, mechanisms, and identification, Theranostics. 10 (2020) 3503–3517, https://doi.org/10.7150/thno.42174.

[34] P.R. Pandey, R. Munk, G. Kundu, S. De, K. Abdelmohsen, M. Gorospe, Methods for analysis of circular RNAs, Wiley Interdiscip. Rev. RNA. 11 (2019) 1–11, https://doi.org/10.1002/wrna.1566.

[35] W.R. Jeck, N.E. Sharpless, Detecting and characterizing circular RNAs, Nat. Biotechnol. 32 (2014) 453–461, https://doi.org/10.1038/nbt.2890.

[36] A. Dieterich, C. Papantonis, in: Circular RNAs, Springer New York, New York, NY, 2018, https://doi.org/10.1007/978-1-4939-7562-4.

[37] P.R. Bejugam, A. Das, A.C. Panda, Seeing is believing: visualizing circular RNAs, Non-Coding RNA. 6 (2020) 45, https://doi.org/10.3390/ncrna6040045.

[38] L.V.W. Stagsted, K.M. Nielsen, I. Daugaard, T.B. Hansen, Noncoding AUG circRNAs constitute an abundant and conserved subclass of circles, Life Sci. Alliance. 2 (2019) 1–16, https://doi.org/10.26508/lsa.201900398.

[39] H. Ho-Xuan, P. Glažar, C. Latini, K. Heizler, J. Haase, R. Hett, M. Anders, F. Weichmann, A. Bruckmann, D. Van Den Berg, S. Hüttelmaier, N. Rajewsky, C. Hackl, G. Meister, Comprehensive analysis of translation from overexpressed circular RNAs reveals pervasive translation from linear transcripts, Nucleic Acids Res. 48 (2020) 10368–10382, https://doi.org/10.1093/nar/gkaa704.

[40] T.B. Hansen, Signal and noise in circRNA translation, Methods 21 (2021) 1046–2023, https://doi.org/10.1016/j.ymeth.2021.02.007.

[41] L. Szabo, J. Salzman, Detecting circular RNAs: bioinformatic and experimental challenges, Nat. Rev. Genet. 17 (2016) 679–692, https://doi.org/10.1038/nrg.2016.114.

[42] C. Pfafenrot, C. Preußer, Establishing essential quality criteria for the validation of circular RNAs as biomarkers, Biomol. Detect. Quantif. 17 (2019) 100085, https://doi.org/10.1016/j.bdq.2019.100085.

[43] L. Chen, C. Wang, H. Sun, J. Wang, Y. Liang, Y. Wang, G. Wong, The bioinformatics toolbox for circRNA discovery and analysis, Brief. Bioinform. 22 (2020) 1–23, https://doi.org/10.1093/bib/bbaa001.

[44] D. Tsitsipatis, M. Gorospe, Practical guide for circular RNA analysis: steps, tips, and resources, Wiley Interdiscip. Rev. RNA. 12 (2021) 1–11, https://doi.org/10.1002/wrna.1633.

[45] R. Xin, Y. Gao, Y. Gao, R. Wang, K.E. Kadash-Edmondson, B. Liu, Y. Wang, L. Lin, Y. Xing, isoCirc catalogs full-length circular RNA isoforms in human transcriptomes, Nat. Commun. 12 (2021) 266, https://doi.org/10.1038/s41467-020-20459-8.

[46] I.L. Patop, S. Wüst, S. Kadener, Past, present, and future of circRNAs, EMBO J. 38 (2019) 1–13, https://doi.org/10.15252/embj.2018100836.

[47] K.J. Riley, J.A. Steitz, The "observer effect" in genome-wide surveys of protein-RNA interactions, Mol. Cell. 49 (2013) 601–604, https://doi.org/10.1016/j.molcel.2013.01.030.

[48] Y. Zhang, X.-O. Zhang, T. Chen, J.-F. Xiang, Q.-F. Yin, Y.-H. Xing, S. Zhu, L. Yang, L.-L. Chen, Circular intronic long noncoding RNAs, Mol. Cell. 51 (6) (2013) 792–806, https://doi.org/10.1016/j.molcel.2013.08.017.

[49] L.M. Holdt, A. Stahringer, K. Sass, G. Pichler, N.A. Kulak, W. Wilfert, A. Kohlmaier, A. Herbst, B.H. Northoff, A. Nicolaou, G. Gäbel, F. Beutner, M. Scholz, J. Thiery, K. Musunuru, K. Krohn, M. Mann, D. Teupser, Circular non-coding RNA ANRIL modulates ribosomal RNA maturation and atherosclerosis in humans, Nat. Commun. 7 (2016) 12429, https://doi.org/10.1038/ncomms12429.

[50] A.C. Panda, S. De, I. Grammatikakis, R. Munk, X. Yang, Y. Piao, D.B. Dudekula, K. Abdelmohsen, M. Gorospe, High-purity circular RNA isolation method (RPAD) reveals vast collection of intronic circRNAs, Nucleic Acids Res. 45 (2017), https://doi.org/10.1093/nar/gkx297.

[51] M.S. Xiao, J.E. Wilusz, An improved method for circular RNA purification using RNase R that efficiently removes linear RNAs containing G-quadruplexes or structured 3' ends, Nucleic Acids Res. 47 (2019) 8755–8769, https://doi.org/10.1093/nar/gkz576.

[52] D. Siede, K. Rapti, A.A. Gorska, H.A. Katus, J. Altmüller, J.N. Boeckel, B. Meder, C. Maack, M. Völkers, O.J. Müller, J. Backs, C. Dieterich, Identification of circular RNAs with host gene-independent expression in human model systems for cardiac differentiation and disease, J. Mol. Cell. Cardiol. 109 (2017) 48–56, https://doi.org/10.1016/j.yjmcc.2017.06.015.

[53] Y.-J. Zhu, B. Zheng, G.-J. Luo, X.-K. Ma, X.-Y. Lu, X.-M. Lin, S. Yang, Q. Zhao, T. Wu, Z.-X. Li, X.-L. Liu, R. Wu, J.-F. Liu, Y. Ge, L. Yang, H.-Y. Wang, L. Chen, Circular RNAs negatively regulate cancer stem cells by physically binding FMRP against CCAR1 complex in hepatocellular carcinoma, Theranostics. 9 (2019) 3526–3540, https://doi.org/10.7150/thno.32796.

[54] T. Schneider, S. Schreiner, C. Preußer, A. Bindereif, O. Rossbach, Northern blot analysis of circular RNAs, Methods Mol. Biol. 1724 (2018) 119–133, https://doi.org/10.1007/978-1-4939-7562-4_10.

[55] J. Ule, H.W. Hwang, R.B. Darnell, The future of cross-linking and immunoprecipitation (CLIP), Cold Spring Harb. Perspect. Biol. 10 (2018) a032243, https://doi.org/10.1101/cshperspect.a032243.

[56] E.C. Wheeler, E.L. Van Nostrand, G.W. Yeo, Advances and challenges in the detection of transcriptome-wide protein–RNA interactions, Wiley Interdiscip. Rev. RNA. 9 (2018) 1–11, https://doi.org/10.1002/wrna.1436.

[57] F.C.Y. Lee, J. Ule, Advances in CLIP technologies for studies of protein-RNA interactions, Mol. Cell. 69 (2018) 354–369, https://doi.org/10.1016/j.molcel.2018.01.005.

[58] Z. Li, C. Huang, C. Bao, L. Chen, M. Lin, X. Wang, G. Zhong, B. Yu, W. Hu, L. Dai, P. Zhu, Z. Chang, Q. Wu, Y. Zhao, Y. Jia, P. Xu, H. Liu, G. Shan, Exon-intron circular RNAs regulate transcription in the nucleus, Nat. Struct. Mol. Biol. 22 (2015) 256–264, https://doi.org/10.1038/nsmb.2959.

[59] D. Barbagallo, A. Caponnetto, M. Cirnigliaro, D. Brex, C. Barbagallo, F. D'Angeli, A. Morrone, R. Caltabiano, G.M. Barbagallo, M. Ragusa, C. Di Pietro, T.B. Hansen, M. Purrello, CircSMARCA5 inhibits migration of glioblastoma multiforme cells by regulating a molecular axis involving splicing factors SRSF1/SRSF3/PTB, Int. J. Mol. Sci. 19 (2018) 1–13, https://doi.org/10.3390/ijms19020480.

[60] K. Abdelmohsen, A.C. Panda, R. Munk, I. Grammatikakis, D.B. Dudekula, S. De, J. Kim, J.H. Noh, K.M. Kim, J.L. Martindale, M. Gorospe, Identification of HuR target circular RNAs uncovers suppression of PABPN1 translation by circPABPN1, RNA Biol. 14 (2017) 361–369, https://doi.org/10.1080/15476286.2017.1279788.

[61] D.B. Dudekula, A.C. Panda, I. Grammatikakis, S. De, K. Abdelmohsen, M. Gorospe, Circinteractome: A web tool for exploring circular RNAs and their interacting proteins and microRNAs, RNA Biol. 13 (2016) 34–42, https://doi.org/10.1080/15476286.2015.1128065.

[62] K. Zhang, X. Pan, Y. Yang, H.-B. Shen, CRIP: predicting circRNA–RBP-binding sites using a codon-based encoding and hybrid deep neural networks, RNA 25 (2019) 1604–1615, https://doi.org/10.1261/rna.070565.119.

[63] M. Zhang, T. Wang, G. Xiao, Y. Xie, Large-scale profiling of RBP-circRNA interactions from public CLIP-seq datasets, Genes 11 (2020) 54, https://doi.org/10.3390/genes11010054.

[64] Y. Yang, Z. Hou, Z. Ma, X. Li, K.-C. Wong, iCircRBP-DHN: identification of circRNA-RBP interaction sites using deep hierarchical network, Brief. Bioinform. bbaa274 (2020) 1–11, https://doi.org/10.1093/bib/bbaa274.

[65] L.M. Hellman, M.G. Fried, Electrophoretic mobility shift assay (EMSA) for detecting protein-nucleic acid interactions, Nat. Protoc. 2 (2007) 1849–1861, https://doi.org/10.1038/nprot.2007.249.

[66] S.F. Mitchell, J.R. Lorsch, Standard in vitro assays for protein-nucleic acid interactions - Gel shift assays for RNA and DNA binding, 1st ed., Elsevier Inc., 2014, https://doi.org/10.1016/B978-0-12-420119-4.00015-X.

[67] Q. Li, Y. Wang, S. Wu, Z. Zhou, X. Ding, R. Shi, R.F. Thorne, X.D. Zhang, W. Hu, M. Wu, CircACC1 regulates assembly and activation of AMPK complex under metabolic stress, Cell Metab. 30 (2019) 157-173.e7, https://doi.org/10.1016/j.cmet.2019.05.009.

[68] F. Yang, A. Hu, D. Li, J. Wang, Y. Guo, Y. Liu, H. Li, Y. Chen, X. Wang, K. Huang, L. Zheng, Q. Tong, Circ-HuR suppresses HuR expression and gastric cancer progression by inhibiting CNBP transactivation, Mol. Cancer. 18 (2019) 1–16, https://doi.org/10.1186/s12943-019-1094-z.

[69] L. Wang, H. Long, Q. Zheng, X. Bo, X. Xiao, B. Li, Circular RNA circRHOT1 promotes hepatocellular carcinoma progression by initiation of NR2F6

expression, Mol. Cancer. 18 (2019) 1–12, https://doi.org/10.1186/s12943-019-1046-7.
[70] C.-X. Liu, X. Li, F. Nan, S. Jiang, X. Gao, S.-K. Guo, W. Xue, Y. Cui, K. Dong, H. Ding, B. Qu, Z. Zhou, N. Shen, L. Yang, L.-L. Chen, Structure and degradation of circular RNAs regulate PKR activation in innate immunity, Cell 177 (2019) 865–880.e21, https://doi.org/10.1016/j.cell.2019.03.046.
[71] J. Breuer, O. Rossbach, Production and purification of artificial circular RNA sponges for application in molecular biology and medicine, Methods Protoc. 3 (2020) 1–14, https://doi.org/10.3390/mps3020042.
[72] R.A. Wesselhoeft, P.S. Kowalski, D.G. Anderson, Engineering circular RNA for potent and stable translation in eukaryotic cells, Nat. Commun. 9 (2018) 2629, https://doi.org/10.1038/s41467-018-05096-6.
[73] J.L. Litke, S.R. Jaffrey, Highly efficient expression of circular RNA aptamers in cells using autocatalytic transcripts, Nat. Biotechnol. 37 (2019) 667–675, https://doi.org/10.1038/s41587-019-0090-6.
[74] C. Chu, Q.C. Zhang, S.T. Da Rocha, R.A. Flynn, M. Bharadwaj, J.M. Calabrese, T. Magnuson, E. Heard, H.Y. Chang, Systematic discovery of Xist RNA binding proteins, Cell 161 (2015) 404–416, https://doi.org/10.1016/j.cell.2015.03.025.
[75] C.A. McHugh, C.-K. Chen, A. Chow, C.F. Surka, C. Tran, P. McDonel, A. Pandya-Jones, M. Blanco, C. Burghard, A. Moradian, M.J. Sweredoski, A.A. Shishkin, J. Su, E.S. Lander, S. Hess, K. Plath, M. Guttman, The Xist lncRNA interacts directly with SHARP to silence transcription through HDAC3, Nature 521 (2015) 232–236, https://doi.org/10.1038/nature14443.
[76] B. Rogell, B. Fischer, M. Rettel, J. Krijgsveld, A. Castello, M.W. Hentze, Specific RNP capture with antisense LNA/DNA mixmers, RNA 23 (2017) 1290–1302, https://doi.org/10.1261/rna.060798.117.
[77] W.W. Du, W. Yang, E. Liu, Z. Yang, P. Dhaliwal, B.B. Yang, Foxo3 circular RNA retards cell cycle progression via forming ternary complexes with p21 and CDK2, Nucleic Acids Res. 44 (2016) 2846–2858, https://doi.org/10.1093/nar/gkw027.
[78] X. Huang, M. He, S. Huang, R. Lin, M. Zhan, D. Yang, H. Shen, S. Xu, W. Cheng, J. Yu, Z. Qiu, J. Wang, Circular RNA circERBB2 promotes gallbladder cancer progression by regulating PA2G4-dependent rDNA transcription, Mol. Cancer. 18 (2019) 1–19, https://doi.org/10.1186/s12943-019-1098-8.
[79] P.R. Pandey, J.H. Yang, D. Tsitsipatis, A.C. Panda, J.H. Noh, K.M. Kim, R. Munk, T. Nicholson, D. Hanniford, D. Argibay, X. Yang, J.L. Martindale, M.W. Chang, S. W. Jones, E. Hernando, P. Sen, S. De, K. Abdelmohsen, M. Gorospe, CircSamd4 represses myogenic transcriptional activity of PUR proteins, Nucleic Acids Res. 48 (2020) 3789–3805, https://doi.org/10.1093/nar/gkaa035.
[80] A. Bronisz, A.K. Rooj, K. Krawczynski, P. Peruzzi, E. Salinska, I. Nakano, B. Purow, E.A. Chiocca, J. Godlewski, The nuclear DICER-circular RNA complex drives the deregulation of the glioblastoma cell microRNAome, Sci. Adv. 6 (2020) 1–17, https://doi.org/10.1126/sciadv.abc0221.
[81] Q. Zhao, J. Liu, H. Deng, R. Ma, J.-Y. Liao, H. Liang, J. Hu, J. Li, Z. Guo, J. Cai, X. Xu, Z. Gao, S. Su, Targeting mitochondria-located circRNA SCAR alleviates NASH via reducing mROS output, Cell 183 (2020) 76–93.e22, https://doi.org/10.1016/j.cell.2020.08.009.
[82] C. Preußer, L.-H. Hung, T. Schneider, S. Schreiner, M. Hardt, A. Moebus, S. Santoso, A. Bindereif, Selective release of circRNAs in platelet-derived extracellular vesicles, J. Extracell. Vesicles. 7 (2018), https://doi.org/10.1080/20013078.2018.1424473.
[83] D. Gemmill, S. D'souza, V. Meier-Stephenson, T.R. Patel, Current approaches for RNA-labelling to identify RNA-binding proteins, Biochem. Cell Biol. 98 (2020) 31–41, https://doi.org/10.1139/bcb-2019-0041.
[84] M.L. Winz, A. Samanta, D. Benzinger, A. Jäschke, Site-specific terminal and internal labeling of RNA by poly(A) polymerase tailing and copper-catalyzed or copper-free strain-promoted click chemistry, Nucleic Acids Res. 40 (2012) 1–13, https://doi.org/10.1093/nar/gks062.
[85] S. Schreiner, A. Didio, L.-H. Hung, A. Bindereif, Design and application of circular RNAs with protein-sponge function, Nucleic Acids Res. 48 (2020) 12326–12335, https://doi.org/10.1093/nar/gkaa1085.
[86] P. Bayat, R. Nosrati, M. Alibolandi, H. Rafatpanah, K. Abnous, M. Khedri, M. Ramezani, SELEX methods on the road to protein targeting with nucleic acid aptamers, Biochimie 154 (2018) 132–155, https://doi.org/10.1016/j.biochi.2018.09.001.
[87] T. Adachi, Y. Nakamura, Aptamers: a review of their chemical properties and modifications for therapeutic application, Molecules 24 (2019), https://doi.org/10.3390/molecules24234229.
[88] D.S. Peabody, The RNA binding size of bacteriophage MS2 coat protein, EMBO J. 12 (1993) 595–600, https://doi.org/10.1002/j.1460-2075.1993.tb05691.x.
[89] C.D. Cilley, J.R. Williamson, Analysis of bacteriophage n protein and peptide binding to boxB RNA using polyacrylamide gel coelectrophoresis (PACE), RNA 3 (1997) 57–67, https://doi.org/10.1021/bi0351312.
[90] P. Legault, J. Li, J. Mogridge, L.E. Kay, J. Greenblatt, NMR structure of the bacteriophage λ N peptide/boxB RNA complex: recognition of a GNRA fold by an arginine-rich motif, Cell 93 (1998) 289–299, https://doi.org/10.1016/S0092-8674(00)81579-2.
[91] E. Braselmann, C. Rathbun, E.M. Richards, A.E. Palmer, Illuminating RNA biology: tools for imaging RNA in live mammalian cells, Cell Chem. Biol. 27 (2020) 891–903, https://doi.org/10.1016/j.chembiol.2020.06.010.
[92] A.K. Hollensen, H.S. Thomsen, M. Lloret-Llinares, A.B. Kamstrup, J.M. Jensen, M. Luckmann, N. Birkmose, J. Palmfeldt, T.H. Jensen, T.B. Hansen, C. K. Damgaard, circZNF827 nucleates a transcription inhibitory complex to balance neuronal differentiation, Elife. 9 (2020) 1–29, https://doi.org/10.7554/eLife.58478.
[93] T.W. Nilsen, RNase footprinting to map sites of RNA–protein interactions, Cold Spring Harb. Protoc. 2014 (2014) 677–682, https://doi.org/10.1101/pdb.prot080788.
[94] I.M. Silverman, F. Li, A. Alexander, L. Goff, C. Trapnell, J.L. Rinn, B.D. Gregory, RNase-mediated protein footprint sequencing reveals protein-binding sites throughout the human transcriptome, Genome Biol. 15 (2014) 1–16, https://doi.org/10.1186/gb-2014-15-1-r3.
[95] Z. Ji, R. Song, H. Huang, A. Regev, K. Struhl, Transcriptome-scale RNase-footprinting of RNA-protein complexes, Nat. Biotechnol. 34 (2016) 410–413, https://doi.org/10.1038/nbt.3441.
[96] Y. Qu, M. Boutjdir, RNase protection assay for quantifying gene expression levels, Methods 366 (2007) 145–158, https://doi.org/10.1007/978-1-59745-030-0_8.
[97] M.F. Carey, C.L. Peterson, S.T. Smale, The RNase protection assay, Cold Spring Harb. Protoc. 8 (2013) 276–285, https://doi.org/10.1101/pdb.prot071910.
[98] E.W. Ottesen, D. Luo, J. Seo, N.N. Singh, R.N. Singh, Human survival motor neuron genes generate a vast repertoire of circular RNAs, Nucleic Acids Res. 47 (2019) 2884–2905, https://doi.org/10.1093/nar/gkz034.
[99] R.J. Britten, R.B. Roberts, High-resolution density gradient sedimentation analysis, Science 131 (1960) 32–33, https://doi.org/10.1126/science:131.3392.32.
[100] T. Rösel, J. Medenbach, A. Damianov, S. Schreiner, A. Bindereif, in: Handbook of RNA Biochemistry: Second, Completely Revised and Enlarged Edition, Wiley-VCH Verlag GmbH & Co. KGaA, Weinheim, Germany, 2014, pp. 1055–1066, https://doi.org/10.1002/9783527647064.ch47.
[101] A.W. Heumüller, J.N. Boeckel, Characterization and validation of circular RNA and their host gene mRNA expression using PCR, Methods Mol. Biol. 1724 (2018) 57–67, https://doi.org/10.1007/978-1-4939-7562-4_5.
[102] A. Smirnov, K.U. Förstner, E. Holmqvist, A. Otto, R. Günster, D. Becher, R. Reinhardt, J. Vogel, Grad-seq guides the discovery of ProQ as a major small RNA-binding protein, Proc. Natl. Acad. Sci. U. S. A. 113 (2016) 11591–11596, https://doi.org/10.1073/pnas.1609981113.
[103] M. Caudron-Herger, S.F. Rusin, M.E. Adamo, J. Seiler, V.K. Schmid, E. Barreau, A. N. Kettenbach, S. Diederichs, R-DeeP: proteome-wide and quantitative identification of RNA-dependent proteins by density gradient ultracentrifugation, Mol. Cell. 75 (2019) 184–199.e10, https://doi.org/10.1016/j.molcel.2019.04.018.
[104] D.C. Tatomer, J.E. Wilusz, An unchartered journey for ribosomes: circumnavigating circular RNAs to produce proteins, Mol. Cell. 66 (2017) 1–2, https://doi.org/10.1016/j.molcel.2017.03.011.
[105] T. Schneider, A. Bindereif, Circular RNAs: coding or noncoding? Cell Res. 27 (2017) 724–725, https://doi.org/10.1038/cr.2017.70.
[106] J.U. Guo, V. Agarwal, H. Guo, D.P. Bartel, Expanded identification and characterization of mammalian circular RNAs, Genome Biol. 15 (2014) 1–14, https://doi.org/10.1186/s13059-014-0409-z.
[107] X. You, I. Vlatkovic, A. Babic, T. Will, I. Epstein, G. Tushev, Güney Akbalik, M. Wang, C. Glock, C. Quedenau, X. Wang, J. Hou, H. Liu, W. Sun, S. Sambandan, T. Chen, E.M. Schuman, W. Chen, Neural circular RNAs are derived from synaptic genes and regulated by development and plasticity, Nat. Neurosci. 18 (2015) 603–610, https://doi.org/10.1038/nn.3975.
[108] N.R. Pamudurti, O. Bartok, M. Jens, R. Ashwal-Fluss, C. Stottmeister, L. Ruhe, M. Hanan, E. Wyler, D. Perez-Hernandez, E. Ramberger, S. Shenzis, M. Samson, G. Dittmar, M. Landthaler, M. Chekulaeva, N. Rajewsky, S. Kadener, Translation of circRNAs, Mol. Cell. 66 (2017) 9–21.e7, https://doi.org/10.1016/j.molcel.2017.02.021.
[109] S. van Heesch, F. Witte, V. Schneider-Lunitz, J.F. Schulz, E. Adami, A.B. Faber, M. Kirchner, H. Maatz, S. Blachut, C.-L. Sandmann, M. Kanda, C.L. Worth, S. Schafer, L. Calviello, R. Merriott, G. Patone, O. Hummel, E. Wyler, B. Obermayer, M.B. Mücke, E.L. Lindberg, F. Trnka, S. Memczak, M. Schilling, L. E. Felkin, P.J.R. Barton, N.M. Quaife, K. Vanezis, S. Diecke, M. Mukai, N. Mah, S.-J. Oh, A. Kurtz, C. Schramm, D. Schwinge, M. Sebode, M. Harakalova, F. W. Asselbergs, A. Vink, R.A. de Weger, S. Viswanathan, A.A. Widjaja, A. Gärtner-Rommel, H. Milting, C. dos Remedios, C. Knosalla, P. Mertins, M. Landthaler, M. Vingron, W.A. Linke, J.G. Seidman, C.E. Seidman, N. Rajewsky, U. Ohler, S. A. Cook, N. Hubner, The translational landscape of the human heart, Cell 178 (2019) 242–260.e29, https://doi.org/10.1016/j.cell.2019.05.010.
[110] D. Bartsch, A. Zirkel, L. Kurian, Characterization of circular RNAs (circRNA) associated with the translation machinery, Methods Mol. Biol. 1724 (2018) 159–166, https://doi.org/10.1007/978-1-4939-7562-4_13.
[111] I. Legnini, G. Di Timoteo, F. Rossi, M. Morlando, F. Briganti, O. Sthandier, A. Fatica, T. Santini, A. Andronache, M. Wade, P. Laneve, N. Rajewsky, I. Bozzoni, Circ-ZNF609 is a circular RNA that can be translated and functions in myogenesis, Mol. Cell. 66 (2017) 22–37.e9, https://doi.org/10.1016/j.molcel.2017.02.017.
[112] Y. Yang, X. Fan, M. Mao, X. Song, P. Wu, Y. Zhang, Y. Jin, Y. Yang, L.-L. Chen, Y. Wang, C.CL. Wong, X. Xiao, Z. Wang, Extensive translation of circular RNAs driven by N^6-methyladenosine, Cell Res. 27 (2017) 626–641, https://doi.org/10.1038/cr.2017.31.
[113] M. Kozak, Inability of circular mRNA to attach to eukaryotic ribosomes, Nature 280 (1979) 82–85, https://doi.org/10.1038/280082a0.
[114] B. Capel, A. Swain, S. Nicolis, A. Hacker, M. Walter, P. Koopman, P. Goodfellow, R. Lovell-Badge, Circular transcripts of the testis-determining gene Sry in adult mouse testis, Cell 73 (1993) 1019–1030, https://doi.org/10.1016/0092-8674(93)90279-Y.
[115] T. Toptan, B. Abere, M.A. Nalesnik, S.H. Swerdlow, S. Ranganathan, N. Lee, K. H. Shair, P.S. Moore, Y. Chang, Circular DNA tumor viruses make circular RNAs, Proc. Natl. Acad. Sci. U. S. A. 115 (2018) E8737–E8745, https://doi.org/10.1073/pnas.1811728115.

[116] R. Aviner, The science of puromycin: from studies of ribosome function to applications in biotechnology, Comput. Struct. Biotechnol. J. 18 (2020) 1074–1083, https://doi.org/10.1016/j.csbj.2020.04.014.
[117] C. Ragan, G.J. Goodall, N.E. Shirokikh, T. Preiss, Insights into the biogenesis and potential functions of exonic circular RNA, Sci. Rep. 9 (2019) 1–18, https://doi.org/10.1038/s41598-018-37037-0.
[118] A. Zirkel, A. Papantonis, Detecting circular RNAs by RNA fluorescence in situ hybridization, Methods Mol. Biol. 1724 (2018) 69–75, https://doi.org/10.1007/978-1-4939-7562-4_6.
[119] X. Pichon, M. Lagha, F. Mueller, E. Bertrand, A growing toolbox to image gene expression in single cells: sensitive approaches for demanding challenges, Mol. Cell. 71 (2018) 468–480, https://doi.org/10.1016/j.molcel.2018.07.022.
[120] A. Raj, P. van den Bogaard, S.A. Rifkin, A. van Oudenaarden, S. Tyagi, Imaging individual mRNA molecules using multiple singly labeled probes, Nat. Methods. 5 (2008) 877–879, https://doi.org/10.1038/nmeth.1253.
[121] C. Kocks, A. Boltengagen, M. Piwecka, A. Rybak-Wolf, N. Rajewsky, Single-molecule fluorescence in situ hybridization (FISH) of circular RNA CDR1as, Methods Mol. Biol. 1724 (2018) 77–96, https://doi.org/10.1007/978-1-4939-7562-4_7.
[122] C. Suenkel, D. Cavalli, S. Massalini, F. Calegari, N. Rajewsky, A highly conserved circular RNA is required to keep neural cells in a progenitor state in the mammalian brain, Cell Rep. 30 (2020) 2170–2179.e5, https://doi.org/10.1016/j.celrep.2020.01.083.
[123] T. Gross-thebing, A. Paksa, E. Raz, Two-color whole-mount in situ hybridization to vertebrate and Drosophila embryos, Trends Genet. 10 (1994) 266, https://doi.org/10.1016/0168-9525(90)90008-T.
[124] Q. Zheng, C. Bao, W. Guo, S. Li, J. Chen, B. Chen, Y. Luo, D. Lyu, Y. Li, G. Shi, L. Liang, J. Gu, X. He, S. Huang, Circular RNA profiling reveals an abundant circHIPK3 that regulates cell growth by sponging multiple miRNAs, Nat. Commun. 7 (2016) 11215, https://doi.org/10.1038/ncomms11215.
[125] Y. Bai, Y. Zhang, B. Han, L. Yang, X. Chen, R. Huang, F. Wu, J. Chao, P. Liu, G. Hu, J.H. Zhang, H. Yao, Circular RNA DLGAP4 ameliorates ischemic stroke outcomes by targeting miR-143 to regulate endothelial-mesenchymal transition associated with blood–brain barrier integrity, J. Neurosci. 38 (2018) 32–50, https://doi.org/10.1523/JNEUROSCI.1348-17.2017.
[126] T. Liu, Q. Lu, J. Liu, S. Xie, B. Feng, W. Zhu, M. Liu, Y. Liu, X. Zhou, W. Sun, Y. Zhang, X. Chen, F. Fang, H. Guo, R. Yang, Circular RNA FAM114A2 suppresses progression of bladder cancer via regulating ΔNP63 by sponging miR-762, Cell Death Dis. 11 (2020), https://doi.org/10.1038/s41419-020-2226-5.
[127] X. Zheng, M. Huang, L. Xing, R. Yang, X. Wang, R. Jiang, L. Zhang, J. Chen, The circRNA circSEPT9 mediated by E2F1 and EIF4A3 facilitates the carcinogenesis and development of triple-negative breast cancer, Mol. Cancer. 19 (2020) 1–22, https://doi.org/10.1186/s12943-020-01183-9.
[128] D. Han, Y. Wang, Y. Wang, X. Dai, T. Zhou, J. Chen, B. Tao, J. Zhang, F. Cao, The tumor-suppressive human circular RNA circITCH sponges miR-330-5p to ameliorate doxorubicin-induced cardiotoxicity through upregulating SIRT6, Survivin, and SERCA2a, Circ. Res. 127 (2020) E108–E125, https://doi.org/10.1161/CIRCRESAHA.119.316061.
[129] L. Verduci, S. Strano, Y. Yarden, G. Blandino, The circRNA–microRNA code: emerging implications for cancer diagnosis and treatment, Mol. Oncol. 13 (2019) 669–680, https://doi.org/10.1002/1878-0261.12468.
[130] Z. Lu, G.S. Filonov, J.J. Noto, C.A. Schmidt, T.L. Hatkevich, Y. Wen, S.R. Jaffrey, A.G. Matera, Metazoan tRNA introns generate stable circular RNAs in vivo, RNA 21 (2015) 1554–1565, https://doi.org/10.1261/rna.052944.115.
[131] J.W. Fischer, V.F. Busa, Y. Shao, A.K.L. Leung, Structure-mediated RNA decay by UPF1 and G3BP1, Mol. Cell. 78 (2020) 70–84.e6, https://doi.org/10.1016/j.molcel.2020.01.021.
[132] R. Van Ende, S. Balzarini, K. Geuten, Single and combined methods to specifically or bulk-purify RNA–protein complexes, Biomolecules. 10 (2020) 1–27, https://doi.org/10.3390/biom10081160.
[133] X. Bao, X. Guo, M. Yin, M. Tariq, Y. Lai, S. Kanwal, J. Zhou, N. Li, Y. Lv, C. Pulido-Quetglas, X. Wang, L. Ji, M.J. Khan, X. Zhu, Z. Luo, C. Shao, D.-H. Lim, X. Liu, N. Li, W. Wang, M. He, Y.-L. Liu, C. Ward, T. Wang, G. Zhang, D. Wang, J. Yang, Y. Chen, C. Zhang, R. Jauch, Y.-G. Yang, Y. Wang, B. Qin, M.-L. Anko, A. P. Hutchins, H. Sun, H. Wang, X.-D. Fu, B. Zhang, M.A. Esteban, Capturing the interactome of newly transcribed RNA, Nat. Methods. 15 (2018) 213–220, https://doi.org/10.1038/nmeth.4595.
[134] R. Huang, M. Han, L. Meng, X. Chen, Transcriptome-wide discovery of coding and noncoding RNA-binding proteins, Proc. Natl. Acad. Sci. U. S. A. 115 (2018) E3879–E3887, https://doi.org/10.1073/pnas.1718406115.
[135] J. Trendel, T. Schwarzl, R. Horos, A. Prakash, A. Bateman, M.W. Hentze, J. Krijgsveld, The human RNA-binding proteome and its dynamics during translational arrest, Cell 176 (2019) 391–403.e19, https://doi.org/10.1016/j.cell.2018.11.004.
[136] R.M.L. Queiroz, T. Smith, E. Villanueva, M. Marti-Solano, M. Monti, M. Pizzinga, D.-M. Mirea, M. Ramakrishna, R.F. Harvey, V. Dezi, G.H. Thomas, A.E. Willis, K. S. Lilley, Comprehensive identification of RNA–protein interactions in any organism using orthogonal organic phase separation (OOPS), Nat. Biotechnol. 37 (2019) 169–178, https://doi.org/10.1038/s41587-018-0001-2.
[137] E.C. Urdaneta, C.H. Vieira-Vieira, T. Hick, H.H. Wessels, D. Figini, R. Moschall, J. Medenbach, U. Ohler, S. Granneman, M. Selbach, B.M. Beckmann, Purification of cross-linked RNA-protein complexes by phenol-toluol extraction, Nat. Commun. 10 (2019) 990, https://doi.org/10.1038/s41467-019-08942-3.

cells

MDPI

Article

Molecular Determinants for RNA Release into Extracellular Vesicles

Marie-Luise Mosbach [1], Christina Pfafenrot [1], Elke Pogge von Strandmann [2], Albrecht Bindereif [1,*,†] and Christian Preußer [2,*,†]

[1] Institute of Biochemistry, Justus Liebig University of Gießen, 35392 Gießen, Germany; marie.mosbach@chemie.bio.uni-giessen.de (M.-L.M.); christina.pfafenrot@chemie.bio.uni-giessen.de (C.P.)
[2] Institute for Tumor Immunology, Center for Tumor Biology and Immunology (ZTI), Philipps University of Marburg, 35043 Marburg, Germany; poggevon@staff.uni-marburg.de
* Correspondence: Albrecht.Bindereif@chemie.bio.uni-giessen.de (A.B.); preusserc@staff.uni-marburg.de (C.P.); Tel.: +49-641-99-35420 (A.B.); +49-6421-28-21644 (C.P.)
† These authors contributed equally to this manuscript.

Abstract: Extracellular vesicles (EVs) are important for intercellular communication and act as vehicles for biological material, such as various classes of coding and non-coding RNAs, a few of which were shown to selectively target into vesicles. However, protein factors, mechanisms, and sequence elements contributing to this specificity remain largely elusive. Here, we use a reporter system that results in different types of modified transcripts to decipher the specificity determinants of RNAs released into EVs. First, we found that small RNAs are more efficiently packaged into EVs than large ones, and second, we determined absolute quantities for several endogenous RNA transcripts in EVs (U6 snRNA, U1 snRNA, Y1 RNA, and GAPDH mRNA). We show that RNA polymerase III (pol III) transcripts are more efficiently secreted into EVs compared to pol II-derived transcripts. Surprisingly, our quantitative analysis revealed no RNA accumulation in the vesicles relative to the total cellular levels, based on both overexpressed reporter transcripts and endogenous RNAs. RNA appears to be EV-associated only at low copy numbers, ranging between 0.02 and 1 molecule per EV. This RNA association may reflect internal EV encapsulation or a less tightly bound state at the vesicle surface.

Keywords: extracellular vesicles; exRNA; absolute RNA quantification; Y1 RNA; U1 snRNA; U6 snRNA; GAPDH mRNA

Citation: Mosbach, M.-L.; Pfafenrot, C.; von Strandmann, E.P.; Bindereif, A.; Preußer, C. Molecular Determinants for RNA Release into Extracellular Vesicles. *Cells* **2021**, *10*, 2674. https://doi.org/10.3390/cells10102674

Academic Editors: Alice Conigliaro and Carla Cicchini

Received: 2 September 2021
Accepted: 29 September 2021
Published: 6 October 2021

1. Introduction

Extracellular vesicles (EVs) are omnipresent lipid particles released by nearly every cell and are involved in cell–cell communication [1–3]. As this already implies, EVs are not simply empty lipid bins, but rather represent transport vesicles, which are associated with various biomolecules. Although the composition of EVs is a highly debated topic, a large number of different biomolecules have been identified to be associated with EVs [4–6]. However, the presence or absence of certain molecules appears strongly dependent on the starting material, the type of purification, and the research group [7,8]. Nevertheless, various proteins (e.g., receptors, transcription factors, enzymes, and extracellular matrix proteins), lipids, and nucleic acids (DNA and RNA) have been identified [9–11]. In particular, ribonucleic acids have gained considerable attention in the last few years. While most studies focus on the functionally well-characterized miRNAs [12–14], the advent of the RNA-Seq technologies allowed to analyze extremely low quantities of RNA, revealing different types of EV-associated RNA. Several studies described that, in addition to the already mentioned miRNAs, other non-coding RNAs, such as lncRNAs, snoRNAs, tRNAs, rRNAs, piRNAs, Y RNAs, and circRNAs are also present [15–19]. In some reports, the existence of mRNAs within vesicles could also be demonstrated, transferable to and functionally active in recipient cells [20–22].

Apart from the identification of distinct RNA classes, the question of a specific and direct loading into EVs has remained unanswered. Some mechanisms have been proposed, such as protein-mediated secretion of RNAs, in which RNA-binding proteins assist with selective release of RNAs to EVs, some through recognition of RNA-binding motifs, in particular for miRNAs [23–27]. In addition to protein-mediated exports, less selective export mechanisms and determinants have also been identified, such as size dependence, whereby mainly small RNAs are present in vesicles; a concentration-directed RNA sorting into EVs was also considered [19,28,29]. Interestingly, recent quantitative studies showed that extracellular miRNAs could be relatively rare in EVs, with a range between 0.0001 and 0.1 molecules per EV [30–32]. Likewise, detected mRNAs are less frequently associated with EVs. In contrast, other RNAs, in particular those derived from RNA Polymerase III, such as Y RNAs and tRNA (fragments) as well as snRNA and rRNA fragments, appear to be more abundant in EVs [31]. The previous assessment that miRNAs are enriched in EVs may be related to the fact that miRNAs are predominantly associated with RNA-binding proteins, such as AGO2, and are found as contaminants during isolation or associated with the outside surface of EVs, thus protecting extracellular miRNAs from degradation by RNases [28,33–35].

Here, we used different reporter expression constructs to determine which RNA characteristics mediate the preferential release of RNAs into vesicles. In addition to a length dependence, we were able to show that RNA polymerase III transcripts are preferentially associated with EVs. In addition, we did absolute quantification of various endogenous RNAs in EVs versus total cells. In sum, EV-mediated RNA secretion appears to be inefficient and only a few RNA molecules are present within each vesicle. Our results and EV-RNA quantitation should contribute to our mechanistic understanding of EV-mediated transfer and functional range of RNAs.

2. Materials and Methods

2.1. Cell Culture and Transfection

All cell lines A549, ES-2, HEK293, HepG2, and U373 were maintained at 37 °C in 5% CO_2 in Dulbecco's Modified Eagle Medium (Gibco™, Thermo Fisher Scientific, Waltham, MA, USA) supplemented with 10% fetal bovine serum (Gibco™, Life Technologies, Carlsbad, CA, USA). For EV production, between 8×10^6 and 2×10^7 cells were seeded per T175 flask (Greiner Bio-One GmbH, Frickenhausen, Germany), depending on the cell line. After 24 h, the medium was changed to CD293 medium (Gibco™, Thermo Fisher Scientific) supplemented with 1% penicillin-streptomycin and 1x GlutaMAX™ (Gibco™, Thermo Fisher Scientific), followed by cell culture for 48 h. To generate EV-depleted FBS, FBS-derived EVs were pelleted by ultracentrifugation at 110,000× *g* at 4 °C for 18 h. The EV-depleted supernatant was mixed with DMEM to obtain a final concentration of 5%.

For transfection, 5–6 × 10^6 cells per 15-cm dish (Greiner Bio-One GmbH) were seeded in DMEM supplemented with 10% FBS one day before transfection. Transfection was performed by TurboFect (Thermo Fisher Scientific Waltham, MA, USA), using 20 µg plasmid per plate. After 4 h, the medium was changed to DMEM supplemented with 5% EV-depleted FBS, and cells were cultured for 24 h.

2.2. Isolation of Extracellular Vesicles

EVs were isolated from the cell culture medium by differential centrifugation, first at 2000× *g* for 10 min, and second, at 5000× *g* for 5 min at 4 °C. Supernatants (200 mL) were filtered through a 0.22 µm pore filter (ROTILABO® CME, Carl Roth, Karlsruhe, Germany), followed by ultrafiltration through centrifugal filters (Amicon Ultra-15, 10 kDa, Merck KGaA, Darmstadt, Germany) to a final volume of 500 µL. Subsequently, the concentrated EV samples were subjected to size exclusion chromatography using qEVoriginal 70-nm columns (IZON Science Ltd., Christchurch, New Zealand). The EV-containing fractions were pooled and subjected to a final ultracentrifugation step at 110,000× *g* at 4 °C for two h

(Beckman Coulter, Krefeld, Germany; MAX-XP centrifuge, TLA-100.4 rotor). Finally, the EV pellet was resuspended in filtered 1 × PBS.

2.3. SDS-PAGE and Western Blot Analysis

The 1 × 10^9 EVs were lysed with 2 × SDS sample buffer (for CD63 samples, non-reducing conditions were used) and run on an SDS-12% polyacrylamide protein gel. Proteins were transferred to a nitrocellulose membrane (Bio-Rad Laboratories GmbH, Feldkirchen, Germany) and membranes were blocked with 5% (*w*/*v*) milk powder (Carl Roth) in phosphate-buffered saline supplemented with 0.05% Tween (PBS-T) for one hour. Subsequently, membranes were probed using the following antibodies: mouse anti-human CD63 (1:500, Life Technologies; TS63), rabbit anti-human Alix (1:1000, Abcam, Cambridge, UK; EPR15314), and rat anti-human Flotillin-1 (1:1000, BioLegend, Koblenz, Germany; W16108A) overnight at 4 °C in 5% milk in PBS-T. The blot was washed three times with PBS-T and then incubated with HRP-conjugated anti-mouse, anti-rabbit, and anti-rat secondary antibodies (Sigma-Aldrich, Munich, Germany), respectively, for one hour at room temperature. After washing three times with PBS-T, the blots were incubated for five minutes at room temperature with Lumi-Light Western Blotting Substrate (Roche, Basel, Switzerland) and visualized with Amersham Hyperfilm^{TM} ECL (GE Healthcare, Freiburg, Germany).

2.4. Electron Microscopy

EVs were prepared for electron microscopy as described previously [36] with few modifications: Purified EVs were fixed with an equal amount of 4% PFA. A small volume (5–7 µL) of this suspension was transferred to a formvar/carbon-coated meshed copper grid (Ted Pella Inc., Redding, CA, USA) and air-dried for 20 min. The grids were washed with sterile-filtered PBS and fixed for 5 min with 1% glutaraldehyde. After 8 washing steps (2 min each) with distilled water, the sample was incubated with 1% uranyl acetate for 5 min and then transferred to 2% methylcellulose supplemented with 4% uranyl acetate (ratio 9:1) and incubated for 10 min on ice. Excess fluid was removed, and the grid was air-dried for up to 10 min. Images were taken with a Zeiss EM 900 (Zeiss, Jena, Germany) at 80 kV equipped with a 2k slow-scan CCD camera (TRS-STAR GmbH, Stutensee, Germany).

2.5. Nano-Flow Cytometry (NanoFCM)

For NanoFCM, a Nano Analyzer (NanoFCM Co., Ltd., Nottingham, UK) equipped with a 488 nm laser, was calibrated using 200 nm polystyrene beads (NanoFCM Co.) with a defined concentration of 2.08 × 10^8 particles/mL, which were also used as a reference for particle concentration. In addition, monodisperse silica beads (NanoFCM Co. Ltd.) of four different sizes served as size reference standards to calibrate the size of EVs. Freshly filtered (0.22 µm) 1 × PBS was analyzed as background signal and subtracted from the other measurements. Each distribution histogram or dot plot was derived from data collected for one minute with a sample pressure of 1.0 kPa. The EV samples were diluted with filtered (0.1 µm) 1 × PBS, resulting in a particle count in the optimal range of 2500–12,000 events. Particle concentration and size distribution were calculated using the NanoFCM software (NF Profession V1.08, NanoFCM Co. Ltd.).

For immunofluorescence staining, the following antibodies were used (BioLegend): FITC-conjugated mouse anti-human CD9 antibody (clone HI9a), FITC-conjugated mouse anti-human CD81 antibody (clone TAPA-1), and PE-conjugated mouse anti-human CD63 antibody (clone H5C6); as isotype controls, FITC-conjugated mouse IgG1, κ (clone MOCP-21), and PE-conjugated mouse IgG2a, κ (MOPC-173), 2 ng/µL of each antibody in 100 µL 1 × PBS. After removing antibody aggregates by centrifugation at 12,000× *g* for 10 min, the supernatant was added to 2 × 10^8 purified EVs, followed by incubation overnight at 4 °C under constant shaking and washing with 1 mL 1x PBS by ultracentrifugation at 110,000× *g* for 60 min at 4 °C (Beckman Coulter MAX-XP centrifuge, TLA-145 rotor). The pellet was resuspended in 50 µL 1 × PBS for NanoFCM analysis.

2.6. RNA Isolation, Relative and Absolute qPCR

RNA was isolated using the Total RNA Purification Kit (Norgen BioTek Corp. Thorold, ON, Canada), followed by analysis of RNA concentration and integrity (Agilent 2100 Bioanalyzer; RNA 6000 Pico Kit, Agilent Technologies, Santa Clara, CA, USA). For RT-PCR, 1 ng of total EV-RNA and 1000 ng of total cellular RNA were used for cDNA synthesis (qScript™ Flex cDNA synthesis kit, Quantabio, Berverly, MA, USA), with primers specific for the constant region of the reporter constructs. All primers were designed using primer3 version 4.0 (https://primer3.ut.ee/; accessed on 30 September 2021). All oligonucleotides can be found in Table S1. RT-PCR products were analyzed by 2% agarose gel electrophoresis. For absolute and relative quantification, 2 ng total EV RNA and 1000 ng total cellular RNA were reverse-transcribed, using qScript cDNA synthesis kit (Quantabio). Real-time PCR was carried out on an Eppendorf realplex2 thermocycler (Luna® Universal qPCR Master MIX; New England Biolabs, Ipswich, MA USA). Relative expression levels of transcripts in cells and EVs were calculated by the ΔΔCt-method, with each target normalized to Y1 and vault RNA [37]. Unless otherwise stated, three replicates were used to calculate standard deviations. The relative levels of cellular versus EV transcripts were determined ($2^{-\Delta\Delta Ct}$) and normalized to the geometric mean of two housekeeping genes. For absolute quantification, RNA standards were generated by in vitro transcription (HiScribe™T7 High Yield RNA Synthesis Kit, New England Biolabs), based on templates carrying the T7 promoter and the sequences of U6 snRNA, Y1 RNA and U1 snRNA, respectively. Moreover, 50 ng of each standard was reverse-transcribed (qScript cDNA synthesis Kit; Quantabio) and diluted in six 10-fold steps (50 ng to 5 fg). Based on this, a standard curve was calculated with three replicates for standard deviations. Absolute concentrations of the samples were determined using the following equation:

$$Y\ molecules/\mu L = \frac{X\ RNA\ g/\mu L}{(transcript\ length\ [nts] * 321.47 + 18.02) * 6.022 * 10^{23}}$$

For Xrn1 degradation assays, 200 ng total RNA from EVs and cells were digested with 2 units of Xrn1 (New England Biolabs) for one hour at 37 °C. RNA was purified using Monarch® RNA Cleanup Kit, followed by reverse transcription (qScript cDNA synthesis kit; Quantabio) and PCR, using primers against GAPDH, U6 snRNA and Y1 RNA. For standard agarose gel electrophoresis of RT-PCR products, DNA marker was used GeneRuler Ladder Mix with 500, 400, 300, 200, and 100 bp (Thermo Fisher Scientific).

2.7. Plasmid Constructs

Pol II/poly(A), pol II/U1-3′ box, und pol III/U6-term: based on pCDNA3 as vector, RNA expression constructs were designed and synthesized (GeneArt, Thermo Fisher Scientific), each containing the same random-generated sequence of 40 bp and unique flanking constant regions (20 bp each). The insert for Pol II/U1-3′ box additionally contained the sequence of the U1-3′-box at the 3′ end. Both inserts were flanked by restriction sites for *Hin*dIII at the 5′- and *Xba*1 at the 3′ end. For the Pol III/U6-term construct, first, the CMV promoter in pcDNA3.1 was deleted and replaced by a synthetic insert (GeneArt, Thermo Fisher Scientific) consisting of the U6 promoter, a multiple cloning site, and the U6 termination signal (pcDNA3_U6). Then a synthetic fragment consisting of the random-generated 40-bp sequence and the unique flanking constant regions was inserted (see above). For sequences, see Table S1.

Length constructs (80,120,200,360,680): Based on the pcDNA3_U6 vector (see above), a series of constructs with inserts of different lengths was derived. The synthetic inserts (GeneArt, Thermo Fisher Scientific) consist of two 40-bp sequences of multiple copies thereof, inserted between the *Hin*dIII and *Xba*I sites and generating length constructs 80, 120, 200, 360, 680.

2.8. Northern Blot

For glyoxal Northern blot analysis, 300 ng of both total RNA from cells and the corresponding EV-RNA (isolated from 2.4 × 10^6 cells/mL and 350 mL supernatant) was mixed with glyoxal loading dye (Ambion) and incubated at 50 °C for 30 min. RNA was separated by agarose gel electrophoresis (1.2% in 1 × MOPS buffer). The gel was transferred onto a nylon membrane by semidry blotting followed by RNA crosslinking using UV-light (254 nm; 120 J/cm^2) and probed with a single-stranded RNA probe (DIG RNA Labeling Mix; Roche), directed against GAPDH mRNA. Hybridization was performed in NorthernMax buffer (Thermo Fisher Scientific), and washes of the blot and probe detection with alkaline phosphatase-conjugated anti-DIG-Fab fragments were done as described in the Roche manual (Roche).

3. Results

3.1. Isolation and Characterization of Extracellular Vesicles

In order to characterize the selective release of RNAs into EVs using our reporter system, we isolated EVs from HEK293 cell culture by a combination of differential centrifugation, ultrafiltration, size exclusion chromatography, and a final ultracentrifugation step (Figure 1a).

The isolated EVs were characterized, according to minimal information for studies of extracellular vesicles (MISEV) 2018 guidelines [8]. First, EV samples were analyzed by immunoblotting, using antibodies detecting one of the "classical" tetraspanin markers, CD63, as well as two intravesicular markers, ALIX and FLOT1 (flotillin-1) (Figure 1b). Second, we analyzed EV size distribution by nano-flow cytometry (NanoFCM), which detected particles with a mean of approximately 57 nm in diameter, consistent with the established size of small EVs (Figure 1c). In addition, we assessed the specific enrichment of EVs using transmission electron microscopy (Figure 1d).

To obtain a more detailed view of our isolated samples, we also conducted single-particle analysis by NanoFCM (Figure 1e). The three tetraspanin markers CD81, CD9, and CD63 were used for staining, in which 21% of all measured particles were positive for CD81. Furthermore, we performed co-staining of CD9 and the exosomal marker CD63. Both CD9 and CD63 showed similar staining efficiencies with 31% and 12%, respectively. When analyzing the double-positive events, 8% of all particles stained positive.

3.2. RNA Polymerase III Transcripts Are Preferentially Loaded into EVs

When summarizing the various classes of RNAs reported to be associated with EVs, we noticed a clear propensity towards RNA polymerase III transcripts, such as tRNAs (including fragments thereof), Y RNA, vault RNA, and U6 snRNA. To determine more systematically whether RNAs are EV-loaded in an RNA polymerase-dependent manner, we used reporter constructs and compared three different expression platforms, based on three constructs (Figure 2a): all three constructs contain a specific constant region, enabling the individual detection of the transcripts by RT-PCR, as well as a common, random-generated sequence of 40 nts. First, the pol II-poly(A) construct contains an RNA polymerase II (pol II) promoter (CMV) and terminates with a classical poly(A) signal (AAUAAA), generating an mRNA-like transcript. Second, the pol II/U1-3′ box construct harbors the same pol II promoter, but is terminated at the 3′ end by a U1-3′ box, generating a pol II transcript without a poly(A) tail. As a third reporter, a pol III construct was used, which included a U6 snRNA (RNU6-1)-derived pol III promoter as well as a U6 terminator (U5 in the transcript). All three constructs were co-transfected into HEK293 cells and after a 24 h incubation, EVs were purified, and RNA was isolated. Quantification was subsequently performed by absolute RT-qPCR assays (Figure 2b). For an absolute quantification of transcripts, standard curves were generated with three in vitro transcribed RNAs, derived from the reporter constructs, to obtain similar amplification efficiencies to the targets (Figure 2c). In addition to the EV-RNAs, we performed absolute quantification of the overexpressed RNAs in the progenitor cells of the EVs. Inside the cells, we calculated for pol III/U6-term

4.1 × 10^5, for pol II/U1-3′ box 1.8 × 10^5, and for pol II/poly(A) 1.8 × 10^5 molecules per cell, whereas the number of RNA molecules inside EVs was quite low. The most abundant detectable RNA inside EVs was the pol III/U6-term with 0.1 molecules per EV. Both overexpressed pol II/U1-3′ box and pol II/poly(A) RNAs were even less abundant with 0.02 and 0.003 molecules per EV, respectively (Figure 2b).

3.3. Smaller Transcripts Are Preferentially Loaded into EVs

Since several studies indicate that smaller RNAs are preferentially associated with EVs, we designed five pol III promoter-based reporter constructs, expressing RNAs of different lengths with a random sequence (80, 120, 200, 360, and 680 nts; Figure 2d), all of them consisting of an individual constant region for detection by specific primers. These constructs were transfected and expressed in HEK293 cells, and the released EVs were isolated after 48 h. All five transcripts could be detected in cells and EVs. To analyze whether EV-mediated RNA release depends on transcript size, we performed RT-qPCR and analyzed the relative levels of transcripts in EVs versus cells (Figure 2e). For an internal normalization, we set the shortest transcript (80 nts) as a reference to 1. Based on the size distributions, we conclude there is a clear inverse relationship between transcript size and EV-mediated RNA release, and that thereby RNA length represents an important determinant.

3.4. Absolute Quantification of Endogenous RNAs in EVs

Complementary to reporter constructs, which are under the control of strong promoters and express standardized artificial transcripts, we also quantitatively analyzed a set of endogenous RNAs. To cover a more comprehensive set of transcripts, we focused on pol III-derived U6 snRNA and Y1 RNA, as well as on pol II-derived U1 snRNA and GAPDH mRNA. To exclude potentially cell-specific loading differences, we analyzed in parallel EVs from five different cell lines: ES-2 (ovarian clear cell adenocarcinoma), U373 (glioblastoma), HepG2 (hepatocyte carcinoma), A549 (lung adenocarcinoma), in addition to HEK293 cells. Purified EVs of all these cell lines were measured by NanoFCM (Supplementary Figures S1 and S2), followed by RNA isolation (Supplementary Figure S3). Absolute quantification of the individual RNAs was based on standard curves derived from in vitro transcribed standards, with primer amplification efficiencies of 1.97 for U6 snRNA, 1.96 for U1 snRNA, 1.94 for Y1 RNA, and 1.91 for GAPDH mRNA (Figure 3a). Similarly, to the above-mentioned reporter approaches, RNA pol III transcripts were found to be the most abundant in EVs. In particular, the U6 snRNA with 0.7–4.2 molecules per EV was found most frequently in all tested cells. The Y1, as well as the U1 snRNA as RNA Pol II transcript without poly(A) tail, could be detected in copy numbers between 0.2 and 1.9 molecules per EV. Interestingly, GAPDH mRNA as RNA Pol II transcript with a poly(A) tail, could be found in copy numbers between 6.8 and 0.57 molecules per vesicle (Figure 3b).

3.5. GAPDH mRNA Shows an Aberrant Cap and Poly(A) Status

The specific characteristics of the individual RNAs within EVs have not yet been fully clarified. In particular, whether mRNAs that are detectable in EVs exist in full-length copies and carry of a functional poly(A) tail, could not yet be verified in sufficient detail. To initially analyze this, we isolated RNA from ES-2 cells and their corresponding EVs, followed by semi-quantitative RT-PCR assays (Figure 4a). For cDNA synthesis, either oligo(dT) or random hexamer primers (dT, dN_6) were used to evaluate the presence of a poly(A) tail. In the dN_6 approach, U6 snRNA and Y1 RNA were detectable in cells as well as in EVs, whereas ß-actin (ACTB), could not be detected. However, if cDNA synthesis was performed with oligo(dT) instead, the Y1 RNA signal was strongly reduced, as expected for a non-polyadenylated RNA. In contrast, the signals for GAPDH and ACTB mRNA remained similar in cellular RNA, comparing oligo(dT) and dN_6 approaches, but the GAPDH signal strongly decreased for the EV-RNA in the oligo(dT) assay. This suggests that GAPDH mRNA exists predominantly in a non-polyadenylated form when EV-

associated. To further confirm this quantitatively, we also performed RT-qPCR (Figure 4b), which further supports the results of the semi-quantitative analysis. When using oligo(dT) instead of dN_6 for the cDNA synthesis, a clear difference in the ct cycle number for EV-associated GAPDH RNA was observed, while no difference was detected in cellular RNA indicating a missing or defective poly(A) tail for EV-associated GAPDH mRNA.

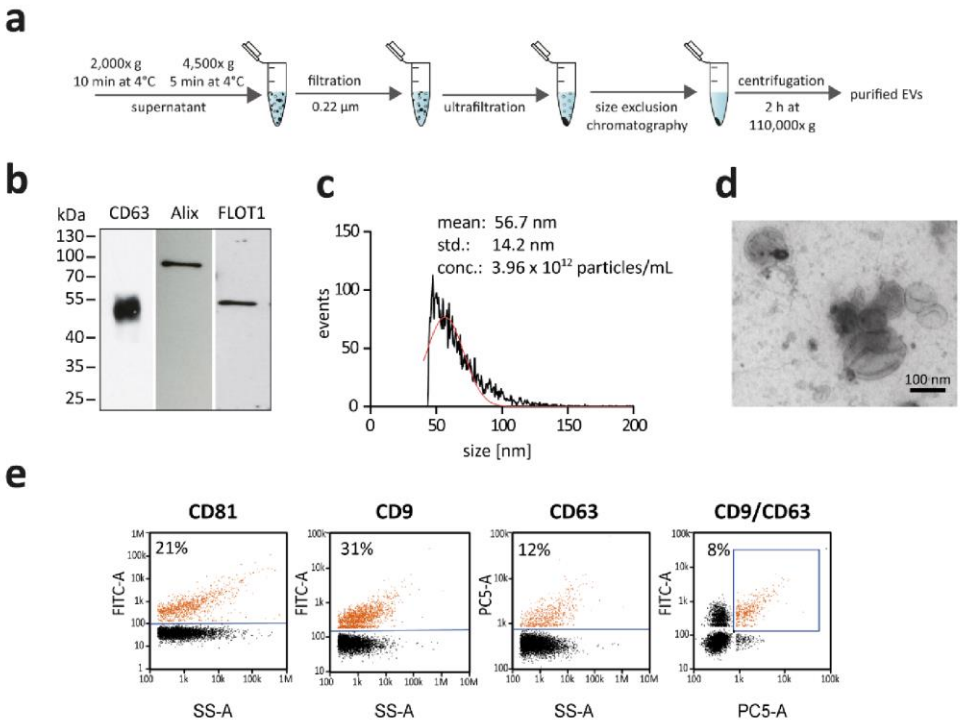

Figure 1. Isolation and characterization of extracellular vesicles from HEK293 cells. (**a**) Schematic overview of EV purification from cell culture supernatant. EVs were purified by a combination of differential centrifugation steps, followed by ultrafiltration and size exclusion chromatography. The EV-containing fractions were pooled and subjected to a final ultracentrifugation step. Subsequently, the EVs were resuspended in PBS. (**b**) Western blot analysis of EV-marker proteins CD63, ALIX, FLOT1. (**c**) Nano-flow cytometry (NanoFCM) analysis, depicting the size distribution (diameter) and concentration of particles and indicating mean and standard deviation (std.) of the size distribution. (**d**) Electron microscopy of purified vesicles. Purified EVs were counterstained by uranyl acetate. (**e**) Single-particle phenotyping of HEK293-derived EVs. EVs were fluorescently labelled with FITC-conjugated antibodies specific to CD81 and CD9 or PE-conjugated CD63. Bivariate dot-plots of indicated fluorescence versus SSC are shown. In addition, double positives for CD9/CD63 are depicted.

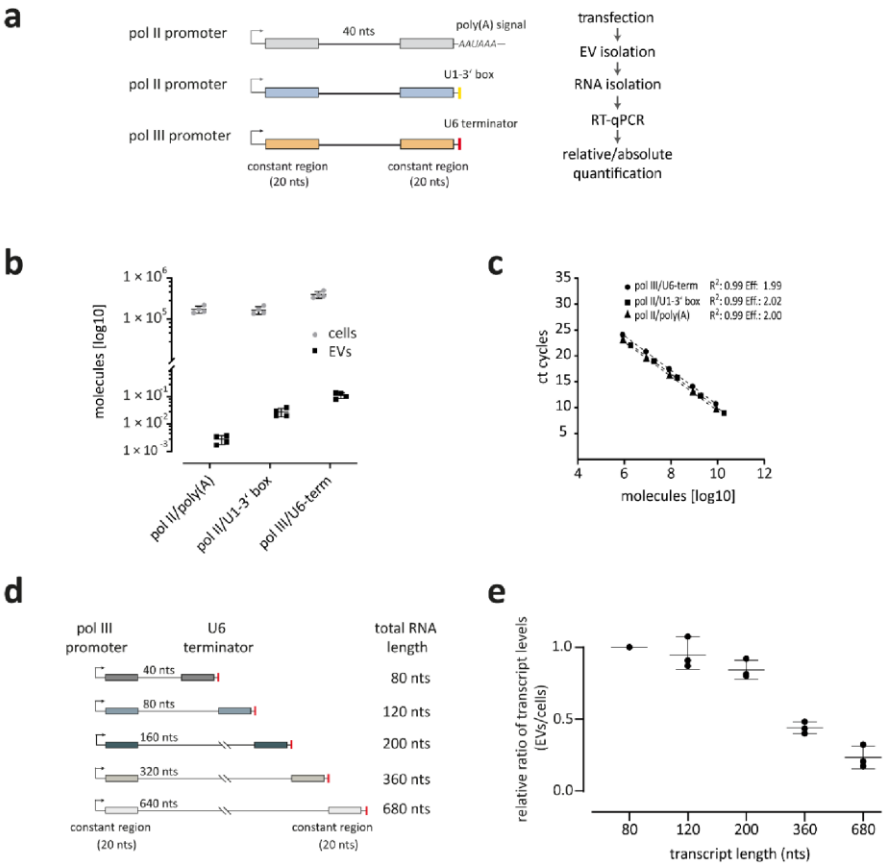

Figure 2. RNA polymerase expression platforms affect RNA packaging into extracellular vesicles. (**a**) Design of expression constructs: pol II/poly(A), pol II/U1-3′ box, and pol III/U6-term. After co-transfection of all three constructs, total RNA was isolated from HEK293 cells and purified EVs, followed by RT-PCR, using primers directed against the respective constant regions. (**b**,**c**) Expression-dependent efficiency of RNA packaging into EVs, quantified by RT-qPCR in absolute copy numbers (molecules per cell and per EV; in log10; panel. For the determination of absolute values, four datasets were used (n = 4), indicating mean and standard deviations (for standard curve with equations and amplification efficiencies, see panel **c**). (**d**,**e**) Size-dependent packaging of RNAs into extracellular vesicles. Design of expression constructs. All constructs harbor an RNA pol III (U6) promotor, followed by a randomly generated sequence with different sizes (40, 80, 160, 320, 640 nts), flanked by two unique constant regions (20 nts). All constructs contain a U6 termination signal (red), resulting in an RNA with a γ-monomethyl cap and no poly(A) tail (panel **d**). Length-dependent efficiency of RNA packaging into EVs, quantified by RT-qPCR as a relative ratio between EV-associated and total cellular RNA (EV/cells). Constructs were transfected in HEK293 cells, followed by total RNA isolation from cells and purified EVs. RT-qPCR was performed and the relative packaging of the individual transcripts (80, 120, 200, 360, 680 nts) into extracellular vesicles was analyzed (n = 3), normalized total expression in cells (panel **e**).

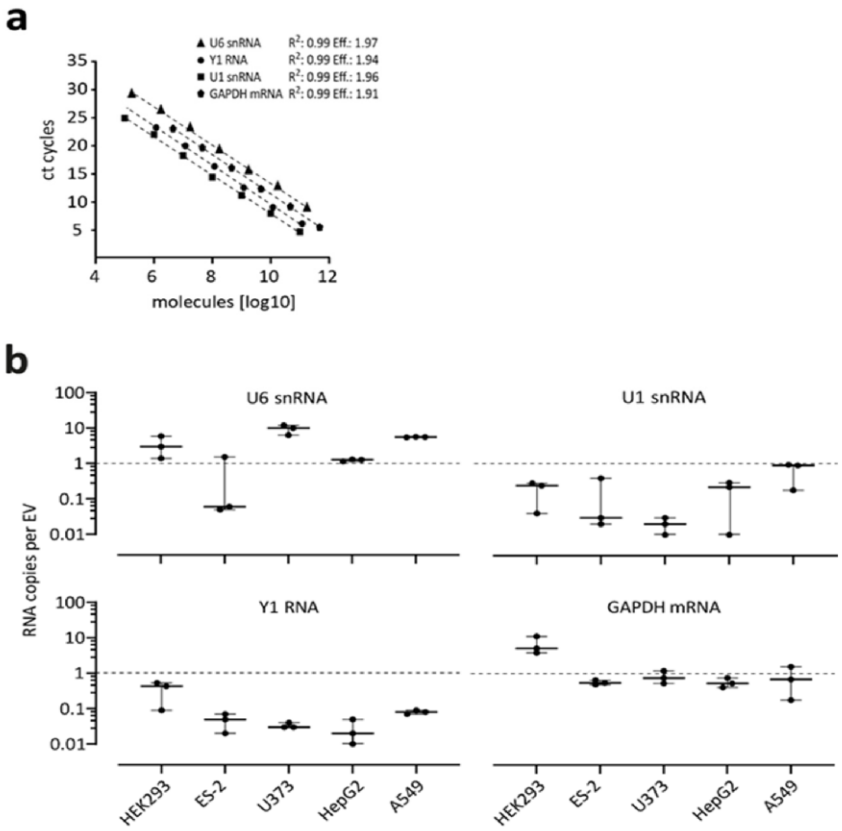

Figure 3. Absolute quantification of endogenous RNAs in EVs: U6 snRNA, Y1 RNA, U1 snRNA, and GAPDH mRNA. (**a**,**b**) Absolute quantification of copy numbers per EV for four different RNAs. For standard curves with equations and amplification efficiencies used for absolute quantification by RT-qPCR, see panel **a**. EVs were purified from five different cell lines (HEK293, ES-2, U373, HepG2, and A549), followed by RT-qPCR assays (panel **b**; copy numbers per EV in log10-scale; $n = 3$, with mean and standard deviations).

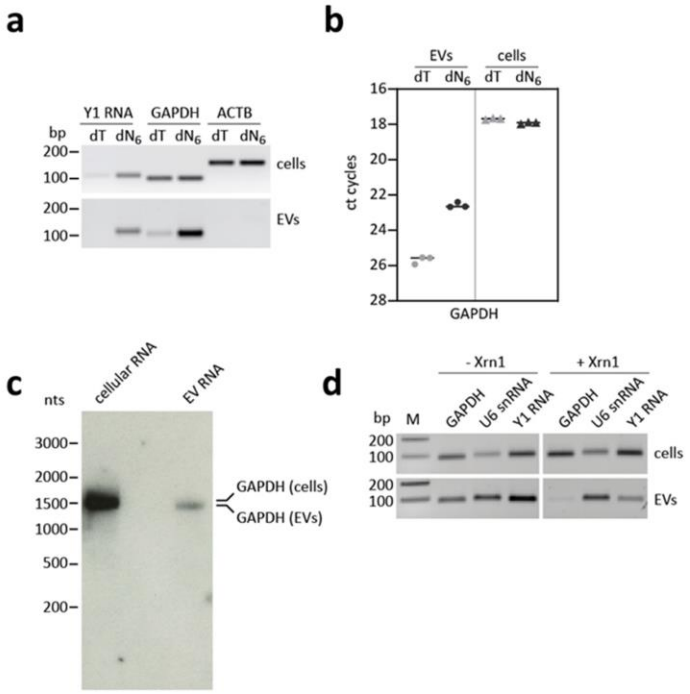

Figure 4. EV-associated and cellular GAPDH mRNA differ in size and polyadenylation status. (**a**) Total RNA from ES-2 cells and their corresponding EVs were isolated, followed by RT-PCR. For reverse transcription, either oligo(dT) or random hexamers (dT, dN_6) were used. Markers (200, 100 bp). (**b**) RNA was isolated from ES-2 cells and their corresponding EVs. For reverse transcription, either oligo(dT) or random hexamers (dT, dN_6) were used, and GAPDH mRNA was quantified by RT-qPCR. (**c**) Detection of GAPDH mRNA in EVs by the glyoxal Northern blot analysis. Total cellular and EV-RNA (300 ng) were analyzed by glyoxal agarose gel electrophoresis and Northern blotting. Exposure time 3 min (**d**) Total RNA from ES-2-derived EVs was isolated and treated with Xrn1 exoribonuclease (+Xrn1). As control, no enzyme was added (−Xrn1). RT-PCR was performed using primers directed against transcripts indicated. Markers (200, 100 bp).

To check whether GAPDH mRNA might be fragmented or shortened in total length in EVs, we used the northern blot analysis to directly visualize GAPDH mRNA. In both cells and EVs, a signal for GAPDH could be detected when the same amount of RNA (300 ng) was used. The GAPDH signal detected in cells corresponds to the expected size of the GAPDH mRNA (approximately 1.6 kb, including 200 nts from the poly(A) tail). However, the signal in EVs appears to be weaker and, furthermore, the band runs slightly below the cellular GAPDH mRNA, which indicates a truncated form (Figure 4c, Supplementary Figure S4). To assay for its 5′-terminal cap, we treated the isolated RNAs with the exoribonuclease Xrn1, which degrades RNAs with a 5′ monophosphate. In contrast, mRNAs with an intact, classical m^7G cap remain protected from degradation. After Xrn1 treatment, the tested GAPDH mRNA was no longer detectable in the EV fraction, while the signal in the cellular fraction remained. In contrast, U6 snRNA with its γ-monomethyl cap was not a substrate for Xrn1 and, thus, remained stable. The same applied to the Y1 RNA signal (Figure 4d). In sum, our data suggest that the detectable GAPDH mRNA in EVs shows altered characteristics with respect to its 5′- and 3′ modifications.

4. Discussion

Research activities on EV-associated RNAs have recently focused on miRNAs, as they represent suitable candidates for biomarkers and, thus, harbor great potential for the diagnosis and early detection of diseases [38]. In addition, an attractive approach to use EVs for therapeutic purposes involves loading the EVs with specific RNAs [39]. In principle, EVs are considered promising candidates for the clinically relevant transport of biomolecules since they are endogenous, and therefore not as immunogenic as synthetic nanoparticles. However, before EVs can be used in this manner, several remaining issues and open questions need to be addressed [40].

The initial assumption that RNA represents one of the major constituents of EVs has recently been challenged by several quantitative studies. In particular, miRNAs were found as stable extracellular RNAs in non-vesicular fractions [11]. Therefore targeted release of RNAs in EVs represents an important issue; several mechanisms for the selective RNA release have been reported (23–27], although so far no general mechanism has been identified. Since the RNA biogenesis pathways may affect EV-mediated packaging, we compared overexpressed transcripts under pol II and pol III promoter control, as well as with and without poly(A) tail. In addition, since our own previous study on RNA release had suggested the length of endogenous RNAs as an important determinant [19]), we compared overexpressed transcripts of different lengths (80–680 nts), carrying oligomerized copies of the same sequence element. As a result, we found pol III transcripts to be most efficiently EV-released and established a reciprocal relationship between transcript length and release efficiency. Therefore, our results from systematic assays in an overexpression system are consistent with and further specify previous findings based on selected endogenous transcripts or RNA-seq. These findings are also reflected by the analysis of endogenous RNAs from EVs, which are for the most part smaller than 200 nts (Figure S3).

Why are small RNAs preferentially secreted? On the one hand, it may represent a disposal pathway whereby RNA fragments are packaged into EVs, or on the other hand, it may be explained by the fact that there is simply not enough space within the vesicle for larger RNA molecules. Assuming that an RNA of approximately 1000 nts can be organized in an ellipsoidal structure of approximately 40 nm in diameter [41] and a size of 40–100 nm for small EVs, based on close packing of equal spheres we would assume that 0.7 to 11 molecules can be loaded per vesicle. Finally, one should not forget that this calculation refers to naked RNA not associated with proteins.

At the same time, we were able to clearly show that the RNA-loading capacity of EVs appears to be limited to a surprisingly low number of molecules, based on measuring absolute copy numbers of specific RNA transcripts, both after overexpression of transcripts and for endogenous RNAs (U6 and U1 snRNAs, Y1 RNA, GAPDH mRNA), as well as by comparing EVs from five different cell lines. Since this limits the application of EVs as effective cargo vehicles, it would be useful to evaluate also expression platforms other than CMV- or U6 promoter-based ones, or other cell lines, as alternatives.

Complementary to artificial transcripts generated by different expression platforms, we quantitatively compared EV packaging of a set of natural RNAs that represent different biogenesis pathways resulting in different terminal modifications: Y1 RNA, U1, U6 snRNA, and GAPDH mRNA. Y1 RNA and U6 snRNA are Pol III-derived, both exhibiting different 5′ modifications (triphosphate for Y1 RNA, γ-monomethyl-triphosphate for U6 snRNA [42,43]. U1 snRNA is a small non-polyadenylated Pol II transcript, and GAPDH a classical mRNA. As a result, we found that even the enriched, naturally occurring small RNAs exist in rather low copy numbers in EVs, ranging between 0.02 (U1 snRNA/U373 cells) and 9 molecules per EV (U6 snRNA/U373 cells), with U6 snRNA being relatively most abundant in all cell lines tested. This appears to be in accordance with a study by Wei et al. [31], where similar numbers were reported based on a stoichiometric estimation of the EV-associated RNAs. In addition, we have not identified dramatic variations between the five cell lines assayed. It is worth noting that due to its abundance and consistent occurrence, the U6 snRNA qualifies as a candidate for a housekeeping EV-RNA.

Interestingly, we detected the GAPDH mRNA at surprisingly high levels of approximately one molecule per EV in all cell lines tested. This appears to be contradictory to what we have shown above, as the GAPDH mRNA with its 1.4 kb length represents the longest transcript we have examined. However, our RT-qPCR quantification did not assess the mRNA integrity. Instead, sequencing data of EV-associated RNAs provide further evidence for RNA fragments, particularly with respect to mRNAs [16,22]. However, our approaches indicate that the mRNA is present as a truncated version but not as detectable fragments. We would like to emphasize that probably are other sorting and selection factors in addition to size and the biogenesis pathway of the individual RNAs and here in particular GAPDH mRNA may exist, as already shown for several RNAs [23–27]. Further methodological approaches such as sequencing of the entire transcript would be necessary to finally clarify this question but are beyond the scope of this study.

In addition, our approaches for examining the 5′ and 3′ status of mRNA suggest that GAPDH mRNA may exist as a mature mRNA, but rather lacks the mRNA-typical cap and part of or the entire poly(A) tail. Because of this limitation to two mRNAs, we cannot exclude that there may indeed be a transfer of a set of translatable mRNAs into EVs, as shown in several studies [21,44,45].

Supplementary Materials: The following are available online at https://www.mdpi.com/article/10.3390/cells10102674/s1, Figure S1: Size distribution (diameter) and concentration of EVs from five different cell lines; Figure S2: Single-particle phenotyping of EVs isolated from five different cell lines; Figure S3: Profiles of EV-derived RNA from five different cell lines. Figure S4: Detection of GAPDH mRNA in EVs by glyoxal Northern blot analysis. Table S1: DNA-oligonucleotides and primers.

Author Contributions: Conceptualization, C.P. (Christian Preußer) and A.B.; investigation and validation, M.-L.M., C.P. (Christina Pfafenrot) and C.P. (Christian Preußer); formal analysis, C.P. (Christian Preußer); data curation, writing—original draft preparation, C.P. (Christian Preußer), A.B. and M.-L.M.; writing—review and editing, C.P. (Christian Preußer); A.B., E.P.v.S.; visualization, M.-L.M. and C.P. (Christian Preußer); supervision, A.B. and C.P. (Christian Preußer); project administration, A.B.; funding acquisition, C.P. (Christian Preußer); A.B. and E.P.v.S. All authors have read and agreed to the published version of the manuscript.

Funding: This research was supported by the *Deutsche Forschungsgemeinschaft* (RTG 2355; project Bi 316/18-1 and 18-2 within SPP 1935; to A.B.), project Bi 316/20-1 within Research Unit FOR 5116 (to A.B. and C.P.); GRK 2573/1 project 416910386 (to E.PvS.). Additional funding was from the State of Hessen, LOEWE Centre DRUID (project E2, to A.B.).

Institutional Review Board Statement: Not applicable.

Informed Consent Statement: Not applicable.

Data Availability Statement: Data is contained within the article or supplementary material.

Conflicts of Interest: The authors declare no conflict of interest.

References

1. Simons, M.; Raposo, G. Exosomes-vesicular carriers for intercellular communication. *Curr. Opin. Cell Biol.* **2009**, *21*, 575–581. [CrossRef]
2. Théry, C.; Ostrowski, M.; Segura, E. Membrane vesicles as conveyors of immune responses. *Nat. Rev. Immunol.* **2009**, *9*, 581–593. [CrossRef] [PubMed]
3. Raposo, G.; Stoorvogel, W. Extracellular vesicles: Exosomes, microvesicles, and friends. *J. Cell Biol.* **2013**, *200*, 373–383. [CrossRef] [PubMed]
4. Kanada, M.; Bachmann, M.H.; Hardy, J.W.; Frimannson, D.O.; Bronsart, L.; Wang, A.; Sylvester, M.D.; Schmidt, T.L.; Kaspar, R.L.; Butte, M.J.; et al. Differential fates of biomolecules delivered to target cells via extracellular vesicles. *Proc. Natl. Acad. Sci. USA* **2015**, *112*, E1433-42. [CrossRef]
5. Zaborowski, M.P.; Balaj, L.; Breakefield, X.O.; Lai, C.P. Extracellular vesicles: Composition, biological relevance, and methods of study. *Bioscience* **2015**, *65*, 783–797. [CrossRef] [PubMed]
6. Doyle, L.M.; Wang, M.Z. Overview of extracellular vesicles, their origin, composition, purpose, and methods for exosome isolation and analysis. *Cells* **2019**, *8*, 727. [CrossRef]

7. Witwer, K.W.; Soekmadji, C.; Hill, A.F.; Wauben, M.H.; Buzás, E.I.; Di Vizio, D.; Falcon-Perez, J.M.; Gardiner, C.; Hochberg, F.; Kurochkin, I.V.; et al. Updating the MISEV minimal requirements for extracellular vesicle studies: Building bridges to reproducibility. *J. Extracell. Vesicles* **2017**, *6*, 1396823. [CrossRef]
8. Théry, C.; Witwer, K.W.; Aikawa, E.; Alcaraz, M.J.; Anderson, J.D.; Andriantsitohaina, R.; Antoniou, A.; Arab, T.; Archer, F.; Atkin-Smith, G.K.; et al. Minimal information for studies of extracellular vesicles 2018 (MISEV2018): A position statement of the International Society for Extracellular Vesicles and update of the MISEV2014 guidelines. *J. Extracell. Vesicles* **2018**, *7*, 1535750. [CrossRef]
9. Mathivanan, S.; Ji, H.; Simpson, R.J. Exosomes: Extracellular organelles important in intercellular communication. *J. Proteomics* **2010**, *73*, 1907–1920. [CrossRef] [PubMed]
10. Thakur, B.K.; Zhang, H.; Becker, A.; Matei, I.; Huang, Y.; Costa-Silva, B.; Zheng, Y.; Hoshino, A.; Brazier, H.; Xiang, J.; et al. Double-stranded DNA in exosomes: A novel biomarker in cancer detection. *Cell Res.* **2014**, *24*, 766–769. [CrossRef]
11. Jeppesen, D.K.; Fenix, A.M.; Franklin, J.L.; Higginbotham, J.N.; Zhang, Q.; Zimmerman, L.J.; Liebler, D.C.; Ping, J.; Liu, Q.; Evans, R.; et al. Reassessment of exosome composition. *Cell* **2019**, *177*, 428. [CrossRef] [PubMed]
12. Gebert, L.F.R.; MacRae, I.J. Regulation of microRNA function in animals. *Nat. Rev. Mol. Cell Biol.* **2019**, *20*, 21–37. [CrossRef]
13. Kesidou, D.; da Costa, M.; Paula, A.; de Windt, L.J.; Brittan, M.; Beqqali, A.; Baker, A.H. Extracellular vesicle miRNAs in the promotion of cardiac neovascularisation. *Front. Physiol.* **2020**, *11*, 579892. [CrossRef]
14. Park, S.; Lee, K.; Park, I.B.; Kim, N.H.; Cho, S.; Rhee, W.J.; Oh, Y.; Choi, J.; Nam, S.; Lee, D.H. The profiles of microRNAs from urinary extracellular vesicles (EVs) prepared by various isolation methods and their correlation with serum EV microRNAs. *Diabetes Res. Clin. Pract.* **2020**, *160*, 108010. [CrossRef]
15. Pegtel, D.M.; Cosmopoulos, K.; Thorley-Lawson, D.A.; Monique, A.J.; Hopmans, E.S.; Lindenberg, J.L.; de Gruijl, T.D.; Würdinger, T.; Middeldorp, J.M. Functional delivery of viral miRNAs via exosomes. *Proc. Natl. Acad. Sci. USA* **2010**, *107*, 6328–6333. [CrossRef] [PubMed]
16. Nolte-'t Hoen, E.N.M.; Buermans, H.P.J.; Waasdorp, M.; Stoorvogel, W.; Wauben, M.H.M.; Peter, A.C. Deep sequencing of RNA from immune cell-derived vesicles uncovers the selective incorporation of small non-coding RNA biotypes with potential regulatory functions. *Nucleic Acids Res.* **2012**, *40*, 9272–9285. [CrossRef]
17. Li, Y.; Zheng, Q.; Bao, C.; Li, S.; Guo, W.; Zhao, J.; Chen, D.; Gu, J.; He, X.; Huang, S. Circular RNA is enriched and stable in exosomes: A promising biomarker for cancer diagnosis. *Cell Res.* **2015**, *25*, 981–984. [CrossRef]
18. van Balkom, B.W.M.; Eisele, A.S.; Pegtel, D.M.; Bervoets, S.; Verhaar, M.C. Quantitative and qualitative analysis of small RNAs in human endothelial cells and exosomes provides insights into localized RNA processing, degradation and sorting. *J. Extracell. Vesicles* **2015**, *4*, 26760. [CrossRef] [PubMed]
19. Preußer, C.; Hung, L.-H.; Schneider, T.; Schreiner, S.; Hardt, M.; Moebus, A.; Santoso, S.; Bindereif, A. Selective release of circRNAs in platelet-derived extracellular vesicles. *J. Extracell. Vesicles* **2018**, *7*, 1424473. [CrossRef]
20. Ratajczak, J.; Miekus, K.; Kucia, M.; Zhang, J.; Reca, R.; Dvorak, P.; Ratajczak, M.Z. Embryonic stem cell-derived microvesicles reprogram hematopoietic progenitors: Evidence for horizontal transfer of mRNA and protein delivery. *Leukemia* **2006**, *20*, 847–856. [CrossRef]
21. Valadi, H.; Ekström, K.; Bossios, A.; Sjöstrand, M.; Lee, J.J.; Lötvall, J.O. Exosome-mediated transfer of mRNAs and microRNAs is a novel mechanism of genetic exchange between cells. *Nat. Cell Biol.* **2007**, *9*, 654–659. [CrossRef] [PubMed]
22. Batagov, A.O.; Kurochkin, I.V. Exosomes secreted by human cells transport largely mRNA fragments that are enriched in the 3′-untranslated regions. *Biol. Direct* **2013**, *8*, 12. [CrossRef] [PubMed]
23. Villarroya-Beltri, C.; Baixauli, F.; Gutiérrez-Vázquez, C.; Sánchez-Madrid, F.; Mittelbrunn, M. Sorting it out: Regulation of exosome loading. *Semin. Cancer Biol.* **2014**, *28*, 3–13. [CrossRef]
24. Santangelo, L.; Giurato, G.; Cicchini, C.; Montaldo, C.; Mancone, C.; Tarallo, R.; Battistelli, C.; Alonzi, T.; Weisz, A.; Tripodi, M. The RNA-binding protein SYNCRIP is a component of the hepatocyte exosomal machinery controlling microRNA sorting. *Cell Rep.* **2016**, *17*, 799–808. [CrossRef]
25. Shurtleff, M.J.; Temoche-Diaz, M.M.; Karfilis, K.V.; Ri, S.; Schekman, R. Y-box protein 1 is required to sort microRNAs into exosomes in cells and in a cell-free reaction. *Elife* **2016**, *5*. [CrossRef]
26. Groot, M.; Lee, H. Sorting mechanisms for microRNAs into extracellular vesicles and their associated diseases. *Cells* **2020**, *9*, 1044. [CrossRef] [PubMed]
27. Zietzer, A.; Hosen, M.R.; Wang, H.; Goody, P.R.; Sylvester, M.; Latz, E.; Nickenig, G.; Werner, N.; Jansen, F. The RNA-binding protein hnRNPU regulates the sorting of microRNA-30c-5p into large extracellular vesicles. *J. Extracell. Vesicles* **2020**, *9*, 1786967. [CrossRef]
28. Arroyo, J.D.; Chevillet, J.R.; Kroh, E.M.; Ruf, I.K.; Pritchard, C.C.; Gibson, D.F.; Mitchell, P.S.; Bennett, C.F.; Pogosova-Agadjanyan, E.L.; Stirewalt, D.L.; et al. Argonaute2 complexes carry a population of circulating microRNAs independent of vesicles in human plasma. *Proc. Natl. Acad. Sci. USA* **2011**, *108*, 5003–5008. [CrossRef]
29. Gámbaro, F.; Li Calzi, M.; Fagúndez, P.; Costa, B.; Greif, G.; Mallick, E.; Lyons, S.; Ivanov, P.; Witwer, K.; Cayota, A.; et al. Stable tRNA halves can be sorted into extracellular vesicles and delivered to recipient cells in a concentration-dependent manner. *RNA Biol.* **2020**, *17*, 1168–1182. [CrossRef] [PubMed]

30. Chevillet, J.R.; Kang, Q.; Ruf, I.K.; Briggs, H.A.; Vojtech, L.N.; Hughes, S.M.; Cheng, H.H.; Arroyo, J.D.; Meredith, E.K.; Gallichotte, E.N.; et al. Quantitative and stoichiometric analysis of the microRNA content of exosomes. *Proc. Natl. Acad. Sci. USA* **2014**, *111*, 14888–14893. [CrossRef]
31. Wei, Z.; Batagov, A.O.; Schinelli, S.; Wang, J.; Wang, Y.; El Fatimy, R.; Rabinovsky, R.; Balaj, L.; Chen, C.C.; Hochberg, F.; et al. Coding and noncoding landscape of extracellular RNA released by human glioma stem cells. *Nat. Commun.* **2017**, *8*, 1145. [CrossRef] [PubMed]
32. Albanese, M.; Chen, Y.-F.A.; Hüls, C.; Gärtner, K.; Tagawa, T.; Mejias-Perez, E.; Keppler, O.T.; Göbel, C.; Zeidler, R.; Shein, M.; et al. Micro RNAs are minor constituents of extracellular vesicles and are hardly delivered to target cells. *bioRvix* **2020**. [CrossRef]
33. Turchinovich, A.; Weiz, L.; Langheinz, A.; Burwinkel, B. Characterization of extracellular circulating microRNA. *Nucleic Acids Res.* **2011**, *39*, 7223–7233. [CrossRef]
34. Olejniczak, S.H.; La Rocca, G.; Gruber, J.J.; Thompson, C.B. Long-lived microRNA-Argonaute complexes in quiescent cells can be activated to regulate mitogenic responses. *Proc. Natl. Acad. Sci. USA* **2013**, *110*, 157–162. [CrossRef]
35. Mateescu, B.; Kowal, E.J.K.; van Balkom, B.W.M.; Bartel, S.; Bhattacharyya, S.N.; Buzás, E.I.; Buck, A.H.; de Candia, P.; Chow, F.W.N.; Das, S.; et al. Obstacles and opportunities in the functional analysis of extracellular vesicle RNA - an ISEV position paper. *J. Extracell. Vesicles* **2017**, *6*, 1286095. [CrossRef] [PubMed]
36. Théry, C.; Amigorena, S.; Raposo, G.; Clayton, A. Isolation and characterization of exosomes from cell culture supernatants and biological fluids. *Curr. Protoc. Cell Biol.* **2006**, *30*, 3–22. [CrossRef]
37. Pfaffl, M.W. A new mathematical model for relative quantification in real-time RT-PCR. *Nucleic Acids Res.* **2001**, *29*, e45. [CrossRef]
38. de Miguel Pérez, D.; Rodriguez Martínez, A.; Ortigosa Palomo, A.; Delgado Ureña, M.; Garcia Puche, J.L.; Robles Remacho, A.; Exposito Hernandez, J.; Lorente Acosta, J.A.; Ortega Sánchez, F.G.; Serrano, M.J. Extracellular vesicle-miRNAs as liquid biopsy biomarkers for disease identification and prognosis in metastatic colorectal cancer patients. *Sci. Rep.* **2020**, *10*, 3974. [CrossRef]
39. Walker, S.; Busatto, S.; Pham, A.; Tian, M.; Suh, A.; Carson, K.; Quintero, A.; Lafrence, M.; Malik, H.; Santana, M.X.; et al. Extracellular vesicle-based drug delivery systems for cancer treatment. *Theranostics* **2019**, *9*, 8001–8017. [CrossRef] [PubMed]
40. Meng, W.; He, C.; Hao, Y.; Wang, L.; Li, L.; Zhu, G. Prospects and challenges of extracellular vesicle-based drug delivery system: Considering cell source. *Drug Deliv.* **2020**, *27*, 585–598. [CrossRef]
41. Gopal, A.; Zhou, Z.H.; Knobler, C.M.; Gelbart, W.M. Visualizing large RNA molecules in solution. *RNA* **2012**, *18*, 284–299. [CrossRef] [PubMed]
42. Singh, R.; Reddy, R. Gamma-monomethyl phosphate: A cap structure in spliceosomal U6 small nuclear RNA. *Proc. Natl. Acad. Sci. USA.* **1989**, *86*, 8280–8283. [CrossRef]
43. Köhn, M.; Pazaitis, N.; Hüttelmaier, S. Why YRNAs? About versatile RNAs and their functions. *Biomolecules* **2013**, *3*, 143–156. [CrossRef] [PubMed]
44. Skog, J.; Würdinger, T.; van Rijn, S.; Meijer, D.H.; Gainche, L.; Sena-Esteves, M.; Curry, W.T.; Carter, B.S.; Krichevsky, A.M.; Breakefield, X.O. Glioblastoma microvesicles transport RNA and proteins that promote tumour growth and provide diagnostic biomarkers. *Nat. Cell Biol.* **2008**, *10*, 1470–1476. [CrossRef] [PubMed]
45. Zomer, A.; Maynard, C.; Verweij, F.J.; Kamermans, A.; Schäfer, R.; Beerling, E.; Schiffelers, R.M.; de Wit, E.; Berenguer, J.; Ellenbroek, S.I.J.; et al. In vivo imaging reveals extracellular vesicle-mediated phenocopying of metastatic behavior. *Cell* **2015**, *161*, 1046–1057. [CrossRef] [PubMed]

Supplementary Figure S1

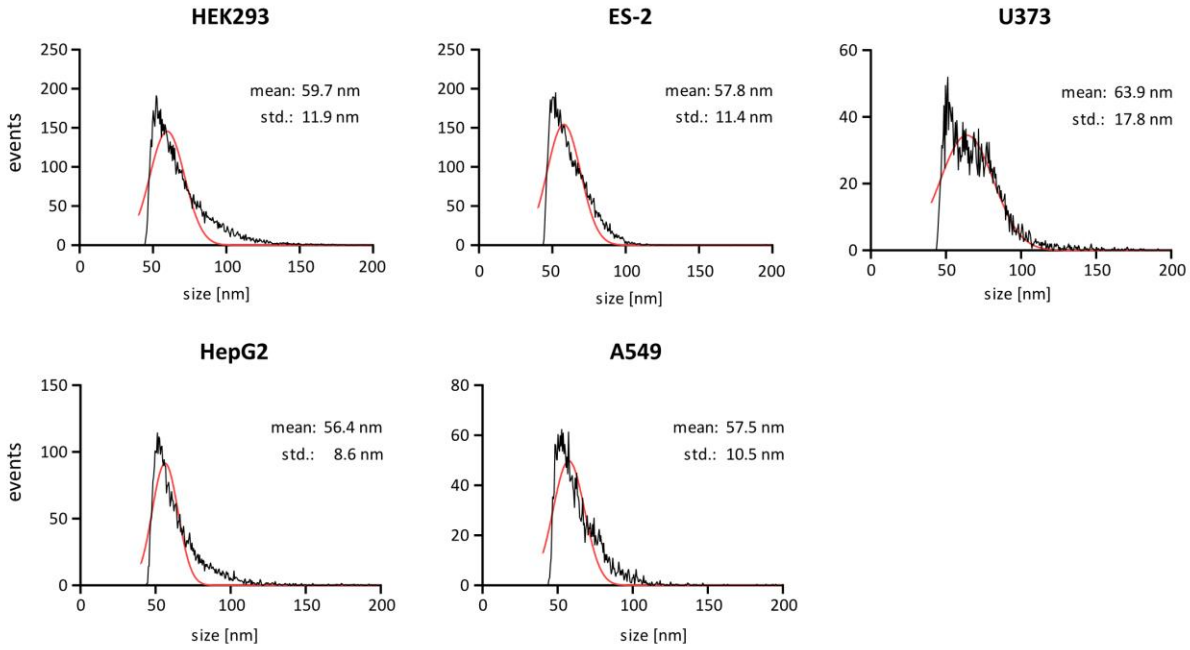

Figure S1. Size distribution (diameter) and concentration of EVs from five different cell lines. Measured by Nano flow cytometry (NanoFCM)

Supplementary Figure S2

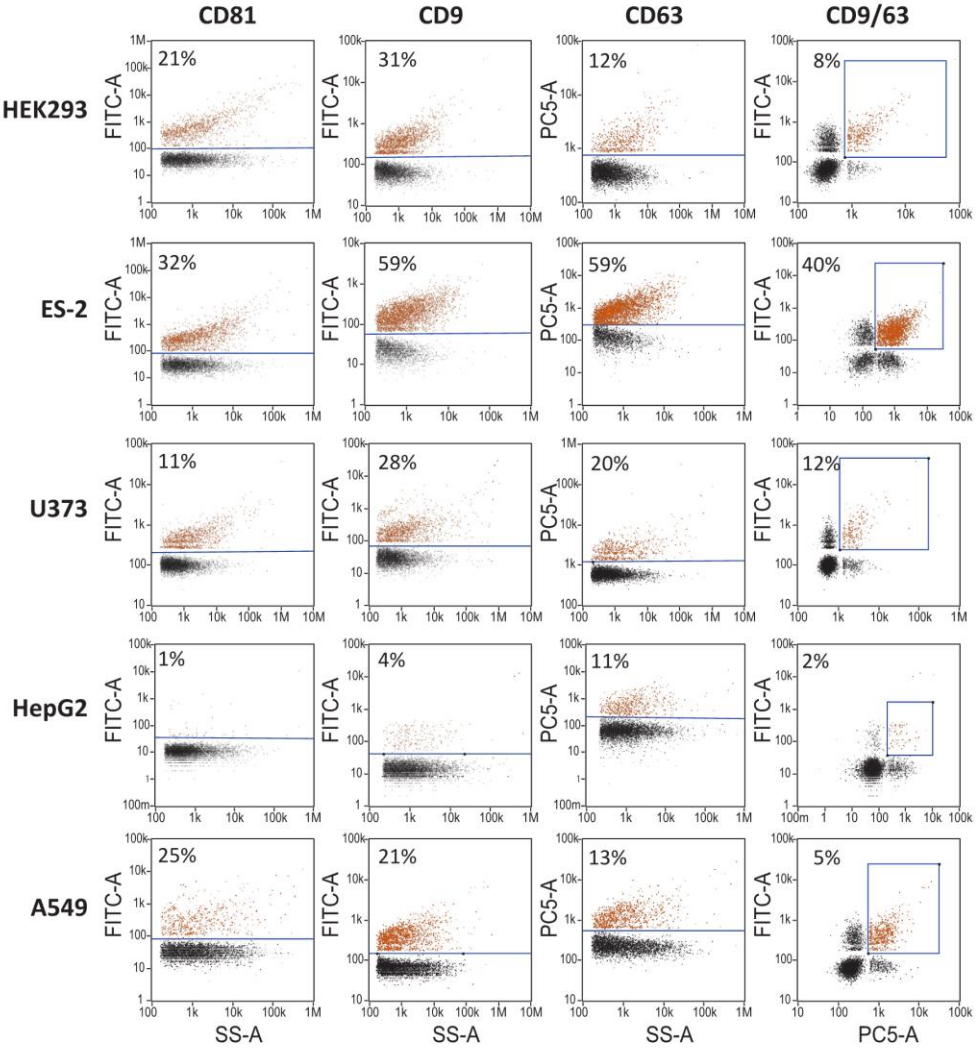

Figure S2. Single-particle phenotyping of EVs isolated from five different cell lines. EVs were fluorescently labeled with FITC-conjugated antibodies specific to CD9 and CD81 or PE-conjugated CD63. Bivariate dot-plots of indicated fluorescence versus SSC are shown. In addition, double positives for CD9/CD63 are depicted on the right-hand side.

Supplementary Figure S3

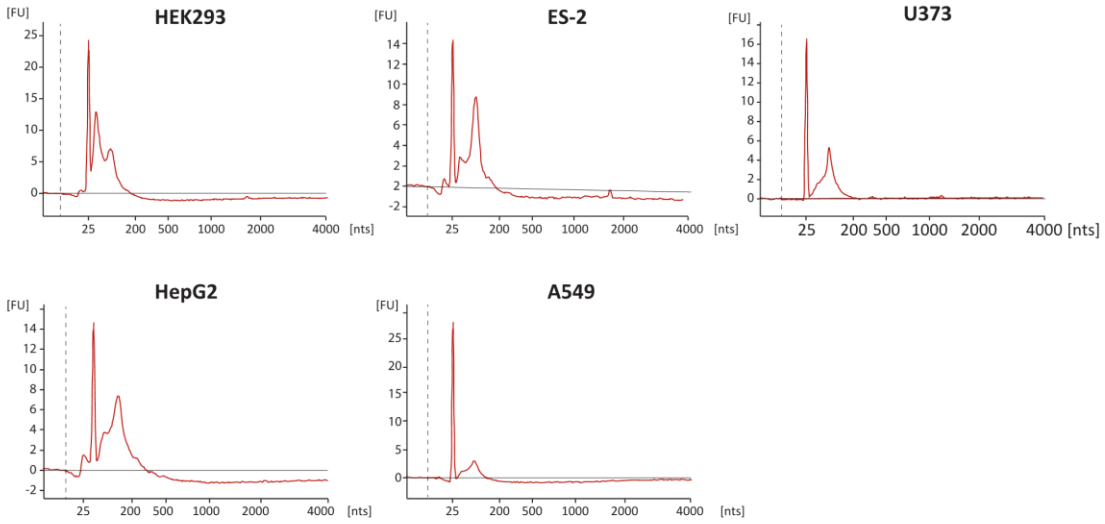

Figure S3. Profile of EV-derived RNA from five different cell lines. Measured with the Bioanalyzer using the Agilent RNA 6000 Pico Kit.

Supplementary Figure S4

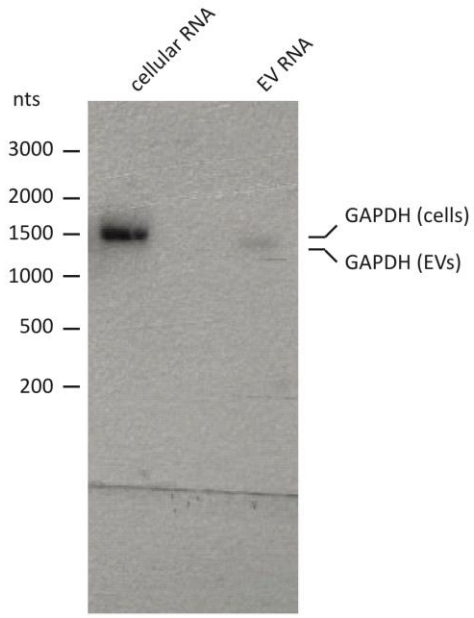

Figure S4. Detection of GAPDH mRNA in EVs by glyoxal Northern blot analysis. Total cellular and EV-RNA (300 ng) were analyzed by glyoxal agarose gel electrophoresis and Northern blotting. One minute exposure time.

Supplementary Table S1

RT-qPCR primers for housekeeping gene detection

Name	*Sequence 5' to 3'*
GAPDH fw	TGCACCACCAACTGCTTAGC
GAPDH rv	GGCATGGACTGTGGTCATGAG
ACTB fw	CTGGAACGGTGAAGGTGACA
ACTB rev	AAGGGACTTCCTGTAACAACGCA
U1 snRNA fw	GCGAGGCTTATCCATTGCAC
U1 snRNA rev	GCAGTCCCCCACTACCACAA
U6 snRNA fw	CTCGCTTCGGCAGCACATA
U6 snRNA rev	GCTTCACGAATTTGCGTGTCA
YRNA 1 fw	GGCTGGTCCGAAGGTAGTGA
YRNA 1 rev	GCAGTAGTGAGAAGGGGGGA

DNA oligonucleotides used for *in vitro* transcription of absolute quantification standards (T7 promoter underlined)

Name	*Sequence 5' to 3'*
GAPDH fw	TAATACGACTCACTATAGGGTGCACCACCAACTGCTTAGCACCCCTGGCCAAGGTCATCCATGACAACTTTGGTATCGTGGAAGGACTCATGACCACAGTCCATGCC
GAPDH rv	GGCATGGACTGTGGTCATGAGTCCTTCCACGATACCAAAGTTGTCATGGATGACCTTGGCCAGGGGTGCTAAGCAGTTGGTGGTGCACCCTATAGTGAGTCGTATTA
Std_U1 fw	TAATACGACTCACTATAGGGGCGAGGCTTATCCATTGCACTCCGGATGTGCTGACCCCTGCGATTTCCCCAAATGTGGGAAACTCGACTGCATAATTTGTGGTAGTGGGGGACTGC
Std_U1 rev	GCAGTCCCCCACTACCACAAATTATGCAGTCGAGTTTCCCACATTTGGGGAAATCGCAGGGGTCAGCACATCCGGAGTGCAATGGATAAGCCTCGCCCCTATAGTGAGTCGTATTA
Std_U6 fw	TAATACGACTCACTATAGGGCTCGCTTCGGCAGCACATATACTAAAATTGGAACGATACAGAGAAGATTAGCATGGCCCCTGCGCAAGGATGACACGCAAATTCGTGAAGC
Std_U6 rev	GCTTCACGAATTTGCGTGTCATCCTTGCGCAGGGGCCATGCTAATCTTCTCTGTATCGTTCCAATTTTAGTATATGTGCTGCCGAAGCGAGCCCTATAGTGAGTCGTATTA
Std_Y1 fw	TAATACGACTCACTATAGGGGGCTGGTCCGAAGGTAGTGAGTTATCTCAATTGATTGTTCACAGTCAGTTACAGATCGAACTCCTTGTTCTACTCTTTCCCCCCTTCTCACTACTGC
Std_Y1 rev	GCAGTAGTGAGAAGGGGGGAAAGAGTAGAACAAGGAGTTCGATCTGTAACTGACTGTGAACAATCAATTGAGATAACTCACTACCTTCGGACCAGCCCCCTATAGTGAGTCGTATTA
Std_PolIII-U6term fw	TAATACGACTCACTATAGGGTGCAATCGGATCGCACTTTTCTCTCTAATGACGTGTTCTTGCCTCAGCTCGATTCGGTAGCACCGCAGAGATTGTCCCTT
Std_PolIII-U6term rev	AAGGGACAATCTCTGCGGTGCTACCGAATCGAGCTGAGGCAAGAACACGTCATTAGAGAGAAAAGTGCGATCCGATTGCACCCTATAGTGAGTCGTATTA
Std_PolII-polyA fw	TAATACGACTCACTATAGGGCGGCTTCAGTTACTTCGCTTCTCTCTAATGACGTGTTCTTGCCTCAGCTCGATTCGGTAGGCTTGTTACAATTGGGCGGA
Std_PolII-polyA rev	TCCGCCCAATTGTAACAAGCCTACCGAATCGAGCTGAGGCAAGAACACGTCATTAGAGAGAAGCGAAGTAACTGAAGCCGCCCTATAGTGAGTCGTATTA
Std_PolII-U1box fw	TAATACGACTCACTATAGGGGTAGGAGGATAGCGGTCGACCTCTCTAATGACGTGTTCTTGCCTCAGCTCGATTCGGTAGTAAAGCCTCGCAGTTCCGA
Std_PolII-U1box rev	TCGGAACTGCGAGGCTTTACTACCGAATCGAGCTGAGGCAAGAACACGTCATTAGAGAGGTCGACCGCTATCCTCCTACCCCTATAGTGAGTCGTATTA

DNA oligonucleotides used for cloning expression constructs (restrictions sites underlined)

Name	*Sequence 5' to 3'*
U6_prom_*Mlu* I fw	AGTACGCGTGAGGGCCTATTTCCCATGATTCCTTCATATTTGCATATACGATACAAGGCTGTTAGAGAGATAATTAGAATTAATTTGACTGTAAACACAAAGATATTAGTACAAAATACGTGACGTAGAAAGTAATAATTTCTTGGGTAGTTTGCAGTTTTAAAATTATGTTTTAAAATGGACTATCAT ATGCTTACCGTAACTTGAAAGTATTTCGATTTCTTGGCTTTATATATCTTGTGGAAAGGACGAAAAGCTTGGTACCGAGCTCGGATCCACTAGTAACGGCCGCCAGTGTGCTGGAATTCTGCAGATATCCATCACACTGGCGGCCGCTCGAGCATGCATCTAGAGGGCCTTTTTTTTGGGCCCAGT
U6_prom_*Apa* I rev	ACTGGGCCCAAAAAAAAGGCCCTCTAGATGCATGCTCGAGCGGCCGCCAGTGTGATGGATATCTGCAGAATTCCAGCACACTGGCGGCCGTTACTAGTGGATCCGAGCTCGGTACCAAGCTTTTCGTCCTTTCCACAAGATATATAAAGCCAAGAAATCGAAATACTTTCAAGTTACGGTAAGCATATG ATAGTCCATTTTAAAACATAATTTTAAAACTGCAAACTACCCAAGAAATTATTACTTTCTACGTCACGTATTTTGTACTAATATCTTTGTGTTTACAGTCAAATTAATTCTAATTATCTCTCTAACAGCCTTGTATCGTATATGCAAATATGAAGGAATCATGGGAAATAGGCCCTCACGCGTACT
PolIII/U6term_*Hin* dIII *fw*	AAGCTTTGCAATCGGATCGCACTTTTCTCTCTAATGACGTGTTCTTGCCTCAGCTCGATTCGGTAGCACCGCAGAGATTGTCCCTTTCTAGA
PolIII/U6term_*Xba* I *rev*	TCTAGAAAGGGACAATCTCTGCGGTGCTACCGAATCGAGCTGAGGCAAGAACACGTCATTAGAGAGAAAAGTGCGATCCGATTGCAAAGCTT
PolII/polyA_*Hin* dIII_ *fw*	AAGCTTCGGCTTCAGTTACTTCGCTTCTCTCTAATGACGTGTTCTTGCCTCAGCTCGATTCGGTAGGCTTGTTACAATTGGGCGGATCTAGA
PolII/polyA_*Xba* I *rev*	TCTAGATCCGCCCAATTGTAACAAGCCTACCGAATCGAGCTGAGGCAAGAACACGTCATTAGAGAGAAGCGAAGTAACTGAAGCCGAAGCTT
PolII/U1box_*Hin* dIII *fw*	AAGCTTGTAGGAGGATAGCGGTCGACCTCTCTAATGACGTGTTCTTGCCTCAGCTCGATTCGGTAGTAAAGCCTCGCAGTTCCGAACTTCTGGAGTTTCAAAAGTAGACTCTAGA
PolII/U1box_*Xba* I *rev*	TCTAGAGTCTACTTTTGAAACTCCAGAAAGTTCGGAACTGCGAGGCTTTACTACCGAATCGAGCTGAGGCAAGAACACGTCATTAGAGAGGTCGACCGCTATCCTCCTACAAGCTT

RT-qPCR primers for expression constructs detection

Name	*Sequence 5' to 3'*
PolIII-U6term fw	TGCAATCGGATCGCACTTTT
PolIII-U6term rev	AAGGGACAATCTCTGCGGTG
PolII-PolyA fw	CGGCTTCAGTTACTTCGCTT
PolII-PolyA rev	TCCGCCCAATTGTAACAAGC
Pol II- U1-3'box	GTAGGAGGATAGCGGTCGAC TCGGAACTGCGAGGCTTTA

DNA oligonucleotides used for cloning of length constructs (LC) (restrictions sites underlined)

Name	*Sequence 5' to 3'*
LC_{80}_*Hin* dIII	AAAGCTTTGCAATCGGATCGCACTTTTCTCTCTAATGACGTGTTCTTGCCTCAGCTCGATTCGGTAGCACCGCAGAGATTGTCCCTTTCTAGA
LC_{80}_*Xba* I rev	TCTAGAAAGGGACAATCTCTGCGGTGCTACCGAATCGAGCTGAGGCAAGAACACGTCATTAGAGAGAAAAGTGCGATCCGATTGCAAAGCTTT
LC_{120}_*Hin* dIII *fw*	AAGCTTCGGCTTCAGTTACTTCGCTTCTCTCTAATGACGTGTTCTTGCCTCAGCTCGATTCGGTAGACTGCCATCACTAGCCACCGCTTCCAATTCCCTACTCTGAGCTTGTTACAATTGGGCGGATCTAGA
LC_{120}_*Xba* I rev	TCTAGATCCGCCCAATTGTAACAAGCTCAGAGTAGGGAATTGGAAGCGGTGGCTAGTGATGGCAGTCTACCGAATCGAGCTGAGGCAAGAACACGTCATTAGAGAGAAGCGAAGTAACTGAAGCCGAAGCTT

LC_{200}_*Hin* dIII *fw*	AAGCTTGTAGGAGGATAGCGGTCGACCTCTCTAATGACGTGTTCTTGCCTCAGCTCGATTCGGTAGACTGCCATCACTAGCCACCGCTTCCAATTCCCTACTCTGACTCTCTAATGACGTGTTCTTGCCTCAGCTCGATTCGGTAGACTGCCATCACTAGCCACCGCTTCCAATTCCCTACTCTGATAA AGCCTCGCAGTTCCGATCTAGA
LC_{200}_*Xba* I rev	TCTAGATCGGAACTGCGAGGCTTTATCAGAGTAGGGAATTGGAAGCGGTGGCTAGTGATGGCAGTCTACCGAATCGAGCTGAGGCAAGAACACGTCATTAGAGAGTCAGAGTAGGGAATTGGAAGCGGTGGCTAGTGATGGCAGTCTACCGAATCGAGCTGAGGCAAGAACACGTCATTAGAGAGGTCG ACCGCTATCCTCCTACAAGCTT
LC_{360}_*Hin* dIII *fw*	AAGCTTGGATTAATGTCAGGCTCCGGCTCTCTAATGACGTGTTCTTGCCTCAGCTCGATTCGGTAGACTGCCATCACTAGCCACCGCTTCCAATTCCCTACTCTGACTCTCTAATGACGTGTTCTTGCCTCAGCTCGATTCGGTAGACTGCCATCACTAGCCACCGCTTCCAATTCCCTACTCTGACTC TCTAATGACGTGTTCTTGCCTCAGCTCGATTCGGTAGACTGCCATCACTAGCCACCGCTTCCAATTCCCTACTCTGACTCTCTAATGACGTGTTCTTGCCTCAGCTCGATTCGGTAGACTGCCATCACTAGCCACCGCTTCCAATTCCCTACTCTGACTGCGCGGTAGGGTAACTTATCTAGA
LC_{360}_*Xba* I rev	TCTAGATAAGTTACCCTACCGCGCAGTCAGAGTAGGGAATTGGAAGCGGTGGCTAGTGATGGCAGTCTACCGAATCGAGCTGAGGCAAGAACACGTCATTAGAGAGTCAGAGTAGGGAATTGGAAGCGGTGGCTAGTGATGGCAGTCTACCGAATCGAGCTGAGGCAAGAACACGTCATTAGAGAGTCA GAGTAGGGAATTGGAAGCGGTGGCTAGTGATGGCAGTCTACCGAATCGAGCTGAGGCAAGAACACGTCATTAGAGAGTCAGAGTAGGGAATTGGAAGCGGTGGCTAGTGATGGCAGTCTACCGAATCGAGCTGAGGCAAGAACACGTCATTAGAGAGCCGGAGCCTGACATTAATCCAAGCTT
LC_{680}_*Hin* dIII *fw*	AAGCTTCAGCCCTGGACACCTGATTACTCTCTAATGACGTGTTCTTGCCTCAGCTCGATTCGGTAGACTGCCATCACTAGCCACCGCTTCCAATTCCCTACTCTGACTCTCTAATGACGTGTTCTTGCCTCAGCTCGATTCGGTAGACTGCCATCACTAGCCACCGCTTCCAATTCCCTACTCTGACTC TCTAATGACGTGTTCTTGCCTCAGCTCGATTCGGTAGACTGCCATCACTAGCCACCGCTTCCAATTCCCTACTCTGACTCTCTAATGACGTGTTCTTGCCTCAGCTCGATTCGGTAGACTGCCATCACTAGCCACCGCTTCCAATTCCCTACTCTGACTCTCTAATGACGTGTTCTTGCCTCAGCTCGA TTCGGTAGACTGCCATCACTAGCCACCGCTTCCAATTCCCTACTCTGACTCTCTAATGACGTGTTCTTGCCTCAGCTCGATTCGGTAGACTGCCATCACTAGCCACCGCTTCCAATTCCCTACTCTGACTCTCTAATGACGTGTTCTTGCCTCAGCTCGATTCGGTAGACTGCCATCACTAGCCACCGC TTCCAATTCCCTACTCTGACTCTCTAATGACGTGTTCTTGCCTCAGCTCGATTCGGTAGACTGCCATCACTAGCCACCGCTTCCAATTCCCTACTCTGAACTGGCCAGAGTCTTGAGTCTCTAGA
LC_{680}_*Xba* I rev	TCTAGAGACTCAAGACTCTGGCCAGTTCAGAGTAGGGAATTGGAAGCGGTGGCTAGTGATGGCAGTCTACCGAATCGAGCTGAGGCAAGAACACGTCATTAGAGAGTCAGAGTAGGGAATTGGAAGCGGTGGCTAGTGATGGCAGTCTACCGAATCGAGCTGAGGCAAGAACACGTCATTAGAGAGTCA GAGTAGGGAATTGGAAGCGGTGGCTAGTGATGGCAGTCTACCGAATCGAGCTGAGGCAAGAACACGTCATTAGAGAGTCAGAGTAGGGAATTGGAAGCGGTGGCTAGTGATGGCAGTCTACCGAATCGAGCTGAGGCAAGAACACGTCATTAGAGAGTCAGAGTAGGGAATTGGAAGCGGTGGCTAGTG ATGGCAGTCTACCGAATCGAGCTGAGGCAAGAACACGTCATTAGAGAGTCAGAGTAGGGAATTGGAAGCGGTGGCTAGTGATGGCAGTCTACCGAATCGAGCTGAGGCAAGAACACGTCATTAGAGAGTCAGAGTAGGGAATTGGAAGCGGTGGCTAGTGATGGCAGTCTACCGAATCGAGCTGAGGCA AGAACACGTCATTAGAGAGTCAGAGTAGGGAATTGGAAGCGGTGGCTAGTGATGGCAGTCTACCGAATCGAGCTGAGGCAAGAACACGTCATTAGAGAGTAATCAGGTGTCCAGGGCTGAAGCTT

RT-qPCR primers for length constructs (LC) detection

Name	***Sequence 5' to 3'***
LC 80 fw	TGCAATCGGATCGCACTTTT
LC 80 rev	AAGGGACAATCTCTGCGGTG
LC 120 fw	CGGCTTCAGTTACTTCGCTT
LC 120 rev	TCCGCCCAATTGTAACAAGC
LC 200 fw	GTAGGAGGATAGCGGTCGAC
LC 200 rev	TCGGAACTGCGAGGCTTTA
LC 360 fw	GGATTAATGTCAGGCTCCGG
LC 360 rev	TAAGTTACCCTACCGCGCAG
LC 680 fw	CAGCCCTGGACACCTGATTA
LC 680 rev	GACTCAAGACTCTGGCCAGT

Northern blot probe GAPDH

Name	***Sequence 5' to 3'***
Probe 1 fw	ACAGTCAGCCGCATCTTCTT
Probe 1 rev	TAATACGACTCACTATAGGGTGTGGTCATGAGTCCTTCCA
Probe 2 fw	ACCCAGAAGACTGTGGATGG
Probe 2 rev	TAATACGACTCACTATAGGGAGGGGTCTACATGGCAACTG

12502–12516 *Nucleic Acids Research, 2021, Vol. 49, No. 21* *Published online 24 November 2021*
https://doi.org/10.1093/nar/gkab1096

Inhibition of SARS-CoV-2 coronavirus proliferation by designer antisense-circRNAs

Christina Pfafenrot[1,†], Tim Schneider[1,†], Christin Müller[2,†], Lee-Hsueh Hung[1], Silke Schreiner[1], John Ziebuhr[2] and Albrecht Bindereif[1,*]

[1]Institute of Biochemistry, Justus Liebig University of Giessen, 35392 Giessen, Germany and [2]Institute of Medical Virology, Justus Liebig University of Giessen, 35392 Giessen, Germany

Received June 25, 2021; Revised October 18, 2021; Editorial Decision October 19, 2021; Accepted October 27, 2021

ABSTRACT

Circular RNAs (circRNAs) are noncoding RNAs that exist in all eukaryotes investigated and are derived from back-splicing of certain pre-mRNA exons. Here, we report the application of artificial circRNAs designed to act as antisense-RNAs. We systematically tested a series of antisense-circRNAs targeted to the SARS-CoV-2 genome RNA, in particular its structurally conserved 5′-untranslated region. Functional assays with both reporter transfections as well as with SARS-CoV-2 infections revealed that specific segments of the SARS-CoV-2 5′-untranslated region can be efficiently accessed by specific antisense-circRNAs, resulting in up to 90% reduction of virus proliferation in cell culture, and with a durability of at least 48 h. Presenting the antisense sequence within a circRNA clearly proved more efficient than in the corresponding linear configuration and is superior to modified antisense oligonucleotides. The activity of the antisense-circRNA is surprisingly robust towards point mutations in the target sequence. This strategy opens up novel applications for designer circRNAs and promising therapeutic strategies in molecular medicine.

INTRODUCTION

Coronaviruses are positive-strand RNA viruses with large polycistronic genomes of around 30 kb, which have been extensively studied since the 2003 SARS outbreak [severe acute respiratory syndrome, reviewed in (1)]. Following receptor-mediated coronavirus entry into susceptible host cells, the two large open reading frames (ORFs), 1a and 1b, located in the 5′-terminal two-thirds of the capped and polyadenylated coronavirus genome, are translated, resulting in two polyproteins that are processed by viral proteases to produce nonstructural proteins that direct viral RNA synthesis (2). Translation requires the 5′-untranslated region (UTR) of the genome RNA, which for SARS-CoV-2 comprises nucleotides 1–265 [for secondary structure models, see (3,4)].

Subsequently, the viral genome RNA serves as a template for negative-strand RNA synthesis. Two types of minus-strand RNAs are produced: first, full-length copies of the plus-strand RNA that are used as templates for the production of new genome RNAs, and second, a set of 5′-coterminal subgenomic (sg) minus-strand RNAs of varying length. The vast majority of sg-minus-strand RNAs carry at their 3′-end an 'antileader' sequence, i.e. a complement of the leader sequence located at the 5′-end of the genome, which they acquire in a process called 'discontinuous extension' of minus strands. The sg-minus strands serve as templates for the production of a nested set of sg-mRNAs that share a common 5′-leader sequence (75 nts in SARS-CoV-2, plus a few nucleotides upstream of the translation start codon of the first ORF in the respective mRNA). This unusual process of discontinuous (minus-strand) RNA synthesis is guided by pairing between complements of the conserved transcription-regulatory sequences (TRS) located upstream of the various ORFs in the 3′-region of the genome ('body-TRS') and the TRS located immediately downstream of the 5′ leader ['leader-TRS', reviewed in (5), and studied by transcriptomics for SARS-CoV-2 (6)].

The current COVID-19 pandemic, with its dramatic worldwide impact on human health and economy, is caused by SARS-CoV-2, which emerged in late 2019 in China. The SARS-CoV-2 genome was sequenced in early 2020 (7,8), and currently there are intense worldwide efforts to develop and apply new therapeutic strategies to fight this life-threatening disease. Most of these approaches focus on, first, small-molecule drugs targeting viral enzymes (nucleoside analogs, protease inhibitors and others), and second, on antibodies interfering with virus entry, in particular virus-receptor interactions. In addition, immunomodulatory agents are being used and a large number of SARS-CoV-2 vaccines (including virus vector-

*To whom correspondence should be addressed. Tel: +49 641 9935420; Fax: +49 641 9935419; Email: albrecht.bindereif@chemie.bio.uni-giessen.de
†The authors wish it to be known that, in their opinion, the first three authors should be regarded as Joint First Authors.

and mRNA-based vaccines) are being developed and tested, many of which providing promising new approaches to prevent or treat COVID-19 more effectively (9).

However, alternative novel strategies should also be considered and pursued. Antisense approaches represent such a classical line of sequence-based interference and have been investigated for the last 30 years [for reviews, see (10–13)]. By targeting specific RNA sequences, antisense approaches aim to modulate RNA structure and activity, mRNA splicing, translation, or stability. Best known examples are antisense oligonucleotides (ASO), with incorporated modified positions, such as 2′-*O*-methyl (2′-OMe), 2′-*O*-methoxyethyl (2′-MOE) nucleotides, locked nucleic acids (LNA), morpholino or other modifications, which can increase RNA base-pairing, metabolic stability, and/or delivery. As a result of antisense research over several decades, ASO-based therapies have been advanced to the stage of approved drugs used in certain genetic diseases (14). Regarding antiviral strategies, earlier studies had evaluated HIV-Tat peptide-coupled morpholino ASO against SARS-CoV and the related mouse hepatitis virus (MHV) (15,16). Here, we investigated the antiviral potential of circular RNAs (circRNAs) as a basis for presenting antisense-RNA sequences, exploiting the unusual metabolic stability of circRNAs to develop them into a new line of RNA-based antiviral therapeutics.

CircRNAs are a large class of RNAs with covalently joined 5′ and 3′ ends that exist in all eukaryotes investigated so far and have been known for more than four decades [(17); reviewed in (18–20)]. More recently, circRNAs were rediscovered as a large class of noncoding RNAs, based on deep sequencing (21–23). The most common type of circRNAs consists of one or several adjacent exons derived from pre-mRNAs. Biogenesis of exonic circRNAs relies on a kind of alternative splicing (24). Functionally, however, circRNAs have remained largely unexplored, except for a few examples of validated miRNA sponges (23,25), which are embedded in regulatory RNA networks (26,27). Several other hypothetical roles have been proposed for circRNAs, for example protein sponging and antisense activity (28). Based on their unusually high stability, circRNAs provide an attractive basis for constructing designer circRNAs in biotechnological applications [see, for example, (29–31)].

Here, we combined for the first time the classical antisense (AS)-RNA approach with synthetic short circRNAs, integrating antisense sequences into a circRNA backbone. Our overall aim was to interfere with SARS-CoV-2 genome expression and viral proliferation by specifically targeting the structurally conserved 5′-UTR of SARS-CoV-2. Based on structure-guided design and a systematic functional screen of a series of AS-circRNAs, we identified a highly accessible subregion in the SARS-CoV-2 5′-leader that could be efficiently targeted by specific AS-circRNAs, resulting in 90% reduction of viral replication in cell culture. Functional antisense activity was consistently higher when the antisense sequence was presented within a circRNA rather than as a corresponding linear RNA. Compared with 2′-OMe- and 2′-MOE-modified antisense oligonucleotides, unmodified antisense-circRNA was superior in its activity; finally, it was surprisingly robust towards point mutations in the target sequence.

In conclusion, our work establishes AS-circRNAs as a novel molecular approach suitable to target and functionally regulate specific RNAs, therefore opening up promising new avenues to develop highly specific, flexible and efficient therapeutic strategies in molecular virology and medicine.

MATERIALS AND METHODS

AS-circRNA design

Antisense target sequences (40–75 nts) were selected based on the SARS-CoV-2 5′-UTR secondary structure (3,4), as well as the presence of specific sequence elements (e.g. 5′-leader, TRS, AUGs). Randomized sequences of equal length (40–75 nts) were used as controls.

RNAs for *in vitro* circularization were composed of a constant backbone sequence, in which the individual antisense target or control sequences were inserted. The constant backbone consists of six complementary nucleotides on either 5′ and 3′ ends of the RNA, followed by four non-complementary nucleotides creating overhanging ends and allowing stem-loop formation and efficient ligation. For enhanced flexibility, and to assure stem loop formation, a spacer of three unrelated nucleotides was added between the constant backbone and the antisense or control sequences on each side (for sequences, see Supplementary Table S1). These sequences were ordered as oligonucleotides (Sigma-Aldrich) including a T7 promoter, and subsequently annealed to yield templates for *in vitro* transcription.

For endogenous overexpression of antisense-circRNAs, oligonucleotide cassettes (see Supplementary Table S1) were cloned into the pAV-U6+27-Tornado-Broccoli vector (32), using the SacII and NotI restriction sites, and replacing the Broccoli aptamer sequence. Again, to allow enhanced flexibility a spacer of unrelated nucleotides was inserted, in this case two nucleotides upstream, and five nucleotides downstream of the AS or control sequence. Since internal poly(U) stretches longer than $(U)_4$, including single nucleotide interruptions, would terminate RNA polymerase III, such sequences were changed by single T→A mutations (see Supplementary Table S1).

In vitro transcription, circularization, gel purification and RNase R treatment of antisense-RNAs

RNAs were transcribed from annealed DNA-oligonucleotide templates (see Supplementary Table S1), using the HighScribe™ T7 high-yield RNA synthesis kit (NEB) in the presence of ATP, CTP, UTP, and GTP (each at 7.5 mM), GMP (30 mM GMP; Merck), and RNaseOut (Thermo Fisher Scientific) for 2 h at 37°C. The DNA template was digested by addition of RQ1 DNase (2 U per reaction, Promega), and incubation for 30 min at 37°C. Transcripts were purified using the Monarch RNA purification kit (NEB) and quantified by the Qubit™ RNA broad-range assay kit (Thermo Fisher Scientific).

For circularization, 60 μg transcribed RNA was incubated with 100 U of T4 RNA ligase (Thermo Fisher Scientific) in 1× T4 RNA ligase buffer, supplemented with 0.1 mg/ml BSA and RNaseOut (Thermo Fisher Scientific),

overnight at 16°C in a final volume of 200 μl. RNA was recovered by phenol/chloroform extraction (Roth) and ethanol precipitation.

Gel purification was performed as described (33). To validate the circular conformation, 250 ng of gel-purified circular or linear RNA was incubated with or without 2 U of RNase R (Biozym; 30 min at 37°C). After digestion, 200 ng of RNAs were separated in a 10% denaturing polyacrylamide gel and visualized by ethidium bromide staining.

Luciferase reporter constructs

5′-UTR (nts 1–265) and 5′-leader (nts 1–75) sequences of SARS-CoV-2 (NC_045512.2) were cloned into pcDNA5-CMV-FF (34) containing the Firefly reporter ORF. Additionally, for the 5′-UTR construct, 24 nucleotides of the ORF1a sequence were included, and, for the 5′-leader construct, 25 nucleotides of the S (spike) ORF, followed in either reporter by the Firefly ORF (for a schematic, see Figure 1A). For the construction of 5′-leader constructs carrying point mutations, oligo cassettes with corresponding nucleotide changes were ordered (Sigma-Aldrich) and cloned in front of the Firefly reporter ORF. Point mutations were selected based on their occurrence frequency and annotation within the ViGTK database (https://www.biosino.org/ViGTK).

Transfection of *in vitro*-transcribed RNAs and Tornado-based circRNA expression constructs; luciferase reporter assays and RT-qPCR

HeLa cells were cultured in DME-medium supplemented with 10% FBS (Gibco) at 37°C and 5% CO_2. For luciferase reporter assays, 1×10^5 cells were seeded per well (12-well plate). RNA transfections were done using Lipofectamine 2000, and Tornado-plasmid transfections with Turbofect reagent, both in a total volume of 1 ml medium/well (Thermo Fisher Scientific). For AS-circRNA screening, cells were transfected either with 1 μg of individual circRNAs, or with a combination of two circRNAs (0.5 μg of each). For titration experiments, different amounts (100, 250, 500, 750, 1000 ng) of circular or corresponding linear RNAs (CTR2 and 1–75 RNA) were used.

To compare the efficiency of AS-circRNAs and ASOs (2′-OMe or 2′-MOE modified; SeqLab), 1 μg of circRNA and a molar equivalent of the corresponding ASOs were used. Control ASOs carry the same modifications as the ASOs tested (for sequence information, see Supplementary Table S1).

For Tornado-circRNA screening, cells were transfected with 1 μg of plasmid DNA. Culture medium was always changed 1 h prior and 4 h after transfection. After one day, cells were co-transfected with 50 ng of 5′-UTR or 5′-leader luciferase reporter plasmids (see above), together with 5 ng of pRL-SCV40 Renilla-reporter (Promega). At 24 h post-transfection, cells were washed three times with PBS (Gibco), and lysed in 250 μl Lysis-Juice (PJK). Luminescence was measured for Firefly and Renilla luciferase (Beetle- and Renilla-Juice kits, respectively; PJK), using a Centro LB 960 Luminometer (Berthold Technologies). Relative luciferase activities were calculated as a ratio of the Firefly and Renilla raw values, with three technical replicates per sample and a total of three independent biological replicates.

For detection of Firefly mRNA expression levels by RT-qPCR, HeLa cells were seeded and transfected as described above. After one day, cells were co-transfected with 50 ng of 5′-leader luciferase reporter plasmid, together with 5 ng of pRL-SCV40 Renilla-reporter (Promega). 24 h post-transfection, cells were washed three times with PBS (Gibco), and lysed by addition of TRIzol reagent (Thermo Fisher Scientific), and the RNA was purified using the RNeasy kit (Qiagen), followed by DNase digestion with RQ1 DNase (Promega) to remove remaining plasmid DNA. Reverse transcription was performed, using 500 ng total RNA with the qScript cDNA synthesis kit (Quantabio). Real-time qPCR was carried out using the Luna qPCR Reaction Mix (NEB) on a StepOne thermocycler (Thermo Fisher Scientific). Firefly and Renilla reporter mRNAs were amplified by specific primer pairs (see Supplementary Table S1). All reactions were performed in technical and biological triplicates; fold-changes (relative to reporter transfection, but without RNA transfection) were calculated using the ΔΔCt method with average cycle threshold (Ct) values, and Firefly mRNA expression was normalized to Renilla mRNA levels.

Viral infection, plaque assays and immunofluorescence

Vero E6 cells were cultured in DME-medium supplemented with 10% FBS and 100 U/ml penicillin and 100 μg/ml streptomycin (Gibco) at 37°C and 5% CO_2. Cells were seeded with a density of 0.5×10^5 per well (24-well plate). RNA transfections were done using Lipofectamine 2000 in a total volume of 0.5 ml medium/well (Thermo Fisher Scientific). For AS-circRNA screening, cells were transfected either with increasing amounts of individual circular RNAs, or their linear counterpart (between 25 and 5000 ng per assay, as described in Results and the figures). Culture medium was exchanged 1 h prior and 4 h after transfection. 24 h post-transfection, cells were inoculated with SARS-CoV-2 at a multiplicity of infection (MOI) of 0.1 pfu/cell at 33°C. At 1 h post-infection, the inoculum was replaced with fresh medium. Virus-containing supernatants were collected at 24 h post-infection, and virus titers were determined by plaque assays (35).

For durability assays (Figure 3E, Supplementary Figure S4), 3×10^5 Vero E6 cells were seeded per well (6-well plate) one day before transfection or infection.

For transfection of RNA prior to viral infection, 5 μg of respective RNAs was transfected, using Lipofectamine 2000 in a total volume of 1 ml medium/well (Thermo Fisher Scientific). The medium was replaced by 2 ml fresh medium after 4 h. 24 h post-transfection, cells were inoculated with SARS-CoV-2 at an MOI of 0.1 pfu/cell at 33°C. At 1 h post-infection, the inoculum was replaced with fresh medium, and cells were subsequently incubated for a total of 72 h.

For transfection post infection, cells were inoculated with SARS-CoV-2 at an MOI of 0.1 pfu/cell at 33°C. At

1 h post-infection, the inoculum was replaced with fresh medium, and 5 μg of respective RNAs was transfected, using Lipofectamine 2000 in a total volume of 1 ml medium per well (Thermo Fisher Scientific). The medium was replaced by 2 ml fresh medium after four hours, followed by incubation of cells for a total of 72 h.

Virus-containing supernatants were collected at 16, 24, 40, 48, 64 and 72 h post-infection or transfection, and virus titers were determined by plaque assays (35).

Cryopreserved normal human bronchial epithelial (NHBE) cells of a non-smoking, healthy donor were obtained from Lonza (CC-2540, Batch No. 18TL269120). The undifferentiated cells were seeded on collagen IV-coated transwell plates (CLS3470-48EA; Corning Costar) and grown in a 1:1 mixture of DMEM (Thermo Fisher Scientific) and BEBM (CC-3171; Lonza), supplemented with BEGM Bronchial Epithelial Single Quots Kits (CC-4175, Lonza) and retinoic acid (74 nM; R2625; Sigma-Aldrich), with medium exchange every second day. After reaching confluence, the cells were cultivated for five (Experiment #1) or seven weeks (Experiment #2) under air–liquid conditions for full differentiation into pseudo-stratified human airway epithelia. The medium from the basolateral compartment was renewed every second day, and the apical surface was washed weekly with PBS (Thermo Fisher Scientific).

The differentiation status of NHBE cells was further validated via immunofluorescence, using antibodies against ZO-1 (Invitrogen, #40-2200, 1:100), mucin 5AC (abcam, #ab198294, 1:100), tubulin IV (abcam, #ab179509, 1:100) and Alexa Fluor 488-coupled F(ab')2 goat anti rabbit IgG (H + L) antibody (Invitrogen, #A-11070, 1:500). Images were acquired by confocal laser-scanning microscopy (Leica TCS SP5), and data were processed, using the Imaris 8.4 software package (Bitplane).

For transfection, the apical surface of the cells was washed three times with 150 μl PBS, and afterwards 5 μg RNA was transfected in a total volume of 125 μl using Lipofectamine 2000 (Thermo Fisher Scientific). Four hours post-transfection, the cells were washed three times with 150 μl PBS. After 24 h the cells were infected with SARS-CoV-2 (MOI of 3 pfu/cell) for 1 h. Afterwards, the inoculum was removed, and at the indicated time points, the apical surface of the cells was incubated with 150 μl/well PBS for 15 min at 33°C, followed by plaque assays to determine virus titers in the supernatants.

Subcellular fractionation

HeLa cells were seeded with a density of 8×10^5 cells per 6-cm plate and transfected with 3 μg of *in vitro* produced linear or circular RNA or with 4 μg of Tornado-plasmids, using Lipofectamine 2000 in a total volume of 4 ml medium/plate. After 24 h, cells were harvested, and 2×10^6 cells subjected to fractionation, using the NE-PER Nuclear and Cytoplasmic Extraction kit (Thermo Fisher Scientific). RNA for Northern blot analysis was prepared from 75% of the nuclear and cytoplasmic fractions using TRIzol LS (Ambion), while 25% was saved for Western blotting (see below).

Western blot

Viral protein accumulation was analyzed by Western blot of Vero E6 cell lysates, previously transfected with 2.5 μg of circRNAs and infected with SARS-CoV-2 at an MOI of 0.1 pfu/cell at 33°C. Total protein lysates obtained at 24 h post-infection were heat-denatured in SDS-loading buffer (50 mM Tris–HCl pH 6.8, 2% SDS, 10% glycerol, 2.5% 2-mercaptoethanol, and 0.05% bromophenol blue) at 95°C for 10 min. Following separation by SDS-polyacrylamide gel electrophoresis (PAGE; 10%), proteins were blotted onto a nitrocellulose membrane (BioRad). Viral proteins were immunostained overnight with rabbit anti-SARS nucleocapsid protein (N, 200-401-A50; Rockland Immunochemicals, 1:500) or mouse anti-GAPDH antibody (monoclonal antibody G8795, GAPDH-71.1; Sigma-Aldrich, 1:5000) and appropriate secondary antibodies (HRP-conjugated anti-rabbit (A0545-1ML) or anti-mouse (A9044-2ML), Sigma-Aldrich, each 1:10,000). The blots were developed using the Lumi-Light Western-Blotting Substrate (Roche). Western blot signals were estimated by densitometry, using GelAnalyzer 19.1 software.

For subcellular fractionation, 1.25% of cytoplasmic or nuclear fractions were analyzed by SDS-PAGE (10%) and Western blotting through detection of hnRNP A1 (monoclonal antibody, sc-32301, 4B10; Santa Cruz Biotechnology, 1:2000) and GAPDH (monoclonal antibody G8795, GAPDH-71.1; Sigma-Aldrich,1:5000).

Northern blot

All Northern blots were performed as previously described (36).

Denaturing polyacrylamide Northern blot. For detection of *in vitro* produced linear and circular RNAs transfected in HeLa or Vero-E6 cells, 1 μg of total RNA or 20% of cytoplasmic/nuclear fractions was used, and for Tornado-derived circRNAs 250 ng of total RNA or 20% of cytoplasmic/nuclear fraction. Samples were separated on a 10% denaturing polyacrylamide gel, transferred to a nylon membrane (Hybond-N+; Amersham) by semi-dry blotting, and crosslinked by UV light (0.125 mJ/cm^2 at 254 nm). Membranes were subsequently hybridized with DIG-UTP-labeled (DIG RNA Labeling Mix, Roche) riboprobes in NorthernMax hybridization buffer (Thermo Fisher Scientific) at 60°C. For *in vitro* produced RNAs, CTR2 or 1–75 specific riboprobes were used that are able to detect both circular and linear molecules. For detection of Tornado circRNAs, a circular-junction-specific probe was used. For oligonucleotide and riboprobe sequences, see Supplementary Table S1. Probe detection with alkaline phosphatase-conjugated anti-DIG-Fab fragments (11093274910, Roche) and CDP-Star chemiluminescence substrate was done as described (Roche).

RNase R and RNase H treatment. To confirm circularity of the detected Tornado-derived circRNAs, 250 ng of total RNA were either incubated with 5 U/μg RNase R (Biozym) in 1x RNase R buffer for 1 h at 37°C, or with 50 ng

of antisense DNA-oligonucleotide in 1x RNase H buffer for 20 min at 37°C, followed by addition of 1 U RNase H (NEB) and incubation for 40 min at 37°C. To assess whether the effect of AS-circRNAs is based on a blocking or cleavage mechanism, 3 μg of total RNA from previously transfected HeLa cells (5 μg circRNA, 500 ng 5′-leader reporter) were incubated with 600 ng antisense DNA-oligonucleotide and RNase H-treated (see above). Samples were analyzed by denaturing polyacrylamide Northern blot as described above.

Glyoxal Northern blot. For detection of the SARS-CoV-2 genome and subgenomic RNAs, 3 μg of total RNA from previously transfected (5 μg *in vitro* produced linear or circular RNAs per 3×10^5 cells on a 6-well plate, in 1 ml total volume), and infected (at 24 h post-infection; MOI = 0.1 pfu/cell) Vero E6 cells were mixed with glyoxal loading buffer (Ambion) and incubated for 30 min at 50°C. RNAs were separated by 1% agarose gel electrophoresis in 1x MOPS buffer, transferred to a nylon membrane (Hybond-N+, Amersham), and hybridized with a DIG-labelled riboprobe complementary to the 3′-UTR common to the positive-strand viral genome as well as the subgenomic RNAs (SARS-CoV-2 genome positions 29,535 to 29,848; for the probe sequence, see Supplementary Table S1; NorthernMax hybridization buffer; Thermo Fisher Scientific; 68°C). The same procedure was used for detection of the full-length 5′-leader reporter transcript: 3 μg of total RNA from previously transfected HeLa cells (5 μg circRNA, 500 ng 5′-leader reporter) were treated and separated as described above, followed by probing with a DIG-labeled riboprobe (position 1 to 997 of the reporter-derived transcript, see Supplementary Table S1). Probe detection was performed as described above.

RNA-Seq and data analysis

For global analysis of viral genome and subgenomic RNA abundance after transfection of *in vitro* produced linear or circular RNA, 3×10^6 Vero E6 cells were seeded in a 6-well plate 1 day before transfection. 5 μg of respective *in vitro* produced RNA was transfected in 1 ml total volume, using Lipofectamine 2000. At 24 h post-transfection, cells were inoculated with SARS-CoV-2 at an MOI of 0.1 pfu/cell at 33°C. At 24 h post-infection, RNA was isolated by TRIzol extraction (Ambion). 1 μg of total RNA, together with 2 μl of a 1:100 dilution of ERCC standard (Ambion) as spike-in, was used to perform poly(A)-selection (NEBNext® Poly(A) mRNA Magnetic Isolation Module; NEB), followed by library preparation (NEBNext Ultra II Directional RNA Library Prep Kit for Illumina; NEB). Libraries were sequenced on an Illumina NextSeq 500 platform (single-read, 150 bp). RNA-seq data were deposited in the Sequence Read Archive (PRJNA693241) of NCBI. Sequence reads were aligned to the SARS-CoV-2 reference genome sequence (NC_045512.2) using STAR (37). Positions of the transcription regulatory sequences (TRS) and subgenomic RNAs (sgRNAs) were based on the SARS-CoV-2 transcriptome tracks (6).

To quantitate the total viral RNA accumulation in each sample (Figure 4B), and to calculate the read coverage in the nine segments across the SARS-CoV-2 viral genome (Figure 4C), the number of uniquely mapped sequence reads of each sample were normalized with the corresponding number of total sequenced reads (mock: 33.4 mio; CTR2_lin: 49.5 mio; CTR2_circ: 66.4 mio; 1–75_lin: 46.5 mio; 1–75_circ: 40.1 mio). For the read coverage across the viral genome, the terminal regions were not used (positions 1–75 and the 3′-terminal 50 nucleotides), due to their low representation.

RESULTS

Design of AS-circRNAs targeting SARS-CoV-2 RNA

To develop new RNA-based therapeutics for antiviral strategies, we designed and tested artificial small circRNAs containing antisense-RNA sequences that target SARS-CoV-2 RNA. We focussed on the 5′-UTR, because its RNA secondary structure is relatively well characterized and highly conserved (2,3), and there is evidence for important functions of the 5′-UTR on multiple levels, including viral genome replication (38) and transcription [subgenomic RNA (sgRNA) synthesis, (5,6)], translational initiation (39), RNA stability (3) and, potentially, RNA packaging (40). To screen for functional antisense sequences and optimal SARS-CoV-2 targets in the 5′-UTR, we initially used two separate luciferase reporter systems (Figure 1A).

First, to assess effects of antisense-circRNAs (AS-circRNAs) on the 5′-UTR of the viral genome, the first 265 nucleotides of the SARS-CoV-2 genome including the ORF1a translation start codon and the first 24 nucleotides of ORF1a, were fused in-frame with the luciferase ORF, resulting in the '5′-UTR' reporter construct (Figure 1A).

Second, to determine effects on the 5′-UTR of viral sgRNAs, the 5′-terminal 75 nucleotides of the SARS-CoV-2 genome were used, comprising the common 'leader' sequence (including the TRS element), which is present on all sgRNAs. That region, followed by 25 nucleotides with AUG start codon and 5′-terminal coding sequence of the S protein, were fused to the luciferase ORF, resulting in the '5′-leader' reporter (Figure 1A).

We selected the exact positioning of the antisense sequences according to the current secondary structure model of the 5′-UTR and 5′-leader regions, containing three highly conserved stem-loop RNA structures [SL 1–3, (3,4)]. Our previous work on AS-circRNAs had indicated that perfect base-pairing between circRNA and target over at least 30 nucleotides was required for stable interaction (Silke Schreiner and Christina Pfafenrot, unpublished observations).

On this basis, a series of six short AS-circRNAs, between 66 and 76 nts in length and with 40–50 nts of antisense sequence, was designed to specifically target the SARS-CoV-2 5′-UTR regions (named according to target boundaries; for a schematic representation and exact SARS-CoV-2 target boundaries, see Figure 1A and B; antisense sequences are listed in Supplementary Table S1). AS-circRNA 1–40 targets the 5′-terminal 40 nucleotides of the SARS-CoV-2 genome (and sgRNAs), including SL1; AS-circRNA 1–65 targets the 5′-terminal 65 nucleotides, but omits the complete 27-nucleotide SL1, and AS-circRNA 1–75 extends this base-pairing interaction by

Nucleic Acids Research, 2021, Vol. 49, No. 21 ***12507***

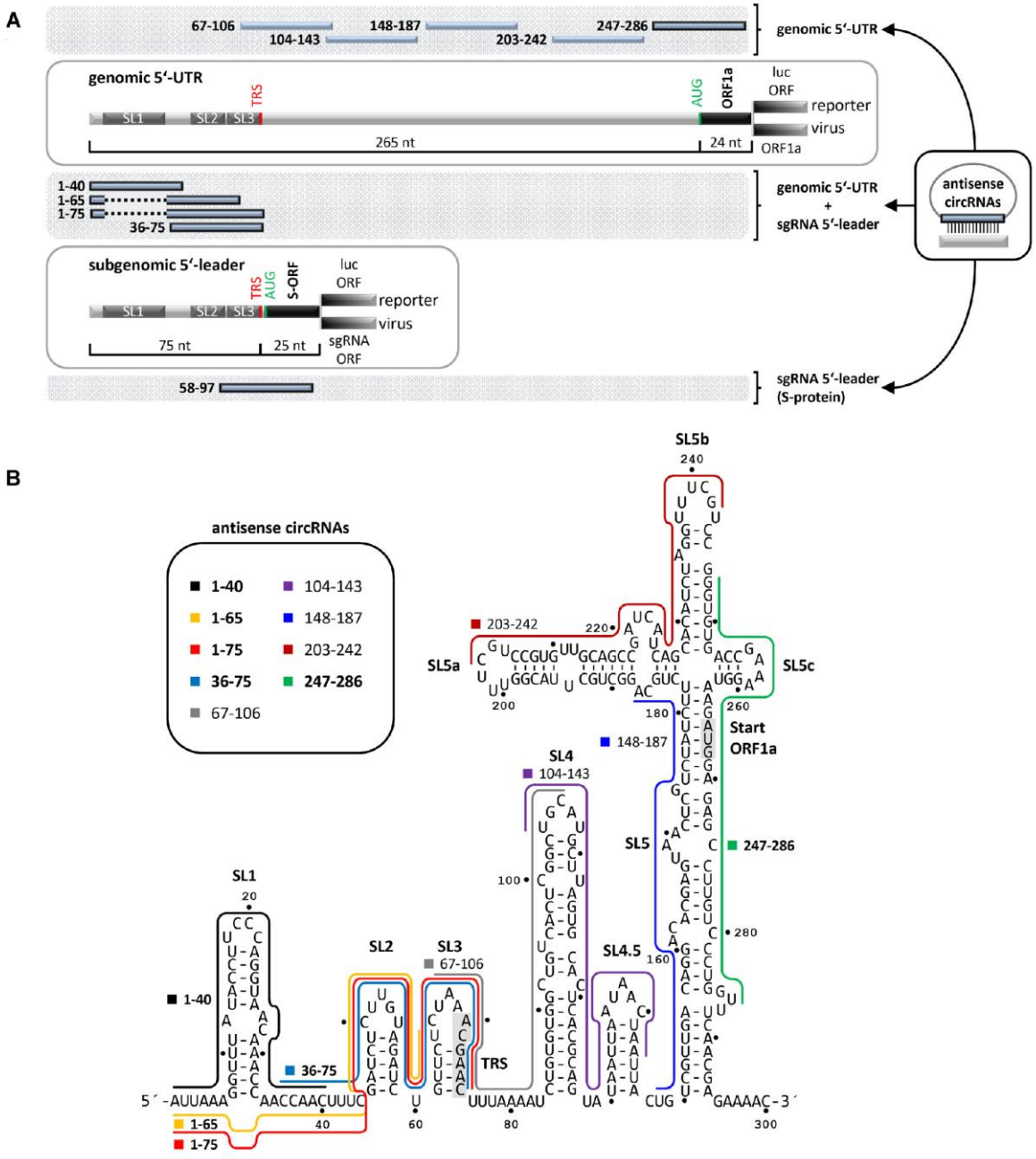

Figure 1. Design of AS-circRNA targeting SARS-CoV-2 RNA. (**A**) Schematic representation of the 5′-UTR (top, nts 1–265) and 5′-leader (bottom; nts 1–75) sequences, targeted by AS-circRNAs, either in a luciferase-reporter (luc), or in the viral SARS-CoV-2 context (ORF1a or S). Target regions of individual AS-circRNAs are represented as blue bars with nucleotide coordinates. The conserved 5′-terminal stem-loop elements (SL1-3) are indicated, as well as the transcription regulatory sequence (TRS) of the 5′-leader. Note that the target regions of AS_1–65 and AS_1–75 circRNAs omit the first stem–loop (SL1), represented as a dashed line. (**B**) Target regions of AS-circRNAs within the 5′-leader (nts 1–75) and 5′-UTR of SARS-CoV-2 (nts 1–265), represented in the context of the secondary structure model of this region [nts 1–300; (3,4)]. For a schematic representation, see panel **A**. The core TRS element (nts 70–75) and the AUG start codon of ORF1a (nts 266–268) are shaded in grey. Note that AS_58–97 circRNA is not included, since it overlaps with the ORF of the S protein.

ten nucleotides, including the TRS element. AS-circRNA 36–75 again was designed to base-pair with the single-stranded region between SL1 and 2, and the less stable SLs 2 and 3, including the TRS element. These four AS-circRNAs have in common that they can base-pair with both the SARS-CoV-2 genomic RNA and all eight major sgRNAs (sgRNAs 2–9) produced in infected cells.

In addition, two AS-circRNAs were designed to specifically target either the ORF1a translation start site, along with flanking regions (in the SARS-CoV-2 genome RNA), or the ORF encoding the viral S protein (in sgRNA 2): AS-circRNA 247–286 spans the 3′-terminal region of the genomic 5′-UTR region and the first 21 nucleotides of the ORF1a, whereas AS-circRNA 58–97 targets SL3, the TRS element and the first 21 nucleotides of the S-protein ORF (Figure 1A). As control and for normalization of luciferase activities, two non-specific circRNAs were used in these experiments, each comprising a randomized sequence of 40 nucleotides instead of the antisense sequences.

Synthetic AS-circRNAs inhibit translation of SARS-CoV-2 reporter constructs

We initially used AS-circRNAs transiently overexpressed in HeLa cells by the so-called Tornado system [Twister-Optimized RNA for Durable Overexpression, see (32)] which relies on an RNA polymerase III-driven and self-cleaving expression cassette, combined with circularization by endogenous RtcB tRNA ligase (Supplementary Figure S1A). One day after transfection of the circRNA expression constructs, either genomic 5′-UTR or subgenomic 5′-leader reporters were transfected, followed by luciferase assays (Supplementary Figure S1B). Overexpression at similarly high levels of all ten SARS-CoV-2 5′-UTR/5′-leader specific AS-circRNAs, as well as of two control circRNAs, was confirmed by Northern blot analysis (Supplementary Figure S1C). In addition, circular configuration was stringently established by RNase H cleavage assays (for AS_1–75 circRNA), and cellular distribution between nucleus and cytoplasm was characterized (for AS_1–75 and CTR2 circRNAs, see Supplementary Figure S1DE). Based on reporter assays with both the genomic (5′-UTR) and subgenomic (5′-leader) constructs, all of these overexpressed anti-SARS-CoV-2 circRNAs, except for AS_67–106 and AS_104–143, were found to reduce luciferase expression to levels between 50 to 60% (Supplementary Figure S1F). Since the four AS-circRNAs against the 5′-leader region (nucleotides 1–75) as well as three AS-circRNAs upstream of or spanning the ORF1a translation initiation site (nucleotides 148–286) reduced reporter expression most profoundly, we decided to focus our subsequent analysis on these regions.

However, the Tornado-based circRNA expression system results in massive overexpression, in the order of 10^6 copies per cell (31), and one cannot rule out effects due to linear precursors or side-products. Therefore we switched for all following assays to synthetic AS-circRNAs transfected in mammalian cells, which is advantageous, because it is a biochemically well-defined system; for example, transfected circRNA quantities can be titrated and the effects of circular and linear forms can be directly compared with each other.

AS-circRNAs were produced *in vitro*, based on transcription by T7 RNA polymerase and circularization by T4 RNA ligase, followed by gel purification (Figure 2A). Each circRNA was designed such that the antisense sequence was linked to a common short stem–loop (6 perfect base-pairs with two overhanging ends that were joined by ligation). The antisense region and the stem–loop are connected by two three-nucleotide linkers, to allow a more flexible presentation of the antisense sequence.

To functionally characterize this series of AS-circRNAs, we first tested their ability to inhibit translation in the two luciferase reporter systems (for a flowchart of analysis, see Figure 2B): HeLa cells were first transfected with circRNA; after 24 h, the reporter construct was transfected and, after another 24 h, luciferase activities were measured.

For quality control and evidence of circularity, purified AS-circRNAs (as well as their linear counterparts) were characterized by denaturing PAGE (Figure 2C): Note that all of these relatively short circRNAs are RNase R resistant, in contrast to the corresponding linear RNAs, and that the circular configuration results in slower mobility relative to the linear form, demonstrating circularity. Regarding cellular distribution after transfection, AS-circRNAs as well as their linear counterparts were detected predominantly in the cytoplasmic compartment (where coronavirus replication is localized), as shown for AS_1–75 and control linear and circular RNAs (Supplementary Figure S2).

Comparing the two reporters, 5′-UTR versus 5′-leader, corresponding effects of AS-circRNAs were observed for the first four AS-circRNAs that target the 5′-terminal region, nucleotides 1–75 (AS_1–40, AS_1–65, AS_1–75, and AS_36–75; see Figure 2D): Only in case of the longest version, AS_1–75, which excludes stem-loop 1, both reporters were strongly reduced in translation (to 39 and 18% residual level, respectively). The two shorter AS-circRNAs (AS_1–40 and AS_1–65) showed smaller or insignificant activities. The strong effect of AS_1–75 circRNA is not simply due to extended base-pairing, since the shorter AS_36–75 was almost as strong as AS_1–75: reduction to 57 and 29%, respectively, for the two reporters.

Moving from the 5′-end to the regions overlapping the translation start codons for the ORF1a and the S-gene, we assayed AS_247–286 circRNA (for the genomic 5′-UTR reporter) and AS_58–97 circRNA (for the 5′-leader reporter): Both had strong effects on reporter activity (reduction to 15% and 54%, respectively). The use of AS-circRNAs (AS_247–286 and AS_58–97) targeting the AUG start codon regions (of ORF1a and S-gene, respectively) in combination with circRNAs targeting the 5′-terminal leader region did not further increase the inhibitory action on reporter translation (see three combinations for each of the two reporters, Figure 2D).

To address the important question of whether the circular configuration of the AS-circRNA is important for inhibitory activity, we compared the two AS-circRNAs with the strongest inhibitory effects with their linear counterparts: AS_1–75 and AS_247–286, using the 5′-UTR reporter, and AS_1–75 and AS_36–75, using the 5′-leader reporter (Figure 2E). To provide additional support for the specificity of the inhibition, we also

Nucleic Acids Research, 2021, Vol. 49, No. 21 ***12509***

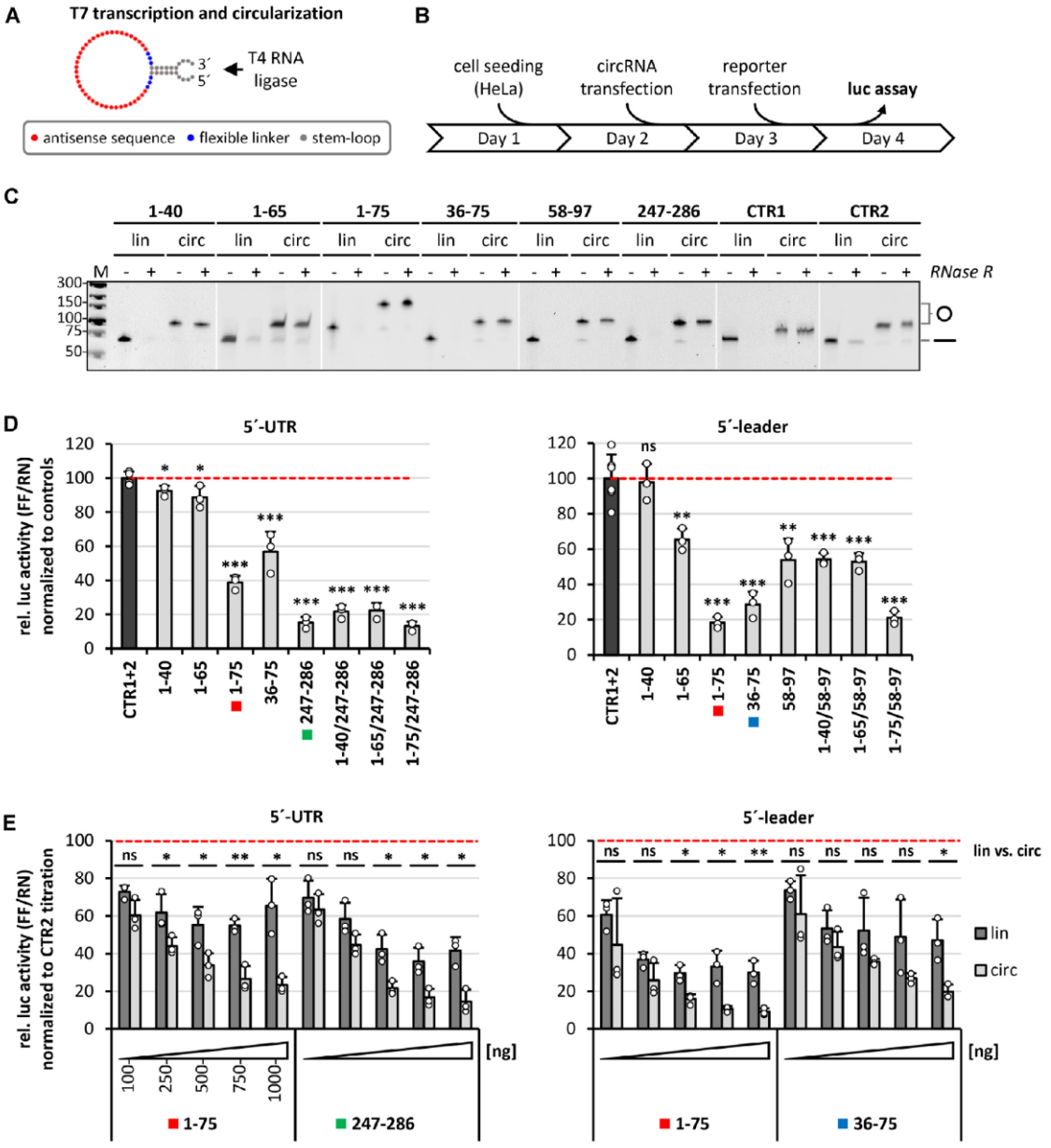

Figure 2. Screening of active AS-circRNAs: 5′-UTR and 5′-leader reporter assays. (**A**) Design of synthetic AS-circRNAs. CircRNAs were produced by *in vitro* T7 transcription and subsequent circularization by T4 RNA ligase. Each circular RNA is composed of a stem–loop with overhangs for efficient ligation (grey), a short stretch of unrelated nucleotides for enhanced flexibility (blue), and the antisense sequence (red). (**B**) Experimental workflow for luciferase reporter assays in HeLa cells transfected with synthetic circRNAs. (**C**) AS-circRNA synthesis. RNase R treatment and aberrant electrophoretic migration confirm the circularity of the produced circRNAs. Gel-purified linear and circular RNAs (lin/circ) were treated with RNase R, or left untreated (–/+), and analyzed by denaturing polyacrylamide electrophoresis and ethidium bromide staining. Mobilities of circular (o) and linear (–) forms are marked. *M*, DNA markers (sizes in bp). (**D**) Luciferase reporter assays reveal regions accessible to AS-circRNAs, based on the repression of luciferase activity by specific SARS-CoV-2 5′-UTR (left) and 5′-leader reporter constructs (right). HeLa cells were transfected with the respective circRNA (as indicated below the diagram) or a combination thereof (e.g. AS_1–40/247–286). The color code highlights those AS-circRNAs that were analyzed in more detail in panel E. After 24 h, the respective reporter was transfected (5′-UTR or 5′-leader), and relative luciferase activities (ratio of Firefly and Renilla expression) were measured, normalized to control circRNAs CTR1 and 2 (mean and standard deviations of three replicates, $*P < 0.05$, $**P < 0.005$, $***P < 0.001$, ns = not significant, two-sided *t*-test). (**E**) Dose dependence and comparison of circular versus linear configuration of selected antisense-RNA regions. HeLa cells were transfected with increasing amounts (100–1000 ng per assay) of circRNAs (light gray), or their linear counterparts (dark grey; as indicated below the diagram). After 24 h, the respective reporter constructs were transfected (5′-UTR or 5′-leader), and relative luciferase activities (Firefly/Renilla expression ratios) were measured, normalized to control circRNA CTR2 (mean and standard deviations of three replicates, $*P < 0.05$, $**P < 0.005$, $***P < 0.001$, ns = not significant, two-sided *t*-test).

12510 Nucleic Acids Research, 2021, Vol. 49, No. 21

measured dosis-dependent reduction in reporter activity for the selected RNAs, with doses ranging between 100 and 1000 ng per assay. For each of the four setups, we observed clear dosis-dependent effects, in particular for the circular configuration. Under the conditions used, maximal activities were attained with 750–1000 ng of AS-circRNA per assay, whereas the inhibition with linear counterparts leveled off at 500 ng and above. Importantly, the circRNAs were consistently more potent than their linear counterparts. At higher concentrations, the circRNA caused a more than 2-fold stronger reduction of reporter activity than the corresponding linear RNA. This superior inhibitory efficacy of the AS-circRNAs may be due to differential stabilities or intracellular localizations of the transfected RNAs, their intrinsic antisense activity, base-pairing potential, structural properties, or a combination thereof.

We conclude that, based on two separate reporters and AS-circRNA transfection in HeLa cells, both the 5′-leader- and the AUG-start codon-proximal regions can be efficiently targeted by AS-circRNAs, resulting in strong translational inhibition down to 10% residual level.

Inhibition of SARS-CoV-2 proliferation by designer AS-circRNAs

Following the identification of specific AS-circRNAs that effectively inhibit translation of reporter RNAs, we sought to corroborate key findings of our study by using SARS-CoV-2-infected cells. To this end, the set of AS-circRNAs we had characterized in our reporter assays, except for inactive AS_1–40, as well as two control RNAs, were transfected in Vero E6 cells, which are permissible for SARS-CoV-2 infection and allow the production of infectious virus progeny (for a flowchart, see Figure 3A). Each AS-circRNAs was transfected in three different quantities (25, 250 and 2500 ng per assay), and 24 h later, cells were infected with SARS-CoV-2 at an MOI of 0.1 pfu/cell. 24 h post-infection, cell culture supernatants were collected, and virus titers were determined by plaque assays to assess the antiviral effects of individual AS-circRNAs on viral replication in cell culture (Figure 3B).

Compared to the controls (untreated cells, mock-transfected cells, two different control AS-circRNAs), the three AS-circRNAs targeting the untranslated leader region differentially affected virus titers: The strongest effect on viral proliferation was measured for AS_1–75, a reduction to 9% of control level, consistent with the strong effect observed in the previous reporter assays (compare Figures 3B and 2D). The shortened version of this circRNA, AS_1–65, still had a moderate, but significant effect on virus titers (reduction to 33% compared to untreated control cells), whereas AS_36–75 had no significant effect (Figure 3B). In contrast to the initial reporter assays, AS_58–97, designed as specific for the subgenomic mRNA encoding the S protein, and AS_247–286, targeting the genomic region including the ORF1a start codon, did not significantly reduce virus titers (Figure 3B). Based on these results, we focussed our further analysis on the AS_1–75 circRNA, which targets both viral genomic and all subgenomic RNA species.

To obtain additional evidence for inhibition of viral replication, we also measured viral protein synthesis by Western blotting, using SARS-CoV-2 nucleocapsid (N) protein-specific antibodies (Figure 3C). Clearly, compared to the controls (untreated, mock, CTR 1 and 2) and four other AS-circRNAs, intracellular accumulation of viral N protein was most profoundly reduced in the cells treated with AS_1–75 circRNA, consistent with the observed inhibitory effects of this particular circRNA on the production of infectious virus progeny.

Finally, we compared effects of circular and linear versions of the antisense sequence of AS_1–75 in their efficiency on viral proliferation, using an extended range of RNA quantities (625–5000 ng per assay; see Figure 3D). We observed a strong and dosis-dependent antiviral effect of AS_1–75 circRNA, with virus titers reduced down to 4% (at 2500 ng per assay); at an even higher dose (5000 ng), virus titers were reduced to 7%, perhaps reflecting some toxic effects at this high circRNA quantity or suboptimal ratios of circRNA to transfection reagent. In contrast, control AS-circRNA had no significant effect. Comparing the effects of circular versus linear RNAs, we observed at all quantities assayed, that circRNA was clearly superior to the corresponding linear version, consistent with our results from reporter assays (see above and Figure 2E).

In addition to the general workflow (Figure 3A), in which we monitored the increase of virus titers until 24 h post-infection, we addressed the question of whether the antiviral effect of AS_1–75 circRNA persists for longer time periods (Figure 3E): We determined virus titers in the culture supernatants of cells transfected with linear versus circular AS_1–75 RNA (along with appropriate controls) and collected at six time points from 16 to 72 h post-infection. Whereas effects of linear and circular control RNA (CTR2) did not significantly differ from the mock control, AS_1–75 circRNA caused a significant reduction of virus titers, especially between 24 to 48 h post-infection. This antiviral effect was specific for the circular configuration and indicates durability of the effect over at least two days under the conditions used. Finally, combining virus titer measurements from several assays of the antiviral effect of AS_1–75 circRNA (all measured at 24 h post-infection and based on Figures 3B, D, E), we estimated an EC_{50} value in the 20–50 nM range for this most effective AS-circRNA (Supplementary Figure S3).

Furthermore, to answer the question whether AS_1–75 circRNA also shows an effect in cells already infected with virus, additional experiments were performed in reverse order of circRNA transfection and virus infection (see Supplementary Figure S4): One hour after virus infection, linear or circular AS_1–75 RNA (together with appropriate controls) was transfected, and virus titers were determined in the culture supernatants at six time points after RNA transfection, from 16 to 72 h post-infection. We chose a one-hour interval between virus infection and circRNA transfection, as used in many published studies. Binding and uptake of virus particles is a relatively fast process (for example, see reference 41). Therefore, one hour is sufficient for establishment of the viral infection, and at the same time, we avoid any potential problems with dying cells, which at later time points would accumulate, obscure any effects, and

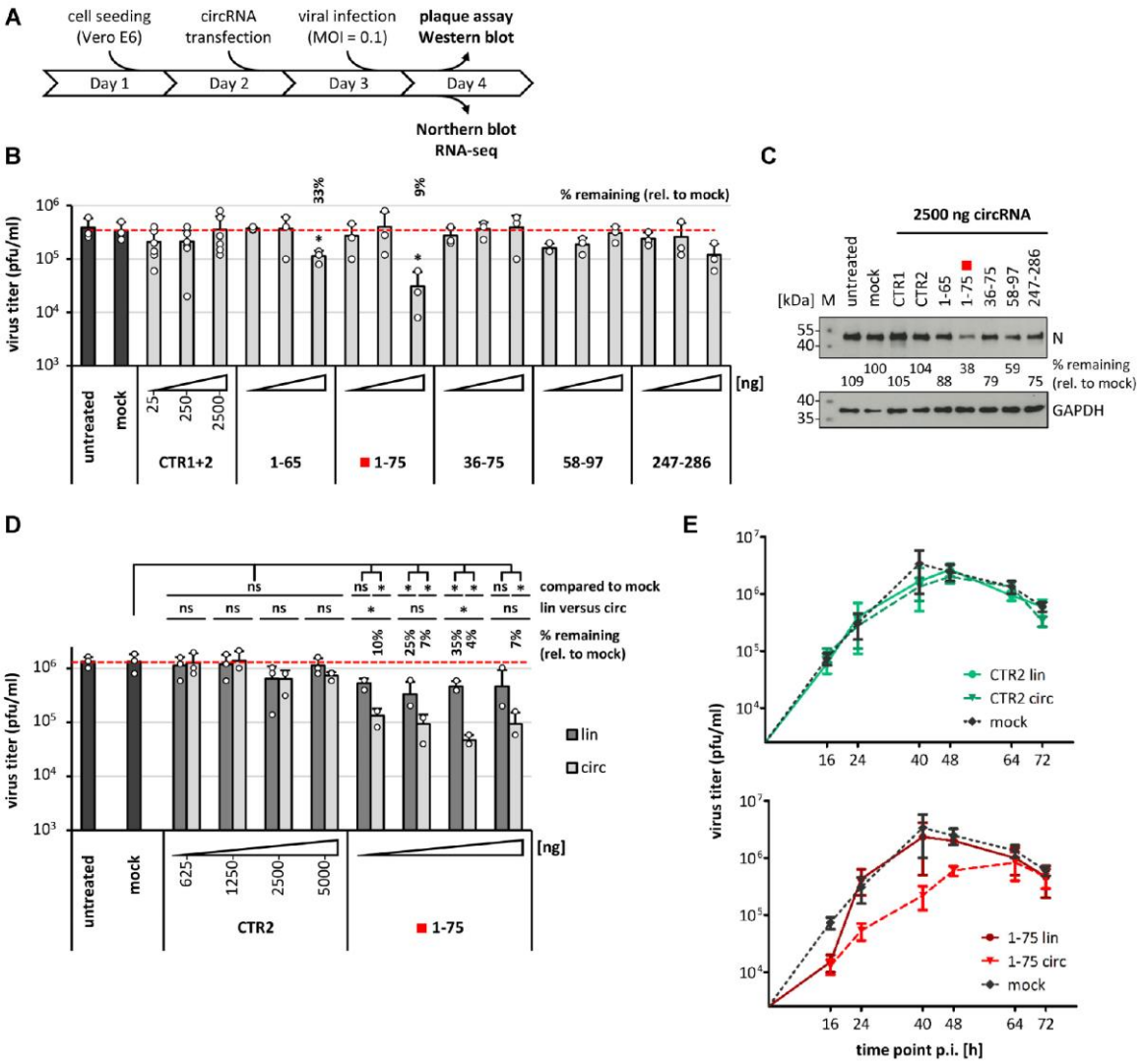

Figure 3. Inhibition of SARS-CoV-2 proliferation by AS-circRNAs: viral infection assays. (**A**) Experimental workflow for viral infection assays using Vero E6 cells. (**B**) Screening of AS-circRNAs by virus titer assays identifies AS_1–75 as the most effective antiviral circRNA. Vero E6 cells were transfected with increasing quantities of circRNAs (25, 250 and 2500 ng per assay; light gray; as indicated below the diagram). After 24 h, cells were infected with SARS-CoV-2 (MOI = 0.1 pfu/cell). The effects on virus titers were measured by virus plaque assays using cell cutlure supernatants collected at 24 h post-infection (mean and standard deviations of three experiments, $*P < 0.05$, ns = not significant, two-sided *t*-test). Untreated (without RNA and transfection reagent) and mock-treated cells (without RNA, but with transfection reagent) served as controls. Residual virus titers of significantly affected samples are indicated as 'percent remaining' relative to mock treatment. (**C**) Viral protein synthesis assays: Western blot analysis of the viral nucleocapsid protein (N) confirms reduction of viral protein accumulation in cells treated with specific AS-circRNAs. Vero E6 cells transfected with 2500 ng of respective circRNAs per assay were harvested, lysed, and equal amounts of protein were analyzed by Western blotting, using the nucleocapsid protein as a marker for viral protein accumulation (quantitation of protein levels relative to mock); GAPDH was used as loading control. *M*, protein markers (sizes in kDa). (**D**) AS_1–75 circRNA: dose dependence of antiviral effect, in comparison to its linear counterpart. Vero E6 cells were transfected with increasing amounts (625, 1250, 2500 and 5000 ng) of AS_1–75 circRNA (light gray), or of its linear counterpart (dark gray), followed by viral infection (MOI = 0.1 pfu/cell) after 24 h. Plaque assays were used to determine virus titers in culture supernatants collected at 24 h post-infection (mean and standard deviations of three experiments, $*P < 0.05$, ns = not significant, two-sided *t*-test). As controls, untreated (without RNA and transfection reagent) and mock-treated cells (without RNA, but with transfection reagent) were used, as well as transfections with linear or circular control RNA (CTR2). The virus titer of significantly affected samples is indicated as 'percent remaining', relative to mock treatment. (**E**) Durability of antiviral activity of AS_1–75 circRNA. Vero E6 cells were transfected with AS_1–75 circRNA or its linear counterpart (bottom panel; in red), followed by viral infection (MOI = 0.1 pfu/cell) after 24 h (mean and SEM of three experiments). Plaque assays were performed to determine virus titers in culture supernatants collected at the indicated time points (16–72 h post-infection). As controls, mock-treated cells (without RNA, but with transfection reagent) were used (top and bottom panels; in black), as well as transfections with linear or circular control RNA (CTR2; top panel; in green).

make interpretations difficult. Again, in this reverse order, the effects of linear and circular control RNA (CTR2) were not significantly different from the mock control, whereas AS_1–75 circRNA caused a significant reduction in viral titers, especially between 24 and 64 h post-transfection. The antiviral effect was also more pronounced for the circular than for the linear configuration, as observed in the usual setup (Figure 3E).

In addition to the standard Vero E6 cell culture system, we evaluated the antiviral effect of AS_1–75 circRNA in a biologically more relevant, *ex-vivo* respiratory cell culture system, based on differentiated primary normal human bronchial epithelial (NHBE) cells grown in air/liquid interface culture (Supplementary Figure S5). This mimicks the tracheobronchial region of the human respiratory tract in a physiologically relevant cellular environment (42). Differentiated NHBE cells were transfected with linear versus circular AS_1–75 RNA or CTR2, followed by viral infection with SARS-CoV-2 after 24 h and determination of virus titers in the culture supernatants at different time points (24–72 h post-infection). Comparing two independent experiments, we conclude that also in this *ex-vivo* model system AS_1–75 circRNA (as well as its linear counterpart) exhibits a strong inhibiting effect on viral replication.

To assess if an elongation of the antisense region of AS_1–75 further improves its antiviral activity, we tested two more AS-circRNAs in virus titer assays: AS_1–100 (S) and (N), both increasing the base-pairing potential of AS_1–75 circRNA by 25 positions and including a small number of nucleotides from the 5′-terminal coding regions of the S and N genes, respectively (Supplementary Figure S6). However, compared to AS_1–75 (virus titer reduced to 1%, relative to control), both elongated AS-circRNAs were slightly less active (reduction to 7 and 4%, respectively, relative to the CTR3 control circRNA of equal length). Note that the elongated AS-circRNAs were designed to specifically target the sgRNAs that are used for S- and N-protein expression, respectively, whereas AS_1–75 has a broader specificity by targeting both genomic RNA and all plus-strand subgenomic RNAs.

Finally, we assessed the effect of AS_1–75 RNA on viral RNA synthesis more directly (Figure 4). Viral genome RNA and all subgenomic mRNAs were detected in infected and transfected cells by Northern blotting with a probe specific for the 3′-terminus of the genome (Figure 4A). We compared the effects of linear and circular versions of AS_1–75 with four different controls (untreated cells, mock, linear and circular control CTR2 RNA). Only the circular configuration of AS_1–75, but not its linear version, strongly reduced viral RNA levels, both genomic RNA and all subgenomic RNAs that can be resolved, indicating a global effect of this most active AS-circRNA on viral RNA synthesis.

Since Northern blotting cannot be quantitated precisely under these conditions, and not all eight subgenomic RNA species (RNAs 2–9) could be unambiguously identified, we performed RNA-seq, using poly(A)-selected RNA from infected cells. By comparing normalized SARS-CoV-2 genome-mapped reads, which reflect total viral RNA accumulation in infected cells, we found that only the read-counts obtained for cells transfected with AS_1–75 circRNA were strongly reduced (to 12.5% of mock levels; Figure 4B).

In order to analyze individual viral RNA species, we measured the read coverage for nine segments across the SARS-CoV-2 viral genome, each of which are delimited by flanking TRS sites (Figure 4C). Due to the characteristic 3′-coterminal structure of each of the viral RNA species, only full-length viral genome RNA (g) can be assessed directly by read coverage between positions 76 and 21,562. In contrast, production of the individual subgenomic RNAs can be determined only as 'cumulative read coverage': For example, the read coverage between positions 21,562 and 25,391 combines reads for both the genome RNA (RNA 1) and the sgRNA 2 (S).

When we compared cumulative read coverage across the viral genome sequence for cells transfected with linear AS_1–75 RNA, AS_1–75 circRNA, or one of the controls, we found that only in the AS_1–75 circRNA-transfected cells viral RNA levels were strongly reduced (to between 37 and 10% relative to mock). Moreover, the extent of reduction increased with a 5′-to-3′ gradient, and most profoundly within the first three segments, proceeding from viral genome RNA to regions that include more and more sgRNAs. This characteristic behavior suggests that the AS_1–75 circRNA interferes, at least in part, with sgRNA synthesis.

AS-circRNAs exhibit robust activity against SARS-CoV-2 mutant sequences and are superior to modified ASOs

Since newly emerging mutations in the viral genome are of great concern in the current SARS-CoV-2 pandemic, we also assayed whether the activity of designer antisense-circRNA was affected by single point mutations in the target sequence. We focussed on the highly conserved 5′-leader region, where the AS_1–75 circRNA had proved most active, in combination with 5′-leader reporter constructs carrying five different single-point mutations, which naturally occur most frequently in this region (https://www.biosino.org/ViGTK/): 21C→T, 34A→T, 35A→T, 36C→T, 66C→T (Figure 5A).

The reduction of reporter activity by AS_1–75 circRNA was not significantly different for the wildtype reporter and for four different mutant versions at positions 21, 34, 35 and 36; only for the 66C→T mutation the antisense activity of AS_1–75 circRNA was reduced, from residual levels of around 25–50% of control levels (Figure 5B–D). These data suggest that the activity of AS_1–75 circRNA is in most cases surprisingly robust and resistant towards single-point mutations.

Finally we compared the activity of AS_1-75 circRNA with corresponding modified, linear antisense oligonucleotides (ASOs), using both the 5′-leader reporter construct as well as viral infection assays (Figure 5BC and EF, respectively). We assayed two different ASOs of standard length, covering positions 1–45 of the 5′-leader sequence (with stem-loop 1 skipped, as in the AS_1–75 circRNA) and positions 56–75, respectively (Figure 5C). These ASOs were modified either by 2′-*O*-methyl (2′-OMe) or 2′-*O*-methoxyethyl (2′-MOE) nucleotides, which

Nucleic Acids Research, 2021, Vol. 49, No. 21 **12513**

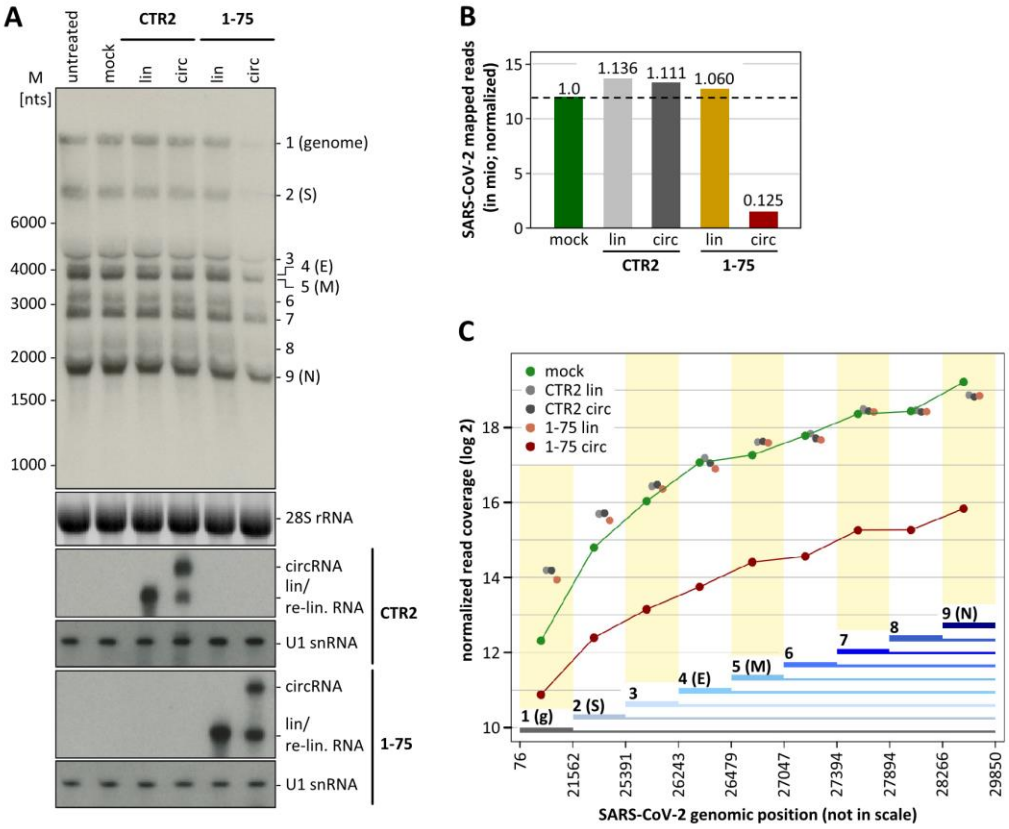

Figure 4. Inhibition of viral RNA synthesis and processing by AS_1–75 circRNA. (**A**) Northern blot analysis of genomic and subgenomic viral RNAs. Vero E6 cells were transfected with AS_1–75 circRNA or its linear counterpart; as controls, untreated (without RNA and transfection reagent) and mock-treated cells (without RNA, but with transfection reagent) were used, as well as cells transfected with linear or circular control RNA (CTR2). At 24 h post-transfection, cells were infected with SARS-CoV-2 (MOI = 0.1 pfu/cell). At 24 h post-infection, total RNA was prepared and subjected to glyoxal-Northern blot analysis, to detect genomic and all subgenomic viral RNA species. *M*, RiboRuler High Range RNA Ladder (Thermo Fisher Scientific). As input control, 28S rRNA was detected by ethidium bromide staining, and CTR2 and AS_1–75 RNAs by specific Northern probes. (**B**) RNA-seq analysis of total viral RNA synthesis. The total numbers of SARS-CoV-2-mapped reads (in mio; normalized to total read number) were compared for RNAs isolated from virus-infected Vero E6 cells that were mock-transfected or transfected with CTR2 control and AS_1–75 RNA, each in linear or circular form, with ratios of read numbers relative to mock conditions indicated. (**C**) Effect of AS_1–75 circRNA on viral genome (g) and subgenomic RNA production in infected cells. Cumulative read coverages (in $\log_2$; normalized to total read number) are plotted for mock-treated, and CTR2 control RNA (lin/circ) or AS_1–75 RNA (lin/circ)-transfected cells. The SARS-CoV-2 genome was divided in nine sections with boundaries defined by the body-TRS sites of the eight subgenomic RNAs (sections used for cumulative read numbers are marked by thick lines; genomic positions are indicated below and drawn not in scale).

should enhance both base-pairing interaction as well as cellular stability. Based on luciferase reporter assays, all four ASOs were clearly less efficient than the AS_1–75 circRNA (by a factor of 3.5–5.4; see Figure 5E). Based on viral infection and virus-titer assays, only the AS_1–75 circRNA, but none of the four ASOs exhibited significant antiviral effects (Figure 5F). We conclude that, comparing antisense-circRNA and state-of-the-art ASOs, these initial assays indicate the superiority of antisense-circRNA as novel and sequence-specific antiviral agents.

DISCUSSION

To our knowledge, this is the first study to report the design and functional evaluation of a series of AS-circRNAs as a novel tool suitable to interfere with gene expression, applied here to block SARS-CoV-2 proliferation. We focussed on the 5′-UTR region, which is not only highly conserved in sequence and structure, but also absolutely essential for the viral life cycle. Based on a series of AS-circRNAs targeting specific 5′-UTR regions of SARS-CoV-2 genome and sgRNAs, we identified a cap-proximal region (including part of the 5′-leader sequence) as the most effective target region. In particular, AS-circRNAs 1–65 and 1–75 strongly interfered with virus proliferation, resulting in at least 10-fold reduced virus titers. Note that the target sequences of these two antisense-RNAs are discontinuous, omitting the first stem–loop. These data suggest that RNA structure information (if available) should be taken into account in the design and optimization of AS-circRNAs.

When evaluating and comparing the efficiencies of AS-circRNAs in our study, one should also take into account that efficiencies are limited by the circRNA transfection efficiencies under our cell culture conditions; therefore the

12514 Nucleic Acids Research, 2021, Vol. 49, No. 21

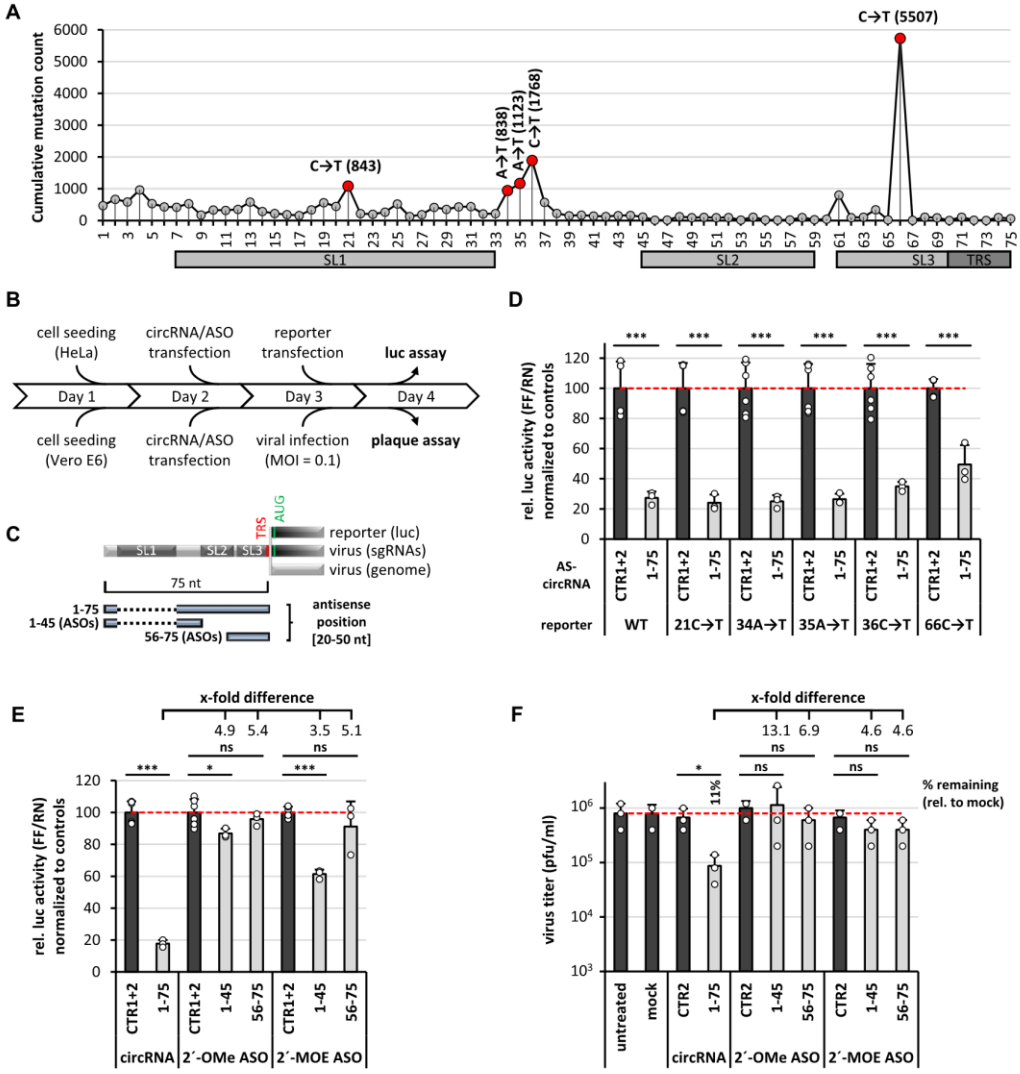

Figure 5. AS-circRNAs exhibit robust activity against SARS-CoV-2 mutant sequences and are superior to modified ASOs. (**A**) Summary of naturally occurring point mutations within the viral 5′-leader of SARS-CoV-2. All annotated mutations are indicated per nucleotide position [cumulative mutation count, as deposited in the ViGTK database (https://www.biosino.org/ViGTK/); as at 30 April 2021). The five most frequent single-point mutations in the 5′-leader region (positions 1–75) are highlighted in red (occurrences given in parentheses) and were selected for mutational analysis. Secondary structures and regulatory elements are marked (SL1–3, TRS). (**B**) Experimental workflow for luciferase reporter assays in HeLa cells, and for viral infection assays using Vero E6 cells, transfected with synthetic circRNAs or modified antisense oligonucleotides (ASOs). (**C**) Schematic representation of the 5′-leader (nts 1–75) sequence, targeted by a AS-circRNA (1–75) or two antisense oligonucleotides (ASOs, 1–45 and 56–75), either in a luciferase-reporter (luc), or in the viral SARS-CoV-2 context (sgRNAs/genome). Target regions of individual AS-circRNA or ASOs are represented as blue bars with nucleotide coordinates. Secondary structures and regulatory elements are marked (SL1–3, TRS, AUG). Note that the targeting regions of AS_1–75 circRNA and 1–45 ASO omit the first stem-loop (SL1), represented as a dashed line. (**D**) Activity of AS_1–75 circRNA in presence of single point mutations within the 5′-leader: luciferase reporter assays. HeLa cells were transfected with 1–75 AS-circRNA or with control circRNAs. After 24 h, the respective 5′-leader reporter plasmids, either without (WT) or with the indicated point mutations, were transfected, and relative luciferase activities (ratio of Firefly and Renilla expression) were measured, normalized to control circRNAs CTR1 and 2 (mean and standard deviations of three replicates, $P < 0.001$***, two-sided *t*-test). (**E**) Activity of 2′-OMe or 2′-MOE modified ASOs: luciferase reporter assays. HeLa cells were transfected with the AS_1–75 circRNA (1 μg) or ASOs (molar equivalents), respectively. After 24 h, the 5′-leader reporter was transfected, and relative luciferase activities (ratio of Firefly and Renilla expression) were measured, normalized to control circRNAs CTR1 and 2, or correspondingly modified control ASOs CTR1 and 2 (mean and standard deviations of three replicates, $P < 0.05$*, $P < 0.001$***, ns = not significant, two-sided t-test). Fold differences in translational repression between AS_1–75 circRNA and ASO treatments are indicated. (**F**) Antiviral activity of 2′-OMe or 2′-MOE modified ASOs: virus infection assays. Vero E6 cells were transfected with AS_1–75 circRNA (2500 ng per assay) or with ASOs (molar equivalents). After 24 h, cells were infected with SARS-CoV-2 (MOI = 0.1 pfu/cell). The antiviral effects were measured by virus plaque assays at 24 h post-infection (mean and standard deviations of three experiments, *$P < 0.05$, ns = not significant, two-sided t-test). Untreated (without RNA and transfection reagent) and mock-treated cells (without RNA, but with transfection reagent) served as controls. In addition, control circRNA CTR2 and the correspondingly modified control ASO CTR2 were used. Residual virus titers of significantly affected samples are indicated as 'percent remaining' relative to mock treatment, as well as fold differences between circRNA and ASO treatments.

'real' activities are likely higher than the apparent values determined here. In addition, the experimental conditions of circRNA lipofection, as well as the *in vivo* stabilities of circRNAs can certainly be further improved, for example by systematically optimizing circRNA delivery, evaluating backbone sequences and structure, or introducing RNA modifications or peptide conjugation.

We were able to demonstrate that the inhibitory potency of circular versions of antisense sequences consistently surpassed that of the corresponding linear versions (Figures 2 and 3); moreover, the optimal AS_1–75 circRNA proved superior to state-of-the-art modified ASOs against the same target region, as used in traditional antisense strategies (Figure 5). Most likely this is due to the relatively high metabolic stability of circular RNAs; in addition, structural peculiarities and constraints of how the antisense sequence is exposed in circular configuration may contribute to the activity of AS-circRNAs. Obviously there are more ASO varieties available, as well as combinations of modified nucleotides, that could be tested more systematically, beyond the 2′-OMe and 2′-MOE moieties assayed here. In addition, integrating modified nucleotide positions within synthetic AS-circRNAs appears an attractive and promising option for follow-up studies to further optimize the antisense-circRNA concept.

Our approach to assay the efficiency of antisense-circRNA against SARS-CoV-2 is based on circRNA transfection followed by virus infection, reflecting a prophylactic treatment. However, we have assayed also in the reverse order, viral infection followed by circRNA transfection, and we were able to confirm the efficiency of AS_1–75 circRNA and durability of the antiviral effect (Supplementary Figure S4). This demonstrates that our antisense-circRNA approach is useful not only for prophylactic strategies, but also for protecting against viral infection and for antiviral therapy.

Finally, we were able to confirm the antiviral effect of AS_1–75 circRNA also in an *ex-vivo* cell culture system (Supplementary Figure S5).

What is the mechanistic basis for the strong antiviral effects observed for these AS-circRNAs? Detailed analyses remain to be performed, but will likely reveal a complex picture, because the 5′-terminal region of SARS-CoV-2 is predicted to be involved in multiple levels of the viral replication cycle, such as translational initiation, viral genome replication, synthesis of the 5′-leader-containing subgenomic RNAs, RNA stability, and RNA packaging. Our analysis of viral RNA synthesis (Figure 4) and the data obtained in reporter assays (Figure 2) indicate that the most potent AS-circRNA, AS_1–75, interferes with both the production of subgenomic RNAs and viral protein translation. Effects on other steps are likely but remain to be corroborated by further studies. Initial direct Northern blot assays with reporters argue against the possibility that an RNAi-type cleavage mechanism induced by perfectly base-paired antisense regions is involved. These results, complemented by measuring luciferase mRNA reporter levels via qPCR, rather support a blockage-type mechanism (Supplementary Figure S7).

The extended length of our optimal, unmodified AS_1–75 circRNA confers a certain robustness towards single point mutations in the antisense target region, as we have demonstrated for several naturally occuring point mutations in the leader region (Figure 5). Obviously this represents an added benefit of an AS-circRNA based antiviral strategy, considering the continuously arising mutant SARS-CoV-2 virus forms.

The confirmed functionality of AS-circRNAs designed and characterized in this study in the context of virus infection, including the superior activity of circular over linear RNAs, suggests that circRNAs with antisense functions may exist in nature and play a role in gene regulation. Our results establish designer AS-circRNAs as a new generation of versatile and adjustable RNA therapeutics with significant potential. Finally, in the context of antiviral therapeutic applications, it is worth noting that AS-circRNAs could be easily adjusted to virus escape mutants potentially arising during viral replication and transmission, particularly during virus pandemics of newly emerging viruses.

DATA AVAILABILITY

RNA-seq data were deposited in the Sequence Read Archive (SRA-ID: PRJNA693241) of NCBI.

SUPPLEMENTARY DATA

Supplementary Data are available at NAR Online.

ACKNOWLEDGEMENTS

We thank Ramakanth Madhugiri for advice on SARS-CoV-2 sequences and subgenomic RNA annotation, Stefan Günther for RNA-seq support, Katharina Rudek for circRNA production, other lab members for discussions, and Zefeng Wang and Guoqing Zhang (PICB Shanghai) for discussions and help with the ViGTK SARS-CoV-2 mutant database.

Author contributions: C.P., T.S., C.M. and S.S. designed and carried out experiments, L.-H.H. did the bioinformatic analysis and J.Z. and A.B. wrote the manuscript.

FUNDING

Deutsche Forschungsgemeinschaft [RTG 2355; project Bi 316/18-1 and 18-2 within SPP 1935 to A.B.; project Bi 316/20-1 within Research Unit FOR 5116 to A.B.; project A01 within SFB1021 to J.Z.; project P3 within KFO309 to J.Z.; project P10 within GRK2581 to J.Z.]; Cardio-Pulmonary Institute (CPI) within the Excellence Strategy Program [Exc 2026 to T.S.]; State of Hessen, LOEWE Centre DRUID [E2 to A.B.; B2 to J.Z.]; German Federal Ministry for Education and Research (COVINET to J.Z.); German Center for Infection Research (DZIF) to J.Z. Funding for open access charge: DFG.

Conflict of interest statement. C.P., T.S., C.M., J.Z. and A.B. filed a patent application on the use of designer antisense-circRNAs (EP 20211415.3, 'Circular nucleic acids and uses thereof for interfering with genome expression and proliferation of coronaviruses'; patent pending).

REFERENCES

1. Perlman,S. and Netland,J. (2009) Coronaviruses post-SARS: update on replication and pathogenesis. *Nat. Rev. Microbiol.*, **7**, 439–450.
2. Perlman,S. and Masters,P.S. (2021) Coronaviridae: the viruses and their replication. In: Howley,P.M., Knipe,D.M. and Whelan,S. (eds). *Fields Virology*. Wolters Kluwer, Philadelphia, PA, Vol. **I**. pp. 410–448.
3. Madhugiri,R., Karl,N., Petersen,D., Lamkiewicz,K., Fricke,M., Wend,U., Scheuer,R., Marz,M. and Ziebuhr,J. (2018) Structural and functional conservation of cis-acting RNA elements in coronavirus 5′-terminal genome regions. *Virology*, **517**, 44–55.
4. Miao,Z., Tidu,A., Eriani,G. and Martin,F. (2021) Secondary structure of the SARS-CoV-2 5′-UTR. *RNA Biol.*, **18**, 447–456.
5. Sola,I., Almazán,F., Zúñiga,S. and Enjuanes,L. (2015) Continuous and discontinuous RNA synthesis in coronaviruses. *Annu. Rev. Virol.*, **2**, 265–288.
6. Kim,D., Lee,J.Y., Yang,J.S., Kim,J.W., Kim,V.N. and Chang,H. (2020) The architecture of SARS-CoV-2 transcriptome. *Cell*, **181**, 914–921.
7. Zhou,P., Yang,X.L., Wang,X.G., Hu,B., Zhang,L., Zhang,W., Si,H.R., Zhu,Y., Li,B., Huang,C.L. *et al.* (2020) A pneumonia outbreak associated with a new coronavirus of probable bat origin. *Nature*, **579**, 270–273.
8. Zhu,N., Zhang,D., Wang,W., Li,X., Yang,B., Song,J., Zhao,X., Huang,B., Shi,W., Lu,R. *et al.* (2020) A novel coronavirus from patients with pneumonia in China, 2019. *N. Engl. J. Med*, **382**, 727–733.
9. Polack,F.P., Thomas,S.J., Kitchin,N., Absalon,J., Gurtman,A., Lockhart,S., Perez,J.L., Pérez Marc,G., Moreira,E.D., Zerbini,C *et al.* (2020) Safety and efficacy of the BNT162b2 mRNA Covid-19 vaccine. *N. Engl. J. Med*, **383**, 2603–2615.
10. Bennett,C.F. and Swayze,E.E. (2010) RNA targeting therapeutics: molecular mechanisms of antisense oligonucleotides as a therapeutic platform. *Annu. Rev. Pharmacol. Toxicol.*, **50**, 259–293.
11. Crooke,S.T., Witztum,J.L., Bennett,C.F. and Baker,B.F. (2018) RNA-targeted therapeutics. *Cell Metab.*, **27**, 714–739.
12. Bennett,C.F., Krainer,A.R. and Cleveland,D.W. (2019) Antisense oligonucleotide therapies for neurodegenerative diseases. *Annu. Rev. Neurosci*, **42**, 385–406.
13. Le,T.K., Paris,C., Khan,K.S., Robson,F., Ng,W.-L. and Rocchi,P. (2021) Nucleic acid-based technologies targeting coronaviruses. *Trends Biochem. Sci.*, **46**, 351–365.
14. Roberts,T.C., Langer,R. and Wood,M.J.A. (2020) Advances in oligonucleotide drug delivery. *Nat. Rev. Drug Discov.*, **19**, 673–694.
15. Neuman,B.W., Stein,D.A., Kroeker,A.D., Churchill,M.J., Kim,A.M., Kuhn,P., Dawson,P., Moulton,H.M., Bestwick,R.K., Iversen,P.L. *et al.* (2005) Inhibition, escape, and attenuated growth of severe acute respiratory syndrome coronavirus treated with antisense morpholino oligomers. *J. Virol.*, **79**, 9665–9676.
16. Burrer,R., Neuman,B.W., Ting,J.P.C., Stein,D.A., Moulton,H.M., Iversen,P.L., Kuhn,P. and Buchmeier,M.J. (2007) Antiviral effects of antisense morpholino oligomers in murine coronavirus infection models. *J. Virol.*, **81**, 5637–5648.
17. Sänger,H.L., Klotz,G., Riesner,D., Gross,H.J. and Kleinschmidt,A.K. (1976) Viroids are single-stranded covalently closed circular RNA molecules existing as highly base-paired rod-likestructures. *Proc. Natl. Acad. Sci. U.S.A.*, **73**, 3852–3856
18. Wilusz,J.E. (2018) A 360° view of circular RNAs: From biogenesis to functions. *Wiley Interdiscip. Rev. RNA*, **9**, e1478.
19. Kristensen,L.S., Andersen,M.S., Stagsted,L.V.W., Ebbesen,K.K., Hansen,T.B. and Kjems,J. (2019) The biogenesis, biology and characterization of circular RNAs. *Nat. Rev. Genet.*, **20**, 675–691.
20. Chen,L.L. (2020) The expanding regulatory mechanisms and cellular functions of circular RNAs. *Nat. Rev. Mol. Cell Biol.*, **21**, 475–490.
21. Salzman,J., Gawad,C., Wang,P.L., Lacayo,N. and Brown,P.O. (2012) Circular RNAs are the predominant transcript isoform from hundreds of human genes in diverse cell types. *PLoS One*, **7**, e30733.
22. Jeck,W.R., Sorrentino,J.A., Wang,K., Slevin,M.K., Burd,C.E., Liu,J., Marzluff,W.F. and Sharpless,N.E. (2013) Circular RNAs are abundant, conserved, and associated with ALU repeats. *RNA*, **19**, 141–157.
23. Memczak,S., Jens,M., Elefsinioti,A., Torti,F., Krueger,J., Rybak,A., Maier,L., Mackowiak,S.D., Gregersen,L.H., Munschauer,M. *et al.* (2013) Circular RNAs are a large class of animal RNAs with regulatory potency. *Nature*, **495**, 333–338.
24. Starke,S., Jost,I., Rossbach,O., Schneider,T., Schreiner,S., Hung,L.-H. and Bindereif,A. (2015) Exon circularization requires canonical splice signals. *Cell Rep.*, **10**, 103–111.
25. Hansen,T.B., Jensen,T.I., Clausen,B.H., Bramsen,J.B., Finsen,B., Damgaard,C.K. and Kjems,J. (2013) Natural RNA circles function as efficient microRNA sponges. *Nature*, **495**, 384–388.
26. Piwecka,M., Glažar,P., Hernandez-Miranda,L.R., Memczak,S., Wolf,S.A., Rybak-Wolf,A., Filipchyk,A., Klironomos,F., Cerda Jara,C.A., Fenske,P. *et al.* (2017) Loss of a mammalian circular RNA locus causes miRNA deregulation and affects brain function. *Science*, **357**, eaam8526.
27. Kleaveland,B., Shi,C.Y., Stefano,J. and Bartel,D.P. (2018) A network of noncoding regulatory RNAs acts in the mammalian brain. *Cell*, **174**, 350–362.
28. Hentze,M.W. and Preiss,T. (2013) Circular RNAs: splicing's enigma variations. *EMBO J.*, **32**, 923–925.
29. Jost,I., Shalamova,L.A., Gerresheim,G.K., Niepmann,M., Bindereif,A. and Rossbach,O. (2018) Functional sequestration of microRNA-122 from Hepatitis C Virus by circular RNA sponges. *RNA Biol.*, **15**, 1032–1039.
30. Müller,S., Wedler,A., Breuer,J., Glaß,M., Bley,N., Lederer,M., Haase,J., Misiak,C., Fuchs,T., Ottmann,A. *et al.* (2020) Synthetic circular miR-21 RNA decoys enhance tumor suppressor expression and impair tumor growth in mice. *NAR Cancer*, **2**, zcaa014.
31. Schreiner,S., Didio,A., Hung,L.-H. and Bindereif,A. (2020) Design and application of circular RNAs with protein-sponge function. *Nucleic Acids Res.*, **48**, 12326–12335.
32. Litke,J.L. and Jaffrey,S.R. (2019) Highly efficient expression of circular RNA aptamers in cells using autocatalytic transcripts. *Nat. Biotechnol.*, **37**, 667–675.
33. Breuer,J. and Rossbach,O. (2020) Production and purification of artificial circular RNA sponges for application in molecular biology and medicine. *Methods Protoc.*, **3**, 42.
34. Medenbach,J., Seiler,M. and Hentze,M.W. (2011) Translational control via protein-regulated upstream open reading frames. *Cell*, **145**, 902–913.
35. Müller,C., Schulte,F.W., Lange-Grünweller,K., Obermann,W., Madhugiri,R., Pleschka,S., Ziebuhr,J., Hartmann,R.K. and Grünweller,A. (2018) Broad-spectrum antiviral activity of the eIF4A inhibitor silvestrol against corona- and picornaviruses. *Antivir. Res.*, **150**, 123–129.
36. Schneider,T., Schreiner,S., Preußer,C., Bindereif,A. and Rossbach,O. (2018) Northern blot analysis of circular RNAs. *Methods Mol. Biol.*, **1724**, 119–133.
37. Dobin,A., Davis,C.A., Schlesinger,F., Drenkow,J., Zaleski,C., Jha,S., Batut,P., Chaisson,M. and Gingeras,T.R. (2013) STAR: ultrafast universal RNA-seq aligner. *Bioinformatics*, **29**, 15–21.
38. Ziv,O., Price,J., Shalamova,L., Kamenova,T., Goodfellow,I., Weber,F. and Miska,E.A. (2020) The Short- and Long-Range RNA-RNA Interactome of SARS-CoV-2. *Mol. Cell*, **80**, 1067–1077.
39. Kim,D., Kim,S., Park,J., Chang,H.R., Chang,J., Ahn,J., Park,H., Park,J., Son,N., Kang,G. *et al.* (2021) A high-resolution temporal atlas of the SARS-CoV-2 translatome and transcriptome. *Nat. Commun.*, **12**, 5120.
40. Cao,C., Cai,Z., Xiao,X., Rao,J., Chen,J., Hu,N., Yang,M., Xing,X., Wang,Y., Li,M. *et al.* (2021) The architecture of the SARS-CoV-2 RNA genome inside virion. *Nat. Commun.*, **12**, 3917.
41. Boulant,S., Stanifer,M. and Lozach,P.Y. (2015) Dynamics of virus-receptor interactions in virus binding, signaling, and endocytosis. *Viruses*, **7**, 2794–2815.
42. Jonsdottir,H.R. and Dijkman,R. (2016) Coronaviruses and the human airway: a universal system for virus-host interaction studies. *Virol. J.*, **13**, 24.

Supplementary Material

Inhibition of SARS-CoV-2 coronavirus proliferation by designer antisense-circRNAs

Christina Pfafenrot [1,3], Tim Schneider [1,3], Christin Müller [2,3], Lee-Hsueh Hung [1], Silke Schreiner [1], John Ziebuhr [2], and Albrecht Bindereif [1*]

[1] Institute of Biochemistry, Justus Liebig University of Giessen, 35392 Giessen, Germany
[2] Institute of Medical Virology, Justus Liebig University of Giessen, 35392 Giessen, Germany

* corresponding author, e-mail: albrecht.bindereif@chemie.bio.uni-giessen.de
[3] These authors contributed equally.

Supplementary Material comprises seven Supplementary Figures and one Supplementary Table.

Supplementary Figure S1.

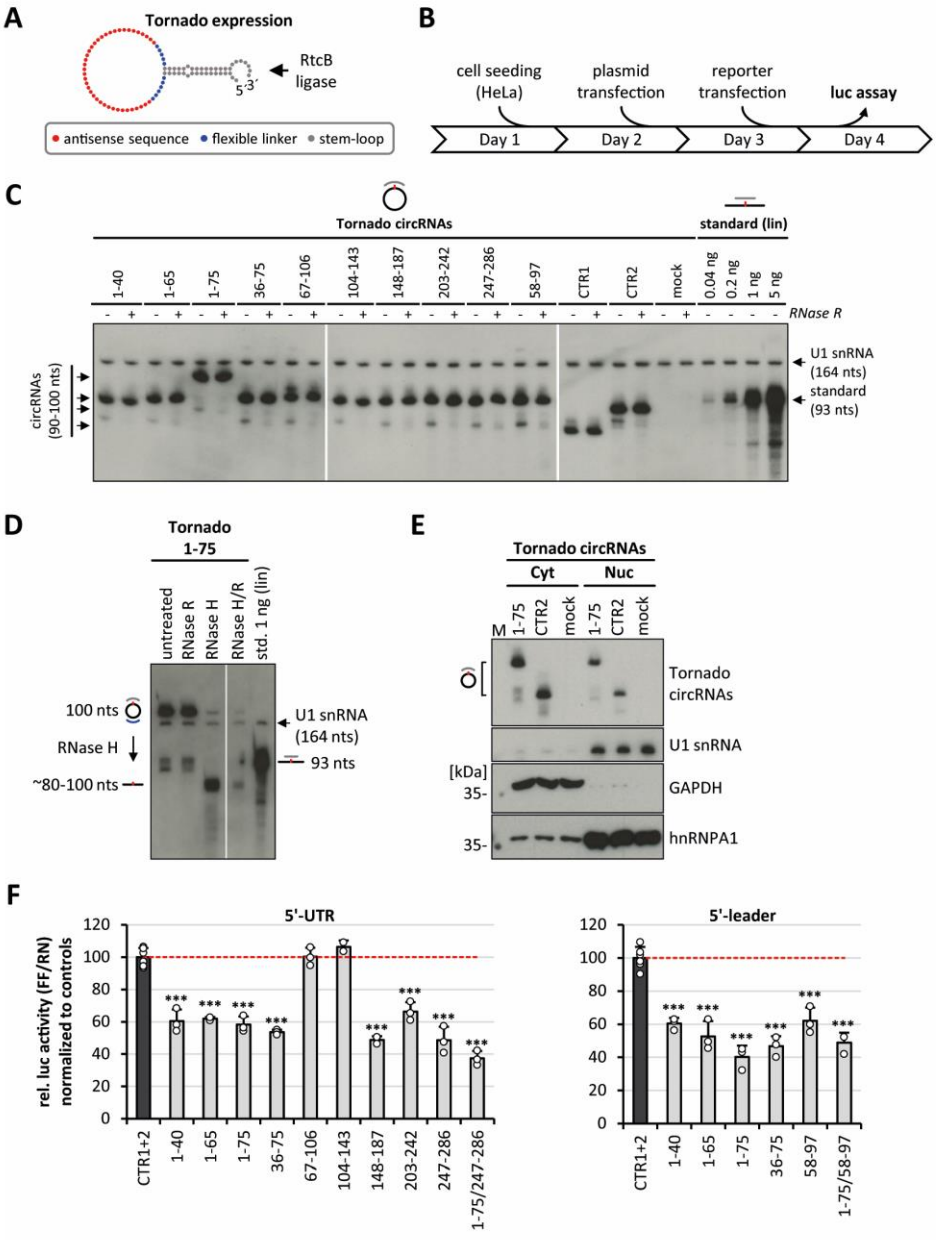

Supplementary Figure S1.
Tornado-based expression of AS-circRNAs in HeLa cells and screening of antisense activities by 5'-UTR and 5'-leader reporter assays.
(A) Design of AS-circRNAs expressed in mammalian cells by the so-called Tornado system (Litke and Jaffrey, 2019), based on RNA-polymerase III-driven expression, ribozyme-mediated processing, and *in vivo* circularization by endogenous RtcB tRNA ligase. Each circular RNA is composed of a stem-loop (grey), a short flexible linker (blue), and the antisense sequence (red).
(B) Experimental workflow for luciferase reporter assays in HeLa cells overexpressing AS-circRNAs.
(C) Tornado-based overexpression of AS-circRNAs in HeLa cells (as indicated) and detection by Northern blot analysis, using a circular-junction specific common probe. Circularity was confirmed by RNase R treatment (-/+). As an input control, U1 snRNA was detected by a U1-specific Northern probe. In addition, a linear standard RNA containing the circular junction (0.04 to 5 ng) served to quantitate Northern signals.
(D) Additional evidence for circularity of Tornado-expressed AS-circRNAs. Total RNA from HeLa cells overexpressing AS_1-75 circRNA was analyzed by Northern blot, using a circular-junction specific probe: RNA aliquots were either left untreated, RNase R digested, treated with RNase H and a junction-specific DNA oligonucleotide (resulting in a cleavage product of ~79 nucleotides), or combining RNase R and H treatment. In addition, 1 ng of the linear standard RNA was applied.
(E) Cellular distribution of Tornado-expressed AS-circRNAs. HeLa cells overexpressing either AS_1-75 or CTR2 control circRNAs were fractionated into cytoplasmic and nuclear fractions, followed by RNA preparation and Northern blot analysis with a common circular-junction probe. In addition, RNA from mock-treated cells were analyzed. For control and as fractionation markers, nuclear U1 snRNA and hnRNP A1 protein, as well as cytoplasmic GAPDH protein were detected by Northern and Western blot.
(F) Translational repression of SARS-CoV-2 5´-UTR and 5´-leader reporter constructs by AS-circRNAs. HeLa cells were transfected with the respective circRNA (as indicated below the diagram) or a combination thereof (e.g. AS_1-40/247-286). After 24 h, the respective reporter was transfected (5'-UTR or 5'-leader), and relative luciferase activities (ratio of Firefly and Renilla expression) were measured, normalized to control circRNAs CTR1 and 2 (mean and standard deviations of three replicates, $p < 0.05$*, $p < 0.005$**, $p < 0.001$***, ns = not significant, two-sided t-test). Source data are provided as a Source Data file.

Supplementary Figure S2.

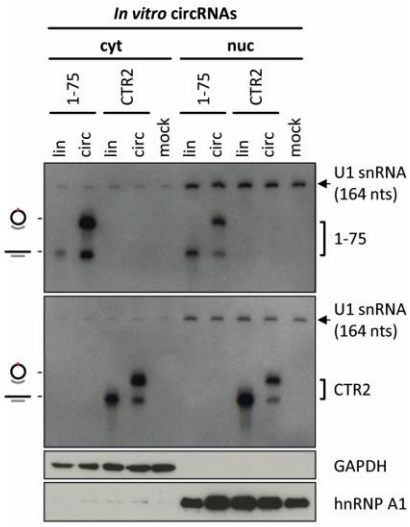

Supplementary Figure S2.
Northern analysis of RNAs transfected in HeLa cells.
Northern blot analysis of fractionated HeLa cells transfected with synthetic AS_1-75 and CTR2 control RNAs, each in linear or circular configuration, or after mock treatment. 24 h after circRNA transfection, cells were fractionated and RNA was prepared, followed by Northern blot analysis (in equivalent quantities), using AS_1-75 (top) and CTR2-specific probes (bottom), which detect both linear and circular forms. As input control, and for confirming nuclear-cytoplasmic fractionation, U1 snRNA was detected by Northern blot, as well as the nuclear hnRNP A1 and the cytoplasmic GAPDH protein by Western blot. Source data are provided as a Source Data file.

Supplementary Figure S3.

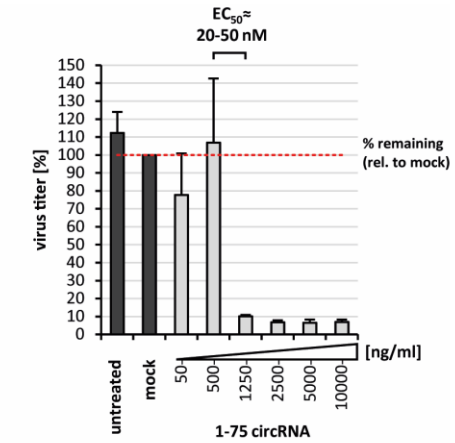

Supplementary Figure S3.
EC_{50} estimation for AS_1-75 circRNA.
EC_{50} value for AS_1-75 circRNA in virus infection assays. Based on combining our data from virus titer assays in Vero E6 cells transfected with different quantities of AS_1-75 circRNA (see **Figures 3BD, Figure 5F and Supplementary Figure S6**), an EC_{50} value between 500 and 1250 ng/ml (20-50 nM) was estimated (mean and SEM of combined data). Source data are provided as a Source Data file.

Supplementary Figure S4.

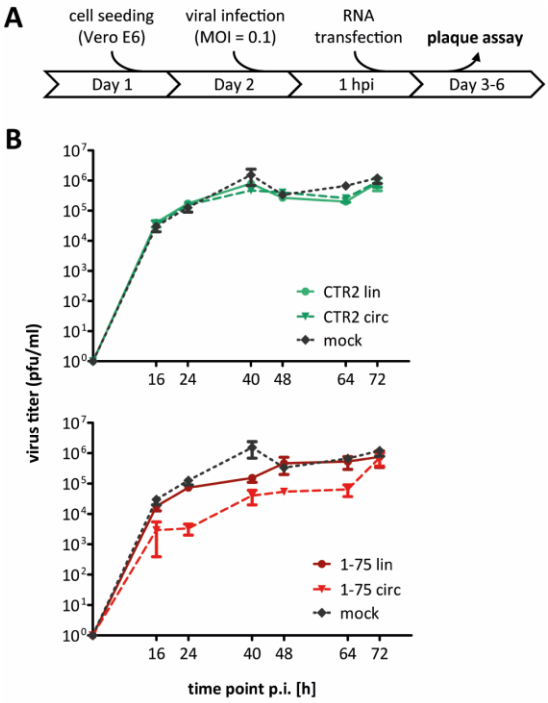

Supplementary Figure S4.
Inhibition of SARS-CoV-2 proliferation by AS-circRNAs transfected post-infection.
(A) Experimental workflow for viral infection assays using Vero E6 cells, transfected with synthetic RNAs (circRNA versus linear RNA) after infection with SARS-CoV-2.
(B) Durability of antiviral activity of AS_1-75 circRNA. Vero E6 cells were infected with SARS-CoV-2 (MOI = 0.1 pfu/cell), followed one hour post-infection by transfection of AS_1-75 circRNA or its linear counterpart (bottom panel; in red; mean and SEM of three experiments). Plaque assays were performed to determine virus titers in culture supernatants collected at the indicated time points (16 to 72 h post-transfection). As controls, mock-treated cells (without RNA, but with transfection reagent) were used (top and bottom panels; in black), as well as transfections with linear or circular control RNA (CTR2; top panel; in green).

Supplementary Figure S5.

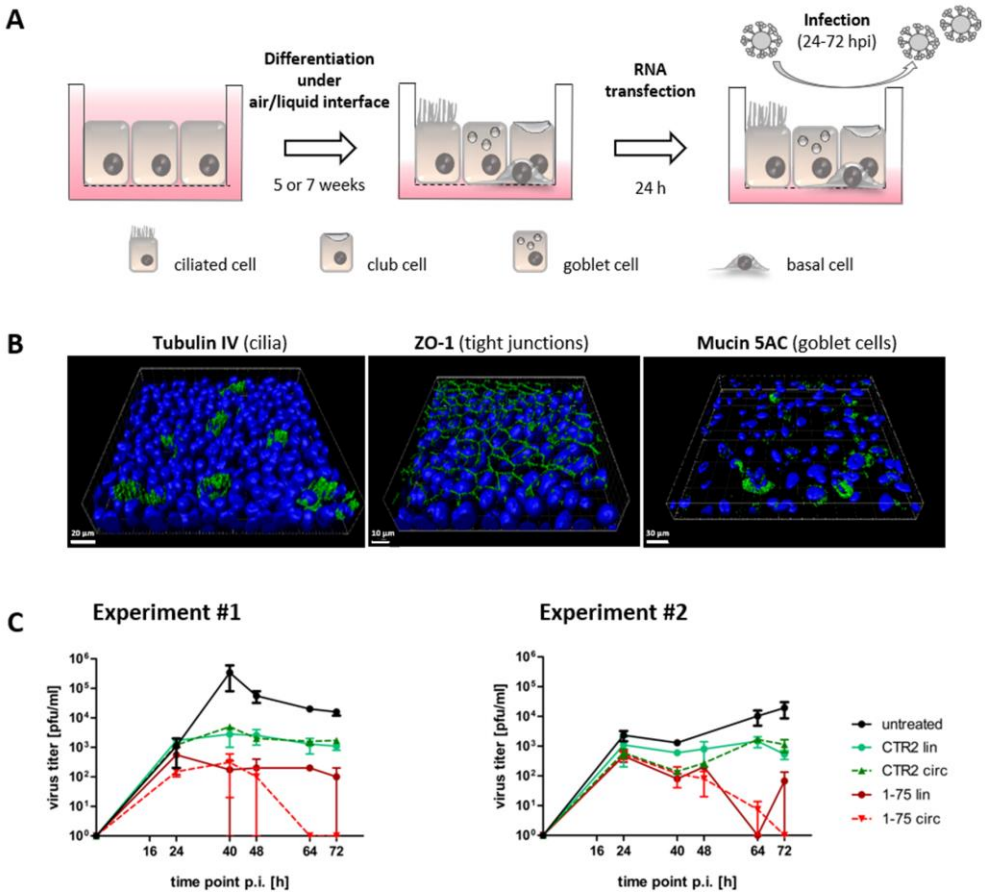

Supplementary Figure S5.
Inhibition of SARS-CoV-2 proliferation by AS-circRNA in primary normal human bronchial epithelial (NHBE) cells
(A) Experimental workflow for viral infection assays using NHBE cells. After reaching confluence, the cells were cultivated under air-liquid conditions for five or seven weeks to allow differentiation into pseudo-stratified human airway epithelia, followed by RNA transfection, virus infection, and plaque assays.
(B) Representative 3D models for validation of the differentiation status of NHBE cells via immunofluorescence analysis, using antibodies against tubulin IV, ZO-1 and mucin 5AC.
(C) Durability of antiviral activity of AS-1-75 circRNA. Differentiated NHBE cells (five weeks: experiment #1; seven weeks: experiment #2) were transfected with AS_1-75 circRNA or its linear counterpart (in red), followed by viral infection (MOI = 3 pfu/cell) after 24 h (mean and SEM of two, Experiment #1, or three, Experiment #2, technical replicates). Plaques assays were performed to determine virus titers in culture supernatants collected at the indicated time points (24-72 h post-infection). As controls, untreated cells (in black) were used, as well as transfections with linear and circular control RNA (CTR2; in green).

Supplementary Figure S6.

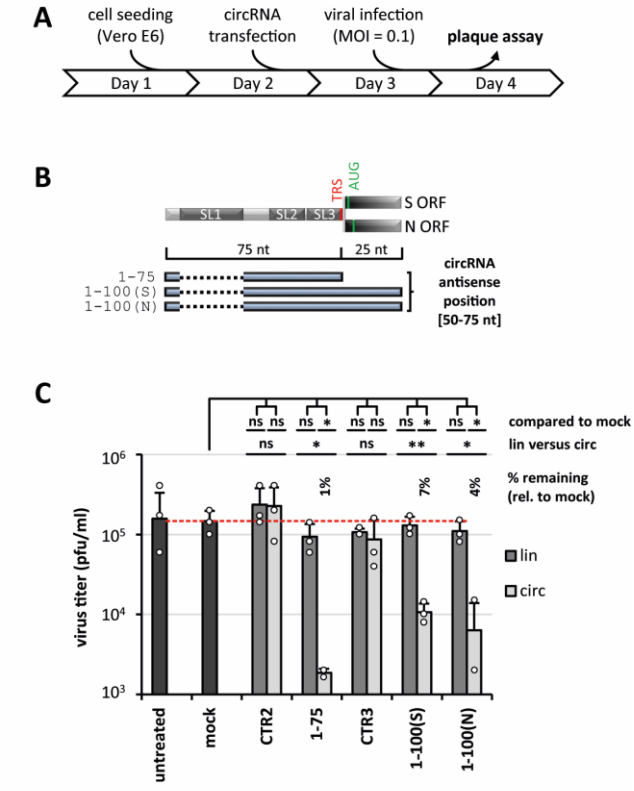

Supplementary Figure S6.
Inhibition of SARS-CoV-2 proliferation by elongated AS-circRNAs: viral infection assays with AS_1-100 (S) and AS_1-100 (N) circRNAs.
(A) Experimental workflow for viral infection assays using Vero E6 cells.
(B) Schematic representation of the S- and N-protein-encoding subgenomic RNAs, including the 75-nucleotide 5'-leader with its stem-loop elements (SL1-3), the transcription regulatory sequence (TRS), and the S- or N-ORF. The two elongated AS-circRNAs are represented below, targeting specifically the S or N subgenomic RNAs, and consisting of 75 nts against the 5'-leader sequence (omitting SL1; dashed line) and 25 nts of 5'-terminal S- or N-ORF. In addition, AS_1-75 RNA (lin/circ) is represented, which was used for comparison.
(C) Viral infection assays with elongated AS-circRNAs. Vero E6 cells were transfected with AS_1-100 (S) and AS_1-100 (N) circRNAs, both in linear or circular form (2500 ng per assay), followed by SARS-CoV-2 viral infection (MOI = 0.1 pfu/cell) and, 24 h post-infection, by virus titer assays (mean and standard deviations of three experiments, $p < 0.05$*, ns = not significant, two-sided t-test). As controls and for comparison, untreated (without RNA and transfection reagent) and mock-treated cells (without RNA, but with transfection reagent), as well as cells transfected with CTR2 and CTR3 control, or with AS_1-75 linear and circular RNAs, were included. Residual virus titers of significantly affected samples are indicated as "percent remaining" relative to mock treatment. Source data are provided as a Source Data file.

Supplementary Figure S7.

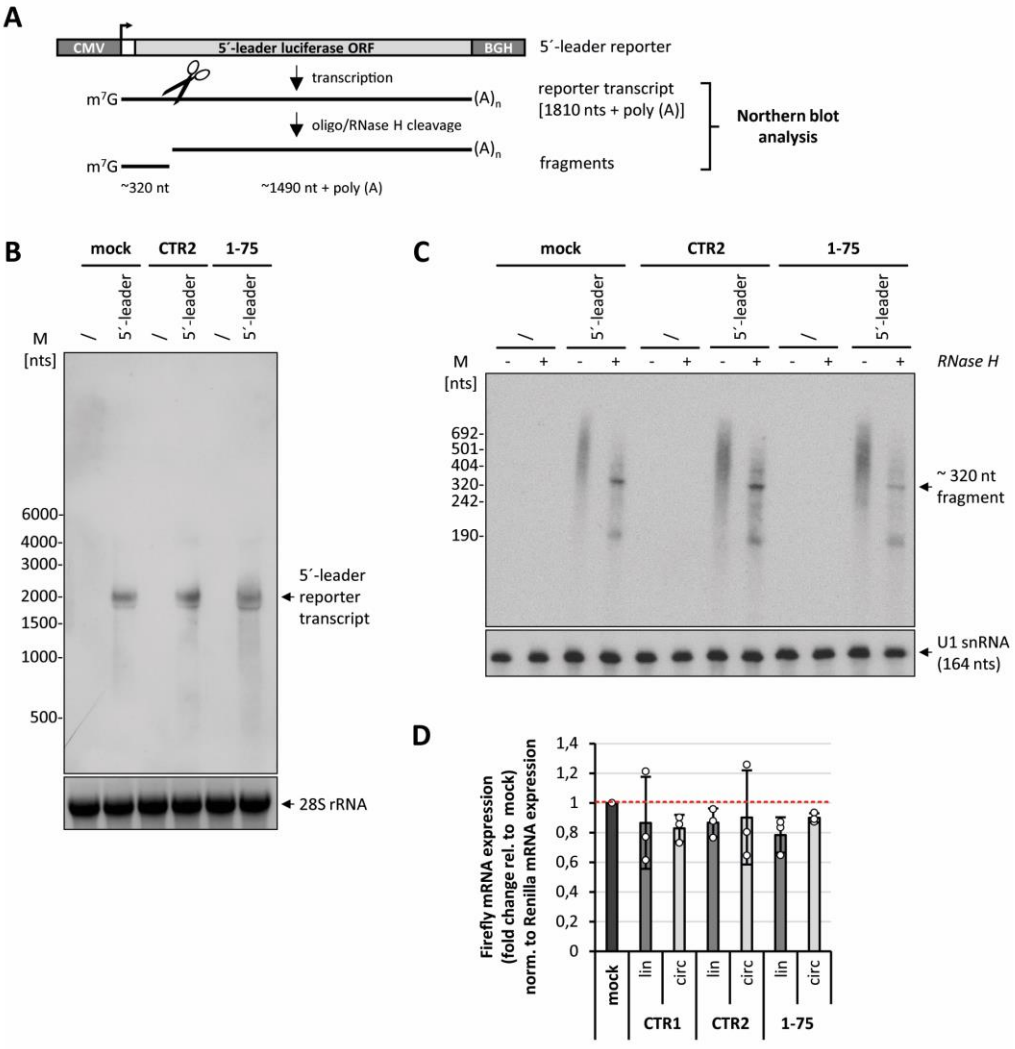

Supplementary Figure S7.
Steric blocking versus cleavage: evidence against an antisense-based cleavage mechanism of AS_1-75 circRNA.
(A) Experimental strategy. The 5´-leader reporter construct is expressed as a capped and polyadenylated mRNA that can be cleaved into two mRNA fragments of characteristic sizes, based on RNase H and a complementary DNA oligonucleotide. Subsequent Northern blot reveals whether the transcript is stable upon AS-1-75 circRNA transfection (evidence for steric blocking) or degraded (evidence for cleavage mechanism).
(B) Northern blot analysis of full-length 5´-leader reporter transcript. HeLa cells were transfected with either no RNA (mock), with 5 µg control (CTR2), or with AS_1-75 circRNA. On the next day, cells were mock-transfected (/ = no plasmid), or transfected with the 5´-leader reporter construct. At 24 h post-transfection, total RNA was prepared and subjected to glyoxal-Northern blot analysis, to detect the 5´-leader reporter transcript [1,810 nts + poly(A)]. *M*, RiboRuler High Range RNA Ladder (Thermo Fisher Scientific). As input control, 28S rRNA was detected by ethidium bromide staining.
(C) Northern blot analysis of RNase H-cleaved fragment of 5´-leader reporter transcript. Total RNA (3 µg each) obtained after mock, control circRNA, or AS_1-75 circRNA transfections (as described in panel **B**) was additionally subjected to RNase H cleavage, followed by Northern blot analysis (denaturing PAGE). The expected cleavage fragment of ~320 nts (see panel **A**) was detected in all RNase H (+) reactions, independently of the circRNA transfected (CTR2 or AS_1-75), and also in the mock transfection. *M*, DNA molecular weight marker, DIG-labelled (Roche). As input control, U1 snRNA was detected by Northern blot. Source data are provided as a Source Data file.
(D) Detection of Firefly mRNA levels by RT-qPCR. HeLa cells were transfected with 1 µg linear or circular RNA. After 24 h, the respective reporter plasmids were transfected (Firefly and Renilla), and relative expression levels of the reporter mRNAs (Firefly mRNA expression normalized to Renilla mRNA expression) were determined by RT-qPCR in comparison to mock transfection (only reporter plasmid transfection, without RNA transfection). Mean and standard deviations are based on three experiments.

Supplementary Table S1.

Tornado circRNAs

Name		Oligonucleotides (with NotI and SacII overhangs) 5´-3´	Final circRNA sequence 5´-3´
1-40	_fwd	GGCCGCAAGTTGGTTGGTTAGTTACCTGGGAAGGTATAAACCTTTAATAAAAACCGC	AACCATGCCGAGTGCGGCCGCAA**GTTGGTTGGTTAGTTACCTGGGAAGGTATAAACCTTTAAT**AAAAACCGCGGTCGGCGT
	_rev	GGTTTTTATTAAAGGTTTATACCTTCCCAGGTAACTAACCAACCAACTTGC	GGACTGTAG
1-65	_fwd	GGCCGCAAAGAACAGATCTACAAGAGATCGAAAGTTGGTTaaTTTAATAAAAACCGC	AACCATGCCGAGTGCGGCCGCAA**AGAACAGATCTACAAGAGATCGAAAGTTGGTTaaTTTAAT**AAAAACCGCGGTCGGCGTG
	_rev	GGTTTTTATTAAAttAACCAACTTTCGATCTCTTGTAGATCTGTTCTTTGC	GACTGTAG
1-75	_fwd	GGCCGCAAGTTCGTTTAGAGAACAGATCTACAAGAGATCGAAAGTTGGTTaaTTTAATAAAAACCGC	AACCATGCCGAGTGCGGCCGCAA**GTTCGTTTAGAGAACAGATCTACAAGAGATCGAAAGTTGGTTaaTTTAAT**AAAAACCG
	_rev	GGTTTTTATTAAAttAACCAACTTTCGATCTCTTGTAGATCTGTTCTCTAAACGAACTTGC	CGGTCGGCGTGGACTGTAG
36-75	_fwd	GGCCGCAAGTTCGTTTAGAGAACAGATCTACAAGAGATCGAAAGTTGGAAAAACCGC	AACCATGCCGAGTGCGGCCGCAA**GTTCGTTTAGAGAACAGATCTACAAGAGATCGAAAGTTGG**AAAAACCGCGGTCGGCGT
	_rev	GGTTTTTCCAACTTTCGATCTCTTGTAGATCTGTTCTCTAAACGAACTTGC	GGACTGTAG
58-97	_fwd	GGCCGCAATAAAACAAGAAAAACAAACATAGTTCGTTTAGAGAACAGAAAAAACCGC	AACCATGCCGAGTGCGGCCGCAA**TAAAACAAGAAAAACAAACATAGTTCGTTTAGAGAACAGA**AAAAACCGCGGTCGGCGT
	_rev	GGTTTTTTCTGTTCTCTAAACGAACTATGTTTGTTTTTCTTGTTTTATTGC	GGACTGTAG
67-106	_fwd	GGCCGCAAGCAGCCGAGTGACAGCCACACAGATATTAAAGTTCGTTTAAAAAACCGC	AACCATGCCGAGTGCGGCCGCAA**GCAGCCGAGTGACAGCCACACAGATATTAAAGTTCGTTTA**AAAAACCGCGGTCGGCGT
	_rev	GGTTTTTTAAACGAACTTTAATATCTGTGTGGCTGTCACTCGGCTGCTTGC	GGACTGTAG
104-143	_fwd	GGCCGCAATTAGATATTAATTATACTGCGTGAGTGCACTAAGCATGCAAAAAACCGC	AACCATGCCGAGTGCGGCCGCAA**TTAGATATTAATTATACTGCGTGAGTGCACTAAGCATGCA**AAAAACCGCGGTCGGCGT
	_rev	GGTTTTTTGCATGCTTAGTGCACTCACGCAGTATAATTAATATCTAATTGC	GGACTGTAG
148-187	_fwd	GGCCGCAATGCAGAAGATAGACGAGTTACTCGTGTCCTGTCAACGACAAAAAACCGC	AACCATGCCGAGTGCGGCCGCAA**TGCAGAAGATAGACGAGTTACTCGTGTCCTGTCAACGACA**AAAAACCGCGGTCGGCGT
	_rev	GGTTTTTTGTCGTTGACAGGACACGAGTAACTCGTCTATCTTCTGCATTGC	GGACTGTAG
203-242	_fwd	GGCCGCAACGAAACCTAGATGTGCTGATGATCGGCTGCAACACGGACGAAAAACCGC	AACCATGCCGAGTGCGGCCGCAA**CGAAACCTAGATGTGCTGATGATCGGCTGCAACACGGACG**AAAAACCGCGGTCGGCG
	_rev	GGTTTTTCGTCCGTGTTGCAGCCGATCATCAGCACATCTAGGTTTCGTTGC	TGGACTGTAG
247-286	_fwd	GGCCGCAAACCAGGGACAAGGCTCTCCATCTTACCTTTCGGTCACACCAAAAACCGC	AACCATGCCGAGTGCGGCCGCAA**ACCAGGGACAAGGCTCTCCATCTTACCTTTCGGTCACACC**AAAAACCGCGGTCGGCGT
	_rev	GGTTTTTGGTGTGACCGAAAGGTAAGATGGAGAGCCTTGTCCCTGGTTTGC	GGACTGTAG
CTR1	_fwd	GGCCGCAAAGATGCGCACCGCACAGATGCGCACCACGCCACGCGTAGAAAAAACCGC	AACCATGCCGAGTGCGGCCGCAA**AGATGCGCACCGCACAGATGCGCACCACGCCACGCGTAGA**AAAAACCGCGGTCGGCG
	_rev	GGTTTTTTCTACGCGTGGCGTGGTGCGCATCTGTGCGGTGCGCATCTTTGC	TGGACTGTAG
CTR2	_fwd	GGCCGCAAAGTCAGTGAGTCAGTGTAATACGGGAGGATACCCGCTGTCAAAAACCGC	AACCATGCCGAGTGCGGCCGCAA**AGTCAGTGAGTCAGTGTAATACGGGAGGATACCCGCTGTC**AAAAACCGCGGTCGGCG
	_rev	GGTTTTTGACAGCGGGTATCCTCCCGTATTACACTGACTCACTGACTTTGC	TGGACTGTAG
			Legend
			AACCATGCCGAGTGCGGCCGCAA**NNNNNNNNNNNNNNNNNNNNNNNNNNNNNNNnnNNNNNN**AAAAACCGCGGTCGGCGT
			GGACTGTAG
			Tornado stem loop, flexible linker, **N** = antisense sequence, **N** = T->A (for extended T-stretches), **nn** = base of SL1

***In vitro* produced RNA**

Name		Oligonucleotides 5´-3´	Final circRNA sequence 5´-3´
1-40	_fwd	TAATACGACTCACTATAGGGAGTAAGCAAAGTTGGTTGGTTTGTTACCTGGGAAGGTATAAACCTTTAATAAAGCTTACAGTA	GGGAGTAAGCAAA**GTTGGTTGGTTTGTTACCTGGGAAGGTATAAACCTTTAAT**AAAGCTTACAGTA
	_rev	TACTGTAAGCTTTATTAAAGGTTTATACCTTCCCAGGTAACAAACCAACCAACTTTGCTTACTCCCTATAGTGAGTCGTATTA	
1-65	_fwd	TAATACGACTCACTATAGGGAGTAAGCAAAAGAACAGATCTACAAGAGATCGAAAGTTGGTTaaTTTAATAAAGCTTACAGTA	GGGAGTAAGCAAA**AGAACAGATCTACAAGAGATCGAAAGTTGGTTaaTTTAAT**AAAGCTTACAGTA
	_rev	TACTGTAAGCTTTATTAAAttAACCAACTTTCGATCTCTTGTAGATCTGTTCTTTTGCTTACTCCCTATAGTGAGTCGTATTA	
1-75	_fwd	TAATACGACTCACTATAGGGAGTAAGCAAAGTTCGTTTAGAGAACAGATCTACAAGAGATCGAAAGTTGGTTaaTTTAATAAAGCTTACAGTA	GGGAGTAAGCAAA**GTTCGTTTAGAGAACAGATCTACAAGAGATCGAAAGTTGGTTaaTTTAAT**AAAGCTTACAGTA
	_rev	TACTGTAAGCTTTATTAAAttAACCAACTTTCGATCTCTTGTAGATCTGTTCTCTAAACGAACTTTGCTTACTCCCTATAGTGAGTCGTATTA	
1-100(S)	_fwd	TAATACGACTCACTATAGGGAGTAAGCAAACAATAAAACAAGAAAAACAAACATTGTTCGTTTAGAGAACAGATCTACAAGAGATCGAAAGTTGGTTaaTTTAATAAAGCTTACAGTA	GGGAGTAAGCAAA**CAATAAAACAAGAAAAACAAACATTGTTCGTTTAGAGAACAGATCTACAAGAGATCGAAAGTTGGTT**
	_rev	TACTGTAAGCTTTATTAAAttAACCAACTTTCGATCTCTTGTAGATCTGTTCTCTAAACGAACAATGTTGTTTTTCTTGTTTTATTGTTTGCTTACTCCCTATAGTGAGTCGTATTA	**aaTTTAAT**AAAGCTTACAGTA
1-100(N)	_fwd	TAATACGACTCACTATAGGGAGTAAGCAAAGGTCCATTATCAGACATTTTAGTTTGTTCGTTTAGAGAACAGATCTACAAGAGATCGAAAGTTGGTTaaTTTAATAAAGCTTACAGTA	GGGAGTAAGCAAA**GGTCCATTATCAGACATTTTAGTTTGTTCGTTTAGAGAACAGATCTACAAGAGATCGAAAGTTGGTT**
	_rev	TACTGTAAGCTTTATTAAAttAACCAACTTTCGATCTCTTGTAGATCTGTTCTCTAAACGAACAAACTAAAATGTCTGATAATGGACCTTTGCTTACTCCCTATAGTGAGTCGTATTA	**aaTTTAAT**AAAGCTTACAGTA
36-75	_fwd	TAATACGACTCACTATAGGGAGTAAGCAAAGTTCGTTTAGAGAACAGATCTACAAGAGATCGAAAGTTGGAAAGCTTACAGTA	GGGAGTAAGCAAA**GTTCGTTTAGAGAACAGATCTACAAGAGATCGAAAGTTGG**AAAGCTTACAGTA
	_rev	TACTGTAAGCTTTCCAACTTTCGATCTCTTGTAGATCTGTTCTCTAAACGAACTTTGCTTACTCCCTATAGTGAGTCGTATTA	
58-97	_fwd	TAATACGACTCACTATAGGGAGTAAGCAAATAAAACAAGAAAAACAAACATTGTTCGTTTAGAGAACAGAAAAGCTTACAGTA	GGGAGTAAGCAAA**TAAAACAAGAAAAACAAACATTGTTCGTTTAGAGAACAGA**AAAGCTTACAGTA
	_rev	TACTGTAAGCTTTTCTGTTCTCTAAACGAACAATGTTTGTTTTTTCTTGTTTTATTTGCTTACTCCCTATAGTGAGTCGTATTA	
247-286	_fwd	TAATACGACTCACTATAGGGAGTAAGCAAAACCAGGGACAAGGCTCTCCATCTTACCTTTCGGTCACACCAAAGCTTACAGTA	GGGAGTAAGCAAA**ACCAGGGACAAGGCTCTCCATCTTACCTTTCGGTCACACC**AAAGCTTACAGTA
	_rev	TACTGTAAGCTTTGGTGTGACCGAAAGGTAAGATGGAGAGCCTTGTCCCTGGTTTTGCTTACTCCCTATAGTGAGTCGTATTA	
CTR1	_fwd	TAATACGACTCACTATAGGGAGTAAGCAAAAGATGCGCACCGCACAGATGCGCACCACGCCACGCGTAGAAAAGCTTACAGTA	GGGAGTAAGCAAA**AGATGCGCACCGCACAGATGCGCACCACGCCACGCGTAGA**AAAGCTTACAGTA
	_rev	TACTGTAAGCTTTTCTACGCGTGGCGTGGTGCGCATCTGTGCGGTGCGCATCTTTTGCTTACTCCCTATAGTGAGTCGTATTA	
CTR2	_fwd	TAATACGACTCACTATAGGGAGTAAGCAAAAGTCAGTGAGTCAGTGTAATACGGGAGGATACCCGCTGTCAAAGCTTACAGTA	GGGAGTAAGCAAA**AGTCAGTGAGTCAGTGTAATACGGGAGGATACCCGCTGTC**AAAGCTTACAGTA
	_rev	TACTGTAAGCTTTGACAGCGGGTATCCTCCCGTATTACACTGACTCACTGACTTTTGCTTACTCCCTATAGTGAGTCGTATTA	
CTR3	_fwd	TAATACGACTCACTATAGGGAGTAAGCAAACTGTCGCCCATAGGAGGGCATAATGTGACTGAGTGACTGACTGTCGCCCATAGGAGGGCATAATGTGACTGAGTGAAAGCTTACAGTA	GGGAGTAAGCAAA**CTGTCGCCCATAGGAGGGCATAATGTGACTGAGTGACTGACTGTCGCCCATAGGAGGGCATAATGT**
	_rev	TACTGTAAGCTTTCACTCAGTCACATTATGCCCTCCTATGGGCGACAGTCAGTCACTCAGTCACATTATGCCCTCCTATGGGCGACAGTTTGCTTACTCCCTATAGTGAGTCGTATTA	**GACTGAGTG**AAAGCTTACAGTA
			Legend
			GGGAGTAAGCAAA**NNNNNNNNNNNNNNNNNNNNNNNNNNNNNNNnnNNNNNN**AAAGCTTACAGTA
			overhang, stem loop, flexible linker, **N** = antisense sequence, **nn** = base of SL1

Northern Blot probes

Name		Oligonucleotides 5´-3´	Riboprobe sequence 5´-3´
Tornado junction	_fwd	TAATACGACTCACTATAGGGTTGCGGCCGCACTCGGCATGGTTCTACAGTCCACGCCGACCGCGGTTTTTTTTTTTTTTTTTTT	GGG**TTGCGGCCGCACTCGGCATGGTTCTACAGTCCACGCCGACCGCGGTTTTT**TTTTTTTTTTTTTTT
	_rev	AAAAAAAAAAAAAAAAAAAACCGCGGTCGGCGTGGACTGTAGAACCATGCCGAGTGCGGCCGCAACCCTATAGTGAGTCGTATTA	
1-75	_fwd	TAATACGACTCACTATAGGGTAACCAACTTTCGATCTCTTGTAGATCTGTTCTCTAAACGAACTTTTTTTTTTTTTTTTTTTTTT	GGG**TAACCAACTTTCGATCTCTTGTAGATCTGTTCTCTAAACGAACTTT**TTTTTTTTTTTTTTTTTTT
	_rev	AAAAAAAAAAAAAAAAAAAAAAAAAGTTCGTTTAGAGAACAGATCTACAAGAGATCGAAAGTTGGTTACCCTATAGTGAGTCGTATTA	
CTR2	_fwd	TAATACGACTCACTATAGGGTTTGACAGCGGGTATCCTCCCGTATTACACTGACTCACTGACTTTTTTTTTTTTTTTTTTTTTTT	GGG**TTTGACAGCGGGTATCCTCCCGTATTACACTGACTCACTGACTTTT**TTTTTTTTTTTTTTTTTTT
	_rev	AAAAAAAAAAAAAAAAAAAAAAAAAGTCAGTGAGTCAGTGTAATACGGGAGGATACCCGCTGTCAAACCCTATAGTGAGTCGTATTA	
U1 snRNA	_fwd	TAATACGACTCACTATAGGGATACTTACCTGGCAGGGGAGATACCATGATTTTTTTTTTTTTTTTTTTTT	GGG**ATACTTACCTGGCAGGGGAGATACCATGAT**TTTTTTTTTTTTTTTTTTT
	_rev	AAAAAAAAAAAAAAAAAAAAAATCATGGTATCTCCCCTGCCAGGTAAGTATCCCTATAGTGAGTCGTATTA	
SARS-CoV-2 genome/sgRNAs	_fwd	CTCATGCAGACCACACAAGG	GGG**AAAATCACATGGGGATAGCACTACTAAAATTAATTTTACACATTAGGGCTCTTCCATATAGGCAGCTCTCCCTAGCA TTGTTCACTGTACACTCGATCGTACTCCGCGTGGCCTCGGTGAAAATGTGGTGGCTCTTTCAAGTCCTCCCTAATGTTAC ACACTGATTAAAGATTGCTATGTGAGATTAAAGTTAACTACATCTACTTGTGCTATGTAGTTACGAGAATTCATTCTGCA CAAGAGTAGACTATATATCGTAAACGGAAAAGCGAAAACGTTTATATAGCCCATCTGCCTTGTGTGGTCTGCATGAG**
	_rev	TAATACGACTCACTATAGGGAAAATCACATGGGGATAGCA	
5´-leader reporter	_fwd	ATTAAAGGTTTATACCTTCCCAG	GGG**AGTGCTTTTGGCGAAGAAGGAGAATAGGGTTGGCACCAGCAGCGCACTTTGAATCTTGTAATCCTGAAGGCTCCTC AGAAACAGCTCTTCTTCAAATCTATACATTAAGACGACTCGAAATCCACATATCAAATATCCGAGTGTAGTAAACATTCC AAAACCGTGATGGAATGGAACAACACTTAAAATCGCAGTATCCGGAATGATTTGATTGCCAAAAATAGGATCTCTGGCA TGCGAGAATCTCACGCAGGCAGTTCTATGAGGCAGAGCGACACCTTTAGGCAGACCAGTAGATCCAGAGGAGTTCATGA TCAGTGCAATTGTCTTGTCCCTATCGAAGGACTCTGGCACAAAATCGTATTCATTAAAACCGGGAGGTAGATGAGATGT GACGAACGTGTACATCGACTGAAATCCCTGGTAATCCGTTTTAGAATCCATGATAATAATTTTTTGGATGATTGGGAGCT TTTTTTGCACGTTCAAAATTTTTTGCAACCCCTTTTTGGAAACGAACACCACGGTAGGCTGCGAAATGCCCATACTGTTG AGCAATTCACGTTCATTATAAATGTCGTTCGCGGGCGCAACTGCAACTCCGATAAATAACGCGCCCAACACCGGCATAA AGAATTGAAGAGAGTTTTCACTGCATACGACGATTCTGTGATTTGTATTCAGCCCATATCGTTTCATAGCTTCTGCCAAC CGAACGGACATTTCGAAGTACTCAGCGTAAGTGATGTCCACCTCGATATGTGCATCTGTAAAAGCAATTGTTCCAGGAA CCAGGGCGTATCTCTTCATAGCCTTATGCAGTTGCTCTCCAGCGGTTCCATCTTCCAGCGGATAGAATGGCGCCGGGCC TTTCTTTATGTTTTTGGCGTCGGATCCCAATAAAACAAGAAAAACAAACATTGTTCGTTTAGAGAACAGATCTACAAGAG ATCGAAAGTTGGTTGGTTTGTTACCTGGGAAGGTATAAACCTTTAAT**
			Legend GGG**NNNNNNNNNNNNNNNNNNNNNNNNNNNNNNNNNNNNNNN**TTTTTTTTTTTTTTTTTTT GGG = transcription start, **NN** = target region , TTT = Oligo(T) for DIG-labeling

Northern Blot standard

Name		Oligonucleotides 5´-3´	Standard sequence 5´-3´
1-40 (Tornado)	_fwd	TAATACGACTCACTATAGGGAAGGTATAAACCTTTAATAAAAACCGCGGTCGGCGTGGACTGTAGAACCATGCCGAGTGCGGCCGCAAGTTGGTTGGTTAGTTACCTGGG	GGG**AAGGTATAAACCTTTAAT**AAAAA<u>CCGCGGTCGGCGTGGACTGTA</u>**GA**<u>ACCATGCCGAGTGCGGCCGC</u>AA**GTTGGTTGGT TAGTTACCTGGG**
	_rev	CCCAGGTAACTAACCAACCAACTTGCGGCCGCACTCGGCATGGTTCTACAGTCCACGCCGACCGCGGTTTTTATTAAAGGTTTATACCTTCCCTATAGTGAGTCGTATTA	
			Legend GGG**NNNNNNNNNNNNNNNNNN**AAAAA<u>CCGCGGTCGGCGTGGACTGTA</u>**GA**<u>ACCATGCCGAGTGCGGCCGC</u>AA**NNNNNNNNNN NNNNNNNNNNNN** GGG = transcription start, **NN** = antisense region, flexible linker, <u>Tornado stem loop</u> , **GA** = circ-junction, **N** = T->A (for extended T-stretches)

RNase H cleavage

Name	Oligonucleotide 5´-3´
1-75	GTTCTCTAAACGAACTTGCGG
5´-leader reporter	GCCCATATCGTTTCATAGCT

Antisense oligonucleotides (ASOs)

Name	Oligonucleotide 5´-3´ (2´-OMe or 2´-MOE modified)
CTR1	CGCACCACGCCACGCGTAGA
CTR2	ACGGGAGGATACCCGCTGTC
1-45	CGAAAGTTGGTTaaTTTAAT
56-75	GTTCGTTTAGAGAACAGATC

RT-qPCR Primer

Name	Oligonucleotide 5´-3´
Firefly fwd	GAGGTTCCATCTGCCAGGTA
Firefly rev	CCGGTATCCAGATCCACAAC
Renilla fwd	AACGCGGCCTCTTCTTATTT
Renilla rev	ATTTGCCTGATTTGCCCATA

Legend for Supplementary Table S1

Supplementary Table S1.
List of oligonucleotides and RNA sequences used in this study
Oligonucleotides used for circRNA production (Tornado-based and *in vitro* production), for Northern Blot analysis, RNase H cleavage, comparison to ASOs (2´-OMe or 2´-MOE modified), and as primers for RT-qPCR.

Inhibition of mRNA translation by designer antisense-circRNAs

Christina Pfafenrot[1], Tim Schneider[1] and Albrecht Bindereif[1]

[1]*Institute of Biochemistry, Justus Liebig University of Giessen, D-35392 Giessen, Germany*

Circular RNAs (circRNAs) belong to a large class of noncoding RNAs that have been detected in all eukaryotes studied so far, and that arise from pre-mRNAs by an alternative splicing mechanism. Here we describe an approach through which small circular antisense RNAs (AS-circRNAs) can be used as molecular tools to inhibit the initiation of translation of specific mRNAs. For a proof-of-principle, we designed AS-circRNAs that specifically target the 5'-UTR of a set of reporter mRNAs and various endogenous MDM2 (mouse double minute 2 homolog) mRNA isoforms. These circRNAs were either synthesized *in vitro* by transcription and enzymatic circularization, or produced *in vivo* by the ribozyme-mediated Tornado expression system. After transfection of synthetic AS-circRNAs, a dose-dependent decrease in the translational activity of a reporter mRNA containing the β-globin (*HBB*, hemoglobin subunit beta gene) 5'-UTR could be detected. In this context, the circRNA proved to be significantly more efficient than its corresponding linear counterpart. Furthermore, functional assays, both with reporter transfections as well as assays with endogenous mRNA, showed that segments of the 5′-untranslated region of MDM2 could be efficiently targeted by specific antisense circRNAs in a position-dependent fashion, thus negatively affecting protein production. In principle, this strategy can be applied to any mRNA and demonstrates the great potential for applications of designer circRNAs in molecular medicine.

This part of the thesis is in preparation for submission.

INTRODUCTION

CircRNAs have been known for more than four decades, but only rediscovered in 2012/13, based on high-throughput sequencing and computer analysis **(Sänger *et al.* 1976**, **Wilusz 2018, Kristensen *et al.* 2019, Chen 2020)**. Most circRNAs are derived from specific exons of canonical mRNA precursors by an alternative RNA processing mechanism also known as *backsplicing*. This process uses the usual splicing signals as well as splicing machinery **(Starke *et al.* 2015)**. CircRNAs are mostly located in the cytoplasm and show a higher stability due to their resistance to exonucleolytic digestion **(Jeck *et al.* 2013)**. Functionally, however, circRNAs are still largely uncharacterized. Only a few studies have shown that naturally occurring circRNAs such as *ciRS-7* and *SRY* can function as microRNA sponges **(Hansen *et al.* 2013, Memczak *et al.* 2013)**. In addition, various other hypothetical functions have been discussed, such as protein sponging and antisense activity **(Hentze and Preiss 2013)**. Due to their unusually high stability compared to their linear counterpart, circRNAs provide an attractive basis for the construction of designer circRNAs for biotechnological applications **(Jost *et al.* 2018, Müller *et al.* 2020, Schreiner *et al.* 2020, Pfafenrot *et al.* 2021)**.

Antisense approaches with linear oligonucleotides have been pursued for over 30 years and thus represent a classic line of sequence-based interference. This strategy offers many approaches to modulate RNA structure and activity, mRNA splicing, translation, or stability **(Bennett and Swayze 2010, Crooke *et al.* 2018, Bennett *et al.* 2019, Le *et al.* 2021)**. This longstanding research has already led to therapeutic approaches against many genetic diseases being approved in the form of drugs **(Roberts *et al.* 2020)**. In this context, antisense oligonucleotides (ASO) are the best-known examples. With additional modifications [2′-*O*-methyl (2′-OMe), 2′-*O*-methoxyethyl (2′-MOE) nucleotides, locked nucleic acids (LNA), morpholino and many more)], RNA base pairing and metabolic stability can be improved.

In this study, the unusual metabolic stability of circRNAs was used to demonstrate the potential of antisense circRNAs to inhibit translation of two different mRNAs: β-globin and MDM2, as a proof-of-principle. Translation of mRNAs is generally a tightly controlled mechanism. The initiation factor eIF4E is an important regulator that recognizes the 5'-cap and forms a trimeric complex (elF4F) responsible for activating the mRNA during translation **(Jackson *et al.* 2010)**. Therefore, we hypothesize that the initiation of translation can be inhibited by blocking the elF4F complex through binding of AS-circRNAs to the 5'-UTR of a particular mRNA.

Hemoglobin is formed from two α- and two β-globin chains. Each of these subunits carries a prosthetic haem group, to which molecular oxygen reversibly binds. β-globin is encoded by the *HBB* gene and consists of a 147-amino-acid long peptide chain. Mutations in this gene often disturb mRNA splicing, resulting, for example, in the β -thalassemia disease, which affects red blood cells **(Cao and Moi 2002)**. The β-globin 5'-UTR is a comparatively short (50 nts) and well-characterized RNA sequence, making it especially suitable for proof-of-principle studies using reporter constructs, independent from its cellular function.

The mouse double minute 2 gene (*MDM2*) encodes a cellular phosphoprotein **(Momand *et al.* 1992)** that plays a key role in the regulation of the tumor suppressor protein p53 by negatively modulating its activity and stability through ubiquitylation and proteasomal-dependent degradation **(Klein and Vassilev 2004)**. Functionally, MDM2 and p53 act in a self-regulatory feedback loop. Under normal conditions, p53 is present only at low levels **(Chène 2003)** since it induces transcription of *MDM2*, which in turn leads to increased MDM2 protein levels. MDM2 can bind p53 with high affinity **(Nag *et al.* 2014)**, inducing its nuclear export **(Kubbutat *et al.* 1997)** and inhibiting its ability to act as a transcription factor **(Oliner *et al.* 1993)**. In addition, MDM2 is able to induce the degradation of p53 by the proteasome through its ubiquitin ligase activity **(Kubbutat *et al.* 1997)**. Upon cellular stress, MDM2-mediated ubiquitination of p53 is abolished. Subsequently, p53 can activate transcription, for example of apoptotic genes **(Wade *et al.* 2013)**. In many cancers, the MDM2-p53 feedback loop is deregulated, which makes it an attractive target for therapeutic strategies. Furthermore, overexpression of MDM2 can promote the formation, progression, and drug resistance of malignant tumors **(Hou *et al.* 2019)**. Initial therapeutic strategies pursued an antisense oligodeoxynucleotide approach, while more recent approaches have shifted to using various small molecule compounds to inhibit the interaction between p53 and MDM2 **(Hou *et al.* 2019)**. These inhibitors are *cis*-imidazolines (Nutlins) which prevent

the interaction between MDM2 and p53 and restore the functionality of p53 by binding MDM2 **(Vassilev 2004)**. Several different inhibitors are currently in various stages of clinical testing.

In this proof-of-principle study, the classical antisense (AS) RNA approach was combined with short designer circRNAs, by integration of antisense sequences into a circRNA backbone. Based on a systematic functional screening of a series of AS-circRNAs, well-accessible subregions of the 5'-UTR of β-globin as well as MDM2 mRNAs could be identified. Efficient reduction of translation in cell cultures could be achieved in reporter assays (β-globin and MDM2) as well as on the endogenous level (MDM2). For β-globin, we could also show a dose-dependent reduction in reporter activity that, in addition, was more pronounced in some cases when the antisense sequence was represented within a circRNA rather than as a linear RNA. Targeting of endogenous MDM2 mRNA was accompanied by significantly decreased mRNA and protein levels.

In summary, this study demonstrates that AS-circRNAs can be used as a novel molecular approach for targeting in principle any mRNA, thus demonstrating great potential for the development of new therapeutic strategies in molecular medicine **(Jost *et al.* 2018, Müller *et al.* 2020, Schreiner *et al.* 2020, Pfafenrot *et al.* 2021)**.

MATERIAL AND METHODS

Most of the methods described in the following sections were performed as reported in **Pfafenrot *et al*. (2021)**.

AS-circRNA design

Antisense target sequences (β-globin: 30-42 nts; MDM2: 40 nts; **Figure 1A**) were selected based on the 5'-UTR of β-globin or MDM2, as well as the presence of specific sequence elements (e.g. two uORFs in the long 5'-UTR of MDM2 Iso1-2; **Figure 3**). Randomized sequences of similar length (β-globin: 25 nts; MDM2: 40 nts) were used as controls.

RNAs for *in vitro* circularization were composed of a constant backbone sequence, in which the individual antisense target or control sequences were inserted. The constant backbone carries six complementary nucleotides on either 5′ and 3′ ends of the RNA, followed by four non-complementary nucleotides creating overhanging ends and allowing stem-loop formation and efficient ligation (for sequences, see **Supplementary Table S1**). These sequences were ordered as oligonucleotides (Sigma-Aldrich) including a T7 promoter, and subsequently annealed to yield templates for *in vitro* transcription.

For endogenous overexpression of antisense circRNAs, oligonucleotide cassettes (see **Supplementary Table S1**) were cloned into the pAV-U6+27-Tornado-Broccoli vector **(Litke and Jaffrey 2019)**, using the SacII and NotI restriction sites, and replacing the Broccoli aptamer sequence. To enhance flexibility, a spacer of unrelated nucleotides was inserted, in this case two nucleotides upstream, and five nucleotides downstream of the AS or control sequence. Since internal poly(U) stretches longer than $(U)_4$, including single-nucleotide insertions, would terminate RNA polymerase III, such sequences were changed by single T→A mutations (see **Supplementary Table S1**).

In vitro transcription, circularization, gel purification and RNase R treatment of antisense-RNAs

RNAs were transcribed from annealed DNA-oligonucleotide templates (see

Supplementary Table S1), using the HighScribe™ T7 high-yield RNA synthesis kit (NEB) in the presence of ATP, CTP, UTP, and GTP (each at 7.5 mM), GMP (30 mM GMP; Merck), and RNaseOut (Thermo Fisher Scientific) for 2 h at 37°C. The DNA template was digested by addition of RQ1 DNase (2 U per 20 µl reaction, Promega), and incubation for 30 min at 37°C. Transcripts were purified using the Monarch RNA purification kit (NEB) and quantified by the Qubit™ RNA broad-range assay kit (Thermo Fisher Scientific).

For circularization, 60 µg transcribed RNA was incubated with 100 U of T4 RNA ligase (Thermo Fisher Scientific) in 1× T4 RNA ligase buffer, supplemented with 0.1 mg/ml BSA and RNaseOut (Thermo Fisher Scientific), overnight at 16°C in a final volume of 200 µl. RNA was recovered by phenol/chloroform extraction (Roth) and ethanol precipitation.

Gel purification was performed as described **(Breuer and Rossbach 2020)**. To validate the circular conformation, 250 ng of gel-purified circular or linear RNA was incubated with or without 2 U of RNase R per 5 µl reaction (Biozym; 30 min at 37°C). After digestion, 200 ng of RNAs were separated on a 12% denaturing polyacrylamide gel and visualized by ethidium bromide staining.

Luciferase reporter constructs

The 5′-UTR (nts 1-50) sequence of β-globin (NM_000518.4) was cloned into pcDNA5-CMV-FF **(Medenbach *et al.* 2011)** containing the Firefly reporter ORF, using the HindIII and BamHI restriction sites.

MDM2 comprises six main isoforms (1: NM_002392, 2: NM_001145339, 3: NM_001145337, 4: NM_001145340, 5: NM_001278462, 6: NM_001367990; see **Figure 3** and **Introduction section E**). Isoforms 1 and 2 contain a long 5'-UTR sequence (nts 1-324) with two additional upstream ORFs (uORFs). Isoforms 3-6 have a short 5'-UTR sequence (nts 1-67; without uORFs). Both the long and short 5'-UTR sequences were cloned into pcDNA5-CMV-FF **(Medenbach *et al.* 2011)**. In addition, 30 nucleotides of the MDM2 ORF sequence, identical in all isoforms, were inserted, followed by the Firefly ORF in both reporters (see **Figure 3**). For the construction of a reporter with mutated uORFs, oligonucleotide cassettes with corresponding nucleotide changes (U→A) were ordered (Sigma-Aldrich) and cloned in front of the Firefly reporter ORF.

Transfection of *in vitro*-transcribed RNAs and Tornado-based circRNA expression constructs; luciferase reporter assays

HeLa cells were cultured in DME-medium supplemented with 10% FBS (Gibco) at 37°C and 5% CO_2. For luciferase reporter assays, 1×10^5 cells were seeded per well (12-well plate). RNA transfections were done using Lipofectamine 2000, and Tornado-plasmid transfections with Turbofect reagent, both in a total volume of 1 ml medium/well (Thermo Fisher Scientific). For titration experiments, different amounts (100, 250, 500, 750, 1000 ng per assay) of circular or corresponding linear RNAs were used.

For durability assays, 1×10^5 HeLa cells were seeded per well (12-well plate) in DME-medium supplemented with 10% FBS (Gibco) one day before transfection. After transfection of RNA, the normal medium was exchanged by DME-medium supplemented with 2% FBS (Gibco).

For Tornado-circRNA screening, cells were transfected with 1 µg of plasmid DNA. Culture medium was always changed 1 h prior and 4 h after transfection. After one day, cells

were co-transfected with 50 ng of 5′-UTR luciferase reporter plasmids, together with 5 ng of pRL-SCV40 Renilla-reporter (Promega). At 24 h post-transfection, cells were washed three times with PBS (Gibco), and lysed in 250 µl Lysis-Juice (PJK). Luminescence was measured for Firefly and Renilla luciferase (Beetle- and Renilla-Juice kits, respectively; PJK), using a Centro LB 960 Luminometer (Berthold Technologies). Relative luciferase activities were calculated as ratios of the Firefly and Renilla raw values, with three technical replicates per sample and a total of three independent biological replicates.

Subcellular fractionation

HeLa cells were seeded at a density of 8×10^5 cells per 6-cm plate and transfected with 4 µg of Tornado-plasmids, using Lipofectamine 2000 in a total volume of 4 ml medium/plate. After 24 h, cells were harvested, and 2×10^6 cells subjected to fractionation, using the NE-PER Nuclear and Cytoplasmic Extraction kit (Thermo Fisher Scientific). RNA for Northern blot analysis was prepared from 75% of the nuclear and cytoplasmic fractions using TRIzol LS (Ambion), while 25% was saved for Western blotting (see below).

Northern Blot

All Northern blots were performed as previously described **(Schneider *et al.* 2018)**.

Denaturing polyacrylamide Northern blot

For detection of Tornado-derived circRNAs in HeLa cells, 250 ng of total RNA, or 20% of cytoplasmic/nuclear fraction, was used. Samples were separated on a 10% denaturing polyacrylamide gel, transferred to a nylon membrane (Hybond-N+; Amersham) by semi-dry blotting, and crosslinked by UV light (0.125 mJ/cm^2 at 254 nm). Membranes were subsequently hybridized with DIG-UTP-labeled (DIG RNA Labeling Mix, Roche) riboprobes in NorthernMax hybridization buffer (Thermo Fisher Scientific) at 60°C. For detection of Tornado circRNAs, a circular-junction-specific probe was used. For oligonucleotide and riboprobe sequences, see **Supplementary Table S1**. Probe detection with alkaline-phosphatase-conjugated anti-DIG-Fab fragments (11093274910, Roche) and CDP-Star chemiluminescence substrate was done as described (Roche).

RNase R and RNase H treatment

To confirm circularity of the detected Tornado-derived circRNAs, 250 ng of total RNA were either incubated with 5 U/µg RNase R (Biozym) in 1x RNase R buffer for 1 h at 37°C, or with 50 ng of antisense DNA-oligonucleotide in 1x RNase H buffer in total volume of 5 µl for 20 min at 37°C, followed by addition of 1 U RNase H (NEB) and incubation for 40 min at 37°C.

Western Blot

MDM2 protein levels were analyzed by Western blot of HeLa cell lysates, previously transfected with 10 µg of Tornado-plasmids in a total volume of 10 ml in 10 cm dishes. Total protein lysates obtained at 24 h post-transfection were heat-denatured in SDS-loading buffer (50 mM Tris–HCl pH 6.8, 2% SDS, 10% glycerol, 2.5% 2-mercaptoethanol, and 0.05% bromophenol blue) at 95°C for 10 min. Following separation by SDS-polyacrylamide gel electrophoresis (PAGE; 10%), proteins were blotted onto a nitrocellulose membrane (BioRad). MDM2 was immunostained overnight with mouse

anti-MDM2 antibody (monoclonal antibody, clone 2A10; Sigma-Aldrich, 1:250) or mouse anti- γ-tubulin antibody (monoclonal antibody TUBG1, GTU-88, Sigma-Aldrich, 1:5000) and appropriate secondary antibody (HRP-conjugated anti-mouse, A9044-2ML, Sigma-Aldrich, 1:10,000). The blots were developed using the Lumi-Light Western-Blotting Substrate (Roche).

For subcellular fractionation, 1.25% of cytoplasmic or nuclear fractions were analyzed by SDS-PAGE (10%) and Western blotting through detection of hnRNP A1 (monoclonal antibody, sc-32301, 4B10; Santa Cruz Biotechnology, 1:2000) and GAPDH (monoclonal antibody G8795, GAPDH-71.1; Sigma-Aldrich, 1:5000).

RT-qPCR of endogenous MDM2 mRNA level

For detection of MDM2 mRNA expression levels by RT-qPCR, HeLa cells were seeded at a density of 1.5×10^6 cells per 10-cm dish and transfected with 10 µg of Tornado-plasmids, using Turbofect (Thermo Fisher Scientific) in a total volume of 10 ml medium/dish. 24 h post-transfection, cells were harvested, and RNA isolation was performed by using TRIzol LS reagent (Thermo Fisher Scientific). A DNase digestion with RQ1 DNase (Promega) followed to remove remaining plasmid DNA. Reverse transcription was performed, using 1 µg total RNA with the qScript cDNA synthesis kit (Quantabio). Real-time qPCR was carried out using the Realplex Mastercycler (Eppendorf) as well as the Luna qPCR Reaction Mix (NEB) according to the manufacturer's instructions. MDM2 Iso1-2 and Iso3-6 mRNAs were amplified by specific primer pairs (see **Figure 3** and **Supplementary Table S1**). All reactions were performed in technical triplicates. The evaluation was carried out using the ΔΔCt method with average cycle threshold (Ct) values **(Pfaffl 2001)**. Normalization was performed with Ct values of housekeeping genes (ACTB and GAPDH) in corresponding samples.

RESULTS

Design of AS-circRNAs targeting the 5'-UTR of β-globin

Circular RNA is characterized, in comparison to its linear counterpart, by being much more stable and thus has great potential for the development of new RNA-based therapeutics. For a proof-of-principle study, artificial small circRNAs with antisense RNA sequences directed against the β-globin 5'-UTR were developed. The focus was placed on the β-globin 5'-UTR, as this RNA sequence is comparatively short (50 nts) and well-characterized. In order to search for optimal β-globin target sequences in the 5'-UTR, a luciferase reporter system was used **(Figure 1A)**. For this purpose, the complete 5'-UTR sequence with its 50 nucleotides including the translation start codon was fused in frame with the luciferase ORF.

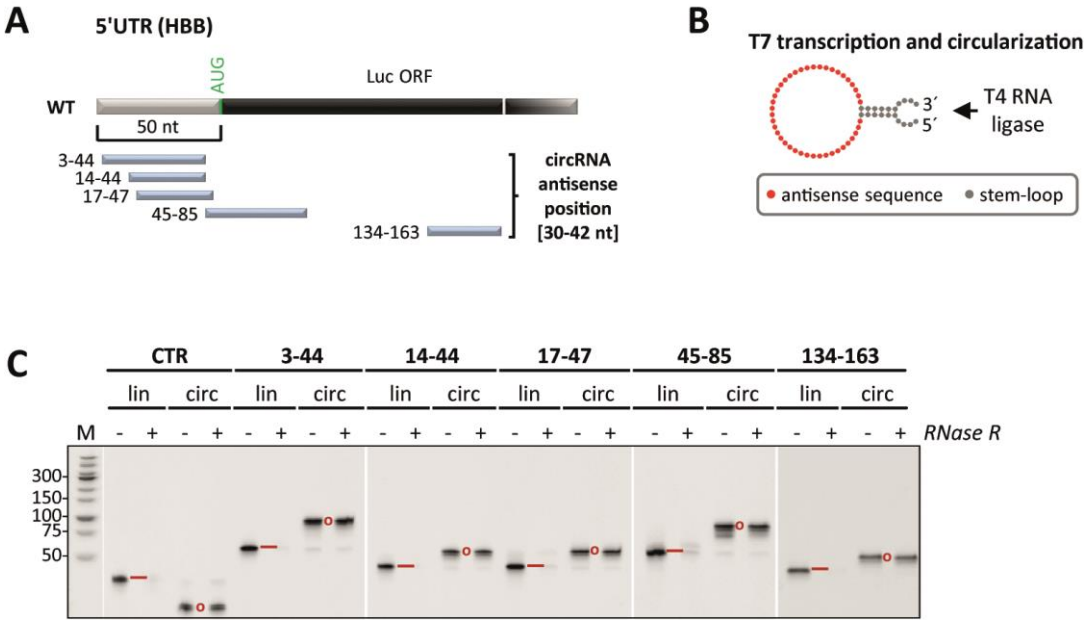

Figure 1: Design of AS-circRNAs targeting the 5´-UTR of human β-globin (*HBB*).
[A] Schematic representation of the β-globin 5′-UTR (nts 1–50), targeted by AS-circRNAs in a luciferase-reporter (luc). Target regions of individual AS-circRNAs are represented as blue bars with nucleotide coordinates.
[B] Design of synthetic AS-circRNAs, which were produced by *in vitro* T7 transcription and subsequent circularization by T4 RNA ligase. Each circular RNA is composed of a stem–loop with overhangs for efficient ligation (grey) and the antisense sequence (red).
[C] AS-circRNA synthesis. RNase R treatment and aberrant electrophoretic migration confirm the circularity of the produced circRNAs. Gel-purified linear and circular RNAs (lin/circ) were treated with RNase R, or left untreated (–/+), and analyzed by denaturing polyacrylamide electrophoresis and ethidium bromide staining. Mobilities of circular (o) and linear (–) forms are marked. *M*, DNA marker (sizes in bp).

In this context, a series of five small AS-circRNAs were designed to specifically target different regions of the β-globin reporter construct (see **Figure 1A**; for secondary structures see **Supplementary Figure S1**). To test in addition, whether the length of the antisense region has an influence on the effect, AS-circRNAs of different lengths were compared with each other (50-62 nts total length, including 30-42 nts antisense sequence; named after the target boundaries; see **Figure 1A**; the circRNA sequences are listed in **Supplementary Table S1**).

The first three AS-circRNAs AS_3-44, AS_14-44, as well as AS_17-47 cover the complete 50 nucleotides of the 5'-UTR. The 45-85 AS-circRNA is directed against the AUG-proximal region with flanking sequences, the AS_134-163 against the luciferase ORF. To control and normalize luciferase activities, a non-specific circRNA with a randomized sequence of 25 nucleotides was used instead of the specific antisense sequences. Each circRNA was designed in a way that the antisense sequence was flanked by a short stem-loop-forming sequence with two overhanging ends (see **Figure 1B**).

Synthetic AS-circRNAs inhibit translation of β-globin reporter constructs in HeLa cells

The production of the respective AS-circRNAs was performed *in vitro* by transcription using T7 RNA polymerase and circularization by T4 RNA ligase.

Circularization was controlled by RNase R treatment followed by denaturing PAGE analysis **(Figure 1C)**. At this point, the circularity can be proven, on the one hand, by a lower gel mobility, and, on the other hand, by a higher RNase R resistance of the circular conformation compared to the linear form.

In order to be able to analyze and compare the effects of circular as well as linear AS-RNA on translation, luciferase assays were performed. After cell seeding (day 1, HeLa cells were transfected with different amounts of synthetic antisense RNAs (100-1000 ng of lin/circ RNA; day 2). After 24 h, Firefly and Renilla luciferase-reporters were co-transfected (day 3), followed by cell lysis and luciferase measurements (day 4; for a flow chart of the analysis, see **Figure 2A**).

The decrease in measurable bioluminescence represents the reduced expression of firefly luciferase due to the interaction of the respective co-transfected circRNA or linear RNA with the β-globin reporter RNA **(Figure 2B)**. Comparing the effects of the various AS-RNAs, a clear dose-dependent effect can be observed for all AS-RNAs tested. Under these conditions, maximal activities were achieved with 750-1000 ng AS-RNA per assay. Overall, for most targets comparable effects were detected between linear and circular, but for two target sequences (AS_3-44 and AS_45-85), a stronger reduction by the respective circRNA could be observed: The AS-circRNA directed against the 5'-terminal region (AS_3-44) showed a reduction of up to 75% (1.2x stronger than linear at titration endpoint), and the AS-circRNA directed against the AUG-proximal region (AS_45-85) showed a reduction of up to 68% (1.4x stronger than linear at titration endpoint). The increased effectiveness of the circRNA in these cases may be due to different stabilities of the transfected RNAs, their intrinsic antisense activity, their base-pairing potential, their structural properties or a combination of these factors.

Based on these results, the question was addressed whether the observed effects of AS_3-44 and AS_45-85 circRNAs persist over a longer period of time compared to linear RNA **(Figure 2C)**. For this purpose, luciferase assays were performed with cells transfected with linear or circular AS_3-44 and AS_45-85 RNA (together with the corresponding control), measuring for five days every 24 h. In this experimental workflow, DME medium with 10% FBS was replaced by DME medium with only 2% FBS. This significantly slows down the doubling time of the cells, preventing that the effects of the RNA were overshadowed by strongly dividing cells throughout this long time period of five days **(Supplementary Figure S2)**.

The comparison of circRNA and its linear counterpart showed that the effect of circRNAs persists significantly longer. In particular, between one and two days after reporter transfection, the effect was the strongest (circRNA: reduction to 31-48% for AS_3-44, and 23-47% for AS_45-85; linear RNA: reduction to 46-69% for AS_3-44, and 31-62% for AS_45-85). After 72 h, the effect of the circular RNA levels off at a reduction of about 20%, whereas the linear RNA completely loses its effectiveness. This effect was specific for the circular conformation and indicates a durability of the effect over at least two days under the conditions used.

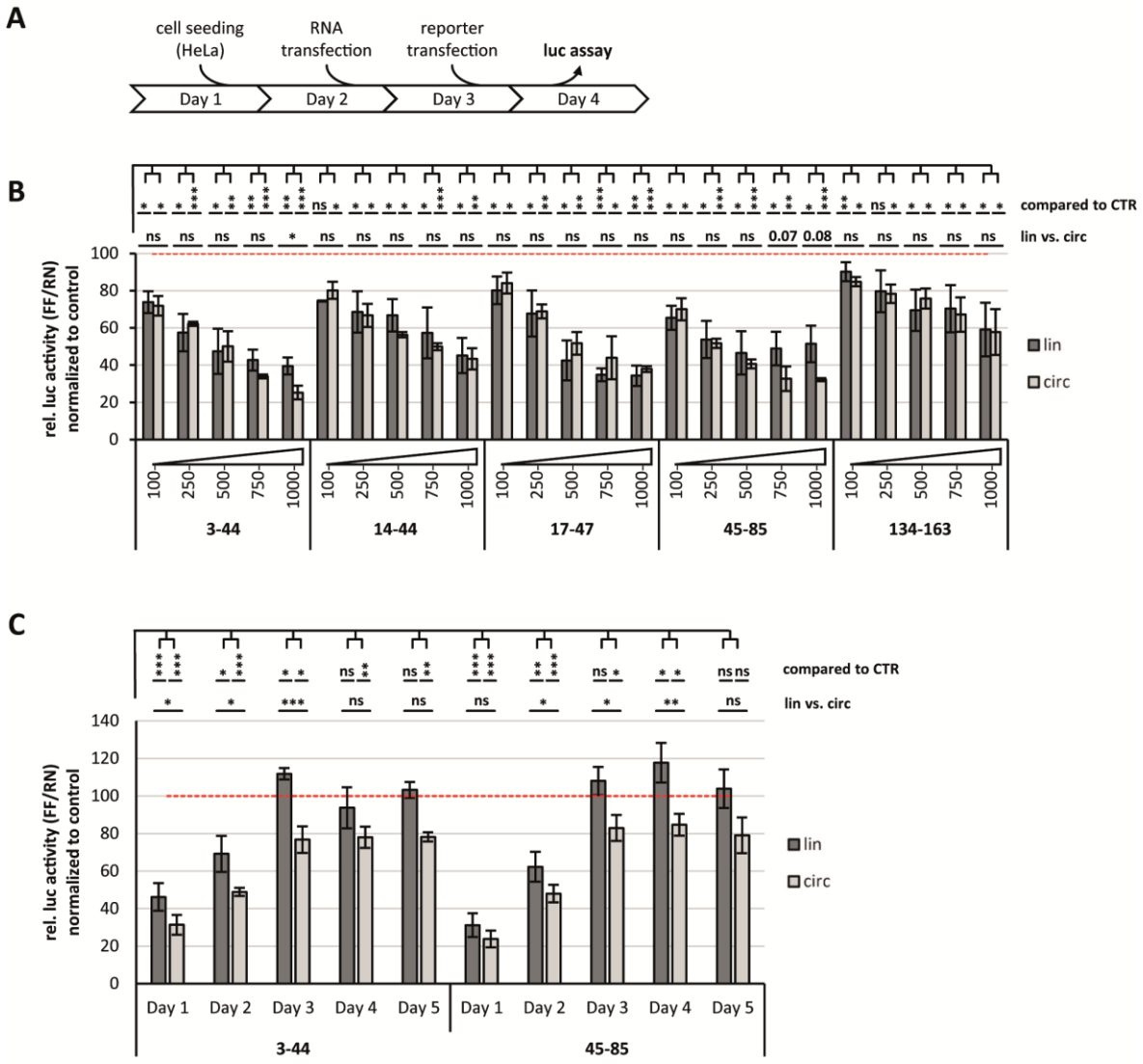

Figure 2: Synthetic circRNAs act as durable inhibitors of translation in a dosis-dependent manner.
[A] Experimental workflow for luciferase reporter assays in HeLa cells transfected with synthetic RNAs (linear or circular).
[B] HeLa cells were transfected with increasing amounts (100 - 1000 ng per assay) of circRNAs (as indicated below; light gray), or their linear counterparts (dark grey). After 24 h, the reporter construct was transfected, and relative luciferase activities (Firefly/Renilla expression ratios) were measured, normalized to control circRNA CTR (mean and standard deviations of three replicates, **P* < 0.05, ***P* < 0.005, ****P* < 0.001, ns = not significant, two-sided *t*-test). For nearly significant samples, the *P*-value is given instead of ns.
[C] Durability of the activity of AS_3-44 and AS_45-85 circRNAs. HeLa cells were transfected with AS_3-44 or AS_45-85 circRNA (light gray) or their linear counterpart (dark grey), followed by transfection of the reporter after 1-5 days. Relative luciferase activities (Firefly/Renilla expression ratios) were measured, normalized to control circRNA CTR (mean and standard deviations of three replicates, **P* < 0.05, ***P* < 0.005, ****P* < 0.001, ns = not significant, two-sided *t*-test).

Based on these findings, we conclude that both the 5′-terminal as well as the AUG start-codon proximal regions are accessible to small synthetic AS-circRNAs, resulting in strong translational inhibition of up to 75%.

Design of AS-circRNAs targeting different isoforms of MDM2

To verify the functionality of small circular RNAs with antisense sequences also at the endogenous level, a series of circRNAs directed against the MDM2 5´-UTR were designed and produced. Again, the focus was on the 5'-untranslated region as well as on the AUG start-codon proximal sequences, as previous studies have shown that these are very effective target regions **(Figure 2B; Pfafenrot *et al.* 2021,** see **section L)**. To search for functional antisense sequences and optimal MDM2 targets in the 5′-UTR, three separate luciferase reporter systems were used **(Figure 3)**.

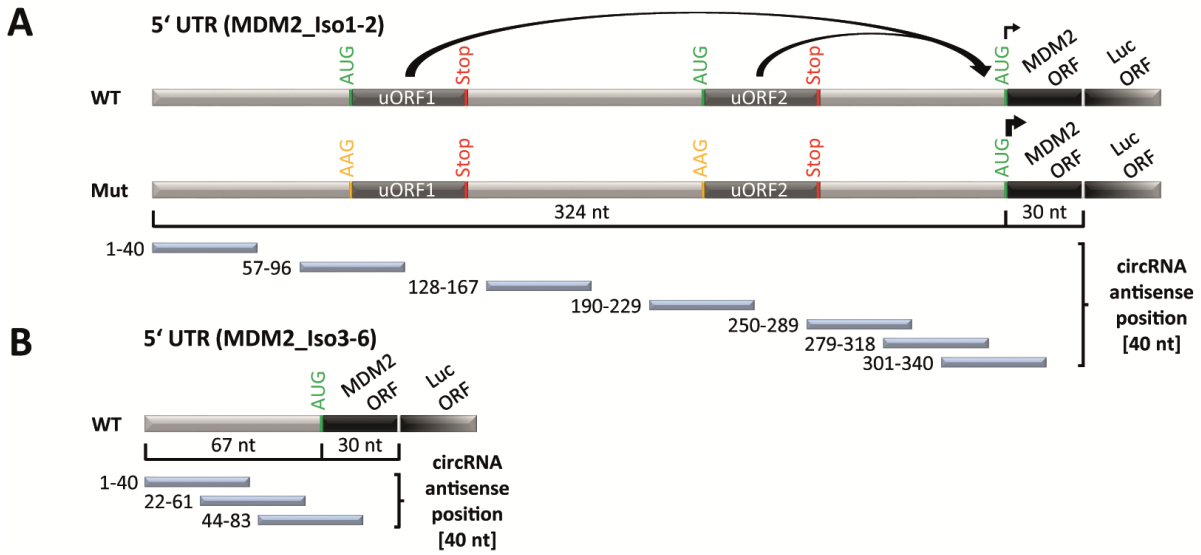

Figure 3: Design of AS-circRNA targeting different human MDM2 isoforms.
[A] Schematic representation of 5'-UTR sequences of MDM2 isoforms 1-2, targeted by AS-circRNAs in a luciferase-reporter (luc). The long 5'-UTR (324 nt), harbouring two upstream open reading frames (uORFs 1-2), are represented in a wildtype (WT) and mutated (Mut) luciferase-reporter (luc). In addition, 30 nts of the MDM2 ORF, starting with the AUG, were fused in-frame with the luciferase ORF. Arrows indicate the effect of the uORFs on the translational output. Target regions of individual AS-circRNAs are represented as blue bars with nucleotide coordinates.
[B] Schematic representation of the third luciferase-reporter, which represents the isoforms 3-6, with a short 5'-UTR (67 nt). Again 30 nts of the MDM2 ORF (together with AUG) were fused in-frame with the luciferase ORF. Blue bars with nucleotide coordinates represent target regions of individual AS-circRNAs.

The first reporter contains the 5'-end of MDM2 isoforms 1 and 2 (long 5'-UTR). Therefore, the first 324 nucleotides, including the ORF translation start codon and the first 30 nucleotides of the MDM2 open reading frame (ORF), were fused in-frame with the luciferase ORF, resulting in the reporter construct '5'-UTR (MDM2_Iso1-2) wild type (WT)' **(Figure 3A upper panel)**. Since the long 5'-UTR of isoforms 1 and 2 also includes two upstream ORFs (uORFs), a second reporter construct was cloned containing mutations in the respective start codons (AUG to AAG) of the first and second uORF. This resulted in the mutant reporter construct '5'-UTR (MDM2_Iso1-2) Mut' **(Figure 3A**

lower panel). In this context we wanted to investigate whether AS-circRNAs can also be used to regulate the translation of the main ORF by blocking the uORFs. The third reporter reflects the 5'-end of MDM2 isoforms 3-6 **(Figure 3B)**, which have a short 5'-UTR compared to isoforms 1 and 2. Here, the first 67 nucleotides, as well as the ORF translation start codon and the first 30 nucleotides of the MDM2 ORF, were fused in-frame with the luciferase ORF, resulting in the '5'-UTR (MDM2_Iso3-6) WT' reporter construct.

In order to cover as many sequence regions as possible, a series of ten short AS-circRNAs was designed, each 90 nts long and including 40 nts antisense sequence, which specifically targets the 5'-UTR regions of MDM2 (named after the target boundaries; for a schematic representation of MDM2 5'-UTR reporters, see **Figure 3**; the circRNA sequences are listed in **Supplementary Table S1**). Both AS-circRNAs 1-40 (Iso1-2 as well as Iso3-6) specifically target the 5'-terminal 40 nucleotides of the respective 5'-UTR. Furthermore, AS-circRNAs were also designed to cover the ORF translation start site together with flanking regions: AS-circRNA 57-96 covers the region of the first uORF (Iso1-2) and AS-circRNA 190-229 the region of the second uORF, whereas AS-circRNAs 301-340 (Iso1-2) and 44-83 (Iso3-6) cover the region of the main ORF. Another AS-circRNA, 128-167, covers an internal region of isoforms 1 and 2. Furthermore, the region upstream of the AUG is covered by three more AS-circRNAs: AS-circRNA 250-289, 279-318 (Iso1-2) as well as 22-61 (Iso3-6). As a control and to normalize the luciferase activities, two non-specific circRNAs (CTR1 and 2) were used in these experiments, each containing a randomized sequence of 40 nucleotides instead of the specific antisense sequences.

Transiently overexpressed AS-circRNAs inhibit translation of MDM2 reporter constructs in HeLa cells

For functional characterization of this series of AS-circRNAs, we first tested their ability to inhibit translation in the three luciferase reporter systems. For this purpose, we used AS-circRNAs that were transiently overexpressed in HeLa cells by the so-called Tornado system (Twister-Optimised RNA for Durable Overexpression, **Litke and Jaffrey 2019)**. This system is based on an RNA polymerase III-guided and self-cleaving expression cassette, combined with circularization by endogenous RtcB-tRNA ligase (**Figure 4A**; for Tornado-derived circRNA secondary structures, see **Supplementary Figure S3**). One day after transfection of the circRNA expression constructs, either the 5′-UTR MDM2 Iso1-2 (WT and Mut) - or the 5′-UTR MDM2 Iso3-6 -reporter was transfected, and after 24 hours, luciferase activities were measured (for a flowchart of the analysis, see **Figure 4B**).

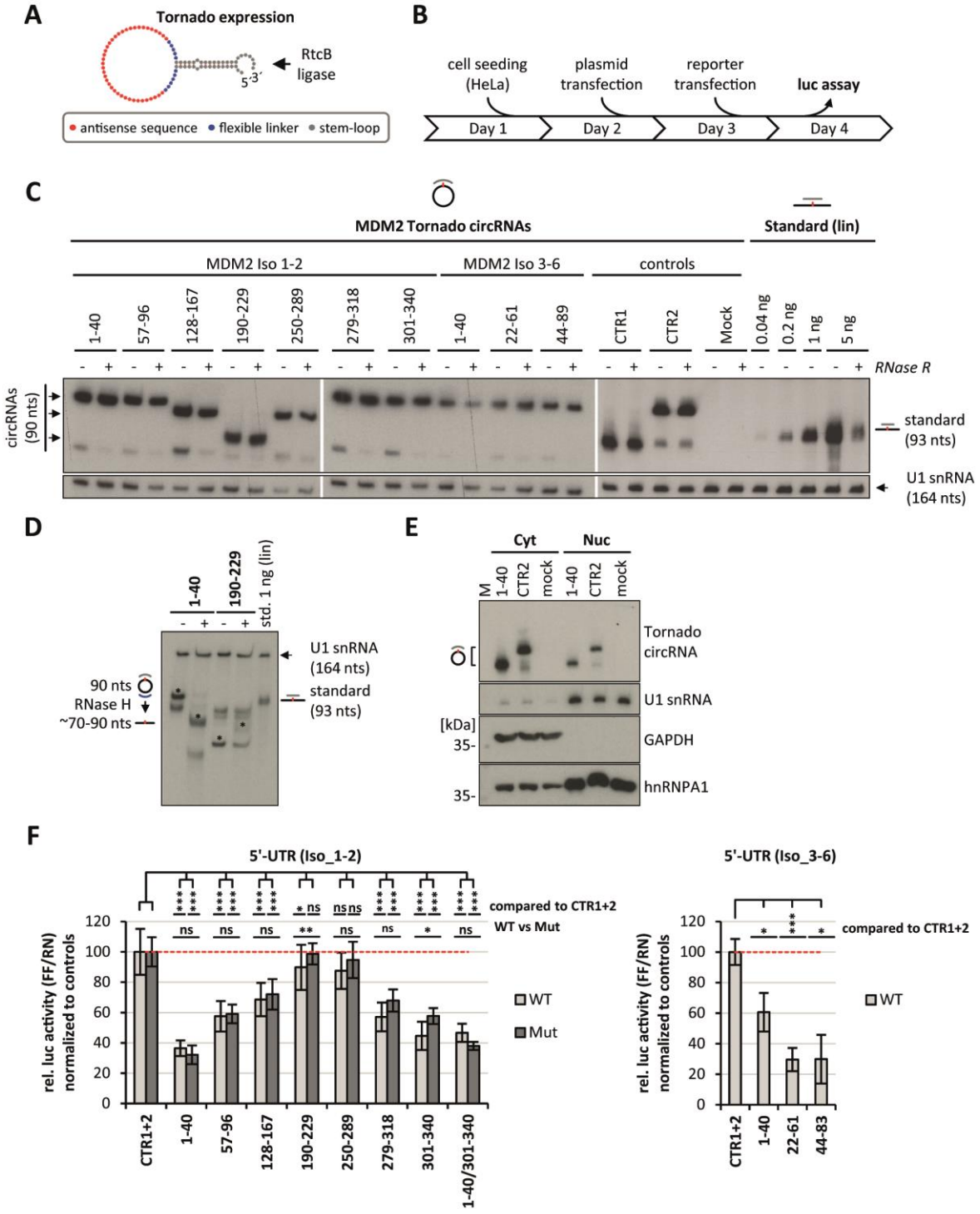

Figure 4: Tornado-based expression of AS-circRNAs in HeLa cells and screening of antisense activities by 5'-UTR reporter assays.

[A] Design of AS-circRNAs expressed in mammalian cells by the so-called Tornado system (Litke and Jaffrey 2019), based on RNA polymerase III-driven expression, ribozyme-mediated processing, and *in vivo* circularization by endogenous RtcB tRNA ligase. Each circular RNA is composed of a stem-loop (grey), a short flexible linker (blue), and the antisense sequence (red).

[B] Experimental workflow for luciferase reporter assays in HeLa cells overexpressing AS-circRNAs.

[C] Tornado-based overexpression of AS-circRNAs in HeLa cells and detection by Northern blot analysis, using a circular-junction specific probe. Circularity was confirmed by RNase R treatment (-/+). As an input control, U1 snRNA was detected by a U1-specific Northern probe. Note that U1 snRNA is partially resistant to degradation by RNase R due to its strong secondary structure. In addition, a linear standard RNA containing the circular junction (0.04 to 5 ng) served to quantitate Northern signals and as a size marker.

Figure 4 legend continued.
[D] Additional evidence for circularity of Tornado-expressed AS-circRNAs. Total RNA from HeLa cells overexpressing AS_1-40 and AS_190-229 circRNAs was analyzed by Northern blot, using a circular-junction specific probe. RNA aliquots were either left untreated, or treated with RNase H and a specific DNA oligonucleotide. Linearization of the circRNA through cleavage of the DNA-RNA hybrid by RNase H resulted in products of ~70-90 nts. In addition, 1 ng of the linear standard RNA (containing the circular junction) was applied, which also serves as a size standard. Asterisks indicate the cirRNA in the untreated (-) and the linearized product after RNase H treatment (+).
[E] Cellular distribution of Tornado-expressed AS-circRNAs. HeLa cells overexpressing either AS_1-40 or CTR2 control circRNAs were fractionated into cytoplasmic and nuclear fractions, followed by RNA preparation and Northern blot analysis of cell-equivalent amounts with a circular-junction probe. In addition, RNA from mock-treated cells was analyzed. For control and as fractionation markers, nuclear U1 snRNA and hnRNP A1 protein, as well as cytoplasmic GAPDH protein, were detected by Northern and Western blot, respectively.
[F] Translational repression of the wildtype (WT; Iso1-2 and Iso3-6) and mutated (Mut; only Iso1-2) 5´-UTR reporter constructs by AS-circRNAs. HeLa cells were transfected with respective circRNAs or a combination thereof (AS_1-40/301-340). After 24 h, the respective reporter was transfected (WT or mutated 5'-UTR), and relative luciferase activities (ratio of Firefly and Renilla expression) were measured, normalized to control circRNAs CTR1 and 2 (mean and standard deviations of three replicates, $P < 0.05$*, $P < 0.005$**, $P < 0.001$***, ns = not significant, two-sided *t*-test).

Overexpression of all ten MDM2 5′-UTR-specific (MDM2 Iso1-2 and Iso3-6) AS-circRNAs as well as two control circRNAs was confirmed by Northern blot analysis **(Figure 4C)**. In addition, Northern blot was combined with RNase R treatment to confirm circularity. Note that all of these circRNAs produced *in vivo* are resistant to RNase R. Furthermore, circular conformation was stringently demonstrated by RNase H cleavage experiments [for AS_1-40 and 190-229 circRNA (both directed against MDM2 Iso1-2) see **Figure 4D**]. In addition, by cell fractionation it was observed that AS-circRNAs are predominantly located in the cytoplasmic compartment **(Figure 4E)**. Based on reporter assays with the MDM2 Iso1-2 (WT as well as Mut) and the MDM2 Iso3-6 5'-UTR constructs, it was determined that all of these overexpressed anti-MDM2 circRNAs, with the exception of AS_250-289, reduce luciferase expression levels to 32-72% **(Figure 4F left panel)**.

Comparing the two reporters, 5'-UTR Iso1-2 WT versus Mut, significant differences were observed for AS_190-229 as well as AS_301-340, although the magnitude of these effects was relatively small. However, when comparing the activity of all AS-circRNAs, a position-dependent effect emerges. The 5'-terminal region covered by AS_1-40 and the main ORF proximal region covered by AS_301-340 showed the strongest effects in translational reduction of the reporter (to 36 and 46% residual level, respectively). The effect of the remaining AS-circRNAs loses intensity with distance to the 5'-terminal region (AS-circRNA 57-96 with 57%, and 128-167 with 68% residual level), whereas the effect increases again upon reaching the AUG-proximal region of the main ORF (AS-circRNA 279-318 with 57% residual level). In a combination between the two strongest AS-circRNAs 1-40/301-340, the inhibitory effect on reporter translation did not increase any further.

In comparison, for the 5'-UTR reporter mRNAs (Iso3-6), a reduction to 60 and 29% could be observed **(Figure 4F right panel)**. The two circRNAs covering the AUG-proximal (AS_22-61) and the direct AUG region (AS_44-83) showed the strongest effect with a reduction to 29% residual level.

Based on these separate reporters and the AS-circRNAs examined, the results indicate that 5'-terminal as well as AUG start-codon proximal regions can be efficiently targeted by AS-circRNAs, resulting in strong

translational inhibition down to ~30% residual levels.

Translational inhibition of endogenous MDM2 RNA

Following the investigation of specific AS-circRNAs (for schematic representation see **Figure 4A**), which effectively inhibit the translation of reporter RNAs, the results were in a next step to be substantiated on the endogenous level. For this purpose, the same setup of AS-circRNAs including the two control RNAs was transfected into HeLa cells (see flow chart in **Figure 5A**) and analysed 48 h later. Here, the cells were first lysed to examine the protein levels of MDM2 by Western blot, using MDM2 protein-specific antibodies (for representative Western blot see **Figure 5B**, for additional replicate see **Supplementary Figure S4**)**.** In parallel, total RNA was isolated to examine the effects of the individual AS-circRNAs at the RNA level by RT-qPCR **(Figure 5C)**.

The expression of MDM2 proteins in HeLa cells was analyzed by Western blotting with an anti-MDM2 monoclonal antibody. Although the calculated molecular weight of the full-length protein (Iso1) is ~56 kDa (see **Introduction, section E**), several MDM2 protein isoforms could be detected, migrating between 80-140 kDa. This observation has been described in the literature and is due to post-translationally phosphorylation and ubiquitination to varying degrees **(Erhardt *et al.* 1997, Cheng and Cohen 2007, Fan and Wang 2017)**. In this analysis, we focused on the protein isoform p140, since it represents the dominant protein variant in HeLa cells. Comparing the protein levels (p140) with each other and the controls (CTR1, CTR2 and mock), a position-dependent effect similar as in the described luciferase assays **(Figure 4F)** could be observed (for representative Western blots, see **Figure 5B** and **Supplementary Figure S4**). AS_1-40 (MDM2 Iso1-2) shows only a moderate effect, whereas AS_301-340 (MDM2 Iso1-2) shows the strongest effect. Interestingly, increased protein levels for the AS-circRNAs that bind in the regions between the first and second uORF (57-96, 128-167 and 190-229) could be detected. Analysis of protein levels after transfection with circRNAs against the 5'- UTR of isoforms 3-6, again showed a significant decrease in protein abundance after treatment with all three circRNAs. In summary, these data support the previous conclusion that the 5'-terminal region (MDM2 Iso3-6 only) and main ORF proximal region (MDM2 Iso1-2 and 3-6) are optimal targets.

To characterize more precisely the effects of the circRNAs and also to be able to conclude on mRNA stability, RT-qPCR was performed **(Figure 5 C)**. For isoform-specific detection, primers were designed to differentiate between isoforms 1-2 and 3-6 (see **Introduction, section E**). Since it is not completely clear which of the isoforms is mainly expressed, the first step was to investigate the expression levels of the various isoform groups in HeLa cells and compare them with each other. A 3.5-fold difference in their abundance was detected **(Supplementary Figure S5)**. These data indicate that the isoform group Iso1-2 is the major expression variant. However, in relation to the observed protein variants formed from the different isoform groups, no definite conclusion can be reached.

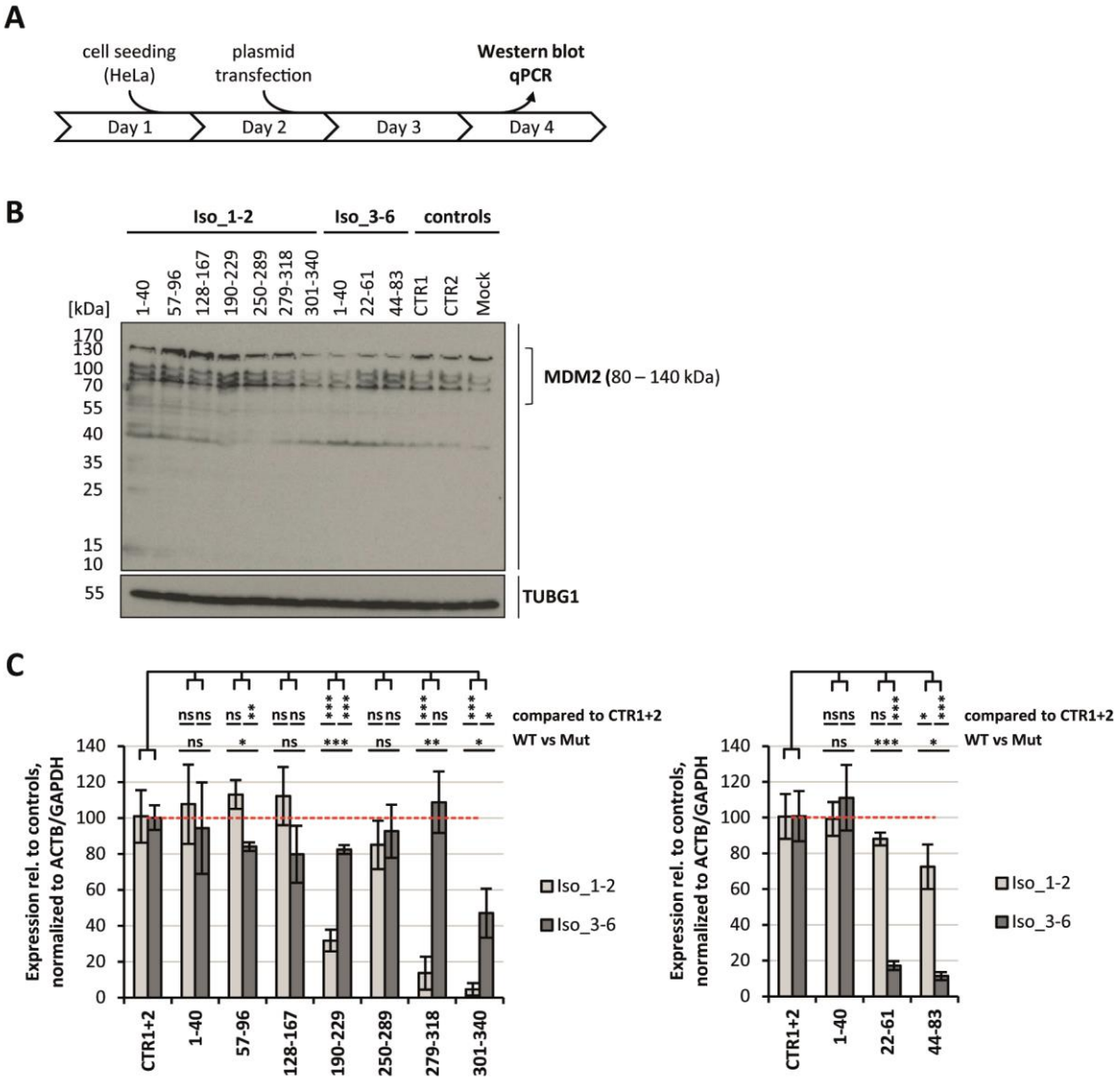

Figure 5: Tornado-based expression of AS-circRNAs in HeLa cells and screening of antisense activities on endogenous MDM2 isoforms by Western blot and qPCR assays.
[A] Experimental workflow for Western Blot and qPCR assays using transfected and circRNA-overexpressing HeLa cells.
[B] Western blot analysis of the endogenous MDM2 protein confirms reduction of protein accumulation in cells treated with specific AS-circRNAs. HeLa cells transfected with 10 µg of respective circRNA-Tornado constructs per assay were harvested 24 h later, lysed, and equal amounts of protein were analyzed by Western blotting. Different detectable MDM2 isoforms are labelled (80-140 kDa). TUBG1 and GAPDH were used as loading controls. *M*, protein markers (sizes in kDa). For an additional replicate, see Supplementary Figure S4.
[C] Detection of MDM2 mRNA levels by RT-qPCR. HeLa cells were transfected with 10 µg of Tornado-plasmids. After 24 h relative expression levels of the MDM2 mRNAs were determined by RT-qPCR, normalized to control circRNAs CTR1 and 2 (mean and standard deviations of three replicates, $P < 0.05$*, $P < 0.005$**, $P < 0.001$***, ns = not significant, two-sided *t*-test). The different isoforms (Iso1-2 and Iso3-6) were detected with specific primer pairs.

In a second step, the aim was to investigate whether an isoform-specific effect on MDM2 mRNA levels could be detected after treatment with the isoform-specific circRNAs. Isoform-specific targeting would be of high importance, since it allows

selective regulation of protein-output from isoforms of a single gene. For this purpose, HeLa cells were transfected with the respective Tornado construct for circRNA overexpression. After 24 hours, total RNA was isolated and RT-qPCR was performed to analyze how the targeting affects mRNA stability at the different antisense positions. Considering the results obtained from Iso1-2 specific AS-circRNAs, we can conclude that AS_190-229, AS_279-318, and AS_301-340 show a significant effect on the stability of isoform 1-2 **(Figure 5C left panel)**. It is clear that there is a discrepancy between the results of the Western blot and the RT-qPCR, as only AS_301-340 shows a reduction in both protein and RNA levels. On the other hand, analysis of the results obtained from Iso3-6 specific AS-circRNAs shows that AS_22-61 and AS_44-83 induce a significant effect on isoforms 3-6 **(Figure 5C right panel)**, which in turn reflects the effects of the Western blot. Thus, both isoform groups show a strong effect after treatment with circRNAs directed against the start codon proximal region.

Notably, AS_301-340 (Iso1-2 'specific') and AS_44-83 (Iso3-6 'specific') also show an effect on the respective other isoforms, which can be explained by the fact that both groups share the same sequence downstream of the AUG, which is covered by 50% of the circRNAs antisense sequence (20 nts).

In summary, these data suggest that for MDM2, the region around the normal AUG initiation site is a good target to achieve significant inhibition of translation.

DISCUSSION

As never before, the development of new RNA-based therapeutics plays a very important role. This is due to the fact that RNA-based drugs can offer new treatment options for many diseases, since they already act at the RNA level, e.g. before a faulty protein is formed. However, because RNA is relatively unstable, development of these therapeutics is a major challenge. The new class of circRNAs could provide a way around this, as one of their greatest advantages is their stability. In this work, artificial antisense circRNAs were designed that specifically target the 5'-UTR of β-globin and MDM2. The aim was to investigate the potential of antisense circRNAs to inhibit translation. Based on a series of AS-circRNAs for both β-globin and MDM2, we identified both the cap-proximal and the AUG start-codon proximal region as the most effective target regions. The data generated indicate a promising antisense function of small circRNAs.

In an initial proof-of-principle study with *in vitro* produced small circRNAs directed against the 5'-UTR of β-globin, luciferase assays demonstrated that translation is efficiently inhibited. As already mentioned, two specific sequence positions have emerged as efficient target sequences in this context: the 5´-cap-proximal and the AUG-proximal region. The activities observed suggest that by binding of AS-circRNAs to the 5'-terminal region of the 5'-UTR, translation initiation can be inhibited by blocking the elF4F complex, which is responsible for mRNA activation. In contrast, circRNAs binding in the AUG-proximal region, could lead to an interruption of ribosome scanning and to degradation of the untranslated mRNA. In a previously published paper **(Pfafenrot *et al.* 2021)**, we were able to substantiate the suspected blockade mechanism on the basis of reporter constructs and using Northern blot and RNase H assays. In contrast, however, we also observed destabilization of endogenous MDM2 mRNA after transfection of AS-circRNAs, indicating a position-dependent effect, and thus further analyses are needed to

clarify the mechanistic principles of AS-circRNA action.

Furthermore, the presented results indicate that the AS sequence length also has an influence on efficiency. Here, AS sequence lengths between 30 and 42 nts were tested, as previous studies have already shown that at least 30 nts are necessary for efficient binding (Silke Schreiner, data not shown). The two most effective circRNAs in the context of the β-globin 5'-UTR (AS_3-44 and AS_45-85) have the longest AS sequence of 41 nts compared to the other circRNAs tested, suggesting that a longer AS sequence has an advantage by forming a more stable duplex. These circRNAs (AS_3-44 and AS_45-85) have been shown to be moderately more efficient (1.2 to 1.4-fold) compared to their linear counterparts, which could also be proven by durability experiments. In this context, it was shown that the circRNAs have the greatest effect within the first two days. After the second day, the effect of circular RNA levelled off at a reduction to 77%, whereas the linear RNA lost its effect completely. This observation can be accounted to the high metabolic stability of circular RNAs. Furthermore, structural features and limitations of the way the antisense sequence is exposed in circular conformation may also contribute to the activity of AS-circRNAs.

In general, it should be noted that the activities of the RNAs are also limited by transfection efficiencies, depending on cell culture conditions used, and therefore the 'true' activities are likely to be higher. The experimental conditions of circRNA lipofection, as well as the *in vivo* stability of circRNAs can and should be further improved.

In comparison to the β-globin study, the circRNAs used to target reporter and endogenous MDM2 RNA were produced by an *in vivo* overexpression system. The ribozyme-mediated Tornado system **(Litke and Jaffrey 2019)** offers the great advantage of high circRNA expression *in vivo*.

MDM2 is an attractive target for cancer therapy and was therefore chosen as a potential target for this study. However, since MDM2 has multiple isoforms, different constructs had to be designed for the respective isoforms, which differ mainly by their 5'-UTR (Iso_1-2 and Iso_3-6, see also **Introduction, section E**). Since isoforms 1 and 2 of MDM2 have two upstream ORFs within the 5'-UTR, we also wanted to test whether the main ORF could be regulated by blocking the uORFs with a corresponding circRNA. For this purpose, we first tested whether a mutant reporter reveals a difference in expression compared to a WT reporter, initially without circRNA treatment. Indeed, the comparison showed that the expression of the mutant reporter was enhanced by 2.8-fold on average **(Supplementary Figure S6)**. However, circRNA treatment induced only insignificant differences between WT and mutant constructs, suggesting that circRNA directed against the uORFs cannot regulate the main ORF at the reporter level.

In the context of MDM2, the β-globin results could generally be reproduced at the reporter level. Again, the results suggest that 5'-terminal as well as AUG start-codon proximal regions can be efficiently targeted by AS-circRNAs.

However, at the endogenous level, only the AUG start-codon proximal region has been shown to be effective. Interestingly, the Western blot indicates slightly increased MDM2 protein levels after targeting the uORFs of isoform 1 and 2 (**Figure 5B**, AS_57-96, 128-167 and 190-229). This difference compared to the reporter assay may be due to the secondary structure of the 5'-UTR, as the secondary structure at the

reporter level may be different from that in the endogenous mRNA.

In addition, qPCR data were also generated, which, however, were not entirely consistent with the MDM2 protein level. Several AS-circRNAs display a reduction on the MDM2 RNA levels (AS_190-229, AS_279-318), which was not observed in the Western blot. Especially for AS_190-229, which showed increased protein levels in the Western blot, a significant reduction to 31% was detected in the qPCR data. If we compare these data with ß-globin or also SARS-CoV-2 data **(Pfafenrot *et al.* 2021)**, in which the mechanism of action could be attributed to blockage, it becomes clear that there appear to be several mechanisms of action in MDM2. This may be due to the complexity of MDM2. MDM2 does not only have different isoforms, but is also integrated in a feedback loop, and interacts with several proteins on certain regulatory processes. Improvements should therefore include multiple cell lines, and more detailed studies should be undertaken regarding the mechanism of action.

Furthermore, synthetic AS-circRNAs should be tested as an alternative for the Tornado-based overexpression system, as these have the advantage of being a biochemically well-defined system; for example, the transfected circRNA amounts can be titrated, and the effects of circular and linear forms can be directly compared with each other. Since circularization is sequence- or secondary structure-dependent, it was not possible in this case to produce the same set of AS-circRNAs synthetically based on transcription by T7 RNA polymerase and circularization by T4 RNA ligase. Due to the high number of by-products, the circular product could neither be determined nor purified by gel purification.

In summary, designer AS-circRNAs have great potential due to their versatility and adaptability. Together with the already published study on the inhibition of SARS-CoV-2 proliferation **(Pfafenrot *et al.* 2021)**, these are the first studies to show an efficient application of such designer antisense circRNAs. The potential is further underlined by the fact that this technology can be applied in all kinds of fields, from medicine to plant pest control, for example. Nevertheless, more targets should be tested to gain more insights, especially for understanding the scope and generality of the underlying mechanism of action.

ACKNOWLEDGMENTS

We thank Jan Medenbach for the initial luciferase plasmids, which were used in a modified form in this study. Furthermore, our thanks also go to Henrik Koch, who started the ß-globin project. We would also like to thank the other lab members for detailed discussions.

REFERENCES

Bennett, C. F., & Swayze, E. E. (2010). RNA targeting therapeutics: molecular mechanisms of antisense oligonucleotides as a therapeutic platform. *Annual review of pharmacology and toxicology*, *50*, 259–293. https://doi.org/10.1146/annurev.pharmtox.010909.105654

Bennett, C. F., Krainer, A. R., & Cleveland, D. W. (2019). Antisense Oligonucleotide Therapies for Neurodegenerative Diseases. *Annual review of neuroscience*, *42*, 385–406. https://doi.org/10.1146/annurev-neuro-070918-050501

Breuer, J., & Rossbach, O. (2020). Production and Purification of Artificial Circular RNA Sponges for Application in Molecular Biology and Medicine. *Methods and protocols*, *3*(2), 42. https://doi.org/10.3390/mps3020042

Cao, A., & Moi, P. (2002). Regulation of the globin genes. *Pediatric research*, *51*(4), 415–421. https://doi.org/10.1203/00006450-200204000-00003

Chen L. L. (2020). The expanding regulatory mechanisms and cellular functions of circular RNAs. *Nature reviews. Molecular cell biology*, *21*(8), 475–490. https://doi.org/10.1038/s41580-020-0243-y

Chène P. (2003). Inhibiting the p53-MDM2 interaction: an important target for cancer therapy. *Nature reviews. Cancer*, *3*(2), 102–109. https://doi.org/10.1038/nrc991

Cheng, T. H., & Cohen, S. N. (2007). Human MDM2 isoforms translated differentially on constitutive versus p53-regulated transcripts have distinct functions in the p53/MDM2 and TSG101/MDM2 feedback control loops. *Molecular and cellular biology*, *27*(1), 111–119. https://doi.org/10.1128/MCB.00235-06

Crooke, S. T., Witztum, J. L., Bennett, C. F., & Baker, B. F. (2018). RNA-Targeted Therapeutics. *Cell metabolism*, *27*(4), 714–739. https://doi.org/10.1016/j.cmet.2018.03.004

Erhardt, P., Tomaselli, K. J., & Cooper, G. M. (1997). Identification of the MDM2 oncoprotein as a substrate for CPP32-like apoptotic proteases. *The Journal of biological chemistry*, *272*(24), 15049–15052. https://doi.org/10.1074/jbc.272.24.15049

Fan, C., & Wang, X. (2017). Mdm2 Splice isoforms regulate the p53/Mdm2/Mdm4 regulatory circuit via RING domain-mediated ubiquitination of p53 and Mdm4. *Cell cycle (Georgetown, Tex.)*, *16*(7), 660–664. https://doi.org/10.1080/15384101.2017.1288327

Hansen, T. B., Jensen, T. I., Clausen, B. H., Bramsen, J. B., Finsen, B., Damgaard, C. K., & Kjems, J. (2013). Natural RNA circles function as efficient microRNA sponges. *Nature*, *495*(7441), 384–388. https://doi.org/10.1038/nature11993

Hentze, M. W., & Preiss, T. (2013). Circular RNAs: splicing's enigma variations. *The EMBO journal*, *32*(7), 923–925. https://doi.org/10.1038/emboj.2013.53

Hou, H., Sun, D., & Zhang, X. (2019). The role of *MDM2* amplification and overexpression in therapeutic resistance of malignant tumors. *Cancer cell international*, *19*, 216. https://doi.org/10.1186/s12935-019-0937-4

Jackson, R., Hellen, C. & Pestova, T. (2010). The mechanism of eukaryotic translation initiation and principles of its regulation. *Nat Rev Mol Cell Biol* **11,** 113–127. https://doi.org/10.1038/nrm2838

Jeck, W. R., Sorrentino, J. A., Wang, K., Slevin, M. K., Burd, C. E., Liu, J., Marzluff, W. F., & Sharpless, N. E. (2013). Circular RNAs are abundant, conserved, and associated with ALU repeats. *RNA (New York, N.Y.)*, *19*(2), 141–157. https://doi.org/10.1261/rna.035667.112

Jost, I., Shalamova, L. A., Gerresheim, G. K., Niepmann, M., Bindereif, A., & Rossbach, O. (2018). Functional sequestration of microRNA-122 from Hepatitis C Virus by circular RNA sponges. *RNA biology*, *15*(8), 1032–1039. https://doi.org/10.1080/15476286.2018.1435248

Klein, C., & Vassilev, L. T. (2004). Targeting the p53-MDM2 interaction to treat cancer. *British journal of cancer*, *91*(8), 1415–1419. https://doi.org/10.1038/sj.bjc.6602164

Kristensen, L. S., Andersen, M. S., Stagsted, L., Ebbesen, K. K., Hansen, T. B., & Kjems, J. (2019). The biogenesis, biology and characterization of circular RNAs. *Nature reviews. Genetics*, *20*(11), 675–691. https://doi.org/10.1038/s41576-019-0158-7

Kubbutat, M. H., Jones, S. N., & Vousden, K. H. (1997). Regulation of p53 stability by Mdm2. *Nature*, *387*(6630), 299–303. https://doi.org/10.1038/387299a0

Le, T. K., Paris, C., Khan, K. S., Robson, F., Ng, W. L., & Rocchi, P. (2021). Nucleic acid-based technologies targeting coronaviruses. *Trends in biochemical sciences*, *46*(5), 351–365. https://doi.org/10.1016/j.tibs.2020.11.010

Litke, J. L., & Jaffrey, S. R. (2019). Highly efficient expression of circular RNA aptamers in cells using autocatalytic transcripts. *Nature biotechnology*, *37*(6), 667–675. https://doi.org/10.1038/s41587-019-0090-6

Medenbach, J., Seiler, M., & Hentze, M. W. (2011). Translational control via protein-regulated upstream open reading frames. *Cell*, *145*(6), 902–913. https://doi.org/10.1016/j.cell.2011.05.005

Memczak, S., Jens, M., Elefsinioti, A., Torti, F., Krueger, J., Rybak, A., Maier, L., Mackowiak, S. D., Gregersen, L. H., Munschauer, M., Loewer, A., Ziebold, U., Landthaler, M., Kocks, C., le Noble, F., & Rajewsky, N. (2013). Circular RNAs are a large class of animal RNAs with regulatory potency. *Nature*, *495*(7441), 333–338. https://doi.org/10.1038/nature11928

Momand, J., Zambetti, G. P., Olson, D. C., George, D., & Levine, A. J. (1992). The mdm-2 oncogene product forms a complex with the p53 protein and inhibits p53-mediated transactivation. *Cell*, *69*(7), 1237–1245. https://doi.org/10.1016/0092-8674(92)90644-r

Müller, S., Wedler, A., Breuer, J., Glaß, M., Bley, N., Lederer, M., Haase, J., Misiak, C., Fuchs, T., Ottmann, A., Schmachtel, T., Shalamova, L., Ewe, A., Aigner, A., Rossbach, O., & Hüttelmaier, S. (2020). Synthetic circular miR-21 RNA decoys enhance tumor suppressor expression and impair tumor growth in mice. *NAR cancer*, *2*(3), zcaa014. https://doi.org/10.1093/narcan/zcaa014

Nag, S., Zhang, X., Srivenugopal, K. S., Wang, M. H., Wang, W., & Zhang, R. (2014). Targeting MDM2-p53 interaction for cancer therapy: are we there yet? *Current medicinal chemistry*, *21*(5), 553–574. https://doi.org/10.2174/09298673113206660325

Oliner, J. D., Pietenpol, J. A., Thiagalingam, S., Gyuris, J., Kinzler, K. W., & Vogelstein, B. (1993). Oncoprotein MDM2 conceals the activation domain of tumour suppressor p53. *Nature*, *362*(6423), 857–860. https://doi.org/10.1038/362857a0

Pfafenrot, C., Schneider, T., Müller, C., Hung, L. H., Schreiner, S., Ziebuhr, J., & Bindereif, A. (2021). Inhibition of SARS-CoV-2 coronavirus proliferation by designer antisense-circRNAs. *Nucleic acids research*, *49*(21), 12502–12516. https://doi.org/10.1093/nar/gkab1096

Pfaffl M. W. (2001). A new mathematical model for relative quantification in real-time RT-PCR. *Nucleic acids research*, *29*(9), e45. https://doi.org/10.1093/nar/29.9.e45

Roberts, T. C., Langer, R., & Wood, M. (2020). Advances in oligonucleotide drug delivery. *Nature reviews. Drug discovery*, *19*(10), 673–694. https://doi.org/10.1038/s41573-020-0075-7

Sänger, H. L., Klotz, G., Riesner, D., Gross, H. J., & Kleinschmidt, A. K. (1976). Viroids are single-stranded covalently closed circular RNA molecules existing as highly base-paired rod-like structures. *Proceedings of the National Academy of Sciences of the United States of America*, *73*(11), 3852–3856. https://doi.org/10.1073/pnas.73.11.3852

Schneider, T., Schreiner, S., Preußer, C., Bindereif, A., & Rossbach, O. (2018). Northern Blot Analysis of Circular RNAs. *Methods in molecular biology (Clifton, N.J.)*, *1724*, 119–133. https://doi.org/10.1007/978-1-4939-7562-4_10

Schreiner, S., Didio, A., Hung, L. H., & Bindereif, A. (2020). Design and application of circular RNAs with protein-sponge function. *Nucleic acids research*, *48*(21), 12326–12335. https://doi.org/10.1093/nar/gkaa1085

Starke, S., Jost, I., Rossbach, O., Schneider, T., Schreiner, S., Hung, L. H., & Bindereif, A. (2015). Exon circularization requires canonical splice signals. *Cell reports*, *10*(1), 103–111. https://doi.org/10.1016/j.celrep.2014.12.002

Vassilev L. T. (2004). Small-molecule antagonists of p53-MDM2 binding: research tools and potential therapeutics. *Cell cycle (Georgetown, Tex.)*, *3*(4), 419–421.

Wade, M., Li, Y. C., & Wahl, G. M. (2013). MDM2, MDMX and p53 in oncogenesis and cancer therapy. *Nature reviews. Cancer*, *13*(2), 83–96. https://doi.org/10.1038/nrc3430

Wilusz J. E. (2018). A 360° view of circular RNAs: From biogenesis to functions. *Wiley interdisciplinary reviews. RNA*, *9*(4), e1478. https://doi.org/10.1002/wrna.1478

SUPPLEMENTARY INFORMATION

Supplementary Figure S1

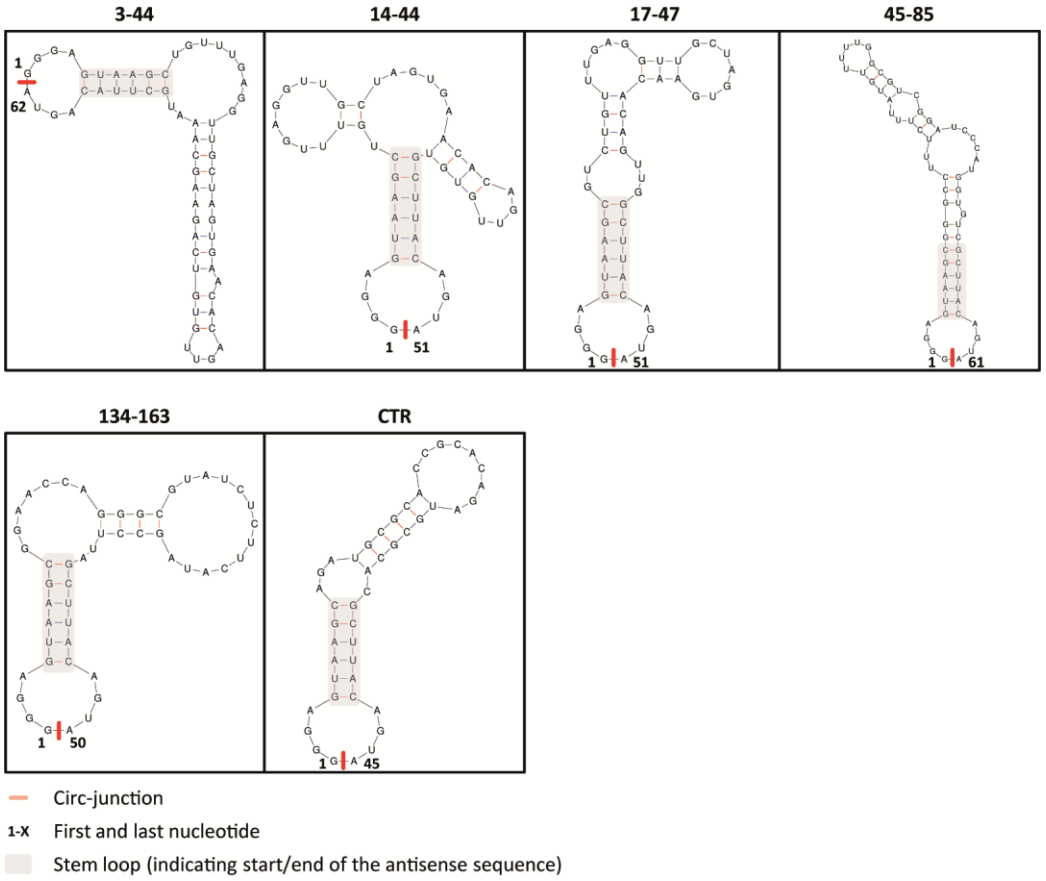

Supplementary Figure S1:
Secondary structure of β-globin antisense circRNAs.
Predicted secondary structure of *in vitro* produced small antisense circular RNAs, used in this study. RNA-folding prediction was performed with mfold. The circ-junction is indicated by a red line. Numbers (1-x) represent the first and the last nucleotide. Stem loops are highlighted in light grey and indicate the start as well as the end of the antisense sequence.

Supplementary Figure S2

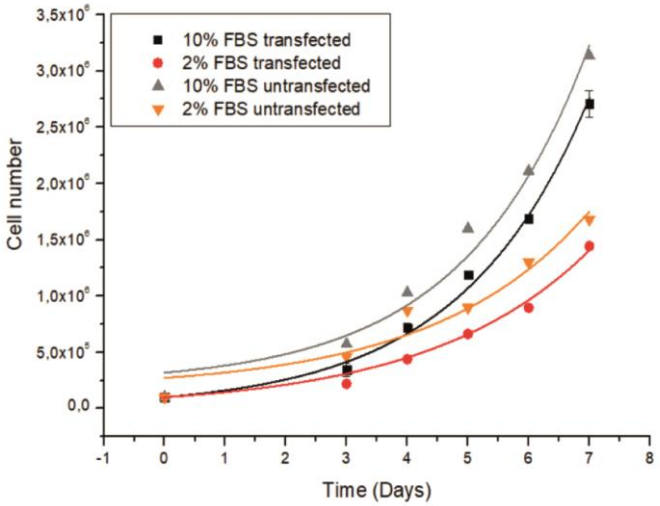

Supplementary Figure S2:
Growth curve analysis of HeLa cells cultured in 2 or 10% FBS-containing medium.
Cellular growth of HeLa cells was compared using DME medium supplemented with 2% or 10% FBS, with or without transfection of the CTR circRNA, over a time period of seven days. Mean and standard deviations of two replicates are shown.

Supplementary Figure S3

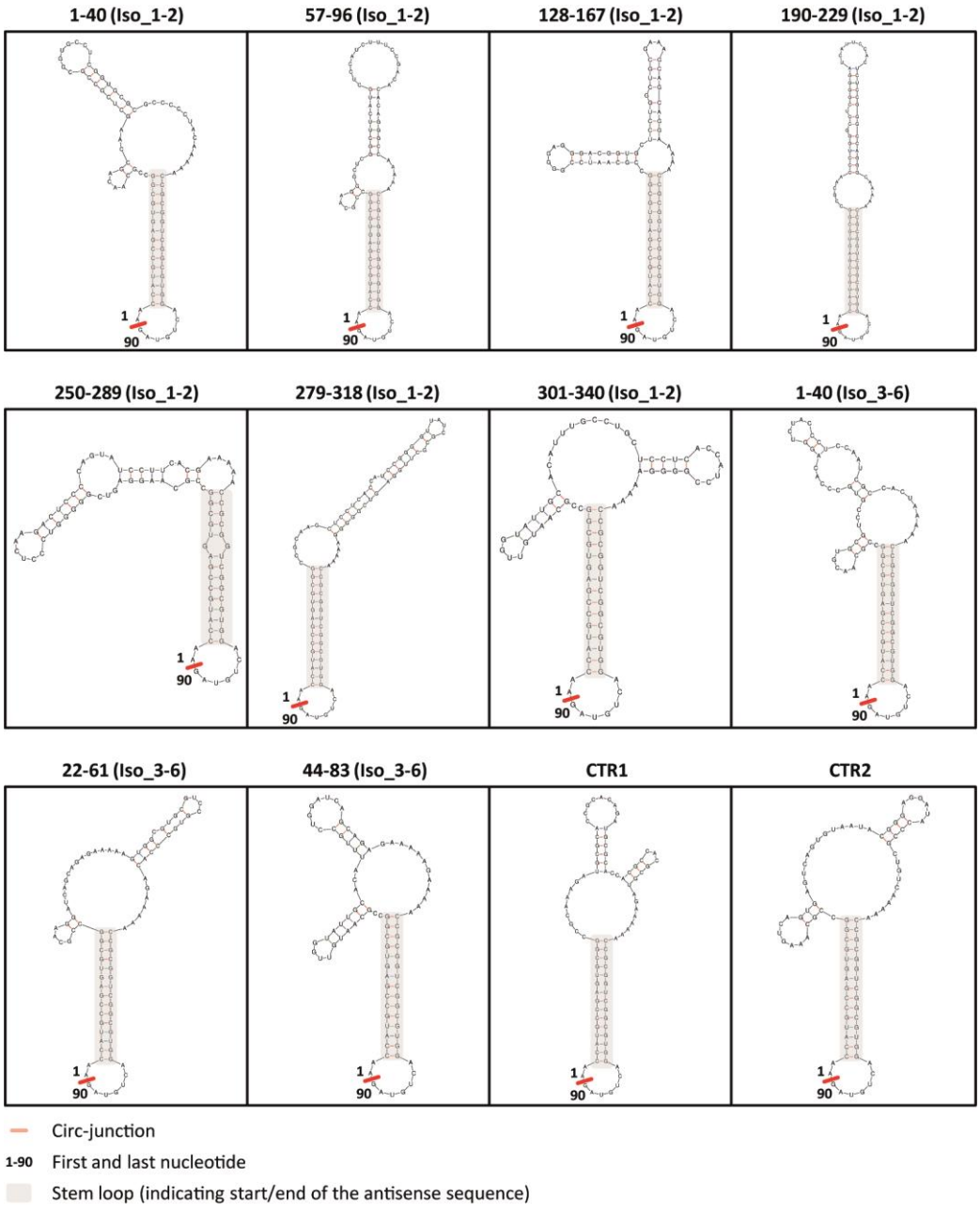

Supplementary Figure S3:
Secondary structure of Tornado-based antisense circRNAs.
Predicted secondary structures of Tornado-based antisense circular RNAs, used in this study. RNA-folding prediction was performed with mfold. The circ-junction is indicated by a red line. Numbers (1-90) represent the first and the last nucleotide. Stem loops are highlighted in light grey, and indicate the start as well as the end of antisense sequence (including the flexible linker sequence).

Supplementary Figure S4

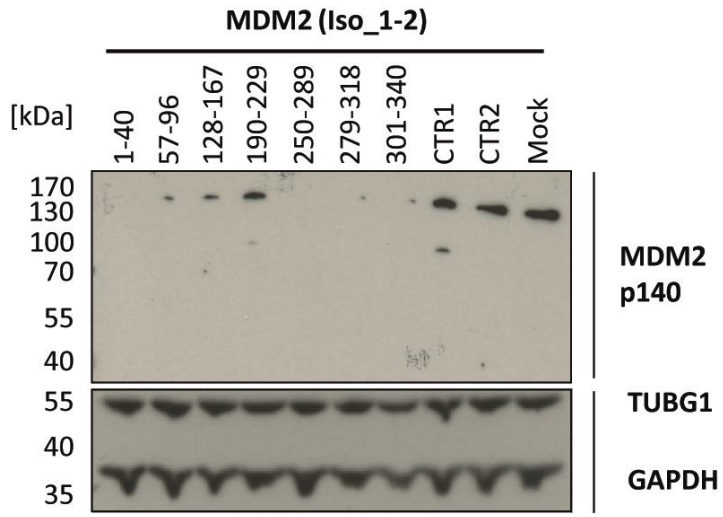

Supplementary Figure S4:
Screening of antisense activities on endogenous MDM2 isoforms by Western blot.
Western blot analysis of the endogenous MDM2 protein confirms reduction of protein accumulation in cells treated with specific AS-circRNAs (results from another replicate, in addition to **Figure 5B**). HeLa cells transfected with 10 µg of respective circRNA-Tornado constructs per assay were harvested 24 h later, lysed, and equal amounts of protein were analyzed by Western blotting, using the MDM2 protein as a marker. Detectable MDM2 isoforms are labelled (140 kDa). TUBG1 and GAPDH were used as loading controls. *M*, protein markers (sizes in kDa).

Supplementary Figure S5

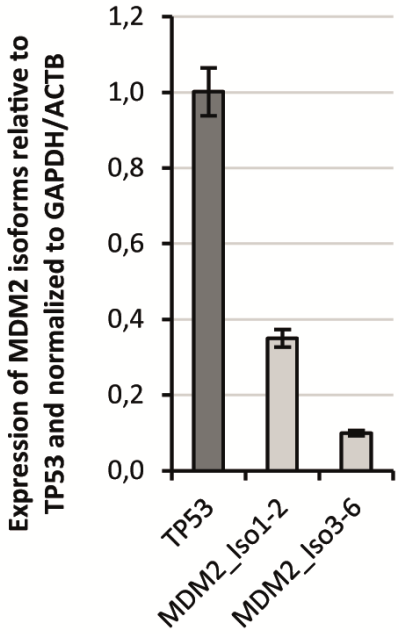

Supplementary Figure S5:
Expression levels of MDM2 mRNA isoforms (Iso1-2 and Iso3-6) in HeLa cells.
Expression of MDM2 isoforms (Iso1-2 and Iso3-6) was detected by RT-qPCR, using specific primer pairs, and plotted relative to the expression of the TP53 mRNA. Normalization was performed against two housekeeping genes (GAPDH and ACTB). Mean and standard deviations of three technical replicates are shown.

Supplementary Figure S6

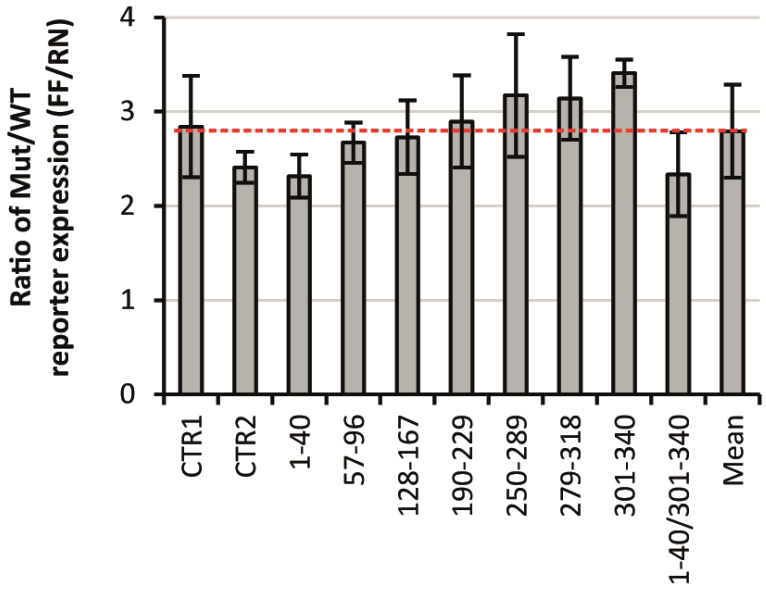

Supplementary Figure S6:
uORFs located in the long MDM2 5´-UTR influence translation of reporter constructs.
Influence of the uORFs located in the 5´-UTR of MDM2 on translational output of the WT/Mut reporter constructs (representing Iso1-2). Reporter expression values (Firefly/Renilla) were derived from the dataset presented in **Figure 4F**, and ratios of the translational output (Mut/WT) were calculated and plotted.

Supplementary Table S1.

***In vitro* produced RNA (β-globin/HBB)**

Name		Oligonucleotides 5´-3´	Final circRNA sequence 5´-3´
3-44	_fwd	TAATACGACTCACTATAGGGAGTAAGCTGTTTGAGGTTGCTAGTGAACACAGTTGTGTCAGAAGCAAATGCTTACAGTA	GGGAGTAAGC**TGTTTGAGGTTGCTAGTGAACACAGTTGTGTCAGAAGCAAAT**GCTTACAGTA
	_rev	TACTGTAAGCATTTGCTTCTGACACAACTGTGTTCACTAGCAACCTCAAACAGCTTACTCCCTATAGTGAGTCGTATTA	
14-44	_fwd	TAATACGACTCACTATAGGGAGTAAGCTGTTTGAGGTTGCTAGTGAACACAGTTGTGTGCTTACAGTA	GGGAGTAAGC**TGTTTGAGGTTGCTAGTGAACACAGTTGTGT**GCTTACAGTA
	_rev	TACTGTAAGCACACAACTGTGTTCACTAGCAACCTCAAACAGCTTACTCCCTATAGTGAGTCGTATTA	
17-47	_fwd	TAATACGACTCACTATAGGGAGTAAGCGTCTGTTTGAGGTTGCTAGTGAACACAGTTGGCTTACAGTA	GGGAGTAAGC**GTCTGTTTGAGGTTGCTAGTGAACACAGTTG**GCTTACAGTA
	_rev	TACTGTAAGCCAACTGTGTTCACTAGCAACCTCAAACAGACGCTTACTCCCTATAGTGAGTCGTATTA	
45-85	_fwd	TAATACGACTCACTATAGGGAGTAAGCGGGCCTTTCTTTATGTTTTTGGCGTCGGATCCCATGGTGTCGCTTACAGTA	GGGAGTAAGC**GGGCCTTTCTTTATGTTTTTGGCGTCGGATCCCATGGTGTC**GCTTACAGTA
	_rev	TACTGTAAGCGACACCATGGGATCCGACGCCAAAAACATAAAGAAAGGCCCGCTTACTCCCTATAGTGAGTCGTATTA	
134-163	_fwd	TAATACGACTCACTATAGGGAGTAAGCGGAACCAGGGCGTATCTCTTCATAGCCTTAGCTTACAGTA	GGGAGTAAGC**GGAACCAGGGCGTATCTCTTCATAGCCTTA**GCTTACAGTA
	_rev	TACTGTAAGCTAAGGCTATGAAGAGATACGCCCTGGTTCCGCTTACTCCCTATAGTGAGTCGTATTA	
CTR	_fwd	TAATACGACTCACTATAGGGAGTAAGCAGATGCGCACCGCACAGATGCGCACGCTTACAGTA	GGGAGTAAGC**AGATGCGCACCGCACAGATGCGCAC**GCTTACAGTA
	_rev	TACTGTAAGCgTGCGCATcTgTGCGgTGCGCATcTGCTTACTCCCTATAGTGAGTCGTATTA	
			Legend GGGAGTAAGC**NNNNNNNNNNNNNNNNNNNNNNNNNNNNNNNNNNNNNNNNNN**GCTTACAGTA overhang, stem loop, **N** = antisense sequence

Tornado circRNAs (MDM2)

Name		Oligonucleotides (with NotI and SacII overhangs) 5´-3´	Final circRNA sequence 5´-3´
1-40 (Iso_1-2)	_fwd	GGCCGCAACAGCCAAGCTCGCCGCGGTGCCTCGGTGCGCGCCCCCTACAAAAACCGC	AACCATGCCGAGTGCGGCCGCAA**CAGCCAAGCTCGCCGCGGTGCCTCGGTGCGCGCCCCCTAC**AAAAACCGCGGTCGGCGTGGACTGTAG
	_rev	GGTTTTTGTAGGGGGCGCGCACCGAGGCACCGCGGCGAGCTTGGCTGTTGC	
57-96 (Iso_1-2)	_fwd	GGCCGCAAGGGCTCGGCTTCATGCTCCATCTTTCCGACACACAGGGCCAAAAACCGC	AACCATGCCGAGTGCGGCCGCAA**GGGCTCGGCTTCATGCTCCATCTTTCCGACACACAGGGCC**AAAAACCGCGGTCGGCGTGGACTGTAG
	_rev	GGTTTTTGGCCCTGTGTGTCGGAAAGATGGAGCATGAAGCCGAGCCCTTGC	
128-167 (Iso_1-2)	_fwd	GGCCGCAATCCGGGGAGGGACGGTGCTCCTGGCTGCGAAAGCAGCAGGAAAAACCGC	AACCATGCCGAGTGCGGCCGCAA**TCCGGGGAGGGACGGTGCTCCTGGCTGCGAAAGCAGCAGG**AAAAACCGCGGTCGGCGTGGACTGTAG
	_rev	GGTTTTTCCTGCTGCTTTCGCAGCCAGGAGCACCGTCCCTCCCCGGATTGC	
190-229 (Iso_1-2)	_fwd	GGCCGCAACCCTGGGCCTCGGGGATCATTCCACTCTCCGGGCCAGGGCAAAAACCGC	AACCATGCCGAGTGCGGCCGCAA**CCCTGGGCCTCGGGGATCATTCCACTCTCCGGGCCAGGGC**AAAAACCGCGGTCGGCGTGGACTGTAG
	_rev	GGTTTTTGCCCTGGCCCGGAGAGTGGAATGATCCCCGAGGCCCAGGGTTGC	
250-289 (Iso_1-2)	_fwd	GGCCGCAAGGAGTCGGGGGTCCCTCAAGACTCCCCAGTATCCTTCACGAAAAACCGC	AACCATGCCGAGTGCGGCCGCAA**GGAGTCGGGGGTCCCTCAAGACTCCCCAGTATCCTTCACG**AAAAACCGCGGTCGGCGTGGACTGTAG
	_rev	GGTTTTTCGTGAAGGATACTGGGGAGTCTTGAGGGACCCCCGACTCCTTGC	
279-318 (Iso_1-2)	_fwd	GGCCGCAAGCTCCTCACCATCCGGGGTTATCGCGCTTGGAGTCGGGGGAAAAACCGC	AACCATGCCGAGTGCGGCCGCAA**GCTCCTCACCATCCGGGGTTATCGCGCTTGGAGTCGGGGG**AAAAACCGCGGTCGGCGTGGACTGTAG
	_rev	GGTTTTTCCCCCGACTCCAAGCGCGATAACCCCGGATGGTGAGGAGCTTGC	
301-340 (Iso_1-2)	_fwd	GGCCGCAATGTTGGTATTGCACATTTGCCTGCTCCTCACCATCCGGGGAAAAACCGC	AACCATGCCGAGTGCGGCCGCAA**TGTTGGTATTGCACATTTGCCTGCTCCTCACCATCCGGGG**AAAAACCGCGGTCGGCGTGGACTGTAG
	_rev	GGTTTTTCCCCGGATGGTGAGGAGCAGGCAAATGTGCAATACCAACATTGC	
1-40 (Iso_3-6)	_fwd	GGCCGCAACGTGCGTCCGTGCCCACAGGTCTACCCTCCAATCGCCACTAAAAACCGC	AACCATGCCGAGTGCGGCCGCAA**CGTGCGTCCGTGCCCACAGGTCTACCCTCCAATCGCCACT**AAAAACCGCGGTCGGCGTGGACTGTAG
	_rev	GGTTTTTAGTGGCGATTGGAGGGTAGACCTGTGGGCACGGACGCACGTTGC	
22-61 (Iso_3-6)	_fwd	GGCCGCAAGGATCAGCAGAGAAAAAGTGGCGTGCGTCCGTGCCCACAGAAAAACCGC	AACCATGCCGAGTGCGGCCGCAA**GGATCAGCAGAGAAAAAGTGGCGTGCGTCCGTGCCCACAG**AAAAACCGCGGTCGGCGTGGACTGTAG
	_rev	GGTTTTTCTGTGGGCACGGACGCACGCCACTTTTTCTCTGCTGATCCTTGC	
44-83 (Iso_3-6)	_fwd	GGCCGCAATGTTGGTATTGCACATTTGCCTGGATCAGCAGAGAAAAAGAAAAACCGC	AACCATGCCGAGTGCGGCCGCAA**TGTTGGTATTGCACATTTGCCTGGATCAGCAGAGAAAAAG**AAAAACCGCGGTCGGCGTGGACTGTAG
	_rev	GGTTTTTCTTTTTCTCTGCTGATCCAGGCAAATGTGCAATACCAACATTGC	
CTR1	_fwd	GGCCGCAAAGATGCGCACCGCACAGATGCGCACCACGCCACGCGTAGAAAAAACCGC	AACCATGCCGAGTGCGGCCGCAA**AGATGCGCACCGCACAGATGCGCACCACGCCACGCGTAGA**AAAAACCGCGGTCGGCGTGGACTGTAG
	_rev	GGTTTTTTCTACGCGTGGCGTGGTGCGCATCTGTGCGGTGCGCATCTTTGC	
CTR2	_fwd	GGCCGCAAAGTCAGTGAGTCAGTGTAATACGGGAGGATACCCGCTGTCAAAAACCGC	AACCATGCCGAGTGCGGCCGCAA**AGTCAGTGAGTCAGTGTAATACGGGAGGATACCCGCTGTC**AAAAACCGCGGTCGGCGTGGACTGTAG
	_rev	GGTTTTTGACAGCGGGTATCCTCCCGTATTACACTGACTCACTGACTTTGC	
			Legend AACCATGCCGAGTGCGGCCGCAA**NNNNNNNNNNNNNNNNNNNNNNNNNNNNNNNNNNNNNNNNNN**AAAAACCGCGGTCGGCGTGGACTGTAG Tornado stem loop, flexible linker, **N** = antisense sequence, **N** = T->A (for extended T-stretches)

Northern Blot probes

Name		Oligonucleotides 5´-3´	Riboprobe sequence 5´-3´
Tornado junction	_fwd	TAATACGACTCACTATAGGGTTGCGGCCGCACTCGGCATGGTTCTACAGTCCACGCCGACCGCGGTTTTTTTTTTTTTTTTTT	GGG**TTGCGGCCGCACTCGGCATGGTTCTACAGTCCACGCCGACCGCGGTTTTT**TTTTTTTTTTTTTT
	_rev	AAAAAAAAAAAAAAAAAAAAACCGCGGTCGGCGTGGACTGTAGAACCATGCCGAGTGCGGCCGCAACCCTATAGTGAGTCGTATTA	
U1 snRNA	_fwd	TAATACGACTCACTATAGGGATACTTACCTGGCAGGGGAGATACCATGATTTTTTTTTTTTTTTTTTTT	GGG**ATACTTACCTGGCAGGGGAGATACCATGAT**TTTTTTTTTTTTTTTTTTT
	_rev	AAAAAAAAAAAAAAAAAAAAATCATGGTATCTCCCCTGCCAGGTAAGTATCCCTATAGTGAGTCGTATTA	
			Legend GGG**NNNNNNNNNNNNNNNNNNNNNNNNNNNNNNNNNNNNNNNN**TTTTTTTTTTTTTTTTTTT GGG = transcription start, **NN** = target region , TTT = Oligo(T) for DIG-labeling

Northern Blot standard

Name		Oligonucleotides 5´-3´	Standard sequence 5´-3´
1-40	_fwd	TAATACGACTCACTATAGGGTCGGTGCGCGCCCCCTACAAAAACCGCGGTCGGCGTGGACTGTAGAACCATGCCGAGTGCGGCCGCA	GGG**TCGGTGCGCGCCCCCTAC**AAAAA<u>CCGCGGTCGGCGTGGACTGTA**GA**ACCATGCCGAGTGCGGCCGC</u>AA**CAGCCAAGCTCGCCG CGGTGCC**
	_rev	ACAGCCAAGCTCGCCGCGGTGCC GGCACCGCGGCGAGCTTGGCTGTTGCGGCCGCACTCGGCATGGTTCTACAGTCCACGCCGACCGCGGTTTTTGTAGGGGGCGCGCACC GACCCTATAGTGAGTCGTATTA	
			Legend GGG**NNNNNNNNNNNNNNNNNN**AAAAA<u>CCGCGGTCGGCGTGGACTGTA**GA**ACCATGCCGAGTGCGGCCGC</u>AA**NNNNNNNNNNNNNNNN NNNNNNN** GGG = transcription start, **NN** = antisense region, flexible linker, <u>Tornado stem loop</u> , **GA** = circ-junction, **N** = T->A (for extended T-stretches)

RNase H cleavage

Name	Oligonucleotide 5´-3´
1-40	CCGCGGCGAGCTTGGCTGTT
190-229	GGAGAGTGGAATGATCCCCG

RT-(q)PCR

Name		Oligonucleotide 5´-3´
MDM2 (Iso_1-2)	_fwd	GCCCGGAGAGTGGAATGAT
	_rev	AGCTGGAATCTGTGAGGTGG
MDM2 (Iso_3-6)	_fwd	CGGACGCACGCCACTTTT
	_rev	CGAAGCTGGAATCTGTGAGG
GAPDH	_fwd	TGCACCACCAACTGCTTAGC
	_rev	GGCATGGACTGTGGTCATGAG
ACTB	_fwd	GTGGAACGGTGAAGGTGACA
	_rev	GGGACTTCCTGTAACAACGCA

Publications and own scientific contributions

2019

- **Christina Pfafenrot and Christian Preußer.** 2019. Establishing essential quality criteria for the validation of circular RNAs as biomarkers. *Biomolecular Detection and Quantification*. **17**:100085, https://doi.org/10.1016/j.bdq.2019.100085.

2021

- **Corinna J. Ulshöfer*, Christina Pfafenrot*, Albrecht Bindereif and Tim Schneider.** 2021. Methods to study circRNA-protein interactions. *Methods*. **196**:36-46, https://doi.org/10.1016/j. ymeth.2021.04.014.

  * *these authors contributed equally to this work.*

  - All parts of the 'CircRNA-centric methods to study circRNA-protein interactions' chapter.

- **Marie-Luise Mosbach, Christina Pfafenrot, Elke Pogge von Strandmann, Albrecht Bindereif and Christian Preußer.** 2021. Molecular Determinants for RNA Release into Extracellular Vesicles. *Cells*. **10:**2674, **https://doi.org/10.3390/cells10102674**.

  - **Figure 1b**. Western blot analysis of EV-marker proteins CD63, ALIX, FLOT1.

- **Christina Pfafenrot*, Tim Schneider*, Christin Müller*, Lee-Hsueh Hung, Silke Schreiner, John Ziebuhr and Albrecht Bindereif.** 2021. Inhibition of SARS-CoV-2 coronavirus proliferation by designer antisense-circRNAs. *Nucleic Acids Research*. **49:**12502-12516, https://doi.org/10.1093/nar/gkab1096.

  * *these authors contributed equally to this work*

  - **Figure 1**. Design of reporter constructs and AS-circRNAs targeting SARS-CoV-2 RNA together with Tim Schneider.
  - **Figure 2CDE.** Production and validation of synthetic AS-circRNAs as well as screening of active AS-circRNAs via luciferase assays.
  - **Figure 3BCDE.** Production and transfection of AS-circRNAs, which served as the basis for infection assays (BDE, Christin Müller) and Western blot analysis (C, Tim Schneider).

- **Figure 4ABC.** Production and transfection of AS-circRNA and library preparation for RNA-seq. Subsequent Northern blot (A) was carried out by Tim Schneider and bioinformatic analysis by Lee-Hsueh Hung (BC).
- **Figure 5DEF.** Production and transfection of AS-circRNAs or modified ASOs and analysis via luciferase reporter assays. Infection assays after transfection (F) were performed by Christin Müller.
- **Supplementary Figure S2.** Production and transfection of AS-circRNAs. Northern blot analysis was performed by Tim Schneider.
- **Supplementary Figure S3-4 and 5C.** Production and transfection of AS-circRNAs. Infection assays were performed by Christin Müller.

Unpublished data

- **Christina Pfafenrot, Tim Schneider and Albrecht Bindereif.** 2022. Inhibition of mRNA translation by designer antisense-circRNAs. *Manuscript in preparation.*

  - **Figure 1**. Design, production and validation of AS-circRNAs targeting the β-globin 5´-UTR.
  - **Figure 2.** Screening of active AS-circRNAs targeting the β-globin 5´-UTR via luciferase assays.
  - **Figure 3.** Design of reporter constructs and AS-circRNAs targeting the MDM2 5´-UTR. (together with Tim Schneider).
  - **Figure 4CF.** Detection of circRNAs overexpressed through the Tornado system via Northern blot and screening of active MDM2-targeting AS-circRNAs via luciferase assay.
  - **Figure 5BC.** Analysis of MDM2 protein and RNA levels via Western blot and RT-qPCR.
  - **Supplementary Figure S1 and S3.** Secondary structure prediction of Tornado derived AS-circRNAs. (together with Tim Schneider).
  - **Supplementary Figure S2.** Transfection and growth curve analysis of HeLa cells.
  - **Supplementary Figure S4.** Transfection and Western blot analysis.

Patent

- EP 20211415.3, Bindereif, Müller, Pfafenrot, Schneider, Ziebuhr, submitted Dec 03, 2020 “Circular nucleic acids and uses thereof for interfering with genome expression and proliferation of coronaviruses”; **patent pending**